October 2022

Biomedical Applications of Protein Films and Polymeric Nanomaterials

Sanjana Gopalakrishnan
University of Massachusetts Amherst

BIOMEDICAL APPLICATIONS OF PROTEIN FILMS AND POLYMERIC NANOMATERIALS

A Dissertation Presented

by

SANJANA GOPALAKRISHNAN

Submitted to the Graduate School of the
University of Massachusetts Amherst in partial fulfillment
of the requirements for the degree of

DOCTOR OF PHILOSOPHY

July 2022

Department of Chemistry

BIOMEDICAL APPLICATIONS OF PROTEIN FILMS AND POLYMERIC NANOMATERIALS

A Dissertation Presented

by

SANJANA GOPALAKRISHNAN

Approved as to style and content by:

_____
Prof. Vincent M. Rotello, Chair

_____
Prof. Dhandapani Venkataraman, Member

_____
Prof. Michael D. Barnes, Member

_____
Prof. Cathal J. Kearney, Member

_____
Prof. Ricardo Metz, Department Head
Department of Chemistry

DEDICATION

To Appa for inspiring me to always ask *why* and Amma for teaching me to never shy away from the *how*.

ACKNOWLEDGMENTS

This work, like most science, was not done in isolation and would not have been possible without the help and support of many individuals.

First and foremost, I would like to thank my advisor, Prof. Vincent M. Rotello for his invaluable guidance and support throughout my PhD. This work would not have been possible without his scientific expertise and vision. Thank you for giving me the freedom to pursue research areas that I was interested in and teaching me the importance of "having fun" while doing science. I deeply appreciate the lessons I have learnt from you and the confidence they have instilled in me.

I would also like to acknowledge the professors who have been a part of my dissertation committee – Prof. Dhandapani Venkataraman, Prof. Michael D. Barnes, Prof. Cathal J. Kearney, and Prof. Laura Bradley. Thank you all for your continued support through the years and for the critical insights and feedback you have provided from time to time.

Much of this research work would not have been possible without the assistance of my collaborators at the Duan lab (Shuting, Yang), Thayumanavan lab (Manisha, Ann), Kearney lab (John, Dorcas) as well as Dr. Lan Zhang and Jinlong. Thank you all for helping me explore new and interesting scientific avenues and for always being generous with your time. I also want to acknowledge the support provided by Dr. Alexander Ribbe and Louis Raboin at the IALS Electron Microscopy facility.

I want to acknowledge the past and current members of the Rotello lab that have been a crucial part of my journey. I am very fortunate to work in a lab full of remarkable scientists that greatly value collaboration and have created an inclusive and positive

workplace. Thank you all for the continued support and friendship that you have afforded to me, and for being the best hype-team one could ask for. I want to especially thank Dr. Li-sheng Wang for being an excellent mentor and for being so patient with me. I am grateful to the contributions that Dave, Jessa, Aarohi, Aritra, Jungmi, and Jonathan have made to this work. I want to thank to Carol for always providing me the help and resources I needed to do my work. I also acknowledge the support provided by the Chemistry staff – Vicki, Caroline, jms, Rebecca, Bob and Dennis.

I want to thank all my friends, near and far – even though I cannot name you all in this document, I greatly value each of your friendships. I especially want to mention Alankrita, Amrita, Anushka, Jaya, Saloni and Shalu for being excellent role models. I am so proud of how far you all have come and the wonderful people you have become.

I want to end by thanking my family –Thank you, Praveen, for being a part of this journey right from the beginning, for believing in my abilities when I didn't, and for being my *partner* in the truest sense of the word. Thank you, Shriya, for always inspiring me to be creative. And finally, thank you Amma and Appa for supporting your 16-year-old daughter when she wanted to leave home to pursue her dream and then every day after, as I travelled further and further to pursue new dreams. Thank you for the trust you have placed in me and for your love and support.

ABSTRACT

BIOMEDICAL APPLICATIONS OF PROTEIN FILMS AND POLYMERIC NANOMATERIALS

JULY 2022

SANJANA GOPALAKRISHNAN, B.S., INDIAN INSTITUTE OF TECHNOLOGY KANPUR

Ph.D., UNIVERSITY OF MASSACHUSETTS AMHERST

Directed by: Professor Vincent M. Rotello

Biomaterials are widely applied for the diagnosis and treatment of numerous diseases. In addition to fulfilling specific biological functions, biomaterials must also be non-toxic, biocompatible, and sterilizable to be regarded as safe-for-use. Polymers are excellent candidates for fabricating functional biomaterials due to their wide availability and varied properties and may be natural or synthetic. Polymer precursors are fabricated into coatings, foams, scaffolds, gels, composites, and nanomaterials for several biomedical applications. This dissertation focuses on two types of polymeric biomaterials – protein-based materials and synthetic polymeric nanoparticles. Proteins are biopolymers that naturally occur with a variety of structural and functional properties. However, the fabrication of protein-based materials is challenging due to their aqueous and mechanical instability. In this work we highlighted the development of an additive-free, thermal treatment approach that relies on heat-curing protein films in fluorous media (fluorous-curing). In doing so, we are able to minimize protein denaturation and retain surface properties. Charged protein films were utilized to prepare antimicrobial coatings and size-sorting devices. We also demonstrated the utility of fluorous-curing to enhance mechanical

and enzymatic stability of collagen films with minimal denaturation. In the latter part of this work, we utilized ultrasound treatment to enhance the activity of biomaterials. Ultrasound is gaining interest as a tool used in combination with biomaterials for applications such as enhanced penetration of therapeutics into tissue, regulating drug release through ultrasound-responsive scaffolds, and sonodynamic therapy. However, these developments are limited and delayed due to the lack of effective in vitro models that prevent uncontrolled cell lysis during ultrasound. We developed 2D and 3D cell cultures for ultrasound treatment using collagen-based materials. We hypothesized that collagen would act as a support for the cells and absorb the energy exerted by ultrasound, thereby protecting the cells. We then utilized ultrasound in combination with antimicrobial polymeric nanomaterials for the synergistic eradication of bacterial biofilms. Antimicrobial polymer nanoparticles are an alternative to traditional antibiotics that prevent development of drug resistance. However, longer incubation durations and higher concentrations are required to allow for penetration into the bacterial biofilms which results in toxicity to mammalian cells. Ultrasound enhances the penetration of these nanoparticles into the biofilm EPS thereby reducing the incubation time and enhancing antimicrobial activity, with minimal toxicity to mammalian cells. Overall, this dissertation discusses significant developments in polymeric materials for varied potential applications as diagnostic sensors, antimicrobial materials, wound-healing, tissue engineering, and drug delivery applications.

TABLE OF CONTENTS

Page

LIST OF TABLES

Table **Page**

LIST OF FIGURES

Figure **Page**

CHAPTER 1

POLYMERIC MATERIALS FOR BIOMEDICAL APPLICATIONS

1.1. Salient features of biomaterials

Body tissues typically feature highly organized structures and unique compositions that enable specific functions such as providing mechanical or structural support, transport of nutrients and by-products, and regulation of cellular functions.[1, 2] However, injury, disease, and aging often result in damage to the tissue architecture and consequently malfunctioning organs.[3] These conditions, if untreated, may result several chronic medical conditions, such as chronic wounds,[4] and a reduced quality of life.

Biomaterials are defined as "a material intended to interface with biological systems to evaluate, treat, augment or replace any tissue, organ or function of the body" as defined in Biomaterials in Hand Surgery.[5] Therefore, they play a significant role in medicine by restoring function and facilitating healing. An ideal biomaterial must have the following features to be regarded as safe for use – 1. The material and its by-products are non-toxic and biocompatible; 2. The material is bioinert and will not cause an immune response in the host; and 3. The material is sterile or easily sterilizable to minimize the risk of infections. Additionally, most biomaterials are designed to have specific functionalities that play a significant role in medicine such as restoring tissue function, treating disease, and facilitate wound-healing.[6, 7] **Figure 1.1** highlights the salient features of biomaterials and show examples of how they are incorporated into implant-based biomaterials.

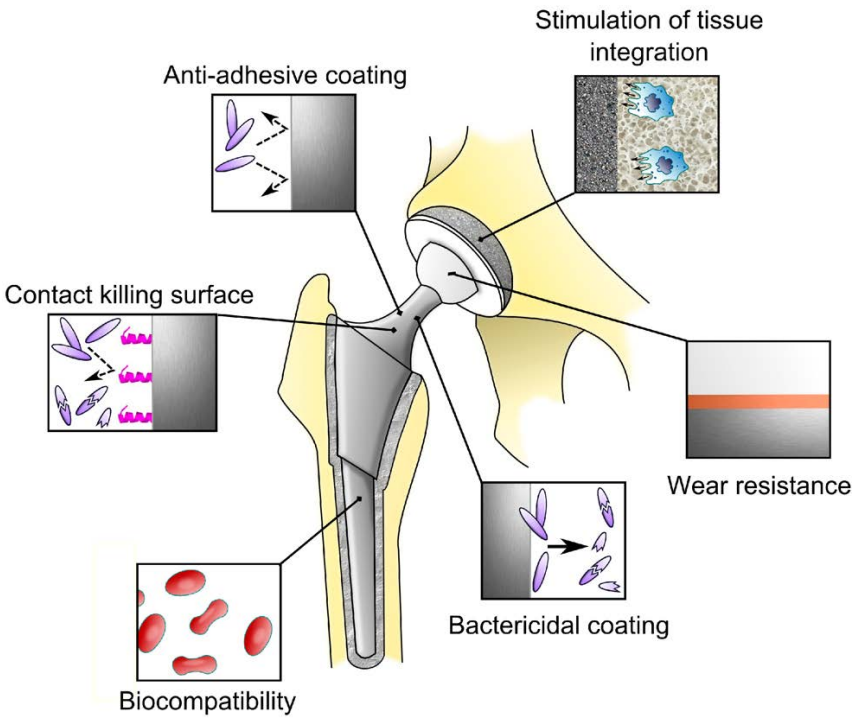

Figure 1.1. Schematic depicting a model medical implant that is non-toxic, biocompatible and bioinert (as it is made of titanium). Biomaterials may also be designed with features such as antimicrobial contact-killing surfaces, anti-adhesive coatings or bactericidal coatings or alternatively to stimulate tissue integration and wound-healing. Reproduced with permission.[6] Copyright 2014, Multidisciplinary Digital Publishing Institute (MDPI).

Biomaterials are often classified on the basis of their function as bioinert or bioactive. Bioinert materials have minimal bonding with the encompassing tissue and are often composed of inert metals or ceramics such as stainless steel, zirconia, alumina, or titanium.[7, 8] They are widely utilized for fabricating implants or joint replacements. On the other hand, bioactive materials is a broad classification for any material that elicits a biochemical or biophysical response in the native tissue environment and may be used to describe a wide variety of materials ranging from therapeutic nanomaterials, tissue engineering scaffolds and grafts, antimicrobial or drug-eluting implant coatings, and drug-loadable hydrogels.[9, 10, 11] Bioactive materials are utilized either on their own, such as therapeutic nanoparticles, tissue grafts, and drug-loaded hydrogels, or in combination with

bioinert materials, such as in the case of implant coatings. Stimuli-responsive biomaterials are also utilized for developing triggerable drug delivery systems that release cargo in response to endogenous or exogenous stimuli.[12] Increasingly, biomaterials are also being designed to be biodegradable or even bioresorbable, enabling the material to be fully digested, into non-toxic by-products and metabolites that the body can process, after fulfilling its function.[13]

1.2. Polymeric Biomaterials

Polymers have recently gained interest as potential building blocks for biomaterials owing to their versatile design space, ready availability, and ease of fabrication. Polymers are being increasingly utilized to develop nanoparticles, hydrogels, coatings, and scaffolds for numerous diagnostic and therapeutic strategies.[14] This chapter summarizes the different types polymeric biomaterials and their varied applications. Both natural (polysaccharides, proteins, and nucleic acids) and synthetic polymers are widely used as precursors and have advantages and potential challenges, that are highlighted in the following sections. There is a special focus of polymeric nanomaterials owing to the recent advances in the field of nanotechnology and the varied applications of polymers. Additionally, stimuli-responsive polymers and their application in development of smart, responsive, and targeted biomaterials are discussed.

1.2.1. Biopolymer-based materials

Biopolymers or natural polymers are polymeric substances derived from biological sources and typically encompass polysaccharides, proteins, and nucleic acids.[15] Biopolymers carry out vital functions in living organisms and therefore exhibit unique

properties, facilitating the fabrication of functional materials. Furthermore, they are abundant in nature, biodegradable, and readily soluble in water. Therefore, biopolymer-based materials can be fabricated in a green and sustainable manner with biodegradable precursors and end-products, and minimal use of organic solvents.[16] Additionally, the wide variety of readily available biopolymers enables the fabrication of functional materials while ensuring biocompatibility. **Figure 1.2.** highlights the different types of biopolymers from different natural sources, including silk, chitosan, gelatin, and cellulose, utilized in the fabrication of wearable sensors.[17]

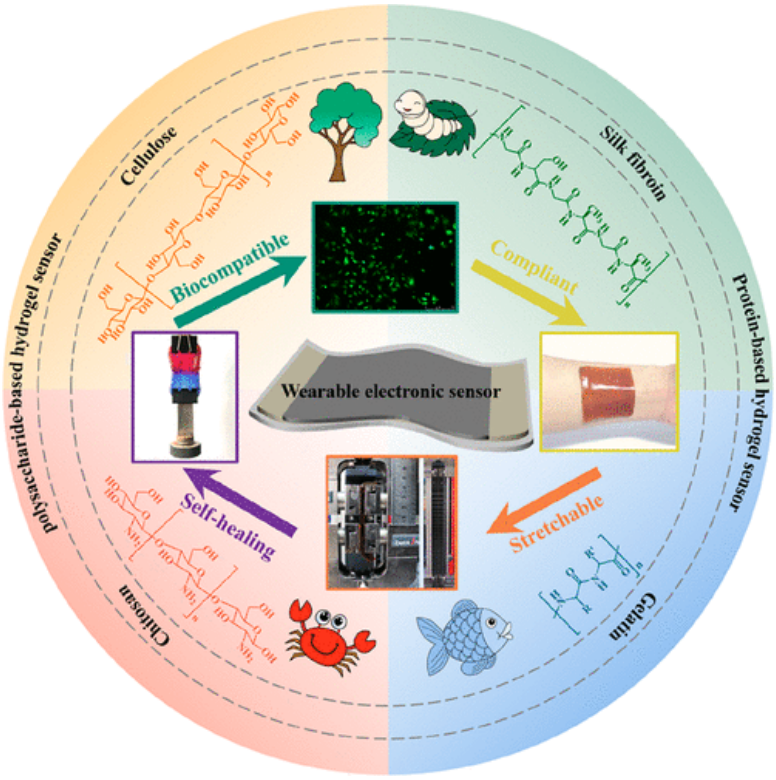

Figure 1.2. Schematic highlighting different natural sources of biopolymers, including gelatin, chitosan, cellulose, and silk fibroin, that are utilized for biomedical applications, such as wearable sensors. Reproduced with permission.[17] Copyright 2020, Elsevier.

Several different types of biopolymers are utilized in the development of biomaterials for a variety of applications. For instance, hyaluronic acid (HA) is a polysaccharide that is widely used for wound-healing applications owing to its inherent anti-inflammatory, anti-edematous, and anti-bacterial properties.[18] Additionally, polysaccharides such as HA, alginate, agar, and chitosan are widely utilized for the fabrication of drug-loadable hydrogels and tissue engineering scaffolds owing to their natural abundance, high hydrophilicity and polyfunctionality.[19] Proteins like silk and collagen, are widely utilized in tissue engineering applications owing to their mechanical and structural properties and the ability to efficiently fabricate scaffolds.[20] Proteins, in particular, have unique functions, often dictated by their structures, that may be translated into functional biomaterials, such as anti-fouling BSA coatings,[21] and lysozyme-based antimicrobial films.[22] Protein- based biomaterials are further elaborated in Chapter 2. Nucleic acids (DNA and RNA)- based materials including nucleic acid-hydrogels (NAHs), DNA origami-based nanostructures, and RNA nanoparticles have been utilized for numerous medical applications including gene and immunotherapy, drug delivery, nanomachinery and catalysis.[23, 24] The ability to program reaction patterns by harnessing the dynamic interactions between nucleic acids and other biomolecules, makes nucleic acids ideal candidates for the fabrication of hierarchical, adaptive, and responsive materials.[24]

1.2.2. Synthetic polymeric biomaterials

The past few decades have seen significant development of synthetic polymeric biomaterials, owing to advances in synthetic technologies and materials processing techniques.[25] Unlike biopolymers, synthetic polymers need to be designed to have specific

properties such as bio-inertness, degradability, and responsiveness to endogenous and exogenous stimuli. Angelova et al. have summarized for rational polymer design to optimize chemical, physical, interfacial, and biomimetic properties.[26] A wide variety of polymers are used in biomedical implants, medical device packaging, and wound-care materials. Polymers are utilized as protective coatings for implantable devices, adhesives, or as substrates for a variety of implantable devices.[27] For example, the wireless Medtronic Bravo pH system was developed as an alternative to traditional pH monitoring systems for GERD, where an epoxy coating was utilized as packaging to minimize discomfort at the time of implantation.[28] Polymeric dressings in the form of films, foams, hydrogels or hydrocolloids are utilized for wound-care owing to their occlusivity and ability to prevent bacterial contamination.[29] Polyurethane (PU) is widely used in many semi-permeable dressings as it is often impermeable to bacteria and liquid but is permeable to air. As compared to control dressings like Tegaderm ™, PU films showed better rate of tissue formation and lower inflammation, enabling better wound-healing.[30, 31]

1.2.3. Composites

The choice of biomaterials is often dictated by its structural and mechanical similarity to native tissue in addition to the previously described characteristics (in section 1.1). Factors such as elastic modulus, adhesion strength, surface morphology and chemical composition play a key role in dictating biomaterial design for a specific application. Often, homogenous biomaterials made of a single type of precursor is unable to satisfy all the biological and mechanical properties required for a specific application. For instance, metals and ceramics are generally preferred over polymers for hard tissue applications such as bone or joint implants. However, the mismatch in the elastic modulus of metals or

ceramics and bones (about 10-20 times), results in differences in the mechanical stress exerted on the implant vs. the bone and ultimately leads to bone atrophy over time. On the other hand, while polymeric materials have similar elastic modulus of bone tissue, they are much weaker than bone tissue. Polymer composite materials, such as fiber-reinforced or carbon nanotube-reinforced polymeric materials, are an alternative to homogenous materials providing similar elastic moduli as well as mechanical strength as the native tissue. Additionally, by controlling the volume fractions of each component, the properties of polymeric composites can be tailored to suit the properties of the tissue.[32] The secondary component in polymer composite materials may be metallic as in the case of titanium/polymethylmethacrylate bone cements,[33] inorganic as in the case of dental fillers containing silica and hydroxyapatite,[34, 35] organic as in the case of carbon fiber-containing polymer composites,[36] or biological wherein biopolymers or live cells are combined with polymers to generate composite biomaterials. There are several soft and hard tissue applications of polymeric composites such as in vascular grafts, abdominal wall prosthesis, bone and joint replacement, and bone cements.[32] **Figure 1.3.** highlights the different types of polymer composite materials and their varied applications.

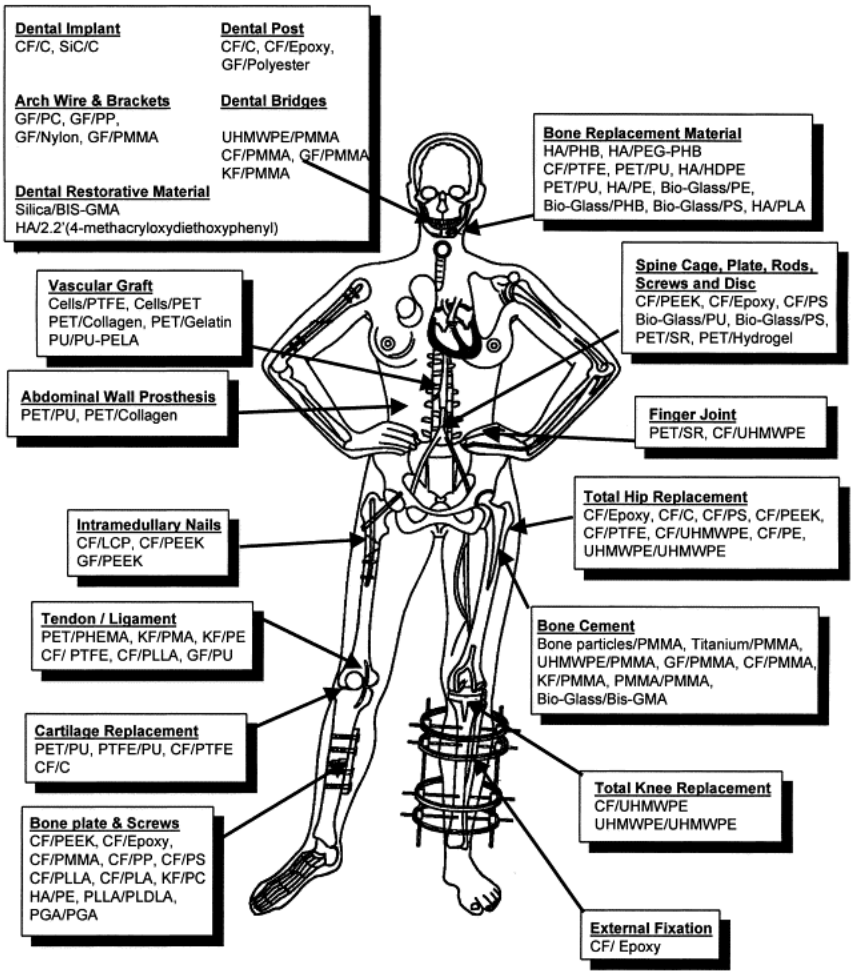

Figure 1.3. Schematic depicting the various types of polymeric composite materials, the secondary components commonly utilized, and their biomedical applications. Polymers are combined with metals, ceramics, other polymers, carbon fibers and even living cells to generate composites for different applications. Reproduced with permission.[32] Copyright 2001, Elsevier.

1.2.4. Polymeric Nanomaterials

Nanomedicine is defined as the design and utilization of diagnostic and/or therapeutic tools on the nanoscale. Many biological, cellular, and sub-cellular processes are regulated by various features of nanomaterials including their size, shape, flexibility,

and chemical composition. Polymeric nanomaterials are promising for the diagnosis and treatment of a wide range of diseases owing to their high degree of uniformity and control on structural and chemical properties,[37] as well as their versatility and flexibility.[38] Polymeric nanomaterials may be designed to carry various hydrophobic or hydrophilic cargoes, have inherent therapeutic or targeting activity owing to their surface functionality, demonstrate triggerable behavior such as assembly, disassembly, or drug activation, in response to endogenous or exogenous stimuli. **Figure 1.4** shows the typical composition of polymeric nanoparticles and the various design elements that may be modified for a particular application.[39]

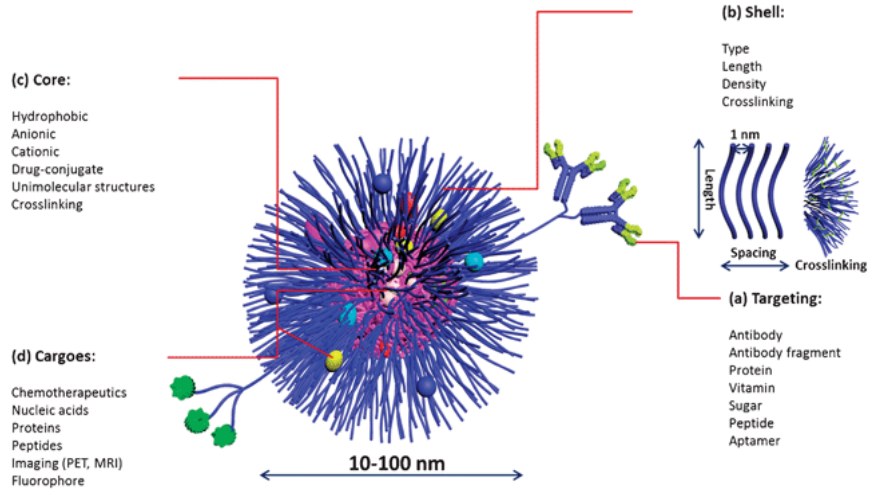

Figure 1.4. Representative polymeric nanoparticle with the following potential design strategies – (a) targeting ability through functional headgroups such as antibodies or sugar moieties; (b) Hydrophilicity, length, density, and permeability of the outer shell; (c) hydrophobicity, charge, and permeability of the core and (d) the properties and applications of the cargo which may be encapsulated in either the core or the shell, or even attached to the headgroup. Reproduced with permission.[39] Copyright 2012, Royal Society of Chemistry.

Polymeric nanomaterials are utilized for a variety of biological applications. Makabenta et al. discuss the applications of polymeric nanoparticles (PNPs) fabricated using natural as well as synthetic polymers for the treatment of multi-drug resistant

bacterial and biofilm infections.[40] PNPs are able to access antimicrobial modalities that are novel to bacteria and therefore bacteria are unable to develop resistance to these systems. Natural polymers such as chitosan-based NPs are utilized for the development of pH-responsive carriers for the controlled and targeted delivery of vancomycin to treat MRSA infections.[41] Synthetic polymers can mimic the activity of antimicrobial peptides.[42] Polymeric nanocomposites incorporating antimicrobial silver NPs[43] or phytochemicals[44] are also utilized for the treatment of bacterial infections. Polymeric carriers are also utilized for the delivery of therapeutic proteins and nucleic acids owing to their versatility, scalability, and biological stability. Polymeric micelles are often utilized for the controlled delivery of biomolecules such as proteins and nucleic acids. González-Toro et al. developed polymeric nanogels that concurrently bind proteins on the exterior of the particle and encapsulate lipophilic molecules within the hydrophobic pocket of the particle. This enables co-delivery of hydrophilic proteins and hydrophobic molecules to the same target region.[45] Synthetic polyoxanorbornene-based polymers have been utilized as mimics of traditional cell-penetrating peptides to deliver proteins.[46] Polymeric nanomaterials have also been utilized to encapsulate hydrophobic transition metal catalysts to develop nanocatalysts for bioorthogonal drug activation. These polymeric nanocatalysts are utilized for both anti-cancer and antimicrobial applications.[47, 48, 49]

1.3. Effect of external stimuli on the activity of biomaterials

Different types of triggers are widely used in combination with biomaterials to enhance, regulate and monitor their activity. These triggers are generally classified into two types – endogenous and exogenous. Endogenous or biological triggers, such as significant changes in pH, changes in glutathione levels, or over-expression of certain

enzymes, are often unique diseased tissue and can therefore be utilized to regulate or enhance the activity of biomaterials.[50] Polymeric nanoparticles that respond to pH and oxidative stress have been utilized for triggered drug delivery.[51] Polymeric hydrogels for triggered drug release are also designed to respond to endogenous triggers, such as pH.[52] An interesting application of enzyme-responsive hydrogels was demonstrated by Alkekhia et al. where they developed polymeric hydrogels that degrade in the presence of β-Lactamase enzymes.[53] β-Lactamases are a class of enzymes specifc to bacteria that are also a leading cause of development of drug resistance in bacteria. Therefore, the β-Lactamase-responsive hydrogels can specifically target bacterial infections and can be effective in prevention of drug-resistant infections. On the other hand, exogenous triggers, such as near IR radiation, ultrasound, temperature, and electromagnetic field, are controlled externally and are therefore independent of inter-patient variations.[50] Conductive polymers such as polyaniline, polypyrrole, and polythiophene have are widely applied in the development of bioactuators, sensors, nerve regenerative implants and tissue engineering scaffolds as their high conductivity enables the cells and tissues cultured on them to be electrically stimulated.[54] Magnetic nanomaterials are utilized in immunotherapy to stimulate naïve T cells, while also allowing for tracking through magnetic resonance imaging.[55] Photo- and ultrasound-induced tissue ablation are widely applied either alone or in combination with drug-loaded biomaterials to enhance tissue penetration.[56, 57] Responsive biomaterials such as thermoresponsive hydrogels[58] and photo-activated nanomaterials[59] are also utilized for controlled and targeted drug delivery.

1.3.1 Biomaterial applications of ultrasound treatment

Ultrasound is of particular interest in drug delivery applications as it is widely available, minimally invasive, and has better tissue penetration as compared other exogenous triggers such as light.[60, 61] In particular, ultrasound has gained interest due to its permeabilization ability to enhance the penetration and consequently the activity of therapeutic agents. For instance, drug diffusion through the skin barrier poses a formidable challenge in transdermal delivery as only a small, lipophilic molecules are able to passively diffuse through the skin.[62] Ultrasound has the ability to reversibly and non-invasively permeabilize the skin enabling localized and controlled delivery of small molecules, biologics, or nanomaterials.[56]

Ultrasound is an oscillating pressure wave with a frequency above 20 kHz. Ultrasound-based treatments are divided into three ranges based on the frequency – low frequency sonophoresis (LFS 20 – 100 kHz), therapeutic ultrasound (0.7 – 3 MHz), and high frequency sonophoresis (HFS > 3 MHz).[63] Ultrasound-based therapies often utilize a combination of one of more of these three main mechanisms – thermal effects, radiation and convection, and acoustic cavitation.[56]Thermal effects are a result of the attenuation of sound energy in the tissue, which heats up the surrounding tissue, resulting in increased blood flow. Convection and radiation both rely on the agitation of surrounding fluid as a result of ultrasound. Lastly, acoustic cavitation is the process of formation and propagation of microbubbles as a result of ultrasound, resulting in tissue permeabilization.

Sonophoresis is widely utilized to enhance the penetration of therapeutic agents in a target region, particularly for transdermal delivery of biomacromolecules, including siRNA and proteins.[64, 65] In these cases, ultrasound is frequently combined with other

biomaterials such as hydrogels or microneedle patches that act as a reservoir for the therapeutic agents. Sonophoresis has also been used in combination with therapeutic nanomaterials to enhance their efficacy for anti-cancer applications.[66] In addition to sonophoresis, ultrasound is also utilized for tissue ablation therapy of the treatment of solid tumors and uterine fibroids.[67] Ultrasound-responsive materials are also gaining wide interest for several drug delivery applications. Ultrasound-triggerable hydrogels are utilized for the controlled and localized delivery of small molecule drugs,[68] nanomaterials[69] and biomacromolecules.[70] Ultrasound acts as an exogenous, on-off trigger whereby the drug is only released in the presence of ultrasound. **Figure 1.5** shows an alginate hydrogel ionically crosslinked with Ca^{2+} ions that is transiently disrupted by ultrasound, as seen in **Figure 1.5 (b), (c)** and **(d)**.[68] This temporary disruption results in an on-off switch that leads to drug release only when the ultrasound is turned on, which is evidenced in **Figure 1.5 (e)** and **(f)** Lastly, sonodynamic therapy, the application of ultrasound in combination with sonosensitizers for on-demand generation of ROS species, is gaining interest for the treatment of both bacterial infections[71] and cancer.[72]

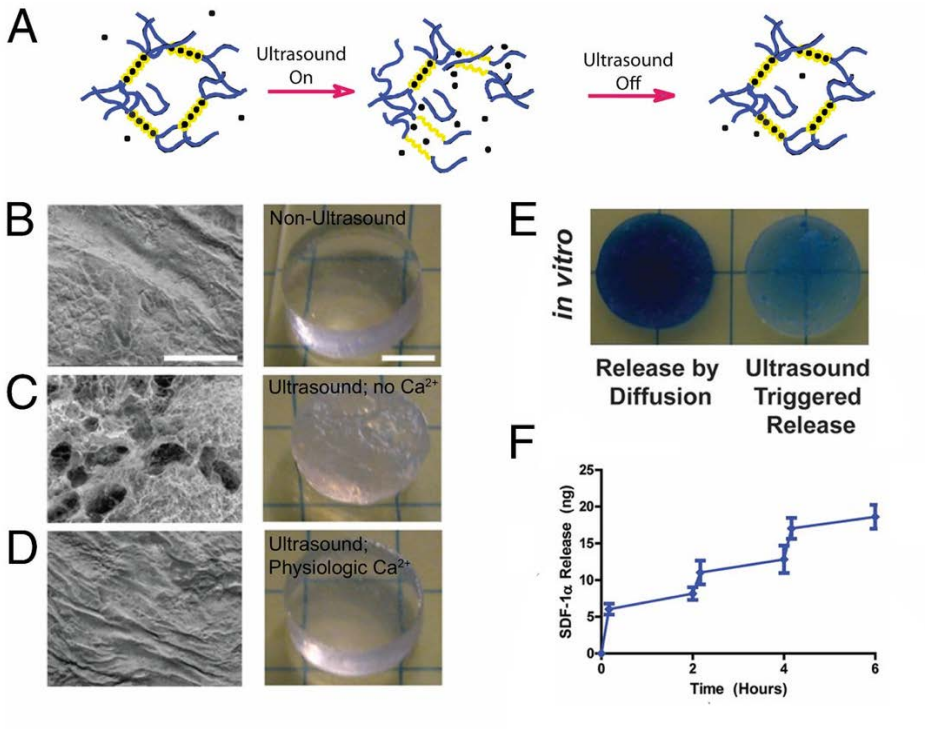

Figure 1.5. (a) Calcium-crosslinked alginate hydrogels are transiently disrupted by ultrasound, leading to release of encapsulated cargo. SEM micrographs and macroscopic images showing the morphology of the gels (b) before, (c) during and (d) after ultrasound treatment. As seen in (d) the disruption is reversible and the structure is preserved post ultrasound treatment. (e) Change in loading of small molecule dye (mitoxantrone) in the gel due to diffusion and ultrasound treatment show that significantly more dye is released by ultrasound. (f) Release profile of SDF-1$^{\alpha}$ from the gels that were treated for 10 min once every 2 h. Reproduced with permission.[68] Copyright 2014, Proceedings of the National Academy of Sciences.

1.4. Conclusions

This chapter summarized the salient features of polymeric biomaterials and their numerous potential applications. Biomaterials are functional materials utilized for the diagnosis and treatment of diseases and therefore must possess the following properties – non-toxicity, biocompatibility, and sterilizability. In this regard, polymers (both natural and synthetic) are excellent candidates for the fabrication of biomaterials. Natural or biopolymers naturally occur with a wide variety of functionalities while synthetic polymers

are easily customizable and scalable to produce a wide range of structural and functional materials on-demand. Natural and synthetic polymers are utilized either by themselves or as composites containing other components to fabricate different materials, such as coatings, foams, scaffolds, hydrogels, and nanomaterials, for innumerable applications including antimicrobial and anti-cancer therapy, drug and biologics delivery, tissue engineering, and medical devices and implants. Additionally, polymeric materials (both natural and synthetic) are utilized in combination with endogenous or exogenous triggers either to enhance their activity or to fabricate stimuli-responsive systems for tissue engineering and drug delivery applications.

The subsequent chapters will focus on two different types of biomaterials – protein-based materials and polymeric nanomaterials. Moreover, there is a special focus on ultrasound-based therapies in combination with biomaterials. Proteins are a class of biopolymers that naturally occur with a wide array of structural, chemical, and functional properties. However, their mechanical and structural instability makes it challenging to fabricate functional materials using proteins. Chapter 2 summarizes the different strategies for fabrication of protein-based materials, including fluorous-curing a thermal treatment strategy that utilizes a fluorous environment. Chapter 3, 4 and 5 then highlight different applications of protein films fabricated by fluorous-curing using a variety of proteins (bovine serum albumin, lysozyme, and collagen). Chapter 6 focuses on the development of a methodology for studying ultrasound-based treatments *in vitro* using collagen-based materials. Collagen films and collagen hydrogels were utilized to generate 2D and 3D fibroblast cultures as in vitro models that protect against the adverse effects of ultrasound. This enables more advances in the field of ultrasound-based therapies by providing a rapid

platform for conducting *in vitro* studies. This *in vitro* model was utilized in Chapter 7 where ultrasound treatment was applied in combination with polymeric nanomaterials for the synergistic eradication of bacterial biofilms. Sonophoresis enhanced the penetration of antimicrobial polymeric NPs into the biofilm enhancing its activity while minimizing damage to healthy tissue.

1.5. References

1. Menon, G. K.; Cleary, G. W.; Lane, M. E. The Structure and Function of the Stratum Corneum. *Int. J. Pharm.* **2012**, *435* (1), 3–9.

2. The cardiac muscle cell - Severs - 2000 - BioEssays - Wiley Online Library https://onlinelibrary.wiley.com/doi/10.1002/(SICI)1521-1878(200002)22:2%3C188::AID-BIES10%3E3.0.CO;2-T

3. Schuliga, M.; Read, J.; Knight, D. A. Ageing Mechanisms That Contribute to Tissue Remodeling in Lung Disease. *Ageing Res. Rev.* **2021**, *70*, 101405.

4. Frykberg, R. G.; Banks, J. Challenges in the Treatment of Chronic Wounds. *Adv. Wound Care* **2015**, *4* (9), 560–582.

5. Tranquilli Leali, P.; Merolli, A. Fundamentals of Biomaterials. *Biomater. Hand Surg.* **2009**, 1–11.

6. Gallo, J.; Holinka, M.; Moucha, C. S. Antibacterial Surface Treatment for Orthopaedic Implants. *Int. J. Mol. Sci. 2014, Vol. 15, Pages 13849-13880* **2014**, *15* (8), 13849–13880.

7. Huebsch, N.; Mooney, D. J. Inspiration and Application in the Evolution of Biomaterials. *Nat. 2009 4627272* **2009**, *462* (7272), 426–432.

8. Ralls, A.; Kumar, P.; Misra, M.; Menezes, P. L. Material Design and Surface Engineering for Bio-Implants. *JOM* **2020**, *72* (2), 684–696.

9. Kokubo, T.; Kim, H. M.; Kawashita, M. Novel Bioactive Materials with Different Mechanical Properties. *Biomaterials* **2003**, *24* (13), 2161–2175.

10. Islam, M. M.; Shahruzzaman, M.; Biswas, S.; Nurus Sakib, M.; Rashid, T. U. Chitosan Based Bioactive Materials in Tissue Engineering Applications-A Review. *Bioact. Mater.* **2020**, *5* (1), 164–183.

11. Pan, H.; Zheng, M.; Ma, A.; Liu, L.; Cai, L. Cell/Bacteria-Based Bioactive Materials for Cancer Immune Modulation and Precision Therapy. *Adv. Mater.* **2021**, *33* (50), 2100241.

12. Mart, R. J.; Osborne, R. D.; Stevens, M. M.; Ulijn, R. V. Peptide-Based Stimuli-Responsive Biomaterials. *Soft Matter* **2006**, *2* (10), 822–835.

13. Godavitarne, C.; Robertson, A.; Peters, J.; Rogers, B. Biodegradable Materials. *Orthop. Trauma* **2017**, *31* (5), 316–320.

14. Griffith, L. G. Polymeric Biomaterials. *Acta Mater.* **2000**, *48* (1), 263–277.

15. Baranwal, J.; Barse, B.; Fais, A.; Delogu, G. L.; Kumar, A. Biopolymer: A Sustainable Material for Food and Medical Applications. *Polymers (Basel).* **2022**, *14* (5).

16. Kaplan, D. L. Introduction to Biopolymers from Renewable Resources. *Biopolym. from Renew. Resour.* **1998**, 1–29.

17. Cui, C.; Fu, Q.; Meng, L.; Hao, S.; Dai, R.; Yang, J. Recent Progress in Natural Biopolymers Conductive Hydrogels for Flexible Wearable Sensors and Energy Devices: Materials, Structures, and Performance. *ACS Appl. Bio Mater.* **2021**, *4* (1), 85–121.

18. Shuborna, N. S.; Chaiyasamut, T.; Sakdajeyont, W.; Vorakulpipat, C.; Rojvanakarn, M.; Wongsirichat, N. Generation of Novel Hyaluronic Acid Biomaterials for Study of Pain in Third Molar Intervention: A Review. *J. Dent. Anesth. Pain Med.* **2019**, *19* (1), 11.

19. Jin, M.; Shi, J.; Zhu, W.; Yao, H.; Wang, D. A. Polysaccharide-Based Biomaterials in Tissue Engineering: A Review. *https://home.liebertpub.com/teb* **2021**, *27* (6), 604–626.

20. Gopalakrishnan, S.; Xu, J.; Zhong, F.; Rotello, V. M. Strategies for Fabricating Protein Films for Biomaterial Applications. *Adv. Sustain. Syst.* **2021**, *5* (1), 2000167.

21. Wang, L. S.; Gopalakrishnan, S.; Lee, Y. W.; Zhu, J.; Nonnenmann, S. S.; Rotello, V. M. Translation of Protein Charge and Hydrophilicity to Materials Surface Properties Using Thermal Treatment in Fluorous Media. *Mater. Horizons* **2018**, *5* (2), 268–274.

22. Xu, X.; Zhang, D.; Gao, S.; Shiba, T.; Yuan, Q.; Cheng, K.; Tan, H.; Li, J. Multifunctional Biomaterial Coating Based on Bio-Inspired Polyphosphate and Lysozyme Supramolecular Nanofilm. *Biomacromolecules* **2018**, *19* (6), 1979–1989.

23. Yue, L.; Wang, S.; Zhou, Z.; Willner, I. Nucleic Acid Based Constitutional Dynamic Networks: From Basic Principles to Applications. *J. Am. Chem. Soc.* **2020**, *142* (52), 21577–21594.

24. Yuan, Y.; Gu, Z.; Yao, C.; Luo, D.; Yang, D. Nucleic Acid–Based Functional Nanomaterials as Advanced Cancer Therapeutics. *Small* **2019**, *15* (26), 1900172.

25. Becker, M. L.; Burdick, J. A. Introduction: Polymeric Biomaterials. *Chem. Rev.* **2021**, *121* (18), 10789–10791.

26. Angelova, N.; Hunkeler, D. Rationalizing the Design of Polymeric Biomaterials. *Trends Biotechnol.* **1999**, *17* (10), 409–421.

27. Teo, A. J. T.; Mishra, A.; Park, I.; Kim, Y. J.; Park, W. T.; Yoon, Y. J. Polymeric Biomaterials for Medical Implants and Devices. *ACS Biomater. Sci. Eng.* **2016**, *2* (4), 454–472.

28. Pandolfino, J. Ambulatory Esophageal PH Monitoring Using a Wireless System. *Am. J. Gastroenterol.* **2003**, *98* (4), 740–749..

29. Mir, M.; Ali, M. N.; Barakullah, A.; Gulzar, A.; Arshad, M.; Fatima, S.; Asad, M. Synthetic Polymeric Biomaterials for Wound Healing: A Review. *Prog. Biomater. 2018 71* **2018**, *7* (1), 1–21.

30. Jenks, M.; Craig, J.; Green, W.; Hewitt, N.; Arber, M.; Sims, A. Tegaderm CHG IV Securement Dressing for Central Venous and Arterial Catheter Insertion Sites: A NICE Medical Technology Guidance. *Appl. Health Econ. Health Policy* **2016**, *14* (2), 135–149.

31. Khil, M. S.; Cha, D. Il; Kim, H. Y.; Kim, I. S.; Bhattarai, N. Electrospun Nanofibrous Polyurethane Membrane as Wound Dressing. *J. Biomed. Mater. Res. Part B Appl. Biomater.* **2003**, *67B* (2), 675–679.

32. Ramakrishna, S.; Mayer, J.; Wintermantel, E.; Leong, K. W. Biomedical Applications of Polymer-Composite Materials: A Review. *Compos. Sci. Technol.* **2001**, *61* (9), 1189–1224.

33. Cools, P.; De Geyter, N.; Vanderleyden, E.; Barberis, F.; Dubruel, P.; Morent, R. Adhesion Improvement at the PMMA Bone Cement-Titanium Implant Interface Using Methyl Methacrylate Atmospheric Pressure Plasma Polymerization. *Surf. Coatings Technol.* **2016**, *294*, 201–209.

34. Moszner, N.; Salz, U. New Developments of Polymeric Dental Composites. *Prog. Polym. Sci.* **2001**, *26* (4), 535–576.

35. Chen, L.; Yu, Q.; Wang, Y.; Li, H. BisGMA/TEGDMA Dental Composite Containing High Aspect-Ratio Hydroxyapatite Nanofibers. *Dent. Mater.* **2011**, *27* (11), 1187.

36. Saito, N.; Aoki, K.; Usui, Y.; Shimizu, M.; Hara, K.; Narita, N.; Ogihara, N.; Nakamura, K.; Ishigaki, N.; Kato, H.; et al. Application of Carbon Fibers to Biomaterials: A New Era of Nano-Level Control of Carbon Fibers after 30-Years of Development. *Chem. Soc. Rev.* **2011**, *40* (7), 3824–3834.

37. Iha, R. K.; Wooley, K. L.; Nyström, A. M.; Burked, D. J.; Kade, M. J.; Hawker, C. J. Applications of Orthogonal, "Click" Chemistries in the Synthesis of Functional Soft Materials. *Chem. Rev.* **2009**, *109* (11), 5620.

38. O'reilly, R. K.; Hawker, C. J.; Wooley, K. L. Cross-Linked Block Copolymer Micelles: Functional Nanostructures of Great Potential and Versatility. *Chem. Soc. Rev.* **2006**, *35* (11), 1068–1083.

39. Elsabahy, M.; Wooley, K. L. Design of Polymeric Nanoparticles for Biomedical Delivery Applications. *Chem. Soc. Rev.* **2012**, *41* (7), 2545.

40. Makabenta, J. M. V.; Nabawy, A.; Li, C. H.; Schmidt-Malan, S.; Patel, R.; Rotello, V. M. Nanomaterial-Based Therapeutics for Antibiotic-Resistant Bacterial Infections. *Nat. Rev. Microbiol.* **2021**, *19* (1), 23.

41. Kalhapure, R. S.; Jadhav, M.; Rambharose, S.; Mocktar, C.; Singh, S.; Renukuntla, J.; Govender, T. PH-Responsive Chitosan Nanoparticles from a Novel Twin-Chain Anionic Amphiphile for Controlled and Targeted Delivery of Vancomycin. *Colloids Surf. B. Biointerfaces* **2017**, *158*, 650–657.

42. Song, J.; Jang, J. Antimicrobial Polymer Nanostructures: Synthetic Route, Mechanism of Action, and Perspective. *Adv. Colloid Interface Sci.* **2014**, *203*, 37–50.

43. Mei, L.; Lu, Z.; Zhang, X.; Li, C.; Jia, Y. Polymer-Ag Nanocomposites with Enhanced Antimicrobial Activity against Bacterial Infection. *ACS Appl. Mater. Interfaces* **2014**, *6* (18), 15813–15821.

44. Landis, R. F.; Gupta, A.; Lee, Y. W.; Wang, L. S.; Golba, B.; Couillaud, B.; Ridolfo, R.; Das, R.; Rotello, V. M. Crosslinked Polymer-Stabilized Nanocomposites for the Treatment of Bacterial Biofilms. *ACS Nano* **2017**, *11* (1), 946.

45. González-Toro, D. C.; Ryu, J. H.; Chacko, R. T.; Zhuang, J.; Thayumanavan, S. Concurrent Binding and Delivery of Proteins and Lipophilic Small Molecules Using Polymeric Nanogels. *J. Am. Chem. Soc.* **2012**, *134* (16), 6964.

46. Sgolastra, F.; Backlund, C. M.; Ilker Ozay, E.; deRonde, B. M.; Minter, L. M.; Tew, G. N. Sequence Segregation Improves Non-Covalent Protein Delivery. *J. Control. Release* **2017**, *254*, 131.

47. Zhang, X.; Landis, R. F.; Keshri, P.; Cao-Milán, R.; Luther, D. C.; Gopalakrishnan, S.; Liu, Y.; Huang, R.; Li, G.; Malassiné, M.; et al. Intracellular Activation of Anticancer Therapeutics Using Polymeric Bioorthogonal Nanocatalysts. *Adv. Healthc. Mater.* **2021**, *10* (5), 2001627.

48. Fedeli, S.; Im, J.; Gopalakrishnan, S.; Elia, J. L.; Gupta, A.; Kim, D.; Rotello, V. M. Nanomaterial-Based Bioorthogonal Nanozymes for Biological Applications. *Chem. Soc. Rev.* **2021**, *50* (24), 13467–13480.

49. Huang, R.; Li, C. H.; Cao-Milán, R.; He, L. D.; Makabenta, J. M.; Zhang, X.; Yu, E.; Rotello, V. M. Polymer-Based Bioorthogonal Nanocatalysts for the Treatment of Bacterial Biofilms. *J. Am. Chem. Soc.* **2020**, *142* (24), 10723–10729.

50. Raza, A.; Rasheed, T.; Nabeel, F.; Hayat, U.; Bilal, M.; Iqbal, H. M. N. Endogenous and Exogenous Stimuli-Responsive Drug Delivery Systems for Programmed Site-Specific Release. *Molecules* **2019**, *24* (6).

51. Colson, Y. L.; Grinstaff, M. W. Biologically Responsive Polymeric Nanoparticles for Drug Delivery. *Adv. Mater.* **2012**, *24* (28), 3878–3886.

52. Gupta, P.; Vermani, K.; Garg, S. Hydrogels: From Controlled Release to PH-Responsive Drug Delivery. *Drug Discov. Today* **2002**, *7* (10), 569–579.

53. Alkekhia, D.; LaRose, C.; Shukla, A. β-Lactamase-Responsive Hydrogel Drug Delivery Platform for Bacteria-Triggered Cargo Release. *ACS Appl. Mater. Interfaces* **2022**, *14* (24), 27538–27550.

54. Guo, B.; Ma, P. X. Conducting Polymers for Tissue Engineering. *Biomacromolecules* **2018**, *19* (6), 1764.

55. Xie, Y. Q.; Wei, L.; Tang, L. Immunoengineering with Biomaterials for Enhanced Cancer Immunotherapy. *Wiley Interdiscip. Rev. Nanomedicine Nanobiotechnology* **2018**, *10* (4), e1506.

56. Oberli, M. A.; Schoellhammer, C. M.; Langer, R.; Blankschtein, D. Ultrasound-Enhanced Transdermal Delivery: Recent Advances and Future Challenges. *Ther. Deliv.* **2014**, *5* (7), 843.

57. Wu, T.; Zhang, D.; Qiao, Q.; Qin, X.; Yang, C.; Kong, M.; Deng, H.; Zhang, Z. Biomimetic Nanovesicles for Enhanced Antitumor Activity of Combinational Photothermal and Chemotherapy. *Mol. Pharm.* **2018**, *15* (3), 1341–1352.

58. Chatterjee, S.; Hui, P. C. L.; Kan, C. wai. Thermoresponsive Hydrogels and Their Biomedical Applications: Special Insight into Their Applications in Textile Based Transdermal Therapy. *Polymers (Basel)*. **2018**, *10* (5).

59. Li, J.; Pu, K. Semiconducting Polymer Nanomaterials as Near-Infrared Photoactivatable Protherapeutics for Cancer. *Acc. Chem. Res.* **2020**, *53* (4), 752–762.

60. Miller, D. L.; Smith, N. B.; Bailey, M. R.; Czarnota, G. J.; Hynynen, K.; Makin, I. R. S. Overview of Therapeutic Ultrasound Applications and Safety Considerations. *J. Ultrasound Med.* **2012**, *31* (4), 623. https://doi.org/10.7863/JUM.2012.31.4.623.

61. Deprez, J.; Lajoinie, G.; Engelen, Y.; De Smedt, S. C.; Lentacker, I. Opening Doors with Ultrasound and Microbubbles: Beating Biological Barriers to Promote Drug Delivery. *Adv. Drug Deliv. Rev.* **2021**, *172*, 9–36.

62. Bos, J. D.; Meinardi, M. M. H. M. The 500 Dalton Rule for the Skin Penetration of Chemical Compounds and Drugs. *Exp. Dermatol.* **2000**, *9* (3), 165–169.

63. Mitragotri, S. Sonophoresis: A 50-Year Journey. *Drug Discov. Today* **2004**, *9* (17), 735–736.

64. Ryu, Y. C.; Kim, D. I.; Kim, S. H.; Wang, H. M. D.; Hwang, B. H. Synergistic Transdermal Delivery of Biomacromolecules Using Sonophoresis after Microneedle Treatment. *Biotechnol. Bioprocess Eng. 2018 233* **2018**, *23* (3), 286–292.

65. Mitragotri, S. Sonophoresis: Ultrasound-Mediated Transdermal Drug Delivery. *Percutaneous Penetration Enhanc. Phys. Methods Penetration Enhanc.* **2017**, 3–14.

66. Tharkar, P.; Varanasi, R.; Wong, W. S. F.; Jin, C. T.; Chrzanowski, W. Nano-Enhanced Drug Delivery and Therapeutic Ultrasound for Cancer Treatment and Beyond. *Front. Bioeng. Biotechnol.* **2019**, *7*, 324.

67. van den Bijgaart, R. J. E.; Eikelenboom, D. C.; Hoogenboom, M.; Fütterer, J. J.; den Brok, M. H.; Adema, G. J. Thermal and Mechanical High-Intensity Focused Ultrasound: Perspectives on Tumor Ablation, Immune Effects and Combination Strategies. *Cancer Immunol. Immunother.* **2017**, *66* (2), 247–258.

68. Huebsch, N.; Kearney, C. J.; Zhao, X.; Kim, J.; Cezar, C. A.; Suo, Z.; Mooney, D. J. Ultrasound-Triggered Disruption and Self-Healing of Reversibly Cross-Linked Hydrogels for Drug Delivery and Enhanced Chemotherapy. *Proc. Natl. Acad. Sci. U. S. A.* **2014**, *111* (27), 9762–9767.

69. Kearney, C. J.; Skaat, H.; Kennedy, S. M.; Hu, J.; Darnell, M.; Raimondo, T. M.; Mooney, D. J. Switchable Release of Entrapped Nanoparticles from Alginate Hydrogels. *Adv. Healthc. Mater.* **2015**, *4* (11), 1634–1639.

70. Arrizabalaga, J. H.; Smallcomb, M.; Abu-Laban, M.; Liu, Y.; Yeingst, T. J.; Dhawan, A.; Simon, J. C.; Hayes, D. J. Ultrasound-Responsive Hydrogels for On-Demand Protein Release. *ACS Appl. Bio Mater.* **2022**.

71. Pourhajibagher, M.; Bahador, A. Synergistic Biocidal Effects of Metal Oxide Nanoparticles-Assisted Ultrasound Irradiation: Antimicrobial Sonodynamic Therapy against Streptococcus Mutans Biofilms. *Photodiagnosis Photodyn. Ther.* **2021**, *35*.

72. Wang, H.; Guo, J.; Lin, W.; Fu, Z.; Ji, X.; Yu, B.; Lu, M.; Cui, W.; Deng, L.; Engle, J. W.; et al. Open-Shell Nanosensitizers for Glutathione Responsive Cancer Sonodynamic Therapy. *Adv. Mater.* **2022**, *34* (15), 2110283.

CHAPTER 2

STRATEGIES FOR FABRICATING PROTEIN FILMS FOR BIOMATERIAL APPLICATIONS

2.1 Introduction

Proteins are sustainable, biocompatible and biodegradable building blocks for designing materials.[1, 2] Proteins naturally feature a variety of functionalities - for instance, structural proteins like collagen are widely used in biomedical applications due to their abundance in the extracellular matrix.[3] Silk fibroin and soy protein isolate films have been used as food packaging materials[4, 5] as well as in the fabrication of medical devices,[6, 7] due to their ready availability, efficient processability, biodegradability and biocompatibility.[8, 9] Furthermore, the process of isolating proteins and fabricating protein-based materials can be conducted with limited use of organic solvents, as most proteins are water soluble.[10, 11, 12] Therefore, protein are an attractive approach for designing sustainable materials for biomedical applications.

Proteins are widely to generate materials including coatings,[13] hydrogels,[14] 3D scaffolds[15] and adhesives.[16] However, the use of proteins in these materials is complicated by their instability in aqueous media, which results in degradation and loss of structure in materials.[17, 18] Therefore, current technologies have been focused on improving the aqueous stability of protein-based materials, while maintaining desirable properties such as biocompatibility, biodegradability, and native functionality.

This chapter focuses on strategies for generating protein films and protein-based coatings, as they are one of the most widely synthesized protein-based material. Currently, three main strategies have been employed, as illustrated in **Figure 2.1** – 1. Naturally self-assembling proteins such as silk fibroin self-assemble into water-stable films upon during; [19] 2. Crosslinking of proteins through physical or chemical approaches;[20, 21] and 3. Thermal treatment of proteins to initiate reorganization of proteins, including recent approaches that retain native structure and properties.[22], [23] Additionally, post-functionalization of the surface[24] or incorporation of additives[25] can be used to enhance native properties of the film or impart new characteristics. Protein films are widely used as food packaging materials,5 tissue engineering scaffolds,7 and coatings for specific biomedical applications such as anti-fouling coatings, cytophilic coatings etc.22 Previous reviews on this subject have focused on either biomedical applications of a particular protein,[26], [27] or on the different types of protein films utilized for a particular application.[28], [29] This progress report serves as a guide to the common methods of protein film fabrication, their application as biomaterials and potential limitations of these approaches.

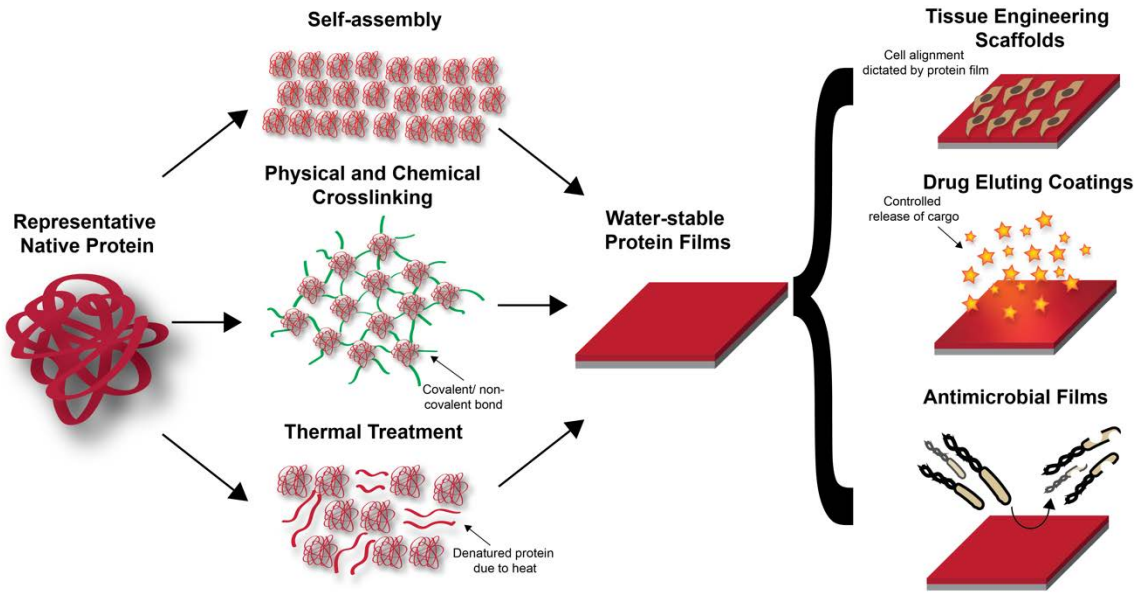

Figure 2.1. Schematic depiction of strategies of fabrication of protein films and examples of biomaterial applications. Stable protein films can be fabricated through self-assembly of proteins, physical or chemical crosslinking, and thermal treatment. Applications of protein films include tissue engineering scaffolds, drug eluting coatings and antimicrobial surfaces.

2.2. Strategies for fabrication of protein films

2.2.1. Structural proteins for self-assembled films

Structural proteins with highly repetitive amino acid sequences such as silk, collagen, keratin, elastin etc. naturally self-assemble into water-stable protein films upon processing through the methods described in Section III of **Figure 2.2**.[19, 30, 31] Protein films can be efficiently fabricated using these naturally self-assembling proteins to form robust, biocompatible and biodegradable coatings. For instance, silk fibroin protein has been used to fabricate protein films for biomedical applications due to the biocompatibility, slow degradation, and robust mechanical properties of the resulting films.[32, 33, 34, 35] Silk fibroin self-assembles into β-sheets that result in water-stable films. Film properties such as mechanical strength and biodegradability can be enhanced by controlling β-sheet

percentage through different strategies such water annealing, methanol annealing and drying speed.[36, 37] **Figure 2.2** summarizes different strategies for the preparation of silk protein solution, processing methods for film formation, and strategies for the manipulation of film properties.

Collagen is a naturally self-assembling protein abundant in the extracellular matrix.[3] It supports cell attachment, migration, and proliferation. It consists of three parallel polypeptide-α chains in a right-handed triple-helical structure that self-associates to form highly ordered cross-linked fibrils. [38] The triple helix structure of collagen and its fibrous structure make collagen films and coatings insoluble in water. For this reason, it is widely used in biomedical applications such as tissue engineering scaffolds, wound healing patches etc.[39, 40] Collagen is usually purified and can be dissolved in acid solutions to form films[41] or alternatively collagen fibers are directly used to prepare films.[42]

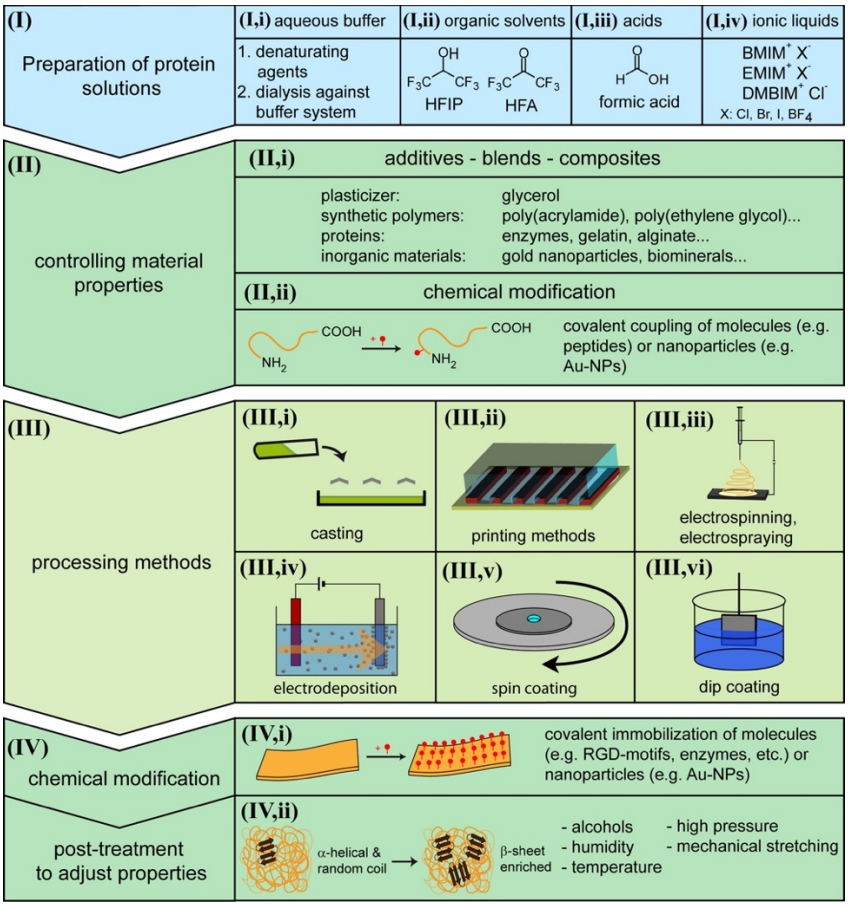

Figure 2.2. Schematic overview of the strategies of fabrication of silk films and coatings. (I) summarizes strategies for preparation of silk solutions and (III) summarizes methods of fabrication of silk films. (II) and (IV) summarize strategies for manipulation of film properties either before (II) or after (IV) film formation. Reproduced with permission. [19] Copyright 2014, American Chemical Society.

Self-assembly is an excellent approach to utilize the natural ability of some proteins to self-assemble through non-covalent crosslinking into water-stable films, without manipulating their native protein primary structure. The resultant protein films retain most of their native protein properties. However, there are a limited number of naturally occurring structural proteins that exhibit this behavior. Therefore, various physical or chemical treatments must be employed to obtain varied functionalities in these self-assembled protein films, which may affect the native protein structure by causing

denaturation, increase cytotoxicity of the film, or affect the functional properties of the protein film.

2.2.2 Crosslinked protein films

Self-assembling structural proteins offer an efficient and additive-free approach for fabricating protein films. However, there are a limited number of these proteins, and they often need to be treated through chemical or physical treatment strategies to suit biomedical applications. Consequently, crosslinkers offer an alternative approach to utilize a wider array of proteins to generate water-stable films while also enhancing film properties. Crosslinking is typically conducted through (1) physical strategies that utilize non-covalent interactions between two proteins such as ionic interactions and hydrogen bonding, or (2) chemical strategies that result in covalent bonding between proteins accomplished through irradiation, sulfur vulcanization and chemical reagents. [20, 21, 43, 44]

Significant research has been conducted in the development of composite protein films fabricated through physical crosslinking strategies, often with other proteins or biopolymers. This approach allows for efficient manipulation of biophysical properties of protein films such as strength, elasticity, roughness, degradability, and biocompatibility. For instance, the physical properties of natively self-assembling silk fibroin films and scaffolds were modulated through blending with biopolymers such as hyaluronic acid (HA) using a freezing-annealing technique to induce self-assembly of stable SF/HA scaffolds. **Figure 2.3(a)** demonstrates the freezing-annealing technique – SF chains for silk 1 form crystal networks upon freezing at -80 ^{o}C, and upon annealing at 3-5 ^{o}C silk crystals trap HA.[45] Increasing HA increases water solubility, indicating that SF crystals are unable to effectively trap the high number of HA chains (**Figure 2.3(b)**). Surface morphologies

observed through SEM imaging (**Figures 2.3(c) – (f)**) show interconnected microporous morphologies with a typical irregular fusiform shape. Increased HA content did not change the morphology significantly, though the average pore size gradually decreased. HA, being a component of the extracellular matrix, enhances cell growth in the composite protein films, while SF provides mechanical stability. [46]

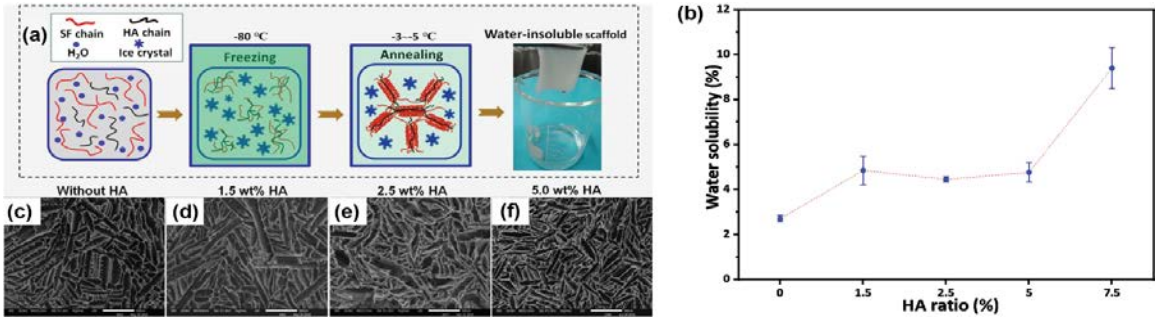

Figure 2.3. (a) Schematic depiction of freezing-annealing technique for the crosslinking of silk-fibroin (SF) and hyaluronic acid (HA) fibers (b) % Water solubility with respect to increase in % HA ratio. (c)-(f) Surface morphology of SF/HA scaffolds with varying wt% of HA obtained through SEM imaging. Scale bars are 500 μm. Adapted with permission.[41] Copyright 2020, Elsevier.

Chemical crosslinking is another strategy to fabricate water-stable protein films. Utilizing chemical crosslinkers allows for precise manipulation of film properties such as mechanical strength, flexibility and rate of degradation. Aldehydes with moderate reactivity such as glutaraldehyde and formaldehyde have been widely utilized as crosslinkers for protein films used in food packaging applications to improve their mechanical properties.[47, 48, 49] However, the use of small molecule aldehydes in biomedical applications is limited due to their high cytotoxicity and environmental hazards.[50] Consequently, biopolymer-based dialdehydes have been developed as non-toxic and biocompatible crosslinkers for protein films. Alginate dialdehyde (AD), synthesized

through peroxidate oxidation of sodium alginate, has been used for crosslinking of casein (CAS), a milk protein, as shown in **Figure 2.4(a)**.[51] Alginate is a non-toxic and biocompatible polysaccharide biopolymer widely used in wound dressing materials.[52] These dialdehyde alginates crosslinked casein (AD-X-CAS), a protein with an overall negative charge due to the presence of COO^- groups. These films are frequently used for loading and controlled release of cationic drugs such as gentamicin sulfate (GS), an antibiotic. **Figure 2.4(b) and 4(c)** shows the surface morphology of AD-X-CAS films and GS-loaded AD-X-CAS films, where GS crystals are clearly observed in the latter. Antimicrobial activity of GS-loaded AD-X-CAS was observed through a disk diffusion assay (**Figure 2.4(d)**) where diffusion of GS inhibited growth of *E. coli*. Similarly, soy protein isolate films have also been generated using dialdehyde carboxymethyl cellulose as a crosslinker, to fabricate water-stable SPI films with significantly improved tensile strength and thermal stability. [53]

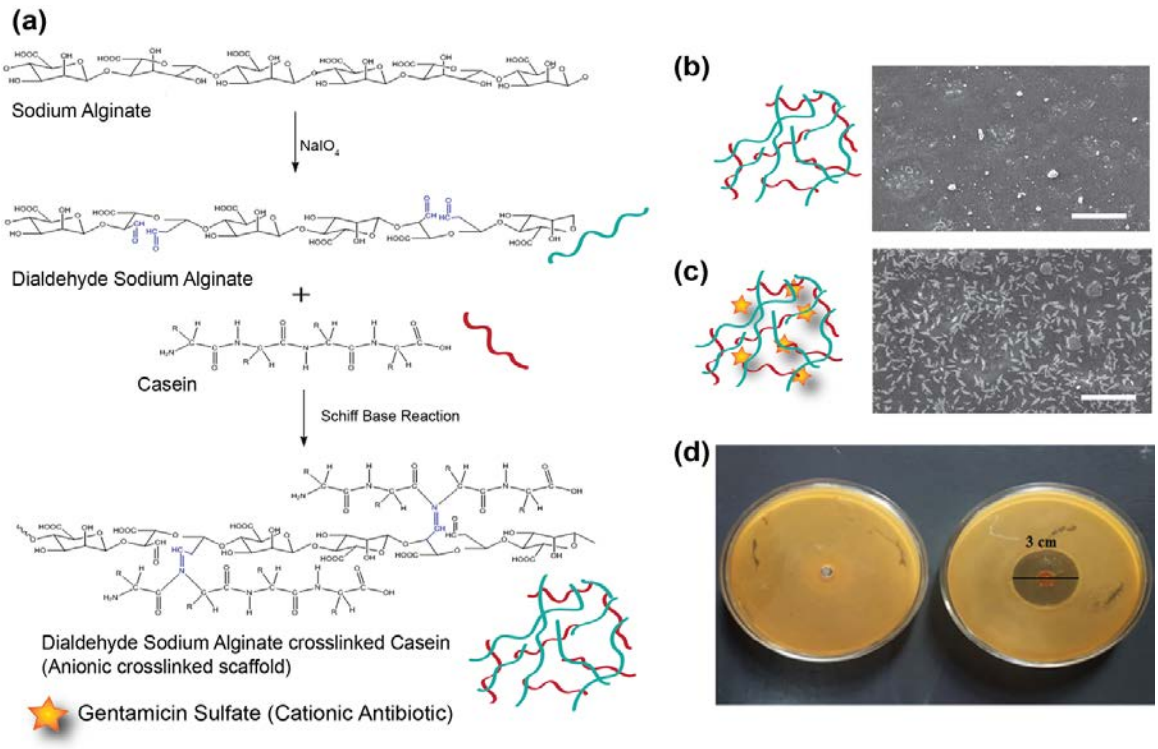

Figure 2.4. (a) Synthesis scheme for fabrication of AD-X-CAS (dialdehyde sodium alginate crosslinked Casein). Schematic representation and SEM image of (b) AD-X-CAS and (c) GS-loaded AD-X-CAS. (d) Disk diffusion assay depicting antimicrobial activity of GS-loaded AD-X-CAS against *E. coli.* Diffusion of GS inhibits bacterial growth around loaded AD-X-CAS as compared to control. Scale bars are 50 μm. Adapted with permission.[47] Copyright 2016, Informa UK Limited, trading as Taylor and Francis Group.

Enzymatic chemical crosslinking is another natural, non-toxic strategy for fabrication of protein films. Enzymes that characterize covalent bond formation between amino acid residues (e.g. sulfhydryl oxidases that catalyze formation of disulfide bonds, peroxidases that catalyze formation of radicals, and transglutaminase (TGase) that catalyzes acyl-transfer reactions between protein residues) are ideal enzymes for this strategy.[54] For instance, TGase has been utilized for the crosslinking of collagen fibers by catalyzing intra- and interchain bonds between lysine and glutamine residues.[55] TGase crosslinking when combined with thermal treatment notably improved crosslinking efficiency, stabilized film thickness, and improved mechanical and thermal stability.

Covalent crosslinking strategies are applicable to a number of proteins, and therefore offer a versatile approach for fabricating protein films. However, a concern with crosslinking strategies is increased cytotoxicity either from the crosslinkers themselves or from the resultant by-products. While this chapter highlights some progress in the development of non-toxic and biodegradable crosslinking strategies, further research on the scalability of these approaches is desired.

2.2.3 Thermal treatment strategies

Thermal treatment of protein films is a promising additive-free strategy to generate water stable films. High temperatures utilized in thermal treatment cause reorganization of native proteins resulting in physical crosslinking, thereby generating water-stable films.[56] Heat-cured films have been generated using plant-isolated proteins such as canola,[57] soy,[58] vicilin,[59] and whey protein.[60] Several reports also indicate that heat-curing improved the mechanical stability in addition to water stability.[61, 62, 63, 64] Furthermore, aging treatments that control both the relative humidity and temperature during treatment have been used to modulate mechanical properties such as tensile strength of collagen films.[65]

One of the main limitations of thermal treatment is the loss of protein structure due to heat-induced denaturation. Loss of protein structure often results in loss of protein properties (e.g. surface charge, hydrophilicity), thereby limiting the applicability of films in functional materials. A recently developed thermal treatment strategy using Nanoimprint lithography (NIL) preserves the structure and surface functionality of native proteins while generating water-stable films. [66] As depicted in **Figure 2.5(a)**, a fluorosilane coated silicon mold was used to apply pressure during heat curing of spin-casted protein films. Treatment at 180 ^{o}C at 3 MPa results in stable, hydrophilic protein films (**Figure 2.5(b)**. Circular

dichroism (CD) spectra (**Figure 2.5(c)**) revealed that most of the secondary structure was retained, while Kelvin Probe Force Microscopy (KPFM) demonstrated retention of the protein native charge in the film. Positive, negative and neutral films were generated using bovine serum albumin (BSA; pI = 4.8), hemoglobin (Hemo; pI = 6.8), and lysozyme (Lyso; pI = 11). Charged protein films were utilized to dictate cell adhesion on the substrate. As seen in **Figure 2.5(d)** anionic and neutral protein films generated using BSA and Hemo result in cytophobic films that prevent cell adhesion, while cationic Lyso results in cytophilic films that enhance cell adhesion. NIL also facilitated fabrication of patterned protein films that dictated cell alignment.

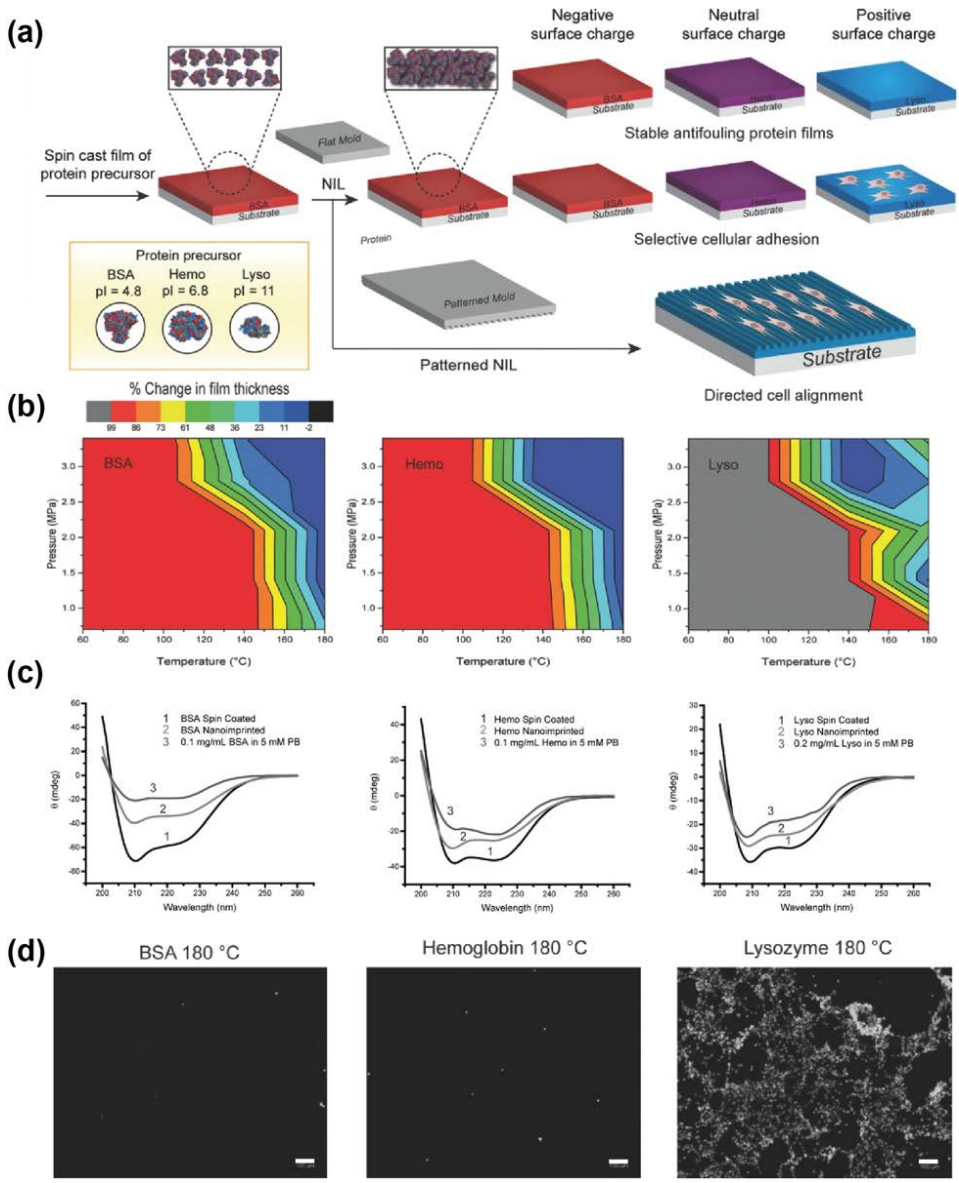

Figure 2.5. (a) Schematic depiction of the NIL treatment of protein films using flat or patterned mold. (b) Heat map depicting the correlation between treatment conditions and stability of the films. Treatment at 180 ºC and 3 MPa resulted in stable BSA, Hemo and Lyso films. (c) CD spectra of 1. Spin-coated protein films 2. NIL films and 3. Protein solution (0.1 mg/ml in 5 mM PB) depicting that treated protein films retained most of their secondary structure. (d) Cell adhesion on BSA, Hemo and Lyso films treated at 180 ºC. BSA and Hemo show minimal cell adhesion while Lyso shows enhanced cell adhesion. Scale bars are 100 µm. Adapted with permission.[62] Copyright 2015, WILEY-VCH Verlag GmbH & Co. KGaA, Weinheim.

While NIL successfully translates native protein properties such as charge into the protein films, one major limitation of this approach is its restriction to 2D substrates. Experiments revealed that the pressure applied during NIL was not the factor that minimized denaturation, as protein films generated in a pressure chamber show significant denaturation.[22] It was hypothesized that the fluorous environment provided by the fluoro-silane mold minimized protein rearrangement at the interface due to the *fluorous effect* - the tendency of fluorous molecules to stay together and segregate from both hydrophobic and hydrophilic molecules.[67] Proteins in the fluorous environment consequently have minimal interaction with the fluorous environment and do not denature to expose their hydrophobic pockets at the interface, thereby preserving the protein structure. Fluorous effect has been previously utilized for thermal stabilization proteins through incorporation of fluorinated amino acids in the hydrophobic pocket of proteins.[68] Consequently, fluorous-cured protein films were generated by heating protein film in a fluorous solvent PFHP (perfluoroperhydrophenanthrene), as shown in **Figure 2.6(a).**[22] This resulted in water-stable protein films that are hydrophilic as compared to heat-cured (HC) protein films both treated at 180 ºC for 15 min, as shown in **Figure 2.6(b)**. PFHP-treated films retain most of their secondary structure as determined by CD spectra (**Figure 2.6(c)**). They also retain their surface charge, as evidenced by KPFM measurements of the surface potential shown in **Figure 2.6(d)**, where the potential difference between HC-BSA and HC-Lyso films is significantly lesser than PFHP-BSA and PFHP-Lyso. This indicates that distinct surface charges of BSA (-) and Lyso (+) is retained during PFHP treatment. Furthermore, this strategy was successfully utilized to generate conformal protein coatings on 3D substrates, as seen in **Figure 2.6(e)** by brilliant blue staining and SEM images of

protein coatings on dental screws – a model medical implant. As shown in **Figure 2.6(f)**, negatively charged BSA protein was used to fabricate anti-fouling protein coatings on medical implants, using this strategy.

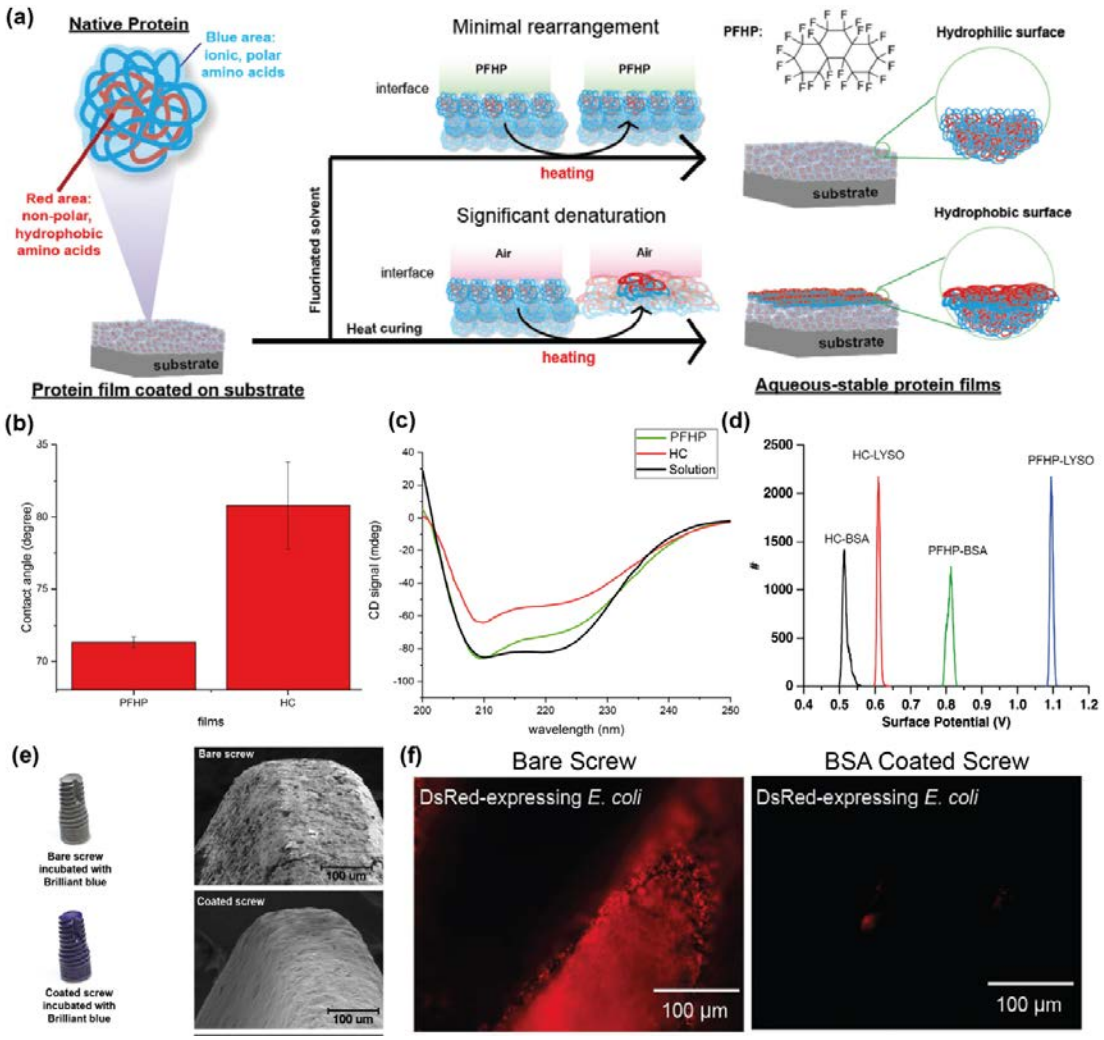

Figure 2.6. (a) Schematic depiction of fluorous treatment using PFHP, showing minimal rearrangement at interface of PFHP as compared to air. (b) Water contact angle measurement through static sessile drop method indicating PFHP treatment results in hydrophilic films as compared to heat-cured films. (c) CD spectra of PFHP treated films (green), heat-cured films (red) and BSA solution (black) shows minimal denaturation of protein due to thermal treatment in the case of PFHP as compared to traditional heat-curing. (d) Surface potential measured by KPFM (Kelvin Probe Force Microscopy) indicating significant potential difference between PFHP-treated BSA (-) and Lyso (+) as compared to heat-cured films. This suggests that PFHP-treated proteins retain their native charges. (e) Bare and BSA coated dental screws stained with Brilliant Blue protein stain. Coated screw shows uniformly dispersed blue color indicative of conformal coating. (f) Conformal coating of BSA on dental screw verified using SEM. BSA forms smooth, uniform coating on the screw. (g) Anti-fouling activity of BSA coating demonstrated through challenge of E. coli ds Red biofilm. No bacteria adhered to BSA coated screw while the bare screw has been completely contaminated. Adapted with permission.[22] Copyright 2018, The Royal Society of Chemistry.

Thermal treatment offers additive-free approaches for fabricating water-stable protein films. However, the high temperatures utilized in most thermal treatment strategies can cause uncontrolled protein denaturation and consequently loss of protein functionality/properties. These losses may be minimized by utilizing the NIL strategy summarized above however, the application of NIL is limited to flat, two-dimensional substrates. Fluorous-curing offers an alternative approach to the NIL-treated protein films by demonstrating similar robustness to the NIL approach. However, this PFHP-based thermal treatment approach is recent and its generalizability to different types of proteins remains untested.

2.2.4 Modification through surface functionalization or incorporation of additives

Modification strategies, either through surface functionalization or incorporation of additives into protein films, offer new areas of film application by endowing them with unique properties. Surface modifications are often conducted to increase either the hydrophilicity or hydrophobicity of protein films, impart specific chemical functionality to the film surface, or enhance biological properties such as cell adhesion. For instance, mussel-inspired dopamine chemistry has been utilized for the surface modification of silk fibroin used to fortify soy-protein adhesives.[24] Silk fibroin films have also been treated with ethanol to induce conformational and morphological modifications in the SF fibers, thereby increasing crystallinity, mechanical strength and water stability.[69] Superhydrophobic and self-cleaning films have also been developed by creating hierarchical micro-/nano-structures on soy protein film surfaces with hydrophobic nanoparticles.[70, 71] Adjusting the precursor concentration and crystal growth time constructed hierarchical micro-/nano-crystals on the soy protein film surface forming a biomimetic film with potential

application as water harvesting materials. Gao et al. developed a strategy for grafting different functional groups on lysozyme protein films to impart different properties to the films.[72] **Figure 2.7(a)** illustrates superhydrophobic and superhydrophilic modifications on phase-transitioned lysozyme (PTL) films. Superhydrophobic coatings were generated through covalent attachment of perfluorooctanyl chloride on the surface, while superhydrophilic films were generated through the grafting of hydrophilic polymer POEGMA. (**Figures 2.7(b) and (c)**). Thermal stability of the superhydrophobic PTL films was evaluated by subjecting modified films to 200 ^{o}C and -196 ^{o}C, followed by recording SEM images of the surface morphology and the contact angle. As seen in **Figures 2.7(d) and (e)**, no changes due to heating or cooling were observed. Mechanical stability was evaluated through the scotch tape test, shown in **Figure 2.7(f)**. No peeling or significant change in contact angle was observed. PTL films have also been utilized to fabricate conformal and transparent coatings on different types of substrates as well as free-floating films with large areas.[73] This strategy of self-assembled phase transitioned proteins to generate amyloid-like aggregates is generalizable to other proteins such as BSA,[74] and has also been utilized to incorporate functional peptides on the protein film surface.[75] Wang et al. have utilized this approach to fabricate amelogenin mimics for controlling enamel remineralization by incorporating amelogenin into PTL films.[75]

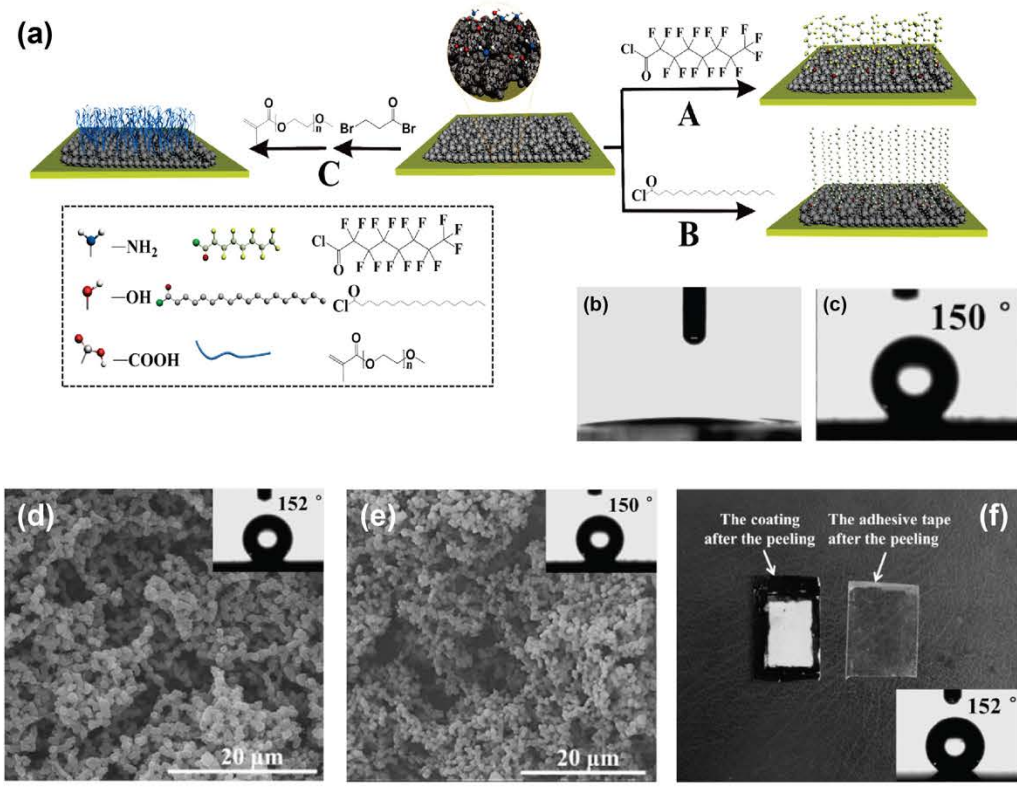

Figure 2.7. (a) Schematic depiction of the surface modification strategies to prepare A. superhydrophobic films, B. Hydrophobic films and C. superhydrophilic films. Contact angle measurements of (b) superhydrophilic film and (c) superhydrophobic film. Thermal stability observed through SEM images and contact angle measurements (inset) at (d) high temperature of 200 °C and (e) low temperature of -196 °C. No significant change due to temperature was observed. (f) Mechanical stability evaluated through scotch-tape test. No significant changes were observed. Adapted with permission.[70] Copyright 2015, WILEY-VCH Verlag GmbH & Co. KGaA, Weinheim.

Incorporation of additives is another common approach to impart specific useful properties to protein films. Carbon nanotubes (CNTs) have been incorporated into different types of protein films to impart mechanical and electric properties to protein films. CNT/silk-elastin-like protein composites showed enhanced mechanical and piezoelectric properties, where mechanical deformation of film correlated with electrical conductivity;[76] Collagen-CNT composites enhanced stability and electrical conductivity, imparted electromagnetic shielding membrane;[77, 78] Hemoglobin-collagen-CNT composites have

also been employed to fabricate a hydrogen peroxide biosensor.[79] Multifunctional films have been made using lysozyme and polyphosphate-based composites. Lysozyme, an antimicrobial enzyme, imparts antimicrobial activity to the film as well as an overall positive charge that enhances cell adhesion, while polyphosphate improves propensity for osteoblast proliferation and bone formation. These composite films provided titanium implant coatings to enhance bone-regenerative properties while preventing infections.[80]

Modification strategies offer efficient and robust methods to obtain protein films with a variety of functionalities. Surface modifications enable the fabrication of multifunctional films, while utilizing additives help overcome inherent limitations of native protein films such as rigidity, mechanical instability etc. A major limitation of both approaches is the cytotoxicity arising from the reagents utilized for modifications or the resultant by-products. Furthermore, often organic solvents must be utilized for some modification strategies, which may result in protein denaturation and loss of function.

2.3. Applications of protein coatings

Protein films are already widely used in biomedical and food packaging applications. Broadly, the applications of protein films may be categorized into the following - tissue engineering and wound-repair scaffolds, antimicrobial coatings, sensing and diagnostic devices, and food-packaging applications.

Tissue-engineering scaffolds must provide a cytophilic surface to enhance cell adhesion, provide support to the cells by mimicking stiffness of natural tissue and degrade at a rate proportional to cell growth.[81] For this reason, materials chosen for fabricating tissue engineering and wound-repair scaffolds must be biocompatible, have modulable mechanical properties and show enzymatic stability. Silk fibroin films are often employed

as scaffolds for tissue engineering, [82] wound repair coatings,[83] and bioelectronic devices such as electrodes.[6, 84] Collagen is another protein that is extensively applied to tissue engineering and wound-healing scaffolds, as it is the dominant protein in the extracellular matrix.[85] Various crosslinking, thermal treatment and additive-based strategies have been utilized to enhance the mechanical and enzymatic stability of collagen films.

Another avenue for the application of protein films is as antimicrobial coatings. Antimicrobial coatings prevent the bacterial contamination of medical devices and consequent infections. Antimicrobial protein coatings are designed by three main strategies – anti-fouling coatings that prevent bacteria adhesion on the surface; contact-killing wherein antimicrobial agent incorporated within protein film kills bacteria adhered to the surface; controlled-release systems wherein the protein film acts as a scaffold to load and release antimicrobial agents. Properties of the native proteins have been translated into the protein film to design anti-fouling[22, 66] and antimicrobial (contact-killing) coatings.[75] Grafting of antimicrobial or anti-fouling polymers onto the surface is another approach to design contact killing systems.[86] Controlled-release coatings have also be prepared through the incorporation of antimicrobial agents such as chlorine,[87] antibiotics[51,88] and phytochemicals[4, 89] within the protein film.

Protein films are potential candidates for sensing and diagnostic tools owing to their varied functionalities. Smart, responsive films that respond to external stimuli have been fabricated using gelatin.[90] Silk fibroin films have been used for immunosensing applications through the incorporation of antibodies within the protein film.[91] Additionally, silk fibroin films have also been used to fabrication of flexible and wearable electronic skins for monitoring human physiological responses.[92, 93] Recently, wearable electronic

devices have been developed using protein nanowire films for humidity sensing.[94] Composite materials of amyloid aggregates and graphene have exhibited shape memory and enzyme sensing properties.[95]

Additionally, protein coatings have been widely used in food packaging applications. Gelatin coatings are commonly used to enhance the shelf-life of vegetables;[96] gelatin,[97] whey[98] and soy[99] protein isolate films are used in meat packaging, while zein[100] and wheat[101] protein films have been used in the packaging of dairy products.

2.4. Conclusions and Perspectives

This chapter discusses strategies for the fabrication of stable protein films, and the application of these biomaterials. Proteins are naturally occurring functional building blocks that are water-processible, making them ideal for designing sustainable and biodegradable materials. Furthermore, the choice of protein can be used to dictate properties such as biocompatibility, cytophilicity, anti-fouling and antimicrobial behavior, all of which are especially attractive for biomedical applications. Protein film stabilization strategies predominantly use one of the three different strategies discussed in this review – (1) using self-assembling structural proteins (2) using chemical or physical crosslinking strategies and (3) using thermal treatment strategies. Additionally, strategies employing post-functional modifications and additives to enhance properties of protein films are frequently utilized in combination with the above approaches.

Protein films have long been used in applications such as edible coatings for food packaging,[102] surface patterning strategies,[103] biodegradable coatings[104] and plastic alternatives,[105] and tissue engineering scaffolds.[106] More recently, fabrication strategies have been developed that greatly expand the range of properties accessible with these

materials. Protein properties have been translated into films to fabricate anti-fouling and bactericidal coatings, [22, 66, 80, 85] and cargo-loaded protein films have been fabricated and applied as biodegradable antimicrobial coatings.[4, 51, 87, 88, 89]

Moving forward, the development of scalable and cost-effective fabrication strategies will allow for the translation of more sophisticated protein-based materials into commercial applications. Development of 2D and 3D patterning strategies will enable complex designs that will facilitate the creation of tissue engineering scaffolds that mimic native tissue properties. Furthermore, the ability to harness native protein properties such as stimuli-responsiveness (enzymes) and binding specificity (receptors) will provide new responsive materials. These active materials will open up numerous applications including bio-sensing, point-of-care diagnostics, and controlled/triggered release systems.

2.5. References

1. DeFrates, K. G.; Moore, R.; Borgesi, J.; Lin, G.; Mulderig, T.; Beachley, V.; Hu, X. Protein-Based Fiber Materials in Medicine: A Review. *Nanomater. (Basel, Switzerland)* **2018**, *8* (7).

2. Wang, L.-S.; Gopalakrishnan, S.; Rotello, V. M. Tailored Functional Surfaces Using Nanoparticle and Protein "Nanobrick" Coatings. **2019**, *35*, 23.

3. Andonegi, M.; Irastorza, A.; Izeta, A.; Cabezudo, S.; de la Caba, K.; Guerrero, P. A Green Approach towards Native Collagen Scaffolds: Environmental and Physicochemical Assessment. *Polymers (Basel)*. **2020**, *12* (7).

4. Lin, L.; Liao, X.; Cui, H. Cold Plasma Treated Thyme Essential Oil/Silk Fibroin Nanofibers against Salmonella Typhimurium in Poultry Meat. *Food Packag. Shelf Life* **2019**, *21*, 100337.

5. Pinheiro Bruni, G.; de Oliveira, J. P.; Gómez-Mascaraque, L. G.; Fabra, M. J.; Guimarães Martins, V.; Zavareze, E. da R.; López-Rubio, A. Electrospun β-

Carotene–Loaded SPI:PVA Fiber Mats Produced by Emulsion-Electrospinning as Bioactive Coatings for Food Packaging. *Food Packag. Shelf Life* **2020**, *23*, 100426.

6. Holland, C.; Numata, K.; Rnjak-Kovacina, J.; Seib, F. P. The Biomedical Use of Silk: Past, Present, Future. *Adv. Healthc. Mater.* **2019**, *8* (1), 1800465.

7. Goder, D.; Matsliah, L.; Giladi, S.; Reshef-Steinberger, L.; Zin, I.; Shaul, A.; Zilberman, M. Mechanical, Physical and Biological Characterization of Soy Protein Films Loaded with Bupivacaine for Wound Healing Applications. *International Journal of Polymeric Materials and Polymeric Biomaterials* **2020**, 1.

8. Valentini, L.; Bittolo Bon, S.; Pugno, N. M. Combining Living Microorganisms with Regenerated Silk Provides Nanofibril-Based Thin Films with Heat-Responsive Wrinkled States for Smart Food Packaging. *Nanomater. 2018, Vol. 8, Page 518* **2018**, *8* (7), 518.

9. Kuruwita, D. P.; Jiang, X.; Darby, D.; Sharp, J. L.; Fraser, A. M. Persistence of Escherichia Coli O157:H7 and Listeria Monocytogenes on the Exterior of Three Common Food Packaging Materials. *Food Control* **2020**, *112*, 107153.

10. Tao, H.; Kaplan, D. L.; Omenetto, F. G. Silk Materials – A Road to Sustainable High Technology. *Adv. Mater.* **2012**, *24* (21), 2824–2837.

11. Arora, A.; Padua, G. W. Review: Nanocomposites in Food Packaging. *J. Food Sci.* **2010**, *75* (1).

12. Zhao, S.; Wang, Z.; Kang, H.; Li, J.; Zhang, S.; Han, C.; Huang, A. Fully Bio-Based Soybean Adhesive in Situ Cross-Linked by Interactive Network Skeleton from Plant Oil-Anchored Fiber. *Ind. Crops Prod.* **2018**, *122*, 366–374.

13. Hassan, B.; Chatha, S. A. S.; Hussain, A. I.; Zia, K. M.; Akhtar, N. Recent Advances on Polysaccharides, Lipids and Protein Based Edible Films and Coatings: A Review. *Int. J. Biol. Macromol.* **2018**, *109*, 1095–1107.

14. Abaee, A.; Mohammadian, M.; Jafari, S. M. Whey and Soy Protein-Based Hydrogels and Nano-Hydrogels as Bioactive Delivery Systems. *Trends Food Sci. Technol.* **2017**, *70*, 69–81.

15. Perez-Puyana, V. M.; Jiménez-Rosado, M.; Romero, A.; Guerrero, A. Highly Porous Protein-Based 3D Scaffolds with Different Collagen Concentrates for Potential Application in Tissue Engineering. *J. Appl. Polym. Sci.* **2019**, *136* (37), 47954.

16. Kord Forooshani, P.; Lee, B. P. Recent Approaches in Designing Bioadhesive Materials Inspired by Mussel Adhesive Protein. *J. Polym. Sci. A. Polym. Chem.* **2017**, *55* (1), 9–33.

17. Zhu, L.; Yin, P.; Xie, T.; Liu, X.; Yang, L.; Wang, S.; Li, J.; Liu, H. Interaction between Soyasaponin and Soy β-Conglycinin or Glycinin: Air-Water Interfacial Behavior and Foaming Property of Their Mixtures. *Colloids Surf. B. Biointerfaces* **2020**, *186*.

18. Zhao, S.; Wang, Z.; Pang, H.; Li, Z.; Zhang, W.; Zhang, S.; Li, J.; Li, L. Designing Biomimetic Microphase-Separated Motifs to Construct Mechanically Robust Plant Protein Resin with Improved Water-Resistant Performance. *Macromol. Mater. Eng.* **2020**, *305* (2), 1900462.

19. Borkner, C. B.; Elsner, M. B.; Scheibel, T. Coatings and Films Made of Silk Proteins. *ACS Appl. Mater. Interfaces* **2014**, *6* (18), 15611–15625.

20. Hu, X.; Cebe, P.; Weiss, A. S.; Omenetto, F.; Kaplan, D. L. Protein-Based Composite Materials. *Mater. Today* **2012**, *15* (5), 208–215.

21. Azeredo, H. M. C.; Waldron, K. W. Crosslinking in Polysaccharide and Protein Films and Coatings for Food Contact – A Review. *Trends Food Sci. Technol.* **2016**, *52*, 109–122.

22. Wang, L. S.; Gopalakrishnan, S.; Lee, Y. W.; Zhu, J.; Nonnenmann, S. S.; Rotello, V. M. Translation of Protein Charge and Hydrophilicity to Materials Surface Properties Using Thermal Treatment in Fluorous Media. *Mater. Horizons* **2018**, *5* (2), 268–274.

23. Zhang, L.; Gopalakrishnan, S.; Li, K.; Wang, L. S.; Han, Y.; Rotello, V. M. Fabrication of Collagen Films with Enhanced Mechanical and Enzymatic Stability through Thermal Treatment in Fluorous Media. *ACS Appl. Mater. Interfaces* **2020**, *12* (5), 6590–6597.

24. Pang, H.; Zhao, S.; Mo, L.; Wang, Z.; Zhang, W.; Huang, A.; Zhang, S.; Li, J. Mussel-Inspired Bio-Based Water-Resistant Soy Adhesives with Low-Cost Dopamine Analogue-Modified Silkworm Silk Fiber. *J. Appl. Polym. Sci.* **2020**, *137* (23), 48785.

25. Zhang, S.; Xia, C.; Dong, Y.; Yan, Y.; Li, J.; Shi, S. Q.; Cai, L. Soy Protein Isolate-Based Films Reinforced by Surface Modified Cellulose Nanocrystal. *Ind. Crops Prod.* **2016**, *80*, 207–213.

26. Huang, W.; Ling, S.; Li, C.; Omenetto, F. G.; Kaplan, D. L. Silkworm Silk-Based Materials and Devices Generated Using Bio-Nanotechnology. *Chem. Soc. Rev.* **2018**, *47* (17), 6486–6504.

27. Feroz, S.; Muhammad, N.; Ranayake, J.; Dias, G. Keratin - Based Materials for Biomedical Applications. *Bioact. Mater.* **2020**, *5* (3), 496–509.

28. Zubair, M.; Ullah, A. Recent Advances in Protein Derived Bionanocomposites for Food Packaging Applications. *Crit. Rev. Food Sci. Nutr.* **2020**, *60* (3), 406–434.

29. Avramescu, S. M.; Butean, C.; Popa, C. V.; Ortan, A.; Moraru, I.; Temocico, G. Edible and Functionalized Films/Coatings—Performances and Perspectives. *Coatings 2020, Vol. 10, Page 687* **2020**, *10* (7), 687.

30. Shavandi, A.; Silva, T. H.; Bekhit, A. A.; Bekhit, A. E. D. A. Keratin: Dissolution, Extraction and Biomedical Application. *Biomater. Sci.* **2017**, *5* (9), 1699–1735.

31. Bax, D. V.; Smalley, H. E.; Farndale, R. W.; Best, S. M.; Cameron, R. E. Cellular Response to Collagen-Elastin Composite Materials. *Acta Biomater.* **2019**, *86*, 158–170.

32. Chen, X.; Knight, D. P.; Shao, Z.; Vollrath, F. Conformation Transition in Silk Protein Films Monitored by Time-Resolved Fourier Transform Infrared Spectroscopy: Effect of Potassium Ions on Nephila Spidroin Films. *Biochemistry* **2002**, *41* (50), 14944–14950.

33. Jiang, C.; Wang, X.; Gunawidjaja, R.; Lin, Y. H.; Gupta, M. K.; Kaplan, D. L.; Naik, R. R.; Tsukruk, V. V. Mechanical Properties of Robust Ultrathin Silk Fibroin Films. *Adv. Funct. Mater.* **2007**, *17* (13), 2229–2237.

34. You, R.; Zhang, J.; Gu, S.; Zhou, Y.; Li, X.; Ye, D.; Xu, W. Regenerated Egg White/Silk Fibroin Composite Films for Biomedical Applications. *Mater. Sci. Eng. C. Mater. Biol. Appl.* **2017**, *79*, 430–435.

35. Liu, H.; Fan, H.; Wang, Y.; Toh, S. L.; Goh, J. C. H. The Interaction between a Combined Knitted Silk Scaffold and Microporous Silk Sponge with Human Mesenchymal Stem Cells for Ligament Tissue Engineering. *Biomaterials* **2008**, *29* (6), 662–674.

36. Jin, H. J.; Park, J.; Karageorgiou, V.; Kim, U. J.; Valluzzi, R.; Cebe, P.; Kaplan, D. L. Water-Stable Silk Films with Reduced β-Sheet Content. *Adv. Funct. Mater.* **2005**, *15* (8), 1241–1247.

37. Lu, Q.; Hu, X.; Wang, X.; Kluge, J. A.; Lu, S.; Cebe, P.; Kaplan, D. L. Water-Insoluble Silk Films with Silk I Structure. *Acta Biomater.* **2010**, *6* (4), 1380–1387.

38. Xu, J.; Liu, F.; Goff, H. D.; Zhong, F. Effect of Pre-Treatment Temperatures on the Film-Forming Properties of Collagen Fiber Dispersions. *Food Hydrocoll.* **2020**, *107*, 105326.

39. Diaz Quiroz, J. F.; Rodriguez, P. D.; Erndt-Marino, J. D.; Guiza, V.; Balouch, B.; Graf, T.; Reichert, W. M.; Russell, B.; Höök, M.; Hahn, M. S. Collagen-Mimetic

Proteins with Tunable Integrin Binding Sites for Vascular Graft Coatings. *ACS Biomater. Sci. Eng.* **2018**, *4* (8), 2934–2942.

40. Chattopadhyay, S.; Raines, R. T. Review Collagen-Based Biomaterials for Wound Healing. *Biopolymers* **2014**, *101* (8), 821–833.

41. McManamon, C.; Cameron, A.; de Silva, J. P.; Daly, R.; O'Brien, F. J.; Cross, G. L. W. Effect of Cross-Linking and Hydration on Microscale Flat Punch Indentation Contact to Collagen-Hyaluronic Acid Films in the Viscoelastic Limit. *Acta Biomater.* **2020**, *111*, 279–289.

42. Xu, J.; Liu, F.; Wang, T.; Goff, H. D.; Zhong, F. Fabrication of Films with Tailored Properties by Regulating the Swelling of Collagen Fiber through PH Adjustment. *Food Hydrocoll.* **2020**, *108*, 106016.

43. Costa, M. J.; Marques, A. M.; Pastrana, L. M.; Teixeira, J. A.; Sillankorva, S. M.; Cerqueira, M. A. Physicochemical Properties of Alginate-Based Films: Effect of Ionic Crosslinking and Mannuronic and Guluronic Acid Ratio. *Food Hydrocoll.* **2018**, *81*, 442–448.

44. Ostrowska-Czubenko, J.; Gierszewska-Druzyńska, M. Effect of Ionic Crosslinking on the Water State in Hydrogel Chitosan Membranes. *Carbohydr. Polym.* **2009**, *77* (3), 590–598.

45. Guan, Y.; You, H.; Cai, J.; Zhang, Q.; Yan, S.; You, R. Physically Crosslinked Silk Fibroin/Hyaluronic Acid Scaffolds. *Carbohydr. Polym.* **2020**, *239*.

46. Stern, R.; Maibach, H. I. Hyaluronan in Skin: Aspects of Aging and Its Pharmacologic Modulation. *Clin. Dermatol.* **2008**, *26* (2), 106–122.

47. Cheung, D. T.; Nimni, M. E. Mechanism of Crosslinking of Proteins by Glutaraldehyde I: Reaction with Model Compounds. *Connect. Tissue Res.* **1982**, *10* (2), 187–199.

48. Chen, X.; Zhou, L.; Xu, H.; Yamamoto, M.; Shinoda, M.; Tada, I.; Minami, S.; Urayama, K.; Yamane, H. The Structure and Properties of Natural Sheep Casing and Artificial Films Prepared from Natural Collagen with Various Crosslinking Treatments. *Int. J. Biol. Macromol.* **2019**, *135*, 959–968.

49. Iahnke, A. O. e. S.; Stoll, L.; Bellé, A. S.; Hertz, P. F.; Rios, A. de O.; Rahier, H.; Flôres, S. H. Gelatin Capsule Residue-Based Films Crosslinked with the Natural Agent Genipin. *Packag. Technol. Sci.* **2020**, *33* (1), 15–26.

50. Mi, X.; Chang, Y.; Xu, H.; Yang, Y. Valorization of Keratin from Food Wastes via Crosslinking Using Non-Toxic Oligosaccharide Derivatives. *Food Chem.* **2019**, *300*.

51. Bajpai, S. K.; Shah, F. F.; Bajpai, M. Dynamic Release of Gentamicin Sulfate (GS) from Alginate Dialdehyde (AD)-Crosslinked Casein (CAS) Films for Antimicrobial Applications. *Des. monomers Polym.* **2016**, *20* (1), 18–32.

52. Sarheed, O.; Abdul Rasool, B. K.; Abu-Gharbieh, E.; Aziz, U. S. An Investigation and Characterization on Alginate Hydogel Dressing Loaded with Metronidazole Prepared by Combined Inotropic Gelation and Freeze-Thawing Cycles for Controlled Release. *AAPS PharmSciTech* **2015**, *16* (3), 601–609.

53. Zheng, T.; Yu, X.; Pilla, S. Mechanical and Moisture Sensitivity of Fully Bio-Based Dialdehyde Carboxymethyl Cellulose Cross-Linked Soy Protein Isolate Films. *Carbohydr. Polym.* **2017**, *157*, 1333–1340.

54. Buchert, J.; Cura, D. E.; Ma, H.; Gasparetti, C.; Monogioudi, E.; Faccio, G.; Mattinen, M.; Boer, H.; Partanen, R.; Selinheimo, E.; et al. Crosslinking Food Proteins for Improved Functionality. *Annu. Rev. Food Sci. Technol.* **2010**, *1* (1), 113–138.

55. Cheng, S.; Wang, W.; Li, Y.; Gao, G.; Zhang, K.; Zhou, J.; Wu, Z. Cross-Linking and Film-Forming Properties of Transglutaminase-Modified Collagen Fibers Tailored by Denaturation Temperature. *Food Chem.* **2019**, *271*, 527–535.

56. Kchaou, H.; Benbettaieb, N.; Jridi, M.; Nasri, M.; Debeaufort, F. Influence of Maillard Reaction and Temperature on Functional, Structure and Bioactive Properties of Fish Gelatin Films. *Food Hydrocoll.* **2019**, *97*, 105196.

57. Li, S.; Donner, E.; Thompson, M.; Zhang, Y.; Rempel, C.; Liu, Q. Preparation and Characterization of Cross-Linked Canola Protein Isolate Films. *Eur. Polym. J.* **2017**, *89*, 419–430.

58. Rhim, J.-W.; Gennadios, A.; Lee, J.-J.; Weller, C. L.; Hanna, M. A. Biodegradation of Cast Soy Protein Films by Aspergillus Oryzae and Bacillus Subtilis. *Food Sci. Biotechnol* **2003**, *12* (1), 96–99.

59. Olsson, E.; Hedenqvist, M. S.; Johansson, C.; Järnström, L. Influence of Citric Acid and Curing on Moisture Sorption, Diffusion and Permeability of Starch Films. *Carbohydr. Polym.* **2013**, *94* (2), 765–772.

60. Amin, S.; Ustunol, Z. Solubility and Mechanical Properties of Heat-Cured Whey Protein-Based Edible Films Compared with That of Collagen and Natural Casings. *Int. J. Dairy Technol.* **2007**, *60* (2), 149–153.

61. Rhim, J. W.; Gennadios, A.; Handa, A.; Weller, C. L.; Hanna, M. A. Solubility, Tensile, and Color Properties of Modified Soy Protein Isolate Films. *J. Agric. Food Chem.* **2000**, *48* (10), 4937–4941.

62. Micard, V.; Belamri, R.; Morel, M. H.; Guilbert, S. Properties of Chemically and Physically Treated Wheat Gluten Films. *J. Agric. Food Chem.* **2000**, *48* (7), 2948–2953.

63. Ali, Y.; Ghorpade, V. M.; Hanna, M. A. Properties of Thermally-Treated Wheat Gluten Films. *Ind. Crops Prod.* **1997**, *6* (2), 177–184.

64. Neo, Y. P.; Perera, C. O.; Nieuwoudt, M. K.; Zujovic, Z.; Jin, J.; Ray, S.; Gizdavic-Nikolaidis, M. Influence of Heat Curing on Structure and Physicochemical Properties of Phenolic Acid Loaded Proteinaceous Electrospun Fibers. *J. Agric. Food Chem.* **2014**, *62* (22), 5163–5172.

65. Shi, D.; Liu, F.; Yu, Z.; Chang, B.; Goff, H. D.; Zhong, F. Effect of Aging Treatment on the Physicochemical Properties of Collagen Films. *Food Hydrocoll.* **2019**, *87*, 436–447.

66. Jeoung, E.; Duncan, B.; Wang, L. S.; Saha, K.; Subramani, C.; Wang, P.; Yeh, Y. C.; Kushida, T.; Engel, Y.; Barnes, M. D.; et al. Fabrication of Robust Protein Films Using Nanoimprint Lithography. *Adv. Mater.* **2015**, *27* (40), 6251–6255.

67. Cametti, M.; Crousse, B.; Metrangolo, P.; Milani, R.; Resnati, G. The Fluorous Effect in Biomolecular Applications. *Chem. Soc. Rev.* **2011**, *41* (1), 31–42.

68. Marsh, E. N. G. Fluorinated Proteins: From Design and Synthesis to Structure and Stability. *Acc. Chem. Res.* **2014**, *47* (10), 2878–2886.

69. Puerta, M.; Arango, M. C.; Jaramillo-Quiceno, N.; Álvarez-López, C.; Restrepo-Osorio, A. Influence of Ethanol Post-Treatments on the Properties of Silk Protein Materials. *SN Appl. Sci.* **2019**, *1* (11), 1–7.

70. Xie, W. Y.; Wang, F.; Xu, C.; Song, F.; Wang, X. L.; Wang, Y. Z. A Superhydrophobic and Self-Cleaning Photoluminescent Protein Film with High Weatherability. *Chem. Eng. J.* **2017**, *326*, 436–442.

71. Liu, H.; Xie, W. Y.; Song, F.; Wang, X. L.; Wang, Y. Z. Constructing Hierarchically Hydrophilic/Superhydrophobic ZIF-8 Pattern on Soy Protein towards a Biomimetic Efficient Water Harvesting Material. *Chem. Eng. J.* **2019**, *369*, 1040–1048.

72. Gao, A.; Wu, Q.; Wang, D.; Ha, Y.; Chen, Z.; Yang, P. A Superhydrophobic Surface Templated by Protein Self-Assembly and Emerging Application toward Protein Crystallization. *Adv. Mater.* **2016**, *28* (3), 579–587.

73. Wang, D.; Ha, Y.; Gu, J.; Li, Q.; Zhang, L.; Yang, P. 2D Protein Supramolecular Nanofilm with Exceptionally Large Area and Emergent Functions. *Adv. Mater.* **2016**, *28* (34), 7414–7423.

74. Hu, X.; Tian, J.; Li, C.; Su, H.; Qin, R.; Wang, Y.; Cao, X.; Yang, P. Amyloid-Like Protein Aggregates: A New Class of Bioinspired Materials Merging an Interfacial Anchor with Antifouling. *Adv. Mater.* **2020**, *32* (23), 2000128.

75. Wang, D.; Deng, J.; Deng, X.; Fang, C.; Zhang, X.; Yang, P. Controlling Enamel Remineralization by Amyloid-Like Amelogenin Mimics. *Adv. Mater.* **2020**, *32* (31).

76. Liu, C.; Ye, X.; Wang, X.; Liao, X.; Huang, X.; Shi, B. Collagen Fiber Membrane as an Absorptive Substrate to Coat with Carbon Nanotubes-Encapsulated Metal Nanoparticles for Lightweight, Wearable, and Absorption-Dominated Shielding Membrane. *Ind. Eng. Chem. Res.* **2017**, *56* (30), 8553–8562.

77. Meiyazhagan, A.; Thangavel, S.; Daniel P., H.; Pulickel M., A.; Palanisamy, T. Electrically Conducting Nanobiocomposites Using Carbon Nanotubes and Collagen Waste Fibers. *Mater. Chem. Phys.* **2015**, *157*, 8–15.

78. Wang, J.; He, C.; Cheng, N.; Yang, Q.; Chen, M.; You, L.; Zhang, Q. Bone Marrow Stem Cells Response to Collagen/Single-Wall Carbon Nanotubes-COOHs Nanocomposite Films with Transforming Growth Factor Beta 1. *J. Nanosci. Nanotechnol.* **2015**, *15* (7), 4844–4850.

79. Li, J.; Mei, H.; Zheng, W.; Pan, P.; Sun, X. J.; Li, F.; Guo, F.; Zhou, H. M.; Ma, J. Y.; Xu, X. X.; et al. A Novel Hydrogen Peroxide Biosensor Based on Hemoglobin-Collagen-CNTs Composite Nanofibers. *Colloids Surf. B. Biointerfaces* **2014**, *118*, 77–82.

80. Xu, X.; Zhang, D.; Gao, S.; Shiba, T.; Yuan, Q.; Cheng, K.; Tan, H.; Li, J. Multifunctional Biomaterial Coating Based on Bio-Inspired Polyphosphate and Lysozyme Supramolecular Nanofilm. *Biomacromolecules* **2018**, *19* (6), 1979–1989.

81. Xing, H.; Lee, H.; Luo, L.; Kyriakides, T. R. Extracellular Matrix-Derived Biomaterials in Engineering Cell Function. *Biotechnol. Adv.* **2020**, *42*.

82. Keirouz, A.; Zakharova, M.; Kwon, J.; Robert, C.; Koutsos, V.; Callanan, A.; Chen, X.; Fortunato, G.; Radacsi, N. High-Throughput Production of Silk Fibroin-Based Electrospun Fibers as Biomaterial for Skin Tissue Engineering Applications. *Mater. Sci. Eng. C. Mater. Biol. Appl.* **2020**, *112*.

83. Arthe, R.; Arivuoli, D.; Ravi, V. Preparation and Characterization of Bioactive Silk Fibroin/Paramylon Blend Films for Chronic Wound Healing. *Int. J. Biol. Macromol.* **2020**, *154*, 1324–1331.

84. Chen, G.; Matsuhisa, N.; Liu, Z.; Qi, D.; Cai, P.; Jiang, Y.; Wan, C.; Cui, Y.; Leow, W. R.; Liu, Z.; et al. Plasticizing Silk Protein for On-Skin Stretchable Electrodes. *Adv. Mater.* **2018**, *30* (21).

85. Pereda, M.; Ponce, A. G.; Marcovich, N. E.; Ruseckaite, R. A.; Martucci, J. F. Chitosan-Gelatin Composites and Bi-Layer Films with Potential Antimicrobial Activity. *Food Hydrocoll.* **2011**, *25* (5), 1372–1381.

86. Li, S.; Donner, E.; Xiao, H.; Thompson, M.; Zhang, Y.; Rempel, C.; Liu, Q. Preparation and Characterization of Soy Protein Films with a Durable Water Resistance-Adjustable and Antimicrobial Surface. *Mater. Sci. Eng. C. Mater. Biol. Appl.* **2016**, *69*, 947–955.

87. Wang, L. S.; Gupta, A.; Duncan, B.; Ramanathan, R.; Yazdani, M.; Rotello, V. M. Biocidal and Antifouling Chlorinated Protein Films. *ACS Biomater. Sci. Eng.* **2016**, *2* (11), 1862–1866.

88. Egozi, D.; Baranes-Zeevi, M.; Ullmann, Y.; Gilhar, A.; Keren, A.; Matanes, E.; Berdicevsky, I.; Krivoy, N.; Zilberman, M. Biodegradable Soy Wound Dressings with Controlled Release of Antibiotics: Results from a Guinea Pig Burn Model. *Burns* **2015**, *41* (7), 1459–1467.

89. Kodal Coşkun, B.; Çalikoğlu, E.; Karagöz Emiroğlu, Z.; Candoğan, K. Antioxidant Active Packaging with Soy Edible Films and Oregano or Thyme Essential Oils for Oxidative Stability of Ground Beef Patties. *J. Food Qual.* **2014**, *37* (3), 203–212.

90. Musso, Y. S.; Salgado, P. R.; Mauri, A. N. Smart Edible Films Based on Gelatin and Curcumin. *Food Hydrocoll.* **2017**, *66*, 8–15.

91. Moraes, M. L.; Lima, L. R.; Vicentini-Oliveira, J. C.; de Souza, A. V. G.; Oliveira, O. N.; Deffune, E.; Ribeiro, S. J. L. Immunosensor for the Diagnostics of Autoimmune Hemolytic Anemia (AIHA) Based on Immobilization of a Monoclonal Antibody on a Layer of Silk Fibroin. *J. Nanosci. Nanotechnol.* **2019**, *19* (7), 3772–3776.

92. Wang, X.; Gu, Y.; Xiong, Z.; Cui, Z.; Zhang, T.; Wang, X. W.; Gu, Y.; Xiong, Z. P.; Zhang, T.; Cui, Z. Silk-Molded Flexible, Ultrasensitive, and Highly Stable Electronic Skin for Monitoring Human Physiological Signals. *Adv. Mater.* **2014**, *26* (9), 1336–1342.

93. Liu, J.; Chen, Q.; Liu, Q.; Zhao, B.; Ling, S.; Yao, J.; Shao, Z.; Chen, X.; Liu, J.; Chen, Q.; et al. Intelligent Silk Fibroin Ionotronic Skin for Temperature Sensing. *Adv. Mater. Technol.* **2020**, *5* (7), 2000430.

94. Liu, X.; Fu, T.; Ward, J.; Gao, H.; Yin, B.; Woodard, T.; Lovley, D. R.; Yao, J. Multifunctional Protein Nanowire Humidity Sensors for Green Wearable Electronics. *Adv. Electron. Mater.* **2020**, *6* (9), 2000721.

95. Li, C.; Adamcik, J.; Mezzenga, R. Biodegradable Nanocomposites of Amyloid Fibrils and Graphene with Shape-Memory and Enzyme-Sensing Properties. **2012**.

96. X. Wang, D. Kong, Z. Ma, R. Zhao, Effect of carrot puree edible films on quality preservation of fresh-cut *Irish Journal of Agricultural and Food Research* **2015**, *54*, 64.

97. Kodal Coşkun, B.; Çalikoğlu, E.; Karagöz Emiroğlu, Z.; Candoğan, K. Antioxidant Active Packaging with Soy Edible Films and Oregano or Thyme Essential Oils for Oxidative Stability of Ground Beef Patties. *J. Food Qual.* **2014**, *37* (3), 203–212.

98. Badr, K. R.; Ahmed, Z. S.; El Gamal, M. S. Evaluation of the Antimicrobial Action of Whey Protein Edible Films Incorporated with Cinnamon, Cumin and Thyme against Spoilage Flora of Fresh Beef. *Int. J. Agric. Res.* **2014**, *9* (5), 242–250.

99. Thaker, M.; Hanjabam, M. D.; Gudipati, V.; Kannuchamy, N. Protective Effect of Fish Gelatin-Based Natural Antimicrobial Coatings on Quality of Indian Salmon Fillets during Refrigerated Storage. *J. Food Process Eng.* **2017**, *40* (1), e12270.

100. Di Pierro, P.; Sorrentino, A.; Mariniello, L.; Giosafatto, C. V. L.; Porta, R. Chitosan/Whey Protein Film as Active Coating to Extend Ricotta Cheese Shelf-Life. *LWT - Food Sci. Technol.* **2011**, *44* (10), 2324–2327.

101. Ünalan, I. U.; Arcan, I.; Korel, F.; Yemenicioğlu, A. Application of Active Zein-Based Films with Controlled Release Properties to Control Listeria Monocytogenes Growth and Lipid Oxidation in Fresh Kashar Cheese. *Innov. Food Sci. Emerg. Technol.* **2013**, *20*, 208–214.

102. Su, J. F.; Huang, Z.; Yuan, X. Y.; Wang, X. Y.; Li, M. Structure and Properties of Carboxymethyl Cellulose/Soy Protein Isolate Blend Edible Films Crosslinked by Maillard Reactions. *Carbohydr. Polym.* **2010**, *79* (1), 145–153.

103. Clemmens, J.; Hess, H.; Lipscomb, R.; Hanein, Y.; Böhringer, K. F.; Matzke, C. M.; Bachand, G. D.; Bunker, B. C.; Vogel, V. Mechanisms of Microtubule Guiding on Microfabricated Kinesin-Coated Surfaces: Chemical and Topographic Surface Patterns. *Langmuir* **2003**, *19* (26), 10967–10974.

104. Gilbert, V.; Rouabhia, M.; Wang, H.; Arnould, A. L.; Remondetto, G.; Subirade, M. Characterization and Evaluation of Whey Protein-Based Biofilms as Substrates for in Vitro Cell Cultures. *Biomaterials* **2005**, *26* (35), 7471–7480.

105. Chen, Y.; Zhang, L.; Lu, Y.; Ye, C.; Du, L. Preparation and Properties of Water-Resistant Soy Dreg/Benzyl Konjac Glucomannan Composite Plastics. *J. Appl. Polym. Sci.* **2003**, *90* (14), 3790–3796.

106. Lévesque, S. G.; Lim, R. M.; Shoichet, M. S. Macroporous Interconnected Dextran Scaffolds of Controlled Porosity for Tissue-Engineering Applications. *Biomaterials* **2005**, *26* (35), 7436–7446.

CHAPTER 3

PROTEIN-BASED FILMS AS ANTI-FOULING AND DRUG ELUTING ANTIMICROBIAL COATINGS FOR MEDICAL IMPLANTS

3.1 Introduction

Infections caused by bacterial contamination of medical devices such as stainless-steel IV poles and implants pose a serious healthcare problem.[1,2] Nosocomial infections are caused by bacterial contamination of the surfaces of medical devices and equipment, usually occurring in healthcare settings.[3,4] In 2011, more than 700,000 nosocomial infections occurred in the United States, resulting in nearly 75,000 deaths.[5] Antimicrobial surfaces have shown promise in the prevention of nosocomial infections.[6]

Antimicrobial coatings are used to prevent bacterial contamination on a wide range of surfaces,[7,8,9,10,11] including medical devices[12,13] and implants.[14,15,16] The general design is based on two main strategies: preventing the adherence of bacteria on the surface,[17] and elimination of bacteria through release of antimicrobial agents.[18] Anti-fouling activity is achieved by tuning the chemical and morphological characteristics of a surface to prevent adhesion or eliminate bacteria upon contact.[19] Antibacterial activity is often imparted with coatings containing antibacterial agents, such as nanoparticles,[20] halogens,[21] and antibiotics.[22] The localized burst release of antimicrobials can efficiently reduce bacteria colonization on biomaterial surfaces as well as the possible risk of bacteria gaining resistance and tolerance to the antimicrobial agents.

Antimicrobials coatings must ensure sufficient loadability and localized burst release of antimicrobials to efficiently mitigate bacterial infections and minimize the risk of bacterial drug resistance. [23, 24] At the same time, the biocompatibility and bioresorbability of coating materials is crucial to minimize immune reactions and cytotoxicity, especially for implants and catheters that are in direct contact with tissue.[25] Therefore, many efforts have focused on improving the biocompatibility of these coatings, while ensuring high drug loadability.[26] Proteins are excellent candidates for fabricating functional biomaterials such as antimicrobial coatings, due to their inherent biocompatibility, biodegradability and functional diversity.[27, 28, 29] However, most of the protein film fabrication strategies utilize cross-linkers to ensure aqueous stability, thereby adversely affecting their biocompatibility, degradability, and protein structure and function. [30, 31] Alternatively, structural proteins that self-assemble into water-stable films such as silk, collagen etc. may be utilized. However, this limits the choice of proteins available and modification strategies must be employed to incorporate functionalities.[32, 33] Recent studies have demonstrated fabrication of protein films through amyloid-like protein aggregation arising from rapid reduction of intramolecular disulfide bonds. This is a non-toxic and versatile strategy that has been utilized for antimicrobial applications.[34, 35]

Previously, we developed an additive-free methodology for fabricating protein films,[36] by heating films in a fluorous environment (using perfluoroperhydrophenanthrene, PFHP) to form water-stable films (fluorous-cured proteins, FCPs) with minimal protein denaturation. Minimal denaturation of protein structure enabled the translation of native protein properties to the film. We generated films that were hydrophilic and retained surface properties such as charge and hydrophilicity.[36, 37, 38] Furthermore, PFHP leaves no

residue on the protein coating and is regarded as safe per FDA guidelines,[39] providing an additive-free, biocompatible strategy for fabrication of protein films. We report here the fabrication of antimicrobial-loaded BSA-based protein coatings that serve as a reservoir for controlled-release of antibiotics while simultaneously retaining their anti-fouling properties, as depicted in **Figure 3.1**. The overall negative charge of the BSA protein film was utilized to imbibe films with cationic cargo, demonstrated through loading of charged fluorescent dyes. Furthermore, we demonstrate that release behavior is also dictated by electrostatic interactions and salt concentration. Lastly, antimicrobial activity was imparted by loading and release of a cationic antibiotic (colistin), providing surfaces featuring both resistance to bacterial colonization and controlled release of antimicrobials. These surfaces provide potential platforms for medical device and implant coatings.

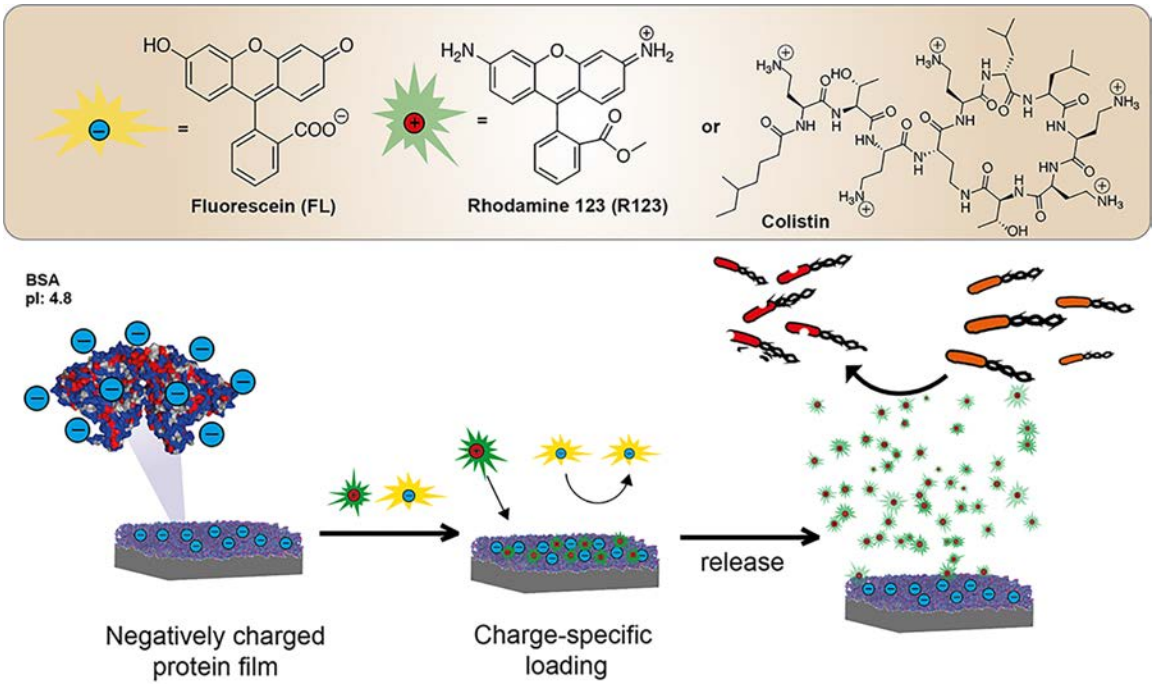

Figure 3.1. Protein nanofilms fabricated by FCP method retain their surface properties and can be loaded with charged cargos via electrostatic interaction. Antimicrobial coatings are fabricated by loading negatively charged BSA nanofilms with cationic antibiotics.

3.2. Results and Discussion

3.2.1. Fabrication and Characterization of BSA Films

Our studies focused on bovine serum albumin (BSA) films generated as per our previous studies as BSA (MW: 66.4 kDa, pI: 4.8) is inexpensive, readily available, and generally considered bioinert. [40, 41] The negative surface charge inherent to BSA films prevents bacterial adhesion, enabling the fabrication of anti-fouling coatings.[42] Coatings were fabricated by spin-casting 20% w/w BSA aqueous solution on plasma-cleaned silicon wafers. The spin-casted films were stabilized by immersing into a preheated fluorous media - perfluoroperhydrophenanthrene (PFHP) for 15 min at 180 °C. After curing, water stable BSA films were generated (**Figure A.1**). Films with different thickness were obtained by changing the concentration of precursor protein solution (**Figure 3.2(a)**). Heat-cured BSA films (treated in air at 180 °C) show significant loss of protein structure and surface charge.[36] Moreover, this loss of charge surfaces is expected to reduce or entirely eliminate electrostatic loading of cargo into the films.

Cargo loadability was demonstrated first using cationic rhodamine 123 (R123) dye. Stabilized BSA films were incubated in 0.05 mM dye solution. The thickness of R123-BSA films was measured before loading, after loading, during release in PBS and post-treatment with protease (trypsin), as shown in **Figure 3.2(b)**. The thickness of BSA films remains constant during incubation in aqueous media for 7 days, indicating good water stability. Moreover, protein films fully degrade within 24 hr in the presence of protease (0.01M trypsin solution) indicating that stabilization process and the cargo-loading do not affect biodegradability of BSA films. The loading capacity of BSA films was quantified by measuring the fluorescent intensity of R123 released from completely degraded films

(using trypsin), normalized by the surface area of substrates **Figure 3.2(c)**. R123-BSA films of different thicknesses were incubated in 1 mL of 0.01% trypsin for 24 hours and the fluorescence intensity of the supernatant was measured. The amount of R123 was determined by a calibration curve generated by measuring fluorescence intensity of different concentrations of R123 (**Figure A.2**). R123 loading increased proportionally to the film thickness, indicating that R123 successfully penetrated into the BSA films and was not simply adhered to the surface. The results indicated that BSA films can be utilized as a reservoir for loading drugs.

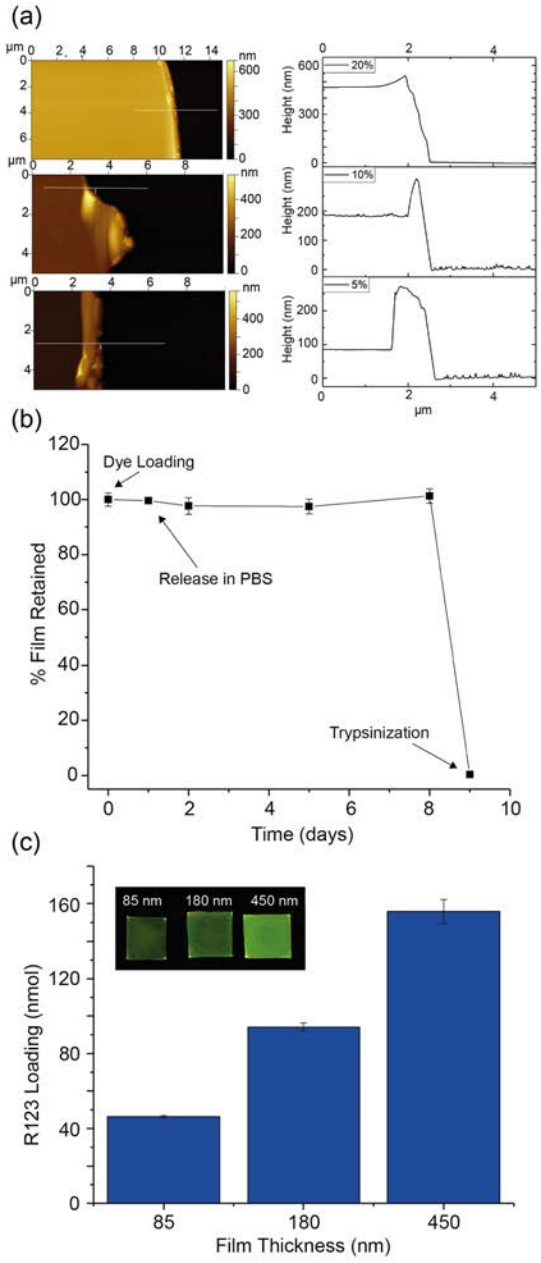

Figure 3.2. (a) Atomic force microscopic images and cross sections for scratched protein films prepared by 5%, 10% and 20% w/w BSA solution. (b) Films stability measured by the change of thickness (quantified using ellipsometry) after loading with dye, incubating in PBS, and treating with protease. (c) Loading capacity of protein films with different thickness (inset is the pictures of films taken under UV irradiation).

3.2.1. Charge-mediated loading and controlled release of fluorescent dyes in BSA films

The role of electrostatic interactions on cargo loading was studied using oppositely charged dyes with similar size and hydrophobicity - anionic fluorescein (FL) and cationic R123.[43] BSA films were incubated in 0.05 mM solutions of both dyes for 1, 3, 6, and 24 hours. We observed that the charge of the molecule significantly affected their loading into the film (**Figure 3.3**). Almost none of the FL was loaded into the film, indicating that the electrostatic interaction between payload and film is the dominant factor for cargo loading. Further evidence for electrostatics driving incorporation was provided by cationic lysozyme films (**Figure A.3**), where inverse behavior was observed. Moreover, R123 loading significantly reduced when the loading solution was mildly acidic (pH = 4). As the isoelectric point of BSA is pI = 4.8, BSA films are expected to be cationic at pH = 4, thereby hindering loading of R123. As expected, the loading of R123 in BSA films at pH 4 decreased substantially when both the cargo and film have the same charge.

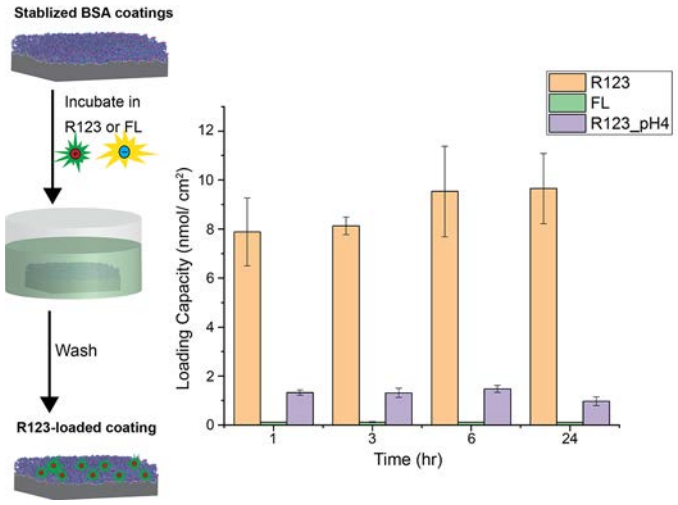

Figure 3.3. Loading capacity of BSA films prepared by incubating with Rhodamine 123 (R123), fluorescein (FL), and R123 in pH 4.

Release behavior of R123-loaded films was monitored by measuring the fluorescence intensity of the supernatant at different time intervals. As **Figure 3.4(a)** shows, burst release was observed within 1hr of incubation. As expected, low loading of FL and R123 at pH = 4 resulted in low release. However, **Figure A.3(a)** indicates that release rate is independent of type of dye loaded as well as pH of loading solution. Following these experiments, the role of ionic strength of the solution on release rate was investigated by varying the salt concentration. We hypothesized that the release behavior of R123 from BSA films will be affected by the salt concentration of the environment due to the change of electrostatic interactions between films and cargos. In low salt conditions (5 mM NaCl), stronger binding between R123 and BSA films led to slow release (**Figure 3.4(b)**). while high salt concentrations (150 mM NaCl) led to weaker the interaction became weaker and lead to an increased release, as seen in **Figure 3.4(b)**.

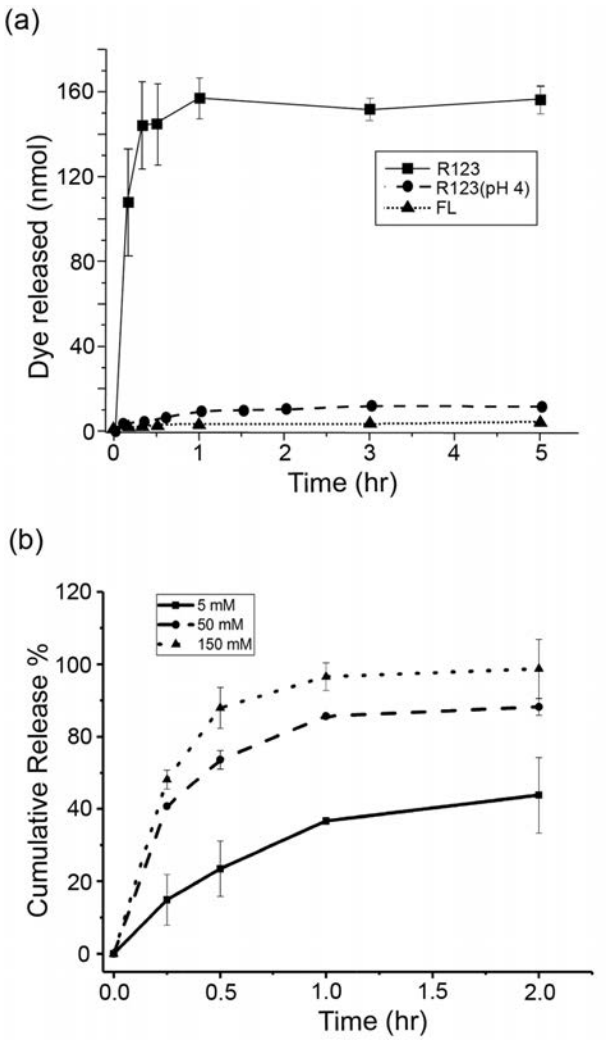

Figure 3.4. (a) Release patterns of dye-loaded BSA films prepared by incubating with R123 and FL. (b) Cumulative release of R123 from BSA films in buffers prepared using different sodium chloride concentrations. Release rates were calculated as 170.8 %release/hr at 150 mM salt concentration, 134.8 %release/hr at 50 mM salt concentration and 49.5 %release/hr at 5 mM salt concentration.

3.2.1. Evaluating the antibacterial efficacy of colistin-loaded BSA Films

The electrostatically regulated interaction of fluorous-cured protein films and cargo was next utilized to develop antifouling drug-eluting coatings for localized burst-release of cationic drugs. We hypothesized that incorporation of a cationic antibiotic into BSA-coated surgical screws would impart active protection from infections through increased antimicrobial activity in the vicinity of the implant, supplementing the passive protection

provided by the anti-fouling behavior of the protein film.[36] We chose colistin as a the antimicrobial due to its polycationic nature and broad-spectrum activity especially against drug-resistant strains.[44] Colistin was loaded into BSA films in a similar manner to R123 loading – films of thickness 85, 180, and 450 nm, generated by varying the concentration of BSA solution during spin coating, were first stabilized in PFHP. Films were then incubated in a 20 mg/ mL colistin solution overnight. The amount of colistin loaded was quantified using LDI-MS, as seen in **Figure 3.5(a)** (calculation described in **Table A.1**). A significant difference in loading was observed between 85 and 180 nm films but not between 180 and 450 nm. This may be attributed to the larger size of the colistin molecule as compared to R123 that would be expected to affect dye penetrability. Next, the antimicrobial activity resulting from release of colistin was tested by the Kirby Bauer Diffusion Assay. Colistin-loaded films of varying thicknesses were placed in a bed of *P. aeruginosa*, prepared by seeding 10 μL of 10^8 cfu/mL of *P. aeruginosa* solution on an agar plate. A clear inhibition zone (**Figure 3.5(b)**) was observed around the colistin-loaded films as well as the colistin-loaded control paper disk due to release of colistin into the agar in the vicinity of the substrate. This serves as a demonstration of localized release as high antibiotic concentrations are observed in the vicinity of the substrate. The normalized inhibition zone (calculations described in **Figure A.5**) was calculated by dividing the total area of the inhibition zone by the area of the BSA film (silicon chips), as shown in **Figure 3.5(c)**. As expected, no inhibition zone was observed in the case of the negative controls: PBS-loaded disks and the BSA film without colistin.

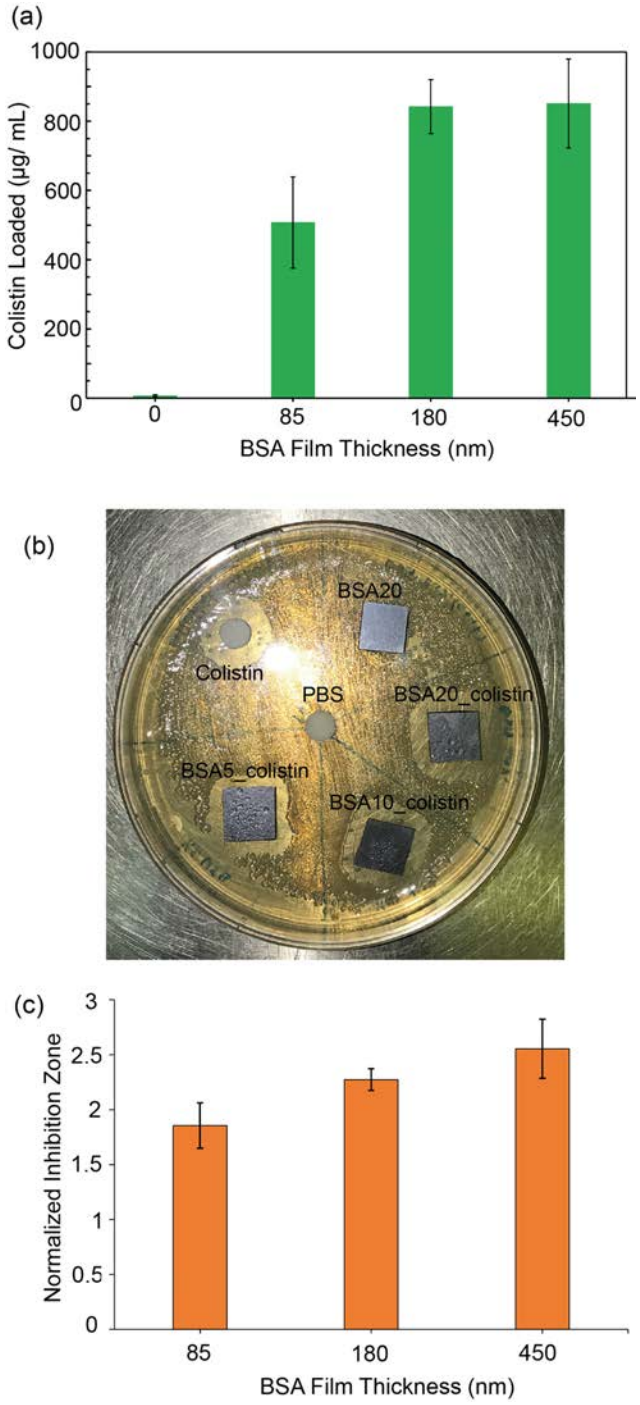

Figure 3.5. (a) Colistin loading in BSA films of varying thicknesses as measured by LDI-MS. (b) Kirby Bauer Diffusion assay showing antimicrobial activity of colistin-loaded films, compared with positive and negative controls. (c) Normalized inhibition zones of Colistin-loaded BSA films calculated disk diffusion assay.

The overall negative charge makes BSA ideal anti-fouling coatings for medical devices and implants. We hypothesized that colistin-loaded BSA films would provide dual protection from bacterial infections through passive resistance to bacterial fouling and active antibacterial activity. Therefore, we utilized surgical screws as a model medical implant to test both the anti-fouling and antimicrobial activity of colistin-loaded BSA coated surgical screws. **Figure 3.6(a)** illustrates the procedure for fabricating colistin-loaded BSA coatings on surgical screws. Plasma-treated clean surgical screws were coated by dipping in a 20% w/v BSA solution, followed by PFHP stabilization. Following this, screws were incubated a 20 mg/ mL colistin solution overnight. Red fluorescent protein (RFP) expressing *E. coli* was incubated with coated screws for 24 hours to evaluate anti-fouling behavior. Fluorescence microscopy images show a significant decrease in bacterial adhesion on BSA films both with and without loaded colistin, as compared to uncoated surgical screws (**Figure 3.6 (b), (c)** and **(d)**).

The biocidal activity of colistin-loaded BSA coatings was quantified by Kirby-Bauer diffusion assay. BSA coated screws with and without colistin were inserted into an agar plate seeded with 10 μL of 10^8 cfu/mL of *P. aeruginosa* solution. A clear inhibition zone was observed around the colistin-loaded BSA coated screws, consistent with the results observed in **Figure 3.5**. As expected, pure BSA coatings as well as uncoated screws showed no antimicrobial activity (**Figure 3.6(e)**). Burst release of antibiotic is expected within two hours, based on the release rates observed in **Figure 3.4(a)**. This rapid release is advantageous, as high concentrations of antibiotics can be released locally. High concentrations minimize the likelihood of development of drug resistance, while localized release is expected to minimize off-target effects. These results demonstrate that colistin-

loaded BSA coatings are viable candidates for designing superior antibacterial coatings for medical implants due to their anti-fouling property and localized antibiotic release.

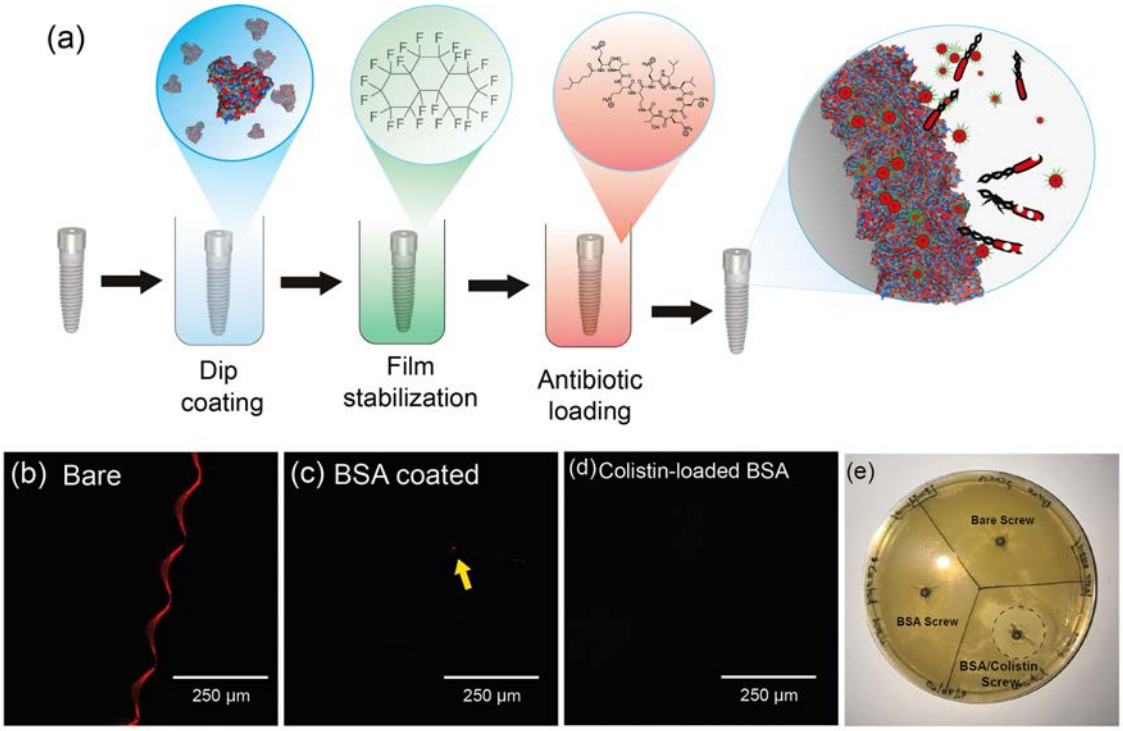

Figure 3.6. (a) Schematic illustration of the fabrication of protein-coating on 3D surgical screw. (b-d) Fluorescence microscopy images of (b) bare, (c) BSA-coated and (d) colistin-loaded surgical screws incubated with red fluorescent protein (RFP) expressing E. coli for 24 hours. (e) Kirby-Bauer disc diffusion antibacterial activity assay for BSA-coated screws.

3.3. Conclusions

In summary, we developed a robust and efficient strategy for fabricating antimicrobial coatings on medical devices using naturally abundant proteins. Fluorous-curing preserves the electrostatic properties of protein precursors, which enabled the fabrication of anionic BSA films that functioned as anti-fouling coatings. Further, the electrostatic interaction between cargo and protein films was harnessed for selective loading and release of oppositely charged cargos. Effective loading and localized release

of cationic antibiotic imparted active protection against bacterial contamination by enhancing antimicrobial activity in the vicinity of the implant. Taken together, fluorous-cured antibiotic-loaded BSA coatings offer dual protection against bacterial contamination of implants through the passive anti-fouling behavior of BSA and the active burst-release of cationic antibiotic in the vicinity of the implant. The rate of drug release is expected to be affected by the type of protein as well as the biological fluid that interacts with the coated implant. Therefore, film surface charge and thickness may be modulated to control rate of release. Utilizing proteins to formulate coatings enables fabrication of biodegradable coatings in a sustainable manner. The choice of protein, in addition to dictating anti-fouling behavior, also ensures biocompatibility. This approach is a sustainable, biocompatible, and effective antimicrobial strategy for the prevention and treatment of implant-related nosocomial infections.

3.4 Experimental Methods

Materials. Bovine serum albumin and lysozyme were purchased from Fisher Scientific and used without further purification. Silica wafers were purchased from WRS Materials. Perfluoroperhydrophenanthrene (PFHP), tetradecafluorohexane, fluorescein, rhodamine 123, and colistin sulfate were purchased from Millipore Sigma. MilliQ water was purified by using a Millipore water purification system. Titanium surgical screws screw was purchased from Alpha Bio Tec.

Film preparation. 5-20% w/v of protein (BSA or Lyso) solutions were prepared in MilliQ water and spin-coated at 3000 rpm for 25 seconds onto plasma-cleaned silicon substrate to yield protein films. As prepared protein films were then incubated in pre-heated

perfluoperhydrophenanthrene (PFHP) at 180 °C for 20 min, followed by washing with tetradecafluorohexane and drying with N_2 gas.

Surgical screws were cleaned in oxygen plasma before dip-coating with 20% w/v BSA solution. The screw was dried in a fume hood for 3 hours before heat-treating in PFHP at 180 ^oC for 20 min. After washing with tetradecafluorohexane, the screws were dried with nitrogen gas.

Dye and antibiotic loaded films. Protein coatings were incubated in either 0.05 mM fluorescein or rhodamine 123 solutions (in PBS) for 24 h followed by with milliQ water. The procedure for antibiotic loading used 20 mg/mL of colistin sulfate solution in PBS followed by the exact same procedure described above. For pH = 4 loading, R123 was dissolved in a pH 4 PBS buffer, adjusted using HCl.

Control release experiment. Dye-loaded protein films were incubated in 3 mL PBS and the release was monitored by fluorescence signal of the supernatant at ex: 490nm, em: 515nm for FL and ex: 500 nm, em: 525 nm for R123 using a plate reader.

Colistin release study. 5, 10 and 20% w/v BSA solutions were used to prepare BSA films with different thicknesses as described above. Stabilized BSA films were then incubated in 20 mg/ mL colistin solution for 24 hr to enable colistin loading. Colistin-loaded BSA films were then incubated in 3 mL PBS for 15 hr to allow for the release of loaded colistin. After 15 hr, the supernatant from each sample was collected, spiked with 500 μg/ mL of Vancomycin solution and analysed using LDI-MS. LDI-MS signal was utilized to calculate the intensity ratio – intensity of colistin signal/ intensity of vancomycin signal. Thereafter, the concentration of vancomycin was utilized to calculate the concentration of colistin in the supernatant. Calculations are further elaborated in Table S1.

Kirby-Bauer disc diffusion. *P. aeruginosa* were inoculated in 3 mL LB broth and grown to stationary phase at 37^{o}C. The cultures were harvested by centrifugation and washed three times with 0.85% sodium chloride solution followed by resuspension in 2 mL PBS. The concentration of the washed bacteria solution was determined by measuring the optical density at 600 nm. Seeding solution were prepared by diluting to 0.1 OD_{600} (10^{8} colony forming units) in M9 minimal media. Agar gel plates were prepared by pouring a sterile solution of 6g Agar and 10g LB in 400 mL of water onto sterile polystyrene petri dishes. 10 µL of the seeding solution was spread onto the agar plates using a sterile glass spreader. Colistin-loaded, BSA Coated as well as uncoated silicon chips were placed onto the agar plate and incubated overnight at 37^{o}C. A paper disc loaded with 1 mg/ mL was utilized as a positive control. The inhibition zone is the area around antibiotic-loaded substrates where no bacterial colonies were observed. The normalized inhibition zone was calculated by dividing the area of inhibition by the area of the substrate (silicon/ paper) for each case.

In the case of the surgical screws, agar plates were prepared and seeded with bacteria using the same protocol. Following this colistin-loaded, BSA coated and bare screws were screwed into the agar to observe colistin release.

Bacterial adhesion experiment. DsRed expressing *E. coli* were inoculated in 3 mL LB broth and grown to stationary phase at 37 ^{o}C. The cultures were then harvested and washed as described above. Seeding solution were made by diluting to 0.1 OD_{600} (10^{8} colony forming units/ mL) in M9 minimal media supplemented with 1mM IPTG (isopropyl

β-D-1-thiogalactopyranoside). 2 ml of this solution was poured onto the bare, BSA-coated and Colistin-loaded screws and incubated for 24 hours in ambient condition to enable bacteria adhesion. The screws were then gently washed 3 times with PBS before imaging by a confocal microscope.

Microscopy. Bacteria were imaged by confocal scanning light microscopy (CLSM). All analysis was performed using the A1SP: Nikon A1 Spectral Detector Confocal.

3.5. References

1. Khalili, H.; Sheikhbabayi, M.; Samadi, N.; Jamalifar, H.; Dalili, D.; Samadi, N. Bacterial Contamination of Single- and Multiple-Dose Vials after Multiple Use and Intravenous Admixtures in Three Different Hospitals in Iran. *Iran. J. Pharm. Res. IJPR* **2013**, *12* (1), 205–209.

2. Kramer, A.; Schwebke, I.; Kampf, G. How Long Do Nosocomial Pathogens Persist on Inanimate Surfaces? A Systematic Review. *BMC Infect. Dis.* **2006**, *6* (1), 130.

3. Khan, H. A.; Ahmad, A.; Mehboob, R. Nosocomial Infections and Their Control Strategies. *Asian Pac. J. Trop. Biomed.* **2015**, *5* (7), 509–514.

4. Klevens, R. M.; Edwards, J. R.; Chesley L. Richards, J.; Horan, T. C.; Gaynes, R. P.; Pollock, D. A.; Cardo, D. M. Estimating Health Care-Associated Infections and Deaths in U.S. Hospitals, 2002. *Public Health Rep.* **2007**, *122* (2), 160–166.

5. Magill, S. S.; Edwards, J. R.; Bamberg, W.; Beldavs, Z. G.; Dumyati, G.; Kainer, M. A.; Lynfield, R.; Maloney, M.; McAllister-Hollod, L.; Nadle, J.; et al. Multistate Point-Prevalence Survey of Health Care–Associated Infections. *N. Engl. J. Med.* **2014**, *370* (13), 1198–1208.

6. Crijns, F. R. L.; Keinänen-Toivola, M. M.; Dunne, C. P. Antimicrobial Coating Innovations to Prevent Healthcare-Associated Infection. *J. Hosp. Infect.* **2017**, *95* (3), 243–244.

7. Cloutier, M.; Mantovani, D.; Rosei, F. Antibacterial Coatings: Challenges, Perspectives, and Opportunities. *Trends Biotechnol.* **2015**, *33* (11), 637–652.

8. Mei, L.; Teng, Z.; Zhu, G.; Liu, Y.; Zhang, F.; Zhang, J.; Li, Y.; Guan, Y.; Luo, Y.; Chen, X.; Wang, Q. Silver Nanocluster-Embedded Zein Films as Antimicrobial Coating Materials for Food Packaging. *ACS Appl. Mater. Interfaces* **2017**, *9* (40), 35297–35304.

9. Yuan, G.; Chen, X.; Li, D. Chitosan Films and Coatings Containing Essential Oils: The Antioxidant and Antimicrobial Activity, and Application in Food Systems. *Food Res. Int.* **2016**, *89*, 117–128.

10. Zhang, R.; Liu, Y.; He, M.; Su, Y.; Zhao, X.; Elimelech, M.; Jiang, Z. Antifouling Membranes for Sustainable Water Purification: Strategies and Mechanisms. *Chem. Soc. Rev.* **2016**, *45* (21), 5888–5924.

11. Miller, D. J; Dreyer, D. R; Bielawski C. W; Paul. D. R; Freeman, B. D; Surface Modification of Water Purification Membranes. *Angew. Chemie Int. Ed.* **2017**, *56* (17), 4662–4711.

12. Keum, H.; Kim, J. Y.; Yu, B.; Yu, S. J.; Kim, J.; Jeon, H.; Lee, D. Y.; Im, S. G.; Jon, S. Prevention of Bacterial Colonization on Catheters by a One-Step Coating Process Involving an Antibiofouling Polymer in Water. *ACS Appl. Mater. Interfaces* **2017**, *9* (23), 19736–19745.

13. Percival, S. L.; Suleman, L.; Donelli, G. Healthcare-Associated Infections, Medical Devices and Biofilms: Risk, Tolerance and Control. *J. Med. Microbiol.* **2015**, *64* (4), 323–334.

14. Cheng, H.; Yue, K.; Kazemzadeh-Narbat, M.; Liu, Y.; Khalilpour, A.; Li, B.; Zhang, Y. S.; Annabi, N.; Khademhosseini, A. Mussel-Inspired Multifunctional Hydrogel Coating for Prevention of Infections and Enhanced Osteogenesis. *ACS Appl. Mater. Interfaces* **2017**, *9* (13), 11428–11439.

15. Raphel, J.; Holodniy, M.; Goodman, S. B.; Heilshorn, S. C. Multifunctional Coatings to Simultaneously Promote Osseointegration and Prevent Infection of Orthopaedic Implants. *Biomaterials* **2016**, *84*, 301–314.

16. Yazici, H.; O'Neill, M. B.; Kacar, T.; Wilson, B. R.; Oren, E. E.; Sarikaya, M.; Tamerler, C. Engineered Chimeric Peptides as Antimicrobial Surface Coating Agents toward Infection-Free Implants. *ACS Appl. Mater. Interfaces* **2016**, *8* (8), 5070–5081.

17. Lejars, M.; Margaillan, A.; Bressy, C. Fouling Release Coatings: A Nontoxic Alternative to Biocidal Antifouling Coatings. *Chem. Rev.* **2012**, *112* (8), 4347–4390.

18. Tobin, E. J. Recent Coating Developments for Combination Devices in Orthopedic and Dental Applications: A Literature Review. *Adv. Drug Deliv. Rev.* **2017**, *112*, 88–100.

19. Masahiro, I.; L., de M. B. K.; J., M. B.; Sonny, B. B.; M., S. E.; Chao, X. Surface Topography of Silicon Nitride Affects Antimicrobial and Osseointegrative Properties of Tibial Implants in a Murine Model. *J. Biomed. Mater. Res. Part A* **2017**, *105* (12), 3413–3421.

20. Knowles, B. R.; Wagner, P.; Maclaughlin, S.; Higgins, M. J.; Molino, P. J. Silica Nanoparticles Functionalized with Zwitterionic Sulfobetaine Siloxane for Application as a Versatile Antifouling Coating System. *ACS Appl. Mater. Interfaces* **2017**, *9* (22), 18584–18594.

21. Bastarrachea, L. J.; Goddard, J. M. Antimicrobial Coatings with Dual Cationic and N-Halamine Character: Characterization and Biocidal Efficacy. *J. Agric. Food Chem.* **2015**, *63* (16), 4243–4251.

22. Yu, M.; You, D.; Zhuang, J.; Lin, S.; Dong, L.; Weng, S.; Zhang, B.; Cheng, K.; Weng, W.; Wang, H. Controlled Release of Naringin in Metal-Organic Framework-Loaded Mineralized Collagen Coating to Simultaneously Enhance Osseointegration and Antibacterial Activity. *ACS Appl. Mater. Interfaces* **2017**, *9* (23), 19698–19705.

23. Lischer, S.; Körner, E.; Balazs, D. J.; Shen, D.; Wick, P.; Grieder, K.; Haas, D.; Heuberger, M.; Hegemann, D. Antibacterial Burst-Release from Minimal Ag-Containing Plasma Polymer Coatings. *J. R. Soc. Interface* **2011**, *8* (60), 1019–1030.

24. Huang, X.; Brazel, C. S. On the Importance and Mechanisms of Burst Release in Matrix-Controlled Drug Delivery Systems. *J. Control. Release* **2001**, *73* (2–3), 121–136.

25. Joseph, M.; J., W. T.; Garima, B. Biocompatibility and Medical Device Coatings. *Medical Coatings and Deposition Technologies*. August 8, 2016.

26. Zheng, W.; Jia, Y.; Chen, W.; Wang, G.; Guo, X.; Jiang, X. Universal Coating from Electrostatic Self-Assembly to Prevent Multidrug-Resistant Bacterial Colonization on Medical Devices and Solid Surfaces. *ACS Appl. Mater. Interfaces* **2017**, *9* (25), 21181–21189.

27. Wang, L. S.; Duncan, B.; Tang, R.; Lee, Y. W.; Creran, B.; Elci, S. G.; Zhu, J.; Tonga, G. Y.; Doble, J.; Fessenden, M.; Bayat, M.; Nonnenmann, S.; Vachet, R. W.; Rotello, V. M. Gradient and Patterned Protein Films Stabilized via Nanoimprint Lithography for Engineered Interactions with Cells. *ACS Appl. Mater. Interfaces* **2017**, *9* (1), 42–46.

28 Aigner, T. B.; Desimone, E.; Scheibel, T. Biomedical Applications of Recombinant Silk-Based Materials. *Adv. Mater.* **2018**, *1704636*, 1–28.

29. Gu, J.; Su, Y.; Liu, P.; Li, P.; Yang, P. An Environmentally Benign Antimicrobial Coating Based on a Protein Supramolecular Assembly. *ACS Appl. Mater. Interfaces* **2017**, *9* (1), 198–210.

30. Chen, L.; Zhou, M.-L.; Qian, Z.-G.; Kaplan, D. L.; Xia, X.-X. Fabrication of Protein Films from Genetically Engineered Silk-Elastin-Like Proteins by Controlled Cross-Linking. *ACS Biomater. Sci. Eng.* **2017**, *3* (3), 335–341.

31. Murphy, A. R.; John, P. St.; Kaplan, D. L. Modification of Silk Fibroin Using Diazonium Coupling Chemistry and the Effects on hMSC Proliferation and Differentiation. *Biomaterials* **2008**, *29* (19), 2829–2838.

32. Gopalakrishnan, S.; Xu, J.; Zhong, F.; Rotello, V. M. Strategies for Fabricating Protein Films for Biomaterial Applications. *Adv. Sustain. Syst.* **2021**, *5* (1), 2000167.

33. Heichel, D. L.; Burke, K. A. Enhancing the Carboxylation Efficiency of Silk Fibroin through the Disruption of Noncovalent Interactions. *Bioconjug. Chem.* **2020**, *31* (5), 1307–1312.

34. X, Hu.; J, Tian.; C, Li.; H, Su.; R, Qin.; Y, Wang.; X, Cao.; P, Yang. Amyloid-Like Protein Aggregates: A New Class of Bioinspired Materials Merging an Interfacial Anchor with Antifouling. *Adv. Mater.* **2020**, *32* (23).

35. Xu, Y.; Liu, Y.; Hu, X.; Qin, R.; Su, H.; Li, J.; Yang, P. The Synthesis of a 2D Ultra-Large Protein Supramolecular Nanofilm by Chemoselective Thiol–Disulfide Exchange and Its Emergent Functions. *Angew. Chemie Int. Ed.* **2020**, *59* (7), 2850–2859.

36. Wang, L.-S.; Gopalakrishnan, S.; Lee, Y.-W.; Zhu, J.; Nonnenmann, S. S.; Rotello, V. M. Translation of Protein Charge and Hydrophilicity to Materials Surface Properties Using Thermal Treatment in Fluorous Media. *Mater. Horizons* **2018**, 5, 268-274

37. Gopalakrishnan, S.; Pan, S.; Fernandez, A.; Lee, J.; Bai, Y.; Wang, L.-S.; Thayumanavan, S.; Duan, X.; Rotello, V. M. Hypersound-Assisted Size Sorting of Microparticles on Inkjet-Patterned Protein Films. *Langmuir* **2021**, *37* (8), 2826–2832.

38. Jeoung, E.; Duncan, B.; Wang, L. S.; Saha, K.; Subramani, C.; Wang, P.; Yeh, Y. C.; Kushida, T.; Engel, Y.; Barnes, M. D.; Rotello, V. M. et al. Fabrication of Robust Protein Films Using Nanoimprint Lithography. *Adv. Mater.* **2015**, *27* (40), 6251–6255.

39. Blinder, K. J.; Peyman, G. A.; Paris, C. L.; Dailey, J. P.; Alturki, W.; Lui, K. R.; Gremillion, C. M.; Clark, L. C. Vitreon, a New Perfluorocarbon. *Br. J. Ophthalmol.* **1991**, *75* (4), 240–244.

40. Lin, Y.; Liu, K.; Wang, C.; Li, L.; Liu, Y. Electrochemical Immunosensor for Detection of Epidermal Growth Factor Reaching Lower Detection Limit: Toward

Oxidized Glutathione as a More Efficient Blocking Reagent for the Antibody Functionalized Silver Nanoparticles and Antigen Interaction. *Anal. Chem.* **2015**, *87,* 8047–8051.

41. Cai, B.; Hu, K.; Li, C.; Jin, J.; Hu, Y. Bovine Serum Albumin Bioconjugated Graphene Oxide: Red Blood Cell Adhesion and Hemolysis Studied by QCM-D. *Appl. Surf. Sci.* **2015**, *356*, 844–851.

42. Wang, L.-S.; Gupta, A.; Duncan, B.; Ramanathan, R.; Yazdani, M.; Rotello, V. M. Biocidal and Antifouling Chlorinated Protein Films. *ACS Biomater. Sci. Eng.* **2016**, *2* (11), 1862–1866.

43. ter Boo, G. J. A.; Richards, R. G.; Moriarty, T. F.; Grijpma, D. W.; Eglin, D. Hyaluronic Acid Derivatives and Its Polyelectrolyte Complexes with Gentamicin as a Delivery System for Antibiotics. *Polym. Adv. Technol.* **2017**, *28* (10), 1325–1333.

44. Garnacho-Montero, J.; Ortiz-Leyba, C.; Jiménez-Jiménez, F. J.; Barrero-Almodóvar, A. E.; García-Garmendia, J. L.; Bernabeu-Wittell, M.; Gallego-Lara, S. L.; Madrazo-Osuna, J. Treatment of Multidrug-Resistant Acinetobacter Baumannii Ventilator-Associated Pneumonia (VAP) with Intravenous Colistin: A Comparison with Imipenem-Susceptible VAP. *Clin. Infect. Dis.* **2003**, *36* (9), 1111–1118.

CHAPTER 4

HYPERSOUND-ASSISTED SIZE SORTING OF MICROPARTICLES ON INKJET-PATTERNED PROTEIN FILMS

4.1 Introduction

Hydrodynamic fluidic systems[1] have enabled rapid developments in numerous applications in biomedical diagnostics,[2, 3, 4, 5] chemical synthesis and analysis,[6, 7, 8] and electronics industries.[9, 10] Fluidic systems can be readily miniaturized, making them ideal platforms for sensors and point-of-care diagnostic devices.[11] Separation and sorting of micron-sized particles is of key importance in areas that involve chemical or biological analysis such as food and chemical processing,[12] medical diagnostics,[13] and environmental assessment.[14]

Fluidic systems that manipulate the translocation of analytes along surfaces is important for useful sorting. The majority of current hydrodynamic approaches utilize microfluidic systems including continuous fluidic systems[15] and droplet systems for chemical detection.[16] However, limited control on flow manipulation[17] and the need for advanced fabrication strategies[18] still remains a challenge in the application of these systems. For instance, flow rate plays an important role in particle movement.[19] However, local manipulation of flow rate requires precise control of the inlet pressure, fluid properties, and channel structure,[20] often needing complex fluid channel design. Surface modification of the fluid channel is an alternate approach to improve the efficiency of these

devices,[21] with translocation of particles guided by electrostatic interactions on surfaces being broadly useful, [22, 23, 24] However, controlled translocation of microparticles is challenging as drag force experienced by particles must be sufficient to overcome friction and other non-specific interactions within the channel. One approach to overcoming this drag is inertial microfluidics that utilize the curvature of fluidic channels for particle manipulation.[25] However, this approach requires precise control on the complex channel design. Another approach is active control of fluidic systems through application of external optical,[26] electromagnetic[27] or acoustic[28] forces fields. These strategies have been effectively utilized for applications such as enriching particle concentration at a designated position,[29] and preventing bio-fouling of fluid channel.[30, 31] However, external fields can alter the structure of soft analytes such as proteins and cause toxicity to cells.[32]

We report here an acoustic streaming[33] approach for enabling the translocation of particles along a protein-based surface.[34] Acoustic streaming is features biocompatibility, high efficiency and straightforward implementation. [33, 35] A key feature of acoustic streaming approaches is the use of a hypersonic resonator to locally manipulate the flow motion. Hypersound-assisted acoustic streaming allows for localized three-dimensional manipulation of the flow rate: the resonator triggers formation of micro-vortices of the fluid upon immersion, thereby generating drag force on the object at the interface between streaming flow and the solid surface.

We hypothesized that the curvature dependence of the drag force generated by the resonator would allow for size-based sorting of analytes. Efficient size sorting using acoustic streaming was demonstrated using carboxylate-functionalized anionic silica microparticles[36] of varying sizes. These particles were sorted electrostatically using

patterned and gradient surfaces generated from cationic lysozyme (Lyso) surfaces and anionic bovine serum albumin (BSA) proteins. We demonstrate in this work that anionic particle translocation to complementary cationic surfaces is dependent on the competition between the drag force from acoustic streaming and non-specific/specific supramolecular interactions between the particle and surface. Particle translocation is dependent on the curvature-dependent drag force and electrostatic interactions with the surface, enabling efficient size sorting.

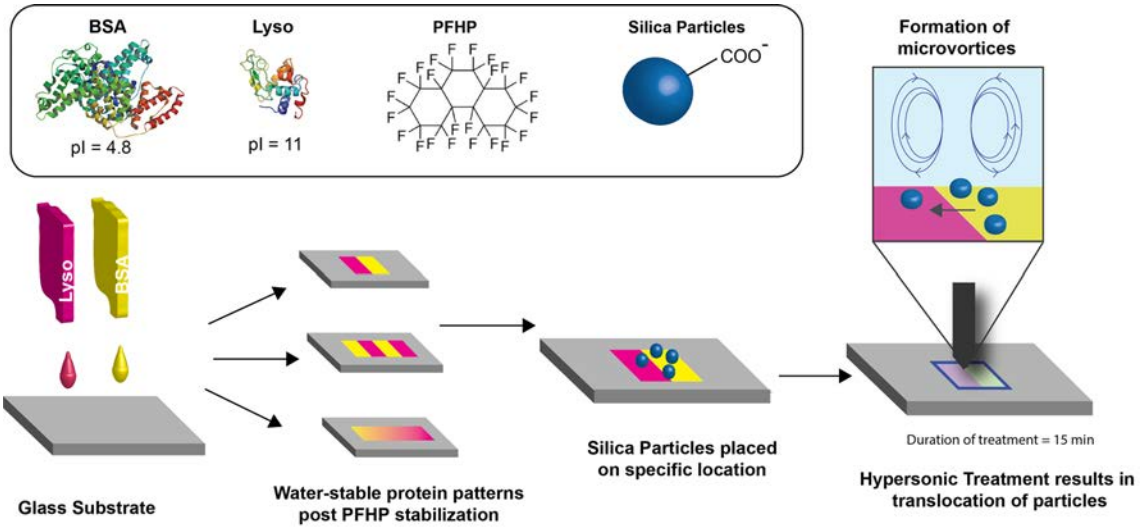

Figure 4.1. Schematic depiction of fabrication of patterned protein films using inkjet printing and controlled translocation of anionic particles to electrostatically complementary lysozyme (Lyso) surfaces through hypersonic resonation. Anionic bovine serum albumin (BSA) provides a repellent surface as a control.

4.2. Results and Discussion

4.2.1. Translocation of silica microparticles on inkjet-patterned protein substrate

Protein patterns (**Figure 4.1**) were generated by loading anionic BSA (pI = 4.8) and cationic Lyso, (pI = 11) into separate ink cartridges to print gradient and patterned protein film on glass slides (See **Figure B.1** for optical micrographs of protein pattern).[36] Protein-

coated slides were then immersed in perfluoroperhydrophenanthrene (PFHP) at 180 °C for 20 min to stabilize the coatings with translation of protein charge to charged surface coatings.[33] A fluidic channel was then fabricated using epoxy glue. The channel length is governed by two key factors – 1) volume of liquid required for effective microvortex formation and 2) size of inkjet-printed protein patterns. Previous reports[37] suggest that channel must be larger than the acoustic field of the hypersonic resonator (of the order of 100 μm). However, larger channels enable effective detection of translocation of particles along the protein patterns. The channels for this study were of the dimensions ~ 1 x 1 x 0.3 cm which allow for effective microvortex formation while providing sufficient area to discern particle translocation.

For particle translocation studies 10 μL of 0.1 mg/mL carboxylate-functionalized silica particle solution (procedure described in SI-2, 3 and 4) was placed at an uncoated location on the substrate away from the protein pattern. After 15 min, the channel was flooded with 500 μL of PBS and the hypersonic treatment was applied as shown in **Figure 4.2(a)**. Images were taken at specific location on the patterned films before and after treatment. As seen in **Figure 4.2(b),** most of the silica particles were present in the region the droplet was placed before treatment. After hypersonic treatment, as expected the anionic particles migrated to the cationic Lyso region. No change was observed on the BSA region of the patterned film. This translocation indicates that the drag force generated by acoustic streaming is able to overcome non-specific interactions of particles to both the unmodified glass surface as well as the negatively charged BSA surface.

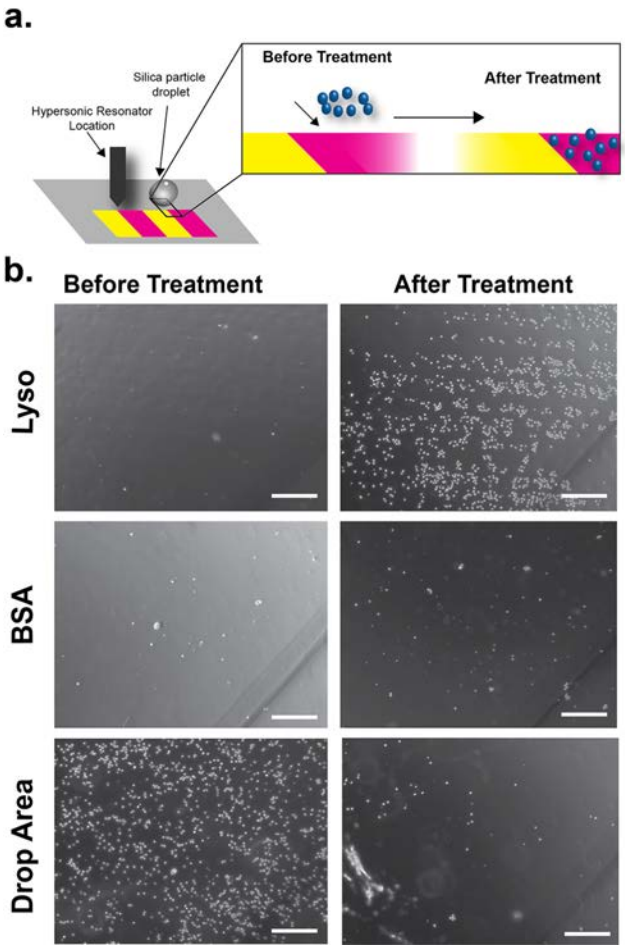

Figure 4.2. (a) Schematic showing the anionic silica particles translocating particles to the cationic lysozyme (Lyso) portion of patterned film. Silica droplet placed at an uncoated portion of the substrate. (b) Micrographs of protein film before and after treatment show that particles are predominantly present in the drop area before treatment. After treatment, most of the particles migrate to Lyso. As expected, no significant change is observed on the anionic BSA portion of the surface. Scale bar = 200 μm.

4.2.2. Size-dependent translocation of silica microparticles on protein surfaces

We then investigated the size-dependence of the drag force exerted by the hypersonic resonator and hence the ability to translocate particles. Previous studies indicate that the drag force is directly proportional to the size of the analytes.[33] We hypothesized that since the translocation of particles depends on the drag force, particles of different sizes would have different velocities. Patterns (**Figure 4.3(a)**) were utilized for this study.

Carboxylate-functionalized silica microparticle solution of different sizes (3, 10, 20 μm, 0.1 mg/mL in PBS) were applied to a fixed location allowed to rest for 15 min. (**Figures S4** and **S5** show charge characterization of particles respectively) The channel was then flooded with PBS and hypersonic treatment was applied as before. Images were taken at specific locations on the patterned films before and after treatment and the number of silica particles were counted for each image. **Figure 4.3(b)** shows optical micrographs of the patterned films before and after treatment. Silica particles that non-specifically adhered to BSA before treatment were removed after hypersonic treatment in the case of larger 10 and 20 μm particles. However, in the case of 3 μm particles, no change was observed post-treatment. This result was further corroborated by quantifying change in particle ratio at several location on the BSA and Lyso region, (**Figure 4.3(c))**. It can be seen that the number of particles on BSA decreased significantly in the case of 10 and 20 μm particles while no significant changes are observed in the case of 3 μm particles. Likewise, the number of particles adhered to Lyso in the case of 10 and 20 μm particles increase. These results were further corroborated by testing 1, 7 and 50 μm sized particles, as shown in **Figure B.6.** Translocation was observed in the case of 7 and 50 μm sized particles but not in the case of 1 μm sized particles. Taken together, these results are consistent with greater force experienced by the larger particles being enough to overcome adhesive interactions and allow the particles to translocate towards the positively charged Lyso film Demonstrating that charge and size-dependent translocation can be utilized for the size-based sorting of analytes.

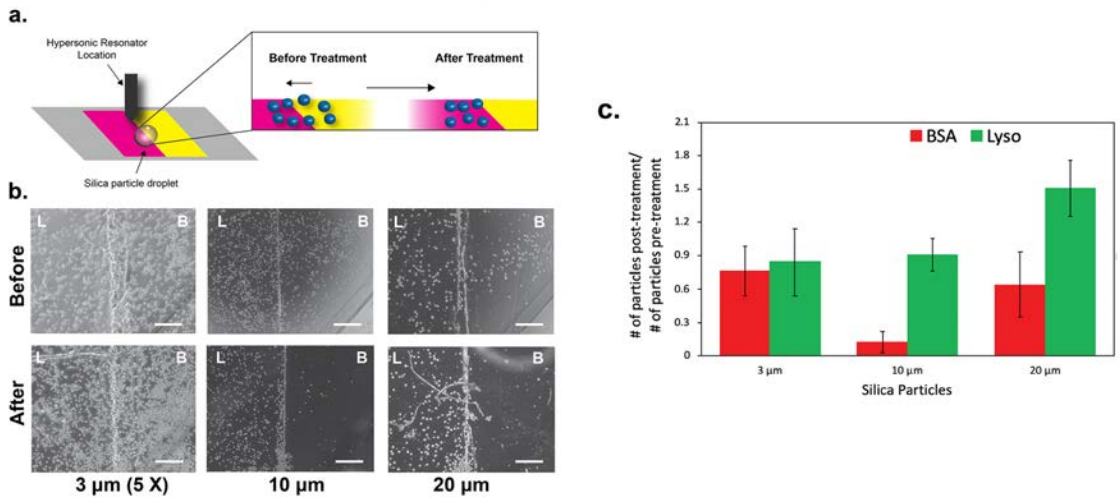

Figure 4.3. (a) Placement of anionic silica particles on protein pattern. (b) Micrographs of 3 µm, 10 µm and 20 µm silica particles adhered to BSA-Lyso pattern before and after treatment. Anionic 10 and 20 µm particles have been dislodged from BSA but not from electrostatically complementary Lyso. No change observed in the case of 3 µm particles (c) Quantification of translocation of silica particles by the ratio of number of particles post-treatment to pre-treatment for multiple images of different areas on the pattern. Particles on Lyso increase while those on BSA decrease in the case of 10 and 20 µm particles. No significant difference is detected in the case of 3 µm patterns. Scale bar = 200 µm for 10 and 20 µm particle images. Scale bar = 40 µm for 3 µm particle images. ~8 images per sample were used for calculation.

4.2.3. Size-sorting of charged silica particles on patterned protein surfaces

Based on the results obtained in **Figure 4.2 and 4.3**, we proceeded to utilize the hypersonic treatment for sorting silica microparticles with our ability to translocate particles based on their size. Treatment was then applied to a specific location as shown in **Figure 4.4(a)** and optical micrographs were obtained post treatment as shown in **Figure 4.4(b).** As anticipated, the 20 µm particles translocate from the drop area to Lyso while the 3 µm particles remain stationery. No particles were present on the BSA region indicating that the electrostatic interaction between Lyso and the silica particles is responsible for the adhesion of the particles on the protein film. The number of particles of both sizes in each region post-treatment was counted and sorting efficiency was calculated as shown in **Table**

4.S1. The sorting efficiency was calculated to be 92% for the 20 μm particles and 95. % for the 3 μm particles This serves as a further demonstration that our system may be employed as a strategy for efficient and rapid sorting of micron-sized analytes.

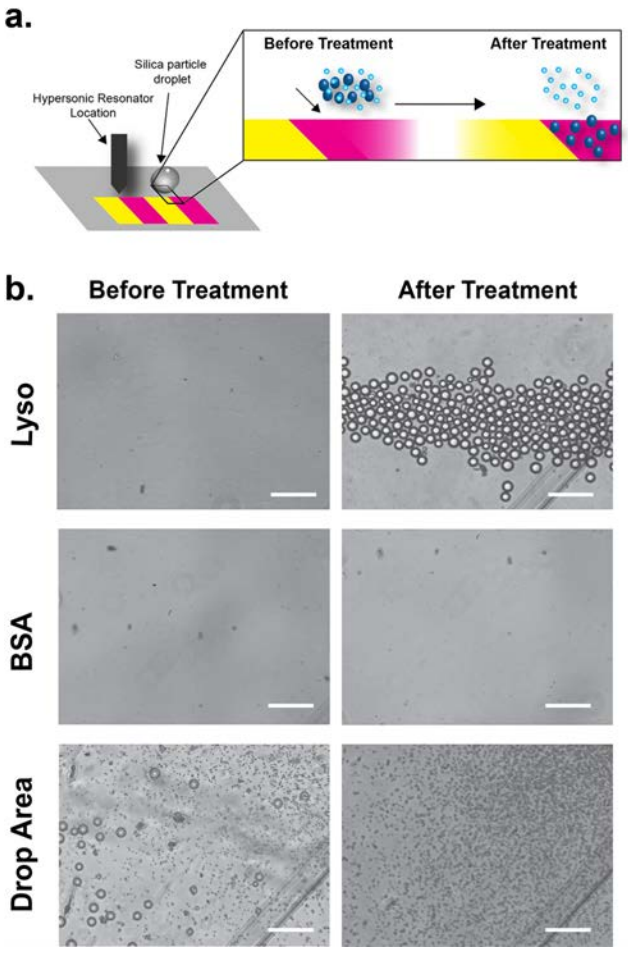

Figure 4.4. (a) Schematic depiction of the experimental setup. Silica droplet is placed at an uncoated portion of the substrate. b) Micrographs of protein film before and after treatment. Most of the particles of both sizes are present in the drop area before treatment. Both BSA and Lyso regions are clean. However, post treatment 20 μm particles move towards Lyso while 3 μm particles remain stationery in the drop area. After treatment micrographs clearly show separated regions containing both particles. Scale bar = 80 μm.

4.2.4. Translocation of silica microparticles along patterned protein surface with charge gradient

A key feature of our sorting strategy is the ability to locally control the motion of particles through a combination of functionalized surfaces and the hypersonic treatment. This synergy was further demonstrated by studying the ability of particles to translocate along protein-based charged gradients. Inkjet printing was used to fabricate a charge gradient going from negative (BSA) to positive (Lyso), as shown in **Figure 4.5(a).** After stabilization and channel fabrication, 500 μL of 0.1 mg/mL silica microparticle solution in PBS (synthesized according to protocol in 4.S1) was added into channel, and allowed to sit for 15 min. As seen in **Figure 4.5(b)**, silica particles adhere in a manner consistent with the charged protein gradient. Hypersonic treatment was then applied for 15 min at 500 milliwatts (mW) with a constant back-and-forth motion, as shown in **Figure 4.5(a)**. As seen in **Figure 4.5(c),** the gradient becomes more pronounced post-treatment due to movement of the silica particles non-specifically adhered to the BSA area of the film. This sorting demonstrates that GHz acoustic streaming coupled with gradient films could be utilized as a sorting strategy.

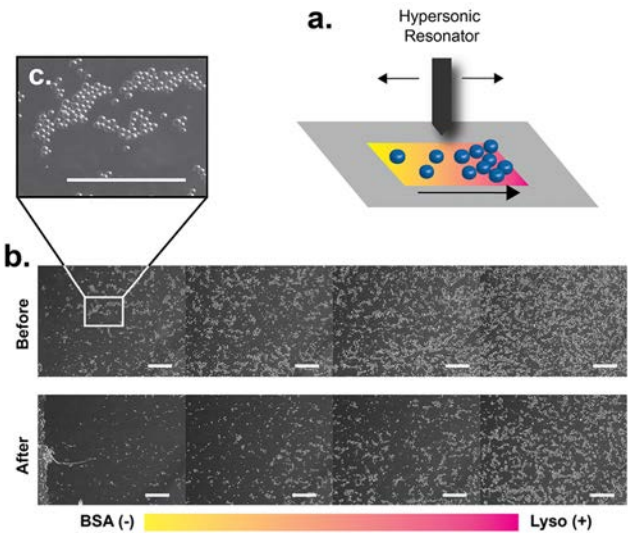

Figure 4.5. (a) Schematic depiction of movement of particles along a charge gradient due to hypersonic treatment. (b) Micrographs of gradient film before and after treatment show more pronounced gradient after treatment. This indicates that particles non-specifically adhered to BSA are dislodged by treatment. Scale bars = 200 μm.

4.3. Conclusions

This study presents a strategy for the translocation and sorting of analytes using a hydrodynamic approach based on gigahertz acoustic streaming. These studies demonstrate the ability of hypersound-based micro-vortices to overcome the limitations of laminar flow in the translocation of particles along charged protein patterns. Moreover, the curvature-dependence of the drag force enabled size-based particle manipulation. Taken together, this hypersonic strategy provides a rapid and efficient method for sorting analytes on the basis of size and charge, with potential applications in chemical and biomedical analysis, point-of-care diagnostic systems and industrial microfluidic systems.

4.4 Experimental Methods

4.4.1. Fabrication of patterned protein films

Inkjet-printing of protein patterns. Printing was done directly onto glass coverslips cleaned through sonication in ethanol, isopropanol and then oxygen-plasma (at 300 mbar for 5 min). Protocol detailed in ref 36 was followed. 10% w/v solutions of BSA (obtained from Fisher Scientific) and Lyso (obtained from Fisher Scientific) were prepared using 20% v/v ethanol in milliQ water as the solvent. The ethanol (obtained from Fisher Scientific) was added to maintain a favorable viscosity for inkjet printing as per the protocol followed in ref 26. Protein solutions were then injected into empty ink cartridges (obtained from Ink owl) through a 0.22 μm PTFE syringe filter compatible with the printer Epson XP830. Syringe filters were used to remove any aggregates or undissolved protein to prevent clogging of the ink head. **Figure B.1** shows micrograph of printed pattern and resolution of inkjet printing.

Following this, protein-loaded ink cartridges were placed into the printer and the head cleaning protocol on the printer was run. Patterns were then generated on the print CD application available through EPSON, using one or more of the three color channels – Magenta, Cyan or yellow – based on the cartridges used for the protein solution. The ink head was flushed after each use with a flushing solution of 70% milliQ water, 20% glycerol and 10% hexanediol spiked with Rhodamine 123, to help with visualization, to remove any debris as well as to prevent clogging of the ink head.

Stabilization of patterned protein films. Printed glass slips were then thermally treated to stabilize the protein, according to protocol established in ref 34. Glass slips were

immersed in perfluoroperhydrophenanthrene (PFHP; obtained from Sigma Aldrich) maintained at 180 ^{o}C for 20 min. Following this glass slips were taken out, allowed to cool and washed with perfluorohexane (obtained from Fisher Scientific) to remove excess PFHP and then dried using a stream of nitrogen. Patterned glass slips were then adhered to glass slides (obtained from Fisher Scientific) using an epoxy AB glue. The same epoxy was used to fashion a channel to contain the water required for PFHP treatment. The dimensions of the channel were ~ 1 x 1 x 0.3 cm. The epoxy was allowed to harden overnight before use.

4.4.2. Synthesis of silica microparticles.

Amine-functionalization of silica microparticle surface. 500 mg of 10 μm, 15 μm and 20 μm SiO_2 particles (obtained from Alfa Aesar; **Figure B.2** shows detailed reaction scheme; **Figure B.4** shows zeta potentials) were charged separately in 2 neck round-bottom flasks. Protocol described in ref 36 was followed. 5 mL toluene was added to the above and dispersed by sonication for 30 min. The dispersion was purged with Argon for 10 minutes, followed by the addition of 1.75 mL (3 Aminopropyl) triethoxysilane (APTES: obtained from Sigma Aldrich). The mixture was refluxed at 110 OC under inert condition for 12 h. The mixture was then centrifuged at 4.4 rpm for 1 h, the precipitate collected, re-dispersed into 25 mL dry toluene (obtained from Fisher Scientific), sonicated for 20 min and centrifuged again at 4.4 rpm for 20 min. The precipitate was washed with ethanol (obtained from Acros Organics) twice and the final product lyophilized. **Figure B.5** shows zeta potential post amine functionalization, indicating a change in surface charge.

Post-functionalization with carboxylate groups. 120 mg of SiO_2- NH_2 was dispersed in 6 mL tetrahydrofuran (THF: obtained from Fisher Scientific) and the suspension sonicated for 30 minutes. 420 mg succinic anhydride (obtained from Acros Organics) was added in 2 portions and stirred at 0 ^oC for 2 h, followed by stirring at room temperature overnight. 10 mL distilled water was then added to quench unreacted succinic anhydride, sonicated for 15 min and centrifuged at 4.4 rpm. for 1 h. The precipitate was re-dispersed in THF and centrifuged again for 15 min at the same rpm. The precipitate was collected, re-dispersed in water and centrifuged for 30 min and lyophilized. **Figure B.5** shows zeta potential post-treatment indicating overall negative surface charge of all particles.

4.4.3. Hypersonic Resonator treatment.

The fabrication process and working mechanism of the hypersonic resonator are explained in our previous work ref 33. In general, a sandwich structure composed of a piezoelectric material between two electrodes is utilized to stimulate gigahertz acoustics, which is acoustically isolated from substrates by Bragg Reflector. A signal generator (Agilent, N5181A) was introduced to generate an RF signal, which was then amplified by a power amplifier (Mini-Circuits, ZHL-5 W-422), and applied to the resonator. The signal generator was also utilized to control the power amplitude and mode of hypersonic resonator. When the hypersonic resonator is immersed into liquid, it suffers from an acoustic damping effect and the acoustic energy is radiated into the liquid, triggering acoustic streaming. For our experiments, the device was immersed into the channel and fixed at a 1.5 mm relative distance to the protein film. The resonator was triggered with amplified RF signal at 1.65 GHz for 15 min.

4.4.4. Optical microscopy measurements.

Bright-field optical microscopy images were obtained through Olympus IX51 at 4X, 10X and 20X as needed. For the graph shown in **Figure 3(c)**, several images were taken at pre-defined locations on the sample before and after treatment and the ratio between number of particles after treatment to number of particles before treatment was calculated to quantify the degree of reorganization. The number of particles were counted using ImageJ.

4.5. References

1. Bae, J.; Lee, J.; Zhou, Q.; Kim, T. Micro-/Nanofluidics for Liquid-Mediated Patterning of Hybrid-Scale Material Structures. *Adv. Mater.* **2019**, *31* (20), 1804953.

2. Zhang, D.; Bi, H.; Liu, B.; Qiao, L. Detection of Pathogenic Microorganisms by Microfluidics Based Analytical Methods. *Anal. Chem.* **2018**, *90* (9), 5512–5520.

3. Haidas, D.; Bachler, S.; Köhler, M.; Blank, L. M.; Zenobi, R.; Dittrich, P. S. Microfluidic Platform for Multimodal Analysis of Enzyme Secretion in Nanoliter Droplet Arrays. *Anal. Chem.* **2019**, *91* (3), 2066–2073.

4. Bandodkar, A. J.; Gutruf, P.; Choi, J.; Lee, K. H.; Sekine, Y.; Reeder, J. T.; Jeang, W. J.; Aranyosi, A. J.; Lee, S. P.; Model, J. B.; et al. Battery-Free, Skin-Interfaced Microfluidic/Electronic Systems for Simultaneous Electrochemical, Colorimetric, and Volumetric Analysis of Sweat. *Sci. Adv.* **2019**, *5* (1), 3294.

5. Devendran, C.; Choi, K.; Han, J.; Ai, Y.; Neild, A.; Collins, D. J. Diffraction-Based Acoustic Manipulation in Microchannels Enables Continuous Particle and Bacteria Focusing. *Lab Chip* **2020**, *20* (15), 2674–2688.

6. Gençer, A.; Schütz, C.; Thielemans, W. Influence of the Particle Concentration and Marangoni Flow on the Formation of Cellulose Nanocrystal Films. *Langmuir* **2017**, *33* (1), 228–234.

7. Kim, J. H.; Jeon, T. Y.; Choi, T. M.; Shim, T. S.; Kim, S. H.; Yang, S. M. Droplet Microfluidics for Producing Functional Microparticles. *Langmuir* **2014**, *30* (6), 1473–1488.

8. Yin, C. Y.; Nikoloski, A. N.; Wang, M. Microfluidic Solvent Extraction of Platinum and Palladium from a Chloride Leach Solution Using Alamine 336. *Miner. Eng.* **2013**, *45*, 18–21.

9. Khoshmanesh, K.; Tang, S. Y.; Zhu, J. Y.; Schaefer, S.; Mitchell, A.; Kalantar-Zadeh, K.; Dickey, M. D. Liquid Metal Enabled Microfluidics. *Lab on a Chip*. Royal Society of Chemistry March 14, 2017, pp 974–993.

10. Chen, G.; Zheng, J.; Liu, L.; Xu, L. Application of Microfluidics in Wearable Devices. *Small Methods* **2019**, *3* (12), 1900688.

11. Gao, B.; Li, X.; Yang, Y.; Chu, J.; He, B. Emerging Paper Microfluidic Devices. *Analyst*. Royal Society of Chemistry November 21, 2019, pp 6497–6511.

12. Tan, Y. C.; Fisher, J. S.; Lee, A. I.; Cristini, V.; Lee, A. P. Design of Microfluidic Channel Geometries for the Control of Droplet Volume, Chemical Concentration, and Sorting. *Lab Chip* **2004**, *4* (4), 292–298.

13. Dalili, A.; Samiei, E.; Hoorfar, M. A Review of Sorting, Separation and Isolation of Cells and Microbeads for Biomedical Applications: Microfluidic Approaches. *Analyst*. Royal Society of Chemistry January 7, 2019, pp 87–113.

14. Yew, M.; Ren, Y.; Koh, K. S.; Sun, C.; Snape, C. A Review of State-of-the-Art Microfluidic Technologies for Environmental Applications: Detection and Remediation. *Glob. Challenges* **2019**, *3* (1), 1800060.

15. Sun, J.; Wu, K.; Su, D.; Guo, G.; Shi, Z. Continuous Separation of Magnetic Beads Using a Y-Shaped Microfluidic System Integrated with Hard-Magnetic Elements. *J. Phys. D. Appl. Phys.* **2020**, *53* (3), 035004.

16. Jeon, J.; Choi, N.; Chen, H.; Moon, J. Il; Chen, L.; Choo, J. SERS-Based Droplet Microfluidics for High-Throughput Gradient Analysis. *Lab Chip* **2019**, *19* (4), 674–681.

17. Shang, L.; Cheng, Y.; Zhao, Y. Emerging Droplet Microfluidics. *Chemical Reviews*. American Chemical Society June 28, 2017, pp 7964–8040.

18. Waheed, S.; Cabot, J. M.; Macdonald, N. P.; Lewis, T.; Guijt, R. M.; Paull, B.; Breadmore, M. C. 3D Printed Microfluidic Devices: Enablers and Barriers. *Lab on a Chip*. Royal Society of Chemistry May 24, 2016, pp 1993–2013.

19. Sollier, E.; Go, D. E.; Che, J.; Gossett, D. R.; O'Byrne, S.; Weaver, W. M.; Kummer, N.; Rettig, M.; Goldman, J.; Nickols, N.; et al. Size-Selective Collection of Circulating Tumor Cells Using Vortex Technology. *Lab Chip* **2014**, *14* (1), 63–77.

20. Zhou, Y.; Ma, Z.; Ai, Y. Dynamically Tunable Elasto-Inertial Particle Focusing and Sorting in Microfluidics. *Lab Chip* **2020**, *20* (3), 568–581.

21. Gokaltun, A.; Yarmush, M. L.; Asatekin, A.; Usta, O. B. Recent Advances in Nonbiofouling PDMS Surface Modification Strategies Applicable to Microfluidic Technology. *TECHNOLOGY* **2017**, *05* (01), 1–12.

22. Duffadar, R. D.; Davis, J. M. Dynamic Adhesion Behavior of Micrometer-Scale Particles Flowing over Patchy Surfaces with Nanoscale Electrostatic Heterogeneity. *J. Colloid Interface Sci.* **2008**, *326* (1), 18–27.

23. Schachermeyer, S.; Ashby, J.; Kwon, M. J.; Zhong, W. Impact of Carrier Fluid Composition on Recovery of Nanoparticles and Proteins in Flow Field Flow Fractionation. *J. Chromatogr. A* **2012**, *1264*, 72–79. https://doi.org/10.1016/j.chroma.2012.09.050.

24. Liu, Y.; Cánovas, R.; Crespo, G. A.; Cuartero, M. Thin-Layer Potentiometry for Creatinine Detection in Undiluted Human Urine Using Ion-Exchange Membranes as Barriers for Charged Interferences. *Anal. Chem.* **2020**, *92* (4), 3315–3323.

25. Gou, Y.; Jia, Y.; Wang, P.; Sun, C. Progress of Inertial Microfluidics in Principle and Application. *Sensors (Switzerland)*. MDPI AG June 1, 2018.

26. Paiè, P.; Zandrini, T.; Vázquez, R.; Osellame, R.; Bragheri, F. Particle Manipulation by Optical Forces in Microfluidic Devices. *Micromachines* **2018**, *9* (5), 200.

27. Haehnel, V.; Khan, F. Z.; Mutschke, G.; Cierpka, C.; Uhlemann, M.; Fritsch, I. Combining Magnetic Forces for Contactless Manipulation of Fluids in Microelectrode-Microfluidic Systems. *Sci. Rep.* **2019**, *9* (1), 1–11.

28. Wu, M.; Ozcelik, A.; Rufo, J.; Wang, Z.; Fang, R.; Jun Huang, T. Acoustofluidic Separation of Cells and Particles. *Microsystems and Nanoengineering*. Nature Publishing Group December 1, 2019, pp 1–18.

29. Schultz, T.; Vogt, S.; Schlupp, P.; Von Wenckstern, H.; Koch, N.; Grundmann, M. Influence of Oxygen Deficiency on the Rectifying Behavior of Transparent-Semiconducting-Oxide-Metal Interfaces. *Phys. Rev. Appl.* **2018**, *9* (6).

30. Mutafopulos, K.; Spink, P.; Lofstrom, C. D.; Lu, P. J.; Lu, H.; Sharpe, J. C.; Franke, T.; Weitz, D. A. Traveling Surface Acoustic Wave (TSAW) Microfluidic Fluorescence Activated Cell Sorter (MFACS). *Lab Chip* **2019**, *19* (14), 2435–2443.

31. Hu, X. J.; Liu, H. L.; Jin, Y. X.; Liang, L.; Zhu, D. M.; Zhu, X. Q.; Guo, S. S.; Zhou, F. L.; Yang, Y. Precise Label-Free Leukocyte Subpopulation Separation Using Hybrid Acoustic-Optical Chip. *Lab Chip* **2018**, *18* (22), 3405–3412.

32. Song, K.; Li, G.; Zu, X.; Du, Z.; Liu, L.; Hu, Z. The Fabrication and Application Mechanism of Microfluidic Systems for High Throughput Biomedical Screening: A Review. *Micromachines* **2020**, *11* (3), 297.

33. Pan, S.; Zhang, H.; Liu, W.; Wang, Y.; Pang, W.; Duan, X. Biofouling Removal and Protein Detection Using a Hypersonic Resonator. *ACS Sensors* **2017**, *2* (8), 1175–1183.

34. Wang, L. S.; Gopalakrishnan, S.; Lee, Y. W.; Zhu, J.; Nonnenmann, S. S.; Rotello, V. M. Translation of Protein Charge and Hydrophilicity to Materials Surface Properties Using Thermal Treatment in Fluorous Media. *Mater. Horizons* **2018**, *5* (2), 268–274.

35. Pan, S.; Jeon, T.; Luther, D. C.; Duan, X.; Rotello, V. M. Cytosolic Delivery of Functional Proteins *In Vitro* through Tunable Gigahertz Acoustics. *ACS Appl. Mater. Interfaces* **2020**, *12* (13), 15823–15829.

36. Feifel, S. C.; Lisdat, F. Silica Nanoparticles for the Layer-by-Layer Assembly of Fully Electro-Active Cytochrome c Multilayers. *J. Nanobiotechnology* **2011**, *9* (1), 59.

37. Cui, W.; Zhang, H.; Zhang, H.; Yang, Y.; He, M.; Qu, H.; Pang, W.; Zhang, D.; Duan, X. Localized Ultrahigh Frequency Acoustic Fields Induced Micro-Vortices for Sub-milliseconds Microfluidic Mixing. *Appl. Phys. Lett.* **2016**, 109 (25), 253503.

CHAPTER 5

FABRICATION OF COLLAGEN FILMS WITH ENHANCED MECHANICAL AND ENZYMATIC STABILITY THROUGH THERMAL TREATMENT IN FLUOROUS MEDIA

5.1 Introduction

Collagen I (Col-I) is the major component of the extracellular matrix in mammalian tissue.[1] The unique triple helix structure provides multiple cell attachment sites and plays an essential role in promoting cell behavior including adhesion, proliferation, migration, and differentiation.[2] Col-I has been utilized as a biomaterial in several forms, such as injectable hydrogels,[3] sponges,[4] nanofibers,[5] hollow spheres,[6] and films[7]. Col-I based materials have been used in conjunction with biomaterial applications such as soft/ hard tissue repair strategies,[7] tissue engineering scaffolds,[8] and wound healing systems[9]. Furthermore, as collagen is a naturally derived protein, it enables sustainable fabrication of biomaterials.[10]

Collagen-based biomaterials often lack sufficient strength and stability and are prone to both mechanical damage and rapid enzymatic digestion.[4] Several processes have been used to enhance the mechanical properties of collagen matrix. For instance, incorporating components such as graphene increases the stiffness of collagen-based matrix.[10, 11] However, this incorporation can jeopardize both the cytophilic properties and biocompatibility of the resulting materials. Crosslinking is a common way to modify collagen to enhance strength as well as improve enzymatic stability.[12] The usual methods

of crosslinking are chemical and physical crosslinking.[1] Chemical cross-linkers (e.g. glutaraldehyde, carbodiimide) can reduce cytocompatibility because either the linkers themselves or the byproducts are cytotoxic.[12] Using a physical method such as dehydrothermal treatment or irradiation can avoid cytotoxicity from the added cross-linking agent. Thermal treatment in particular has been shown to induce crosslinking and tight packing of collagen fibers.[13, 14, 15] However, collagen tends to undergo uncontrolled denaturation during such treatments, unfavorably affecting materials properties.[16]

Perfluorocarbons provide an inert, stable environment due to their immiscibility with water as well as most organic solvents.[17, 18, 19] Furthermore, proteins in perfluorocarbon solvents are not prone to denaturation like proteins in organic solvents.[20] We have previously demonstrated our ability to stabilize protein films from aqueous degradation through thermal treatment in a fluorous media (perfluoroperhydrophenanthrene, PFHP). We also showed that the native secondary structures and surface properties of the proteins are retained after treatment in PFHP.[21] Therefore, we hypothesized that the stability and mechanical properties of the Col-I matrix could be improved by thermal treatment in PFHP, *without* compromising the protein structure. We report here the use of fluorous thermal treatment to improve both the mechanical and biostability of collagen films. In this study, the stability and mechanical properties of Col-I were evaluated after thermal treatment in PFHP and compared to as-prepared Col-I and Col-I heat-treated in air **(Figure 5.1)**, with clear improvements in mechanical properties and enzymatic stability observed with fluorous treatment. Cytocompatibility was retained, as demonstrated through the incubation of fibroblast cells.

Overall, thermal treatment in PHFP enhances both the stability and mechanical properties of Col-I while retaining cytocompatibility and preventing significant denaturation.

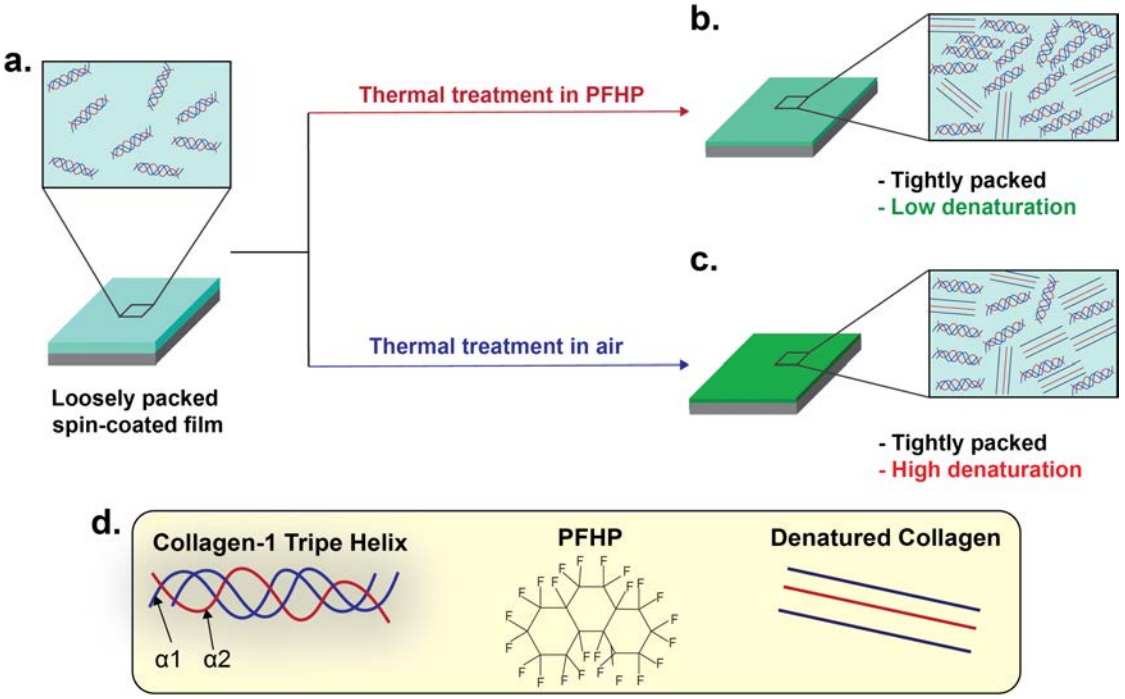

Figure 5.1. Schematic Representation of the fabrication strategy for stable collagen films. (a) Spin-coating of Col-I solution on cleaned silicon substrates produces films with loosely packed collagen fibers. (b) Low degree of denaturation of Col-I with fluorous heat treatment and (c) a high degree of denaturation after heat treatment in air. (d) Schematic showing representative structure of Col-I triple helix, PFHP and denatured col-I fibers.

5.2. Results and Discussion

5.2.1. Fabrication and characterization of collagen films

The post-treatment surface topographies of collagen coatings prepared on Si wafers are shown in **Figure 5.2**. The SC (spin-coated) surface is smooth, with collagen covering the surface homogeneously, forming a net-like structure with an average roughness (R_a) of 0.48 nm **(Figure 5.2(a))**. Fluorous-cured (FC) or air-cured (AC) collagen films treated at 75, 135 and 180 °C showed no significant changes in roughness as compared to SC films **(Figures 5.2(b)-5.2(g))**. We therefore concluded that thermal treatment does not

significantly affect the nano-topography of the surface. The surface morphologies observed by FESEM **(Figure C.1)** are also in accordance with the AFM results indicated in **Figure 5.2**.

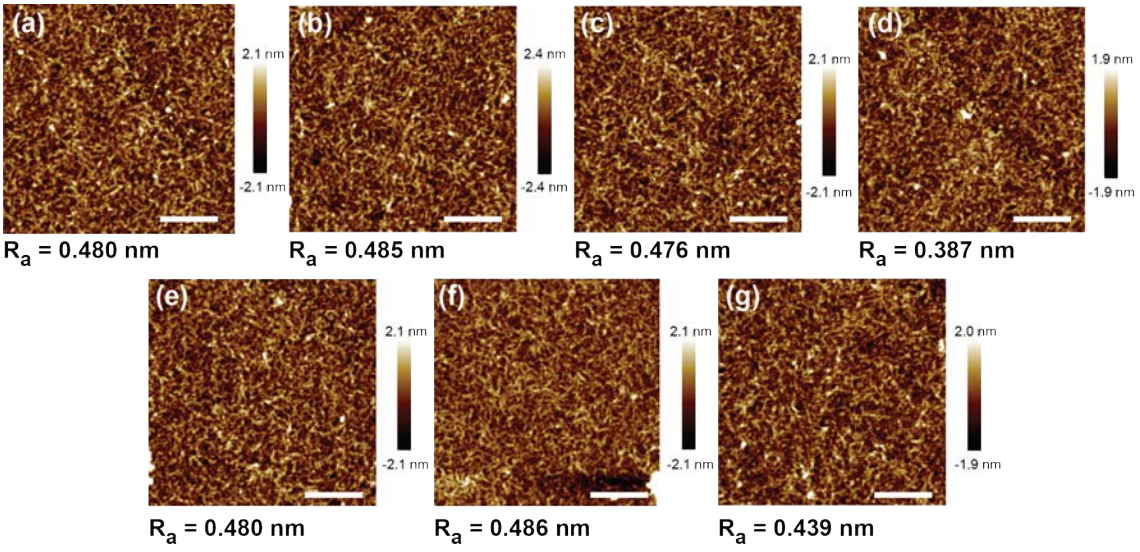

Figure 5.2. Surface-topographies of different coating surfaces imaged by AFM: (a) SC, (b)FC75 (c) FC135, (d)FC180, (e)AC75, (f)AC135, (g)AC180. Scale bar is 1 μm. Height profiles indicate surface roughness of each film. Roughness (R_a) of each sample is reported under the image. Thermal treatment does not significantly affect the nano-topography of the surface.

The thickness of different coatings as measured by ellipsometry are shown in **Figure 5.3(a)**. As the temperature is increased, the thickness of coating decreases, indicating tighter packing of the collagen fibers due to thermal treatment Additionally, there is no significant difference between FC films and AC films, which indicates that the fluorous treatment does not significantly affect the temperature-induced reorganization of the collagen fibers. The thickness of FC-180 obtained through the cross-sectional image obtained by FESEM as seen in **Figure 5.3(b)**, agrees with the ellipsometry measurements in **Figure 5.3(a)** (see also **Figure C.2)**. Thermal treatment of Col-I is known to induce reaction between two or more collagen molecules via carboxylic acids and amines,

inducing intermolecular crosslinking without inducing cytotoxicity.[15] Furthermore, collagen chains shrink and pack tightly during thermal treatment.[15, 16]

Changes in the hydrophilicity of the collagen films due to thermal treatment was assessed through water contact angle measurements. As shown in **Figure 5.3(c)**, Fluorous-cured films (FC75, FC135 and FC180) have increased contact angles as compared to the spin-cast (SC) film (by ~30°) and air-cured films (AC75, AC135 and AC180). This change in contact angle indicates that there is a difference in the reorganization behavior of collagen fibers during both treatments. We hypothesized that PFHP treatment results in tighter packing of collagen fibers than air curing, contributing to lower wettability and therefore a greater increase in contact angles.

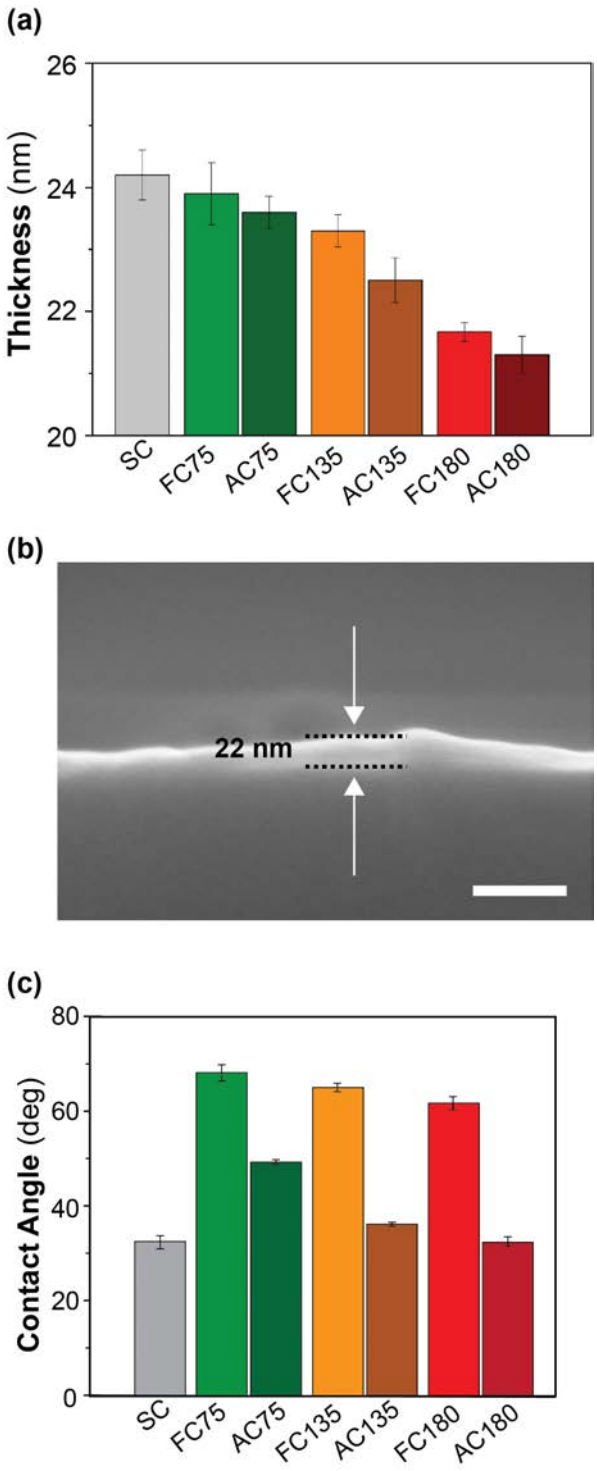

Figure 5.3. (a) Thickness of different coatings as measured by ellipsometry. Thickness decreases as temperature of treatment is increased, during both fluorous-curing as well as air-curing, due to tighter packing of collagen fibers (b) cross-section image of FC180 is in agreement with thickness measurements obtained through ellipsometry (c) Water contact angle measurement on treated and SC films using the static sessile drop method with 2 μL of water. PFHP treatment results in increased hydrophobicity as compared to treatment in air. Scale bar is 250 nm.

5.2.2. Evaluating the structural integrity of the fluorous-cured collagen films

We next evaluated the stability of treated collagen films in aqueous media. Structural and mechanical properties of collagen-based materials are greatly affected by their tendency to swell in aqueous media, often resulting in a loss of structural features.[22] Based on the results in **Figure 3**, we expected samples treated at 180 °C to be resistant to swelling. Results from treatment conducted at other temperatures can be found in **Figure C.4**. Samples were immersed in PBS for different time durations and the thickness of Col-I films were measured through ellipsometry, as seen in **Figure 5.4(a)**. After immersion for 24 h, the thickness of the SC film was reduced by ~50%. By comparison, only slight changes in thickness were observed in the case of FC180 and AC180. This demonstrates that heat treatment at 180° C improved significantly aqueous stability of collagen films. As duration of immersion is increased up to 4 days, FC180 continues to show no significant changes in thickness while AC180 shows significant *increase* in thickness, presumably due to swelling. This difference in stability suggests that collagen fibers are packed tighter post-PFHP treatment, as compared to air treatment. To further evaluate the difference between treatments in air and PFHP, nano-topographies of FC180 and AC180 after a 4-day immersion period were observed by AFM and shown in **Figures 5.4(b), (c)** (see also **Figure C.3**). While the surface of FC180 **(Figure 5.4(b))** showed no significant changes post-immersion, the roughness of AC180 **(Figure 5.4(c))** sharply increased by ~2 nm. The morphology AC180 **(Figure 5.4(d))** observed by FESEM indicates the presence of a porous surface (nanopores and protuberances on the surface marked by the arrows) that may be responsible for the swelling. We hypothesized that the difference in the swelling behavior of FC180 and AC180 may be due to denaturation of collagen in the latter air-

cured film. Collagen fibers heated in air are prone to denaturation and oxidation resulting in an amorphous polymer much like gelatin, which results in a higher degree of swelling as well as lower contact angles.[23]

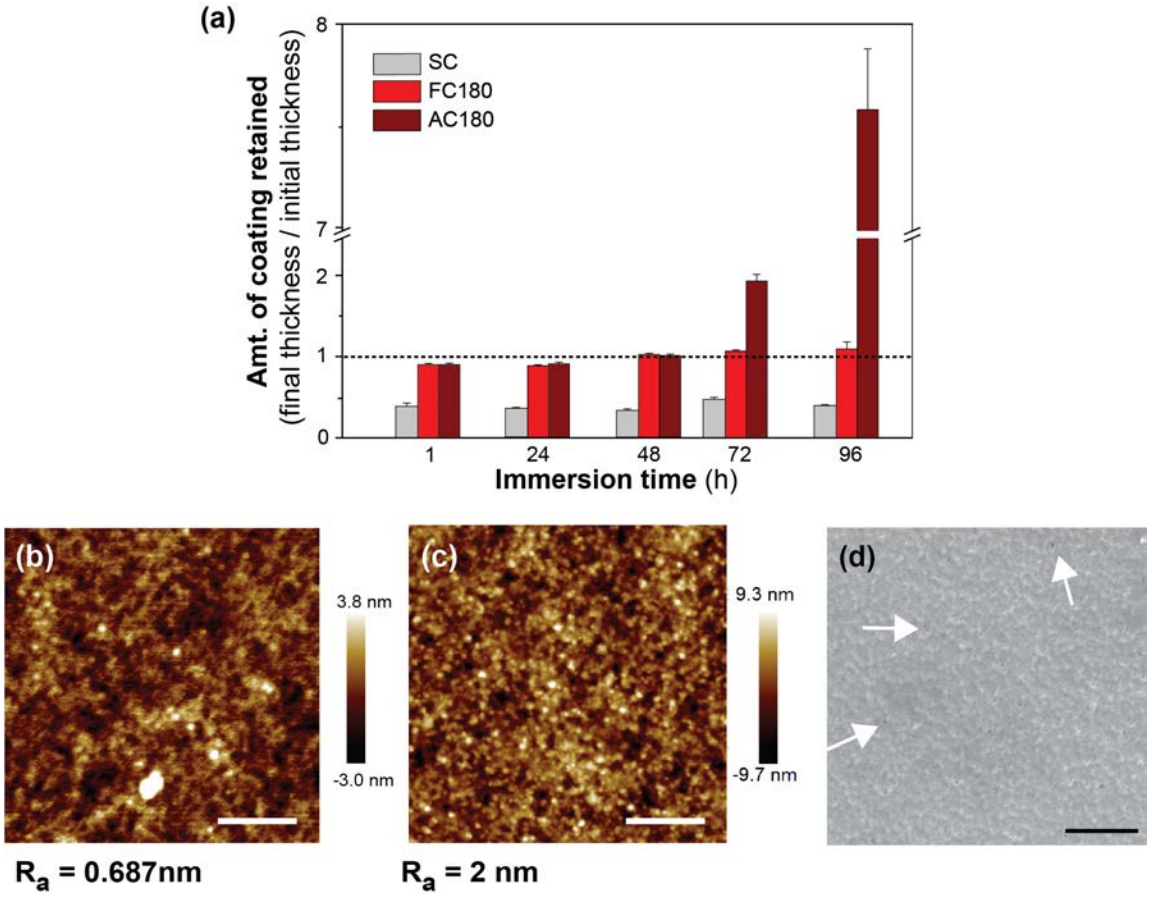

Figure 5.4. Stability of coatings in DPBS: (a) Thickness changes in coatings after immersion in PBS for different time durations. PFHP thermal treatment results in films less prone to swelling (b) and (c) nano-topographies of FC180 and AC180 after immersion in DPBS for 4 days, AC180 has significantly higher roughness compared to FC180. Average roughness calculated on the basis of two images per sample (d) surface morphology of AC180 immersed in PBS. Arrows indicate pores on the surface, which may contribute to increased swelling.

The structure of collagen I plays a key role in interaction with cells and dictates cell behavior such as alignment and phenotype. Based on the swelling studies in **Figure 5.4(a)**, we hypothesized that the rapid increase in swelling of AC180 was most likely a

result of significant denaturation and oxidation of collagen resulting in a gelatin-like[24] material. We evaluated the effect of thermal treatment on the structure of collagen-1 through ATR-FTIR and CD as shown in **Figure 5.5,** to assess the extent of denaturation. [25,26,27] The ATR-FTIR spectra of SC, FC180 and AC180 (**Figure 5.5(a))** all exhibited absorption peaks of amide I (1700-1600 cm^{-1}, C=O stretching vibration), amide II ((1590-1500 cm^{-1}, N-H and C-N stretching vibration), 1454 cm^{-1} (bending vibration), 1300-1000 cm^{-1} (C-O stretching vibration), and amide III (1123, 1225cm^{-1}, the vibrations in C-N and N-H groups of bound amide). [25] The shape of amide I band is characteristic of the collagen secondary structure. Therefore, the Amide I (1700-1600 cm^{-1}) of SC, FC180 and AC180 were deconvoluted, transferred, baselined and resolved as shown in **Figure 5.5(b)**, according to established protocols. [25] The fitting of the band at 1660 cm^{-1} was assigned to prolyl carbonyls directed inside the triple helix (capable of intramolecular hydrogen bonding), and the band at 1630 cm^{-1} was assigned to the random coil form outwards in the triple helix. Thereafter, the calculated ratio of absorbance at 1660 and 1630 cm^{-1} was used to evaluate the denaturation of second structure of amide I. **Figure 5.5(c)** shows the area percentages of each band for different samples. Compared with SC, the ratio of □-helix/random coils decrease slightly for FC180, but strongly for AC180 **(Figure 5.5(c))**. The degree of denaturation, as calculated from **Figure 5.5(c)**, for AC180 and FC180are about 27% and 5% respectively with respect to SC. This indicated that PFHP treatment was able to resist heat-associated denaturation of collagen. This reduced denaturation was further confirmed by the CD spectra as shown in **Figure 5.5(d)**. SC, FC180 and AC180 were examined and compared with a 2 mg/ml Col-I. For SC and FC180, the rotatory maxima and minima are at 221 and 197 nm respectively, and crossover points (zero

rotation) are at approximately 214 nm, which are consistent with the native collagen I solution. However, for AC180, the intensities of rotatory maxima and minima both decrease considerably as compared to SC, indicating significant denaturation.[28] CD spectra of samples incubated in PBS for 4 days post-treatment (**Figure C.5**) also show a similar trend indicating that post-treatment, there is no change in the protein structure and the swelling behavior is solely a result of the denaturation of protein in the air-cured sample.

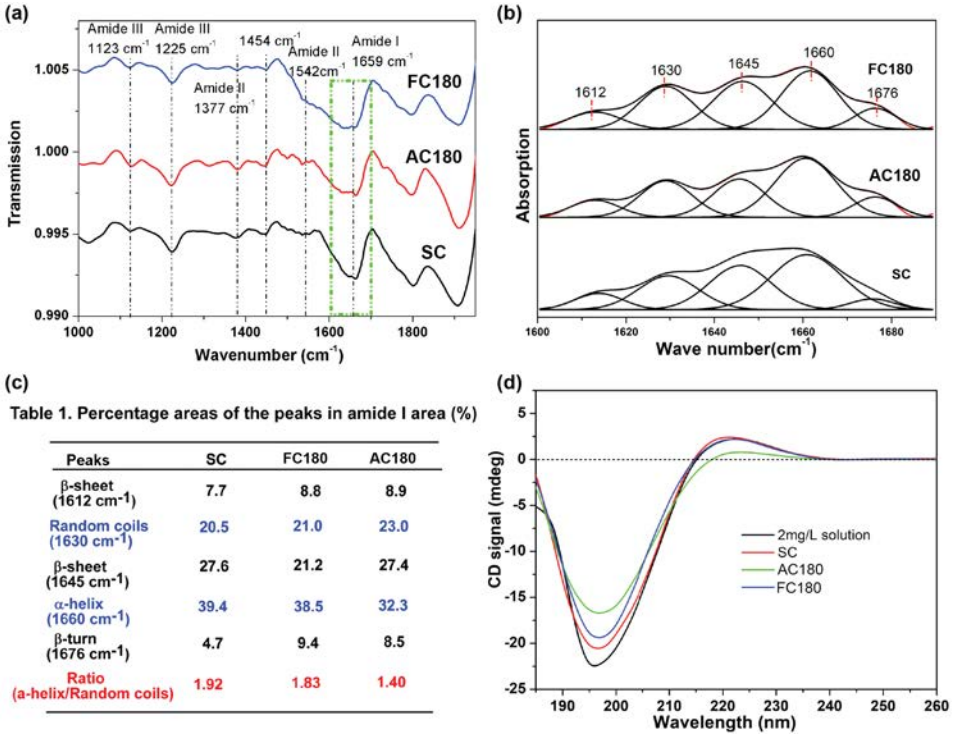

Peaks	SC	FC180	AC180
β-sheet (1612 cm-1)	7.7	8.8	8.9
Random coils (1630 cm-1)	20.5	21.0	23.0
β-sheet (1645 cm-1)	27.6	21.2	27.4
α-helix (1660 cm-1)	39.4	38.5	32.3
β-turn (1676 cm-1)	4.7	9.4	8.5
Ratio (a-helix/Random coils)	1.92	1.83	1.40

Figure 5.5. (a) Fourier-transform infrared spectra of SC, FC180 and AC180; (b) Amide I peak deconvolution of ß-sheet, random coils, □-helix and ß -turn contributes (red lines) elaborated by experimental curves for SC, FC180 and AC180; (c) Percentage areas of different peaks in amide I for SC, FC180 and AC180; (d) CD spectra of SC, FC180 and AC180 compared to Col-I solution. Results indicate significant denaturation of Col-I in the case of AC180.

5.2.3. Evaluating the mechanical and enzymatic stability of fluorous-cured collagen films

Biomaterials are subjects to wear-and-tear during handling and within the body where mechanical failure can result in complications including delayed healing and chronic pain.[29] Improving the mechanical properties of collagen fibers is crucial for biomaterial applications, as mechanical failure is one of the major limitations of collagen-based materials.[30] Furthermore, the mechanical properties of the material must be tunable based on its intended application. For instance, tissue engineering scaffolds must mimic the mechanical properties of native tissue.[3132] Therefore, the ability to tune the mechanical properties of collagen films is important for designing novel biomaterials. We evaluated the mechanical properties of the fluorous-cured coatings by testing the cohesion strength, reduced modulus and hardness. The cohesion strength of the films was evaluated through sonication in aqueous media. Treated and untreated films were sonicated in PBS for 5 and 25 min respectively and thickness before and after treatment was compared **(Figure 5.6(a))** (see also **Figure C.6**). As expected, films treated at 180°C remained stable after 25 min of ultrasound treatment. In contrast, the untreated spin-coated film showed low cohesion strength, with only 50% of the film retained after 5 min of ultrasonic treatment. The thickness of films treated at 75°C reduced by 20% after 5 min and by > 80% after 25 min **(S2).** These results further support our hypothesis that heat treatment induces tighter packing of collagen fibers, thereby increasing the stability and cohesion strength of films. Based on these results, the reduced modulus and hardness of SC, FC180 and AC180 were evaluated through nanoindentation. **Figure 5.6(b)** shows the load-displacement curves obtained through nanoindentation. With increased load, the indenter displaced significantly in the case of SC - ~100 nm during load maintaining and ~190 nm of residual

displacement after unloading. This displacement indicates good plasticity of as-prepared Col-I. In contrast, the displacements for FC180 and AC180 decreased considerably (~ 50 nm during or after loading). The reduced modulus and hardness were calculated and tabulated in **Figure 5.6(c)**. A significant increase in reduced modulus and hardness was observed - ~10 times SC in the case of FC180. Additionally, XPS measurements **(Figure C.7)** showed that no fluorine was incorporated into the film due to the treatment.

Collagen-based coatings are widely studied for wound-healing and tissue repair applications. However, rapid enzymatic digestion of coatings can lead to improper tissue repair due to lack of support for the growing tissue. Ideally, the scaffold should degrade at a rate proportional to the grown of new tissue.[33] For this reason, the ability to tune the rate of degradation of the collagen coating is crucial. We tested the enzymatic degradability of FC180, AC180 and SC by incubating them in trypsin solution for 5-120 min **(Figure 5.6(d))**. After 5 min incubation in trypsin, ~ 70% of the SC film was digested, while both heat-treated films remained relatively stable. However, as treatment was prolonged, marked differences in FC180 and AC180 was observed. After 120 min treatment, while most of the SC and AC180 films were digested, ~30% of the FC180 film was retained. These results indicate that PFHP treatment significantly improved the enzymatic stability of collagen films as compared to untreated collagen films.

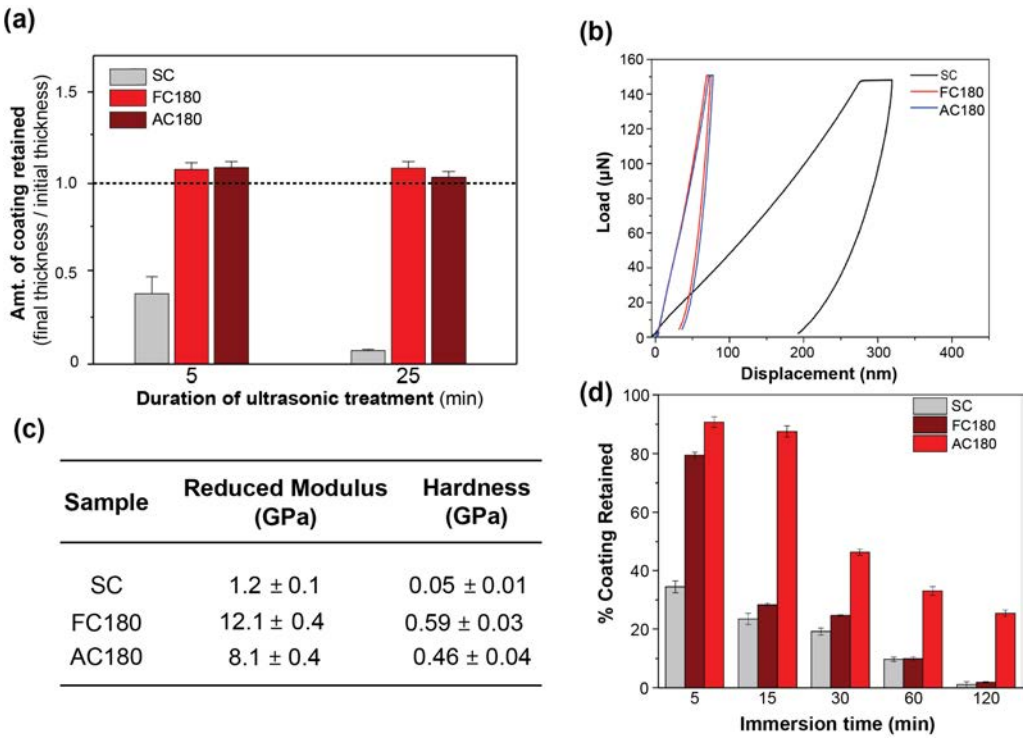

(c)

Sample	Reduced Modulus (GPa)	Hardness (GPa)
SC	1.2 ± 0.1	0.05 ± 0.01
FC180	12.1 ± 0.4	0.59 ± 0.03
AC180	8.1 ± 0.4	0.46 ± 0.04

Figure 5.6. (a) Thickness changes in coatings post ultrasonic treatment in PBS for different time durations. Treated films show greater cohesion strength. Scale bars are 1 μm. b) Load-displacement curves of SC, FC180 and AC180 recorded with increasing the applied load; (c) reduced modulus and hardness calculated and tabulated for SC, FC180 and AC180; PFHP treatment results in mechanically robust films (d) percentage of coatings retained post exposure to enzyme (0.025% trypsin solution) for different durations. PFHP treatment enhances enzymatic stability of collagen films.

5.2.4. Evaluating the cell viability of cells grown on fluorous-cured collagen films

Collagen coatings are widely applied as tissue engineering scaffolds due to their excellent cytocompatibility.[7,8] Surface properties such as chemical composition, nanotopography, and wettability dictate cell behavior such as adhesion, proliferation and differentiation.[34] We therefore evaluated the effect of the PFHP treatment on the cytocompatibility of collagen films by studying the behavior of mouse fibroblasts (L-929) to our treated collagen coatings. Cell adhesion and viability studies were performed on FC180, AC180, SC and bare Si **(Figure 5.7)**. There was no significant statistical difference

in the cell viability of the different coatings, according to the results obtained from the alamar Blue assay **(Figure 5.7(a))**. The % cell viability was calculated with respect to that of bare Si. The cell adhesion and morphology was evaluated through Live/Dead staining in the fluorescence images in **Figure 5.7(b)-(d)**. Most of the cells were live (stained green) indicating that all surfaces exhibited high cell viability. The adherent cells were mostly spherical on Si; larger spindle-like cells were observed on coated surfaces. We therefore concluded that PFHP treatment has no significant effect on the biocompatibility of collagen films.

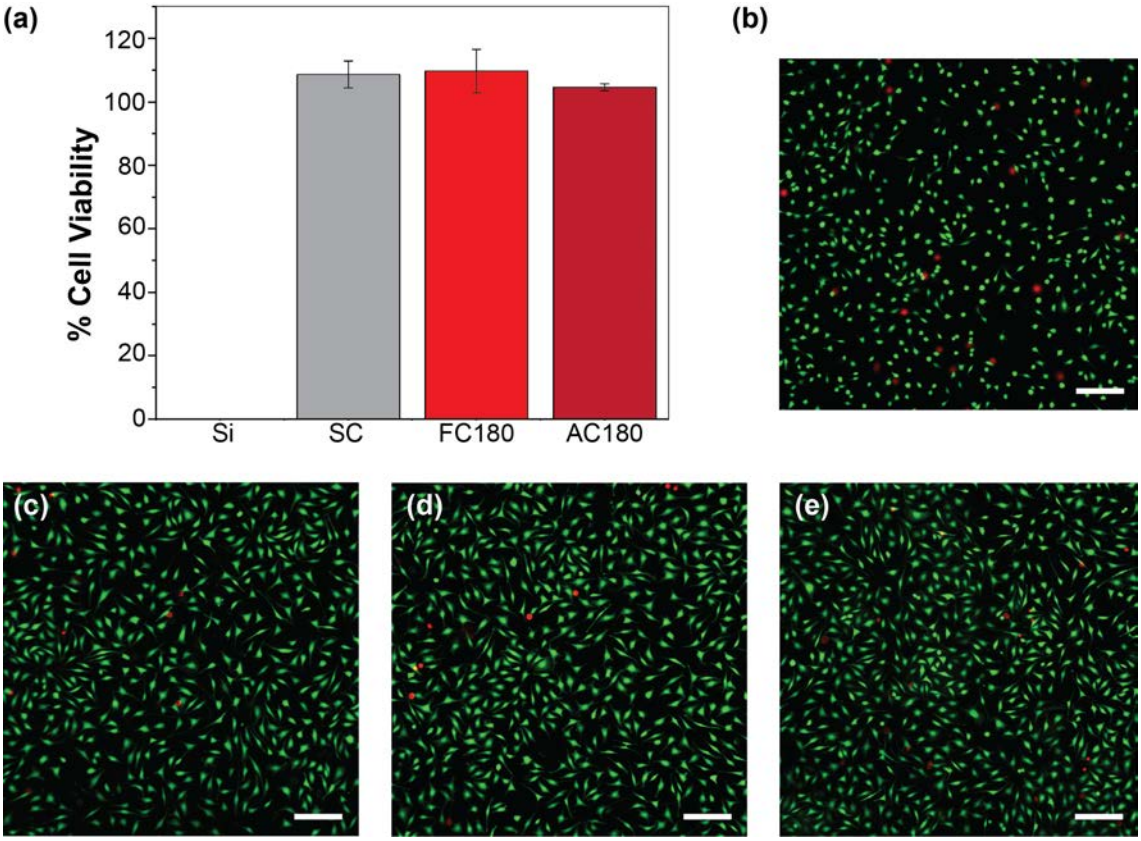

Figure 5.7. (a) % Cell viability of L-929 cells after incubation for 1d with respect to growth control (Bare Si), as determined by alamar Blue assay and (b) Live-dead staining of L-929 cells adhered on the surface of (b) Si, (c) SC, (d)FC180, (e) AC180 after 1d incubation time. No significant effect on viability observed post treatment. % cell viability was calculated with respect to bare Si. Scale bars are 200 μm.

5.3. Conclusions

This study discusses an approach for the fabrication of collagen-based materials utilizing a thermal treatment strategy in a fluorous-based solvent. We demonstrate our ability to enhance the stability relative to uncured or air-cured collagen films and our ability to tune the mechanical properties and enzymatic degradation solely by controlling the temperature of stabilization. Furthermore, the PFHP-based thermal treatment strategy can be successfully used strengthen and stabilize Col I-based biomaterials without compromising biocompatibility and native protein structure. This strategy provides an additive-free approach to design collagen-based biomaterials with improved mechanical and enzymatic stability.

5.4. Experimental Methods

5.4.1. Fabrication of collagen coatings.

Silicon wafers (1cm×1cm, WRS Materials) were ultrasonically washed in ethanol and isopropanol for 10 min each and then treated with oxygen plasma (ITHCA, PDC-001, New York) at an oxygen pressure of 300 Pa for 5 min. A 3 mg/ml Col-I solution (A1048301, Thermo Fisher Scientific) was then spin-coated on cleaned Si wafer at 300 rpm for 50 s. The spin-coated samples were thermally treated in PFHP (perfluoroperhydrophenanthrene, procured from Sigma Aldrich) or air for 15 min at 75, 135 and 180 °C, respectively. Samples were then washed with perfluorohexane (Sigma Aldrich) to remove excess PFHP and dried with a stream N_2 gas. The as spin-coated samples were abbreviated as SC, the samples treated in PFHP solution as FC-T and the

samples treated in air as AC-T, where T represents the temperature according to the treatment.

5.4.2. Structural characterization of collagen films.

The nano-topographies of the coatings were examined by atomic force microscopy (AFM, Bruker Dimension Icon) using Tapping Mode recorded at 2 kHz. The thickness of the coatings was measured by a Rudolph Research Auto EL ellipsometer (GAERTNER Scientific Corporation). Far-UV circular dichroism (CD) spectra were measured on a JASCO J-815 spectropolarimeter (Jasco UK, Essex, UK) with a quartz cuvette at 25 °C. The spectra were recorded from 185 to 260 nm with acetic acid (pH=4) at a rate of 10 nm/min. Attenuated total reflection micro-infrared（ATR-IR）spectra were recorded on a Bruker Vertex70 spectrometer at a spectral resolution of 4 cm^{-1}. The spectra of selected area were dealt with PeakFit4.12（SPSS Inc., Chicago, IL, USA to find the baseline, deconvolve Gaussian IRF, and resolve peaks.

The wettability of different surfaces was determined by measuring the water contact angle through the static sessile drop method (DSA30, Kruss, Germany). A 2.0 μL drop of milliQ water was dropped onto the substrate and an image was captured. The contact angle was then measured by the equipped analysis software (DSAI). This process was repeated thrice per sample to obtain a statistically relevant average.

5.4.3 Stability and mechanical characterization of the collagen films.

The cohesion strength of the collagen films was evaluated by ultrasonic treatment of the coatings in Dulbecco's Phosphate Buffered Saline (DPBS) at 60 Hz for 5 and 25

min. The samples were then gently rinsed with MilliQ water, dried with N_2, and the change in thickness was calculated through ellipsometry measurements.

The stability of collagen was evaluated by its degree of dissolution or swelling in PBS. Different samples were immersed in 1 ml PBS with or without 0.025% trypsin and incubated in an incubator at 37 °C with 5% CO_2 and 95% air for different times. After treatment for pre-determined times, the samples were rinsed with MilliQ water, dried and the thickness change was evaluated as described above. Additionally, the morphologies of FC180 and AC180 after immersed in PBS for 4 days were observed by field emission scanning electron microscope (FESEM, SU6600, Hitachi, Japan) and AFM, respectively.

For the measurements of elastic modulus and hardness, TriboIndenter system (Hysitron TI 950, USA) with a 100 nm spherical indenter was used to perform nanoindentation. Thick Col-I coatings were prepared to minimize the influence of Si substrate on the elastic modulus and hardness measurements. Each Si wafer was carefully drop-casted with 100 μL Col-I solution, dried in vacuum, and then treated in PHFP or air at 180 °C for 15 min to fabricate a coating with thickness more than 500 nm. During each test, the load was increased up to 150 μN with a constant loading rate dP/dt=30 μN/s and kept for 3 s. Four tests were performed on each sample.

5.4.4. Cell adhesion evaluation

Cell culture. The fibroblast cells (L-929) were purchased from the Institute of Biochemistry and Cell Biology of Chinese Academy of Sciences (Shanghai, China).These cells were inoculated in modified Eagle's medium (MEM, Hyclone, USA) containing 10%

fetal bovine serum (Hyclone, USA) and cultured at 37 °C with 5% CO_2. The media was refreshed every other day.

Cell viability assay. The coated Si substrates were placed in 24-well plates. 10^5 cells/ ml were seeded in each well and incubated for 24 h. Viability of fibroblast cells was assessed by the alamarBlue assay (protocol prescribed by the manufacturer-Thermo Fisher Scientific). Additionally, LIVE/DEAD staining was performed using the LIVE/DEAD Viability/Cytotoxicity Kit (Invitrogen, France) as instructed by the manufacturer. The stained cells were observed using epifluorescence (SMZ745T, Nikon, Japan).

5.5. References

1. Sorushanova, A.; Delgado, L. M.; Wu, Z.; Shologu, N.; Kshirsagar, A.; Raghunath, R.; Mullen, A. M.; Bayon, Y.; Pandit, A.; Raghunath, M.; Zeugolis, D.I. The Collagen Suprafamily: From Biosynthesis to Advanced Biomaterial Development. *Advanced Materials*. Wiley-VCH Verlag **2019**.

2. Hosseinkhani, H.; Hiraoka, Y.; Li, C. H.; Chen, Y. R.; Yu, D. S.; Hong, P. Da; Ou, K. L. Engineering Three-Dimensional Collagen-IKVAV Matrix to Mimic Neural Microenvironment. *ACS Chem. Neurosci.* **2013**, *4* (8), 1229–1235.

3. karimizade, A.; takallu, sakine; Mirzaei, E. Evaluating the Effect of PH on Mechanical Strength and Cell Compatibility of Nanostructured Collagen Hydrogel by the Plastic Compression Method. *Nanomedicine J.* **2018**, *5* (3), 180–185.

4. Sun, L.; Li, B.; Yao, D.; Song, W.; Hou, H. Effects of Cross-Linking on Mechanical, Biological Properties and Biodegradation Behavior of Nile Tilapia Skin Collagen Sponge as a Biomedical Material. *J. Mech. Behav. Biomed. Mater.* **2018**, *80*, 51–58.

5. Gautieri, A.; Vesentini, S.; Redaelli, A.; Buehler, M. J. Hierarchical Structure and Nanomechanics of Collagen Microfibrils from the Atomistic Scale Up. *Nano Lett.* **2011**, *11* (2), 757–766.

6. Tapeinos, C.; Larrañaga, A.; Sarasua, J. R.; Pandit, A. Functionalised Collagen Spheres Reduce H2O2 Mediated Apoptosis by Scavenging Overexpressed ROS. *Nanomedicine Nanotechnology, Biol. Med.* **2018**, *14* (7), 2397–2405.

7. Kaczmarek, B.; Sionkowska, A.; Gołyńska, M.; Polkowska, I.; Szponder, T.; Nehrbass, D.; Osyczka, A. M. In Vivo Study on Scaffolds Based on Chitosan, Collagen, and Hyaluronic Acid with Hydroxyapatite. *Int. J. Biol. Macromol.* **2018**, *118* (Pt A), 938–944.

8. Pettian, M. S.; Plepis, A.M.G.; Martins, V.D.C.A; Dos Santos, G.R..; Pinto, C.A.L.; Galdeano, E. A.; Calegari, A.R.A; de Moraes, C.A.; Cunha, M.R.D. Use of an Anionic Collagen Matrix Made from Bovine Intestinal Serosa for in Vivo Repair of Cranial Defects. **2018**.

9. Gaspar-Pintiliescu, A.; Seciu, A. M.; Miculescu, F.; Moldovan, L.; Ganea, E.; Craciunescu, O. Enhanced Extracellular Matrix Synthesis Using Collagen Dressings Loaded with Artemisia Absinthium Plant Extract. *J. Bioact. Compat. Polym.* **2018**, *33* (5), 516–528.

10. Zhang, D.; Wu, X.; Chen, J.; Lin, K. The Development of Collagen Based Composite Scaffolds for Bone Regeneration. *Bioactive Materials*. KeAi Communications Co. March 1, 2018, pp 129–138.

11. Ferreira, A. M.; Gentile, P.; Chiono, V.; Ciardelli, G. Ferreira, A. M., Gentile, P., Chiono, V., & Ciardelli, G. (2012). Collagen for Bone Tissue Regeneration. *Acta Biomater.* **2012**, *8* (9), 3191–3200.

12. Ryan, A. J.; Kearney, C. J.; Shen, N.; Khan, U.; Kelly, A. G.; Probst, C.; Brauchle, E.; Biccai, S.; Garciarena, C. D.; Vega-Mayoral, V.; Loskill, P.; Kerrigan, S.W.; Schenke-Leyland, K.; Coleman, J.N.; O'Brien, F.J. Electroconductive Biohybrid Collagen/Pristine Graphene Composite Biomaterials with Enhanced Biological Activity. *Adv. Mater.* **2018**, *30* (15), e1706442.

13. Terzi, A.; Storelli, E.; Bettini, S.; Sibillano, T.; Altamura, D.; Salvatore, L.; Madaghiele, M.; Romano, A.; Siliqi, D.; Ladisa, M.; De Caro, L.; Quattrini, A.; Valli, L.; Sannino, A.; Giannini, C. Effects of Processing on Structural, Mechanical and Biological Properties of Collagen-Based Substrates for Regenerative Medicine. *Sci. Rep.* **2018**, *8* (1).

14. Koide, M.; Osaki, K.; Konishi, J.; Oyamada, K.; Katakura, T.; Takahashi, A.; Yoshizato, K. A New Type of Biomaterial for Artificial Skin: Dehydrothermally Cross-Linked Composites of Fibrillar and Denatured Collagens. *J. Biomed. Mater. Res.* **1993**, *27* (1), 79–87.

15. Sionkowska, A.; Skopinska-Wisniewska, J.; Gawron, M.; Kozlowska, J.; Planecka, A. Chemical and Thermal Cross-Linking of Collagen and Elastin Hydrolysates. *Int. J. Biol. Macromol.* **2010**, *47* (4), 570–577.

16. Samouillan, V.; Delaunay, F.; Dandurand, J.; Merbahi, N.; Gardou, J.-P.; Yousfi, M.; Gandaglia, A.; Spina, M.; Lacabanne, C. The Use of Thermal Techniques for

the Characterization and Selection of Natural Biomaterials. J. Funct. Biomater. 2011, 2 (3), 230–248.

17. Zhu, D.-W. Perfluorocarbon Fluids: Universal Suspension Polymerization Media. *Macromolecules* **1996**, *29* (8), 2813–2817.

18. Marsh, E. N. G. Fluorinated Proteins: From Design and Synthesis to Structure and Stability. *Acc. Chem. Res.* **2014**, *47* (10), 2878–2886.

19. Asakura, T.; Adachi, K.; Schwartz, E. Stabilizing Effect of Various Organic Solvents on Protein. *J Bio. Chem.* **1978** 253, 6423-6423.

20. Uversky, V. N.; Narizhneva, N. V.; Kirschstein, S. O.; Winter, S.; Löber, G. Conformational Transitions Provoked by Organic Solvents in β-Lactoglobulin: Can a Molten Globule like Intermediate Be Induced by the Decrease in Dielectric Constant? Fold. Des. 1997, 2 (3), 163–172.

21. Wang, L. S.; Gopalakrishnan, S.; Lee, Y. W.; Zhu, J.; Nonnenmann, S. S.; Rotello, V. M. Translation of Protein Charge and Hydrophilicity to Materials Surface Properties Using Thermal Treatment in Fluorous Media. *Mater. Horizons* **2018**, *5* (2), 268–274.

22. Madaghiele M.; Calo E.; Salvatore L.; Bonfrate V.; Pedone D.; Frigione M.; Sannino A.; Assessment of collagen crosslinking and denaturation for the design of regenerative scaffolds. *J Biomed Mater Res Part A:* **2016** 104A: 186-194,

23. Millington, K. R.; Ishii, H.; Maurdev, G. Chemiluminescence from Thermal Oxidation of Amino Acids and Proteins. *Amino Acids* **2010**, *38* (5), 1395–1405.

24. Bozec, L.; Odlyha, M. Thermal Denaturation Studies of Collagen by Microthermal Analysis and Atomic Force Microscopy. Biophys. J. 2011, 101 (1), 228–236.

25. Payne, K. J.; Veis, A. Fourier Transform Ir Spectroscopy of Collagen and Gelatin Solutions: Deconvolution of the Amide I Band for Conformational Studies. *Biopolymers* **1988**, *27* (11), 1749–1760.

26. Silva, Z. S.; Botta, S. B.; Ana, P. A.; França, C. M.; Fernandes, K. P. S.; Mesquita-Ferrari, R. A.; Deana, A.; Bussadori, S. K. Effect of Papain-Based Gel on Type I Collagen - Spectroscopy Applied for Microstructural Analysis. *Sci. Rep.* **2015**, *5*.

27. De Campos Vidal, B.; Mello, M. L. S. Collagen Type I Amide I Band Infrared Spectroscopy. *Micron* **2011**, *42* (3), 283–289.

28. Kandamchira, A.; Selvam, S.; Marimuthu, N.; Janardhanan, S. K.; Fathima, N. N. Influence of Functionalized Nanoparticles on Conformational Stability of Type I

Collagen for Possible Biomedical Applications. *Mater. Sci. Eng. C. Mater. Biol. Appl.* **2013**, *33* (8), 4985–4988.

29. Prasad, K.; Bazaka, O.; Chua, M.; Rochford, M.; Fedrick, L.; Spoor, J.; Symes, R.; Tieppo, M.; Collins, C.; Cao, A.; Markwell, D.; Ostrikov, K.K.; Bazaka, K. Metallic Biomaterials: Current Challenges and Opportunities. *Materials*. MDPI AG July 31, 2017.

30. Meyer, M. Processing of Collagen-Based Biomaterials, and the Resulting Materials Properties. *Biomed. Eng. Online* **2019**, *18* (1).

31. Akhmanova, M.; Osidak, E.; Domogatsky, S.; Rodin, S.; Domogatskaya, A. Physical, Spatial, and Molecular Aspects of Extracellular Matrix of in Vivo Niches and Artificial Scaffolds Relevant to Stem Cells Research. Stem Cells Int. 2015, 2015.

32. Guarino, V.; Raucci, M. G.; Ronca, A.; Cirillo, V.; Ambrosio, L. Multifunctional Scaffolds for Bone Regeneration. In Bone Substitute Biomaterials; Elsevier Inc., 2014; pp 95–117.

33. Zhang, L.; Liu, X.; Li, G.; Wang, P.; Yang, Y. Tailoring Degradation Rates of Silk Fibroin Scaffolds for Tissue Engineering. J. Biomed. Mater. Res. Part A 2019, 107 (1), 104–113.

34. Richbourg, N. R.; Peppas, N. A.; Sikavitsas, V. I. Tuning the Biomimetic Behavior of Scaffolds for Regenerative Medicine through Surface Modifications. *Journal of Tissue Engineering and Regenerative Medicine*. John Wiley and Sons Ltd 2019.

CHAPTER 6

IN VITRO CELL CULTURE MODELS FOR ULTRASOUND TREATMENTS USING COLLAGEN-BASED MATERIALS

6.1 Introduction

Ultrasound treatment has gained interest as a therapeutic strategy owing to its enhanced tissue penetration,[1, 2] versatile applications,[3, 4, 5, 6, 7] easy accessibility,[8, 9] and minimally invasive procedures.[10, 11] The frequency of ultrasound is easily modulated to localize desired biological effects such as thermal ablation of tissue, cavitation-induced cell permeability, and gas body activation.[3] Ultrasound activatable materials, such as alginate hydrogels, are utilized for developing drug-loadable scaffolds for triggerable and localized drug delivery.[12, 13, 14] More recently, sonodynamic therapy-based approaches have gained interest as potential antimicrobial and anti-cancer strategies where ultrasound is used in combination with sonosensitizers to trigger generation of ROS species.[15, 16, 17] Consequently, ultrasound treatment has been utilized for a variety of applications including – controlled and triggered drug release,[12, 13, 14] sonodynamic therapy,[15, 16, 17] targeted tissue ablation,[18, 19] and enhancing the penetration of drugs.[1, 2]

However, the ability to study and explore new ultrasound-based therapeutic strategies is limited by the dearth of effective *in vitro* models that predict the effects of ultrasound-based treatments.[20] Cells grown *in vitro* often experience different biomechanical environments as compared to cells in native tissue.[21] In the native tissue, the extracellular matrix absorbs a significant amount of ultrasonic energy during treatment, thereby protecting the cells from lysis. In the absence of the ECM *in vitro*, cells are more prone to lysis.[22] This results in inconclusive results from *in vitro* studies and often animal

models have to be utilized to assess the safety and efficacy of ultrasound. However, utilizing *in vivo* models for high throughput testing and screening is expensive and time consuming. For this reason, there is a need for effective *in vitro* models that mimic the mechanical environment of native tissue to enable translation of ultrasound-based therapeutic strategies

We utilized collagen-based materials to generate two-dimensional and three-dimensional cell culture models for ultrasound treatments. Collagen is a natural biopolymer and the primary component of the ECM in native tissues.[23] Therefore, it is inherently biocompatible and non-toxic.[24] Furthermore, there are numerous fabrication strategies available to generate collagen-based materials, such as films and hydrogels, with varying mechanical properties.[25, 26] We hypothesized that the collagen matrix will mimic the ECM, absorbing the mechanical energy generated during ultrasound treatment thereby preserving the cells. We evaluated this using two different types of materials as a support for culturing 3T3 fibroblast cells – 2D collagen coatings and 3D collagen hydrogels.[27, 28] Summarized below is the strategy for fabricating both types of scaffolds, culturing 3T3 cells and conducting ultrasound treatment, and evaluating cell viability. Our results indicated that both the 2D and 3D cell cultures are effective *in vitro* models with different advantages and limitations, as indicated in **Figure 6.1**. The 2D collagen film is easy and quick to prepare and utilizes small amounts of materials. Therefore, this is ideal for preliminary studies and for testing a large number of conditions. However, it cannot withstand prolonged exposure to ultrasound. On the other hand, the 3D hydrogel effectively protects the cells from prolonged exposure to ultrasound and is more representative of native tissue. However, 3D cultures utilize significantly more material

and take longer to fabricate (~ 1 week). Overall, both strategies are potential *in vitro* models for testing ultrasound-based therapies and may be utilized for validating a variety therapeutic applications.

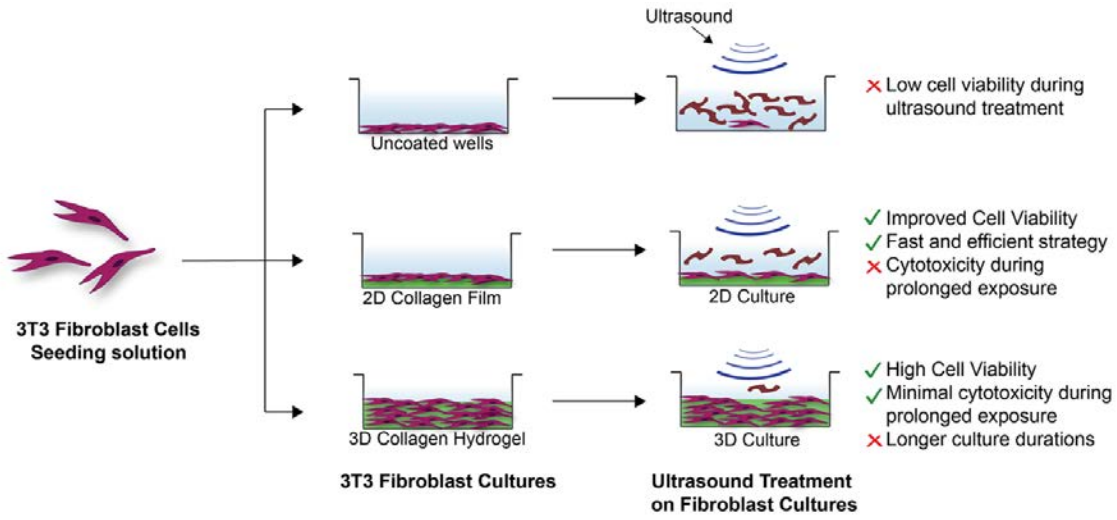

Figure 6.1. Schematic describing 3T3 Fibroblast cells cultured on (top to bottom) uncoated wells , 2D collagen films, and within 3D collagen hydrogels. Cells cultured on uncoated wells show uncontrolled and rapid cell lysis. Cells cultured on collagen films withstand some ultrasound exposure, while cells cultured within the 3D hydrogels withstand prolonged ultrasound exposure.

6.2. Protocols

6.2.1. Protocol 1 - 2D Cell culture

Step 1: Fabrication of 2D collagen coatings

Materials. Fisherbrand sterile 12 well plates (used for all cell cultures), Gibco rat tail collagen 1 solution (concentration 3mg/mL) and phosphate buffer saline (PBS) were purchased from Fisher Scientific. Deionized water produced by a Millipore System (MilliQ water) was utilized post sterilization by autoclaving. All procedures were performed under sterile conditions in a BSL 2 facility inside a biosafety cabinet.

Procedure.

1. Coatings were always prepared in a BSL 2 facility inside a biosafety cabinet to maintain sterile conditions at all times.
2. Coating solution was prepared by diluting the collagen 1 solution in milliQ water to a final concentration of 1 mg/mL. Sufficient solution was prepared to coat all the wells needed to perform the experiment.
3. Following this, 1 mL of the coating solution was placed in each well of a sterile 12 well plate. The plate was then incubated at 37 oC for 30 min to allow for the formation of collagen film. Appropriate number of wells were left uncoated for control groups.
4. The excess collagen solution was then removed, and the coated wells were washed three times using PBS.
5. Plates were then used immediately for cell culture.

Step 2: Fibroblast culture on 2D collagen films

Materials. NIH-3T3 fibroblast cells were purchased from ATCC (ATCC CRL-1658). Dulbecco's modified Eagle's medium (DMEM), fetal bovine serum(FBS), 0.05% trypsin-EDTA, 100X penicillin-streptomycin antibiotic solution, trypan blue and phosphate buffer saline (PBS) were purchased from Fisher Scientific. DMEM was spiked with 10% v/v FBS and 1% v/v antibiotic solution to make the complete growth medium.

Procedure.

Thawing

1. A frozen stock (~1 mL) of NIH-3T3 fibroblast cells was thawed rapidly (<1 minute) in a 37oC water bath.
2. Thawed cells were washed by diluting with 9 mL pre-warmed complete growth medium and then centrifuged at 3000rpm for 5 min to prepare a cell pellet.
3. The growth medium was then removed without disturbing the pellet and the cells were redispersed in 9 mL fresh growth medium to prepare the cell solution.
4. This cell solution was then transferred completely to a T-75 culture flask for further culturing.

Cell culture and cell counting.

1. Once the cells were 80-90% confluent, the growth medium was removed and washed with PBS.
2. The cells were then trypsinized with ~3mL of 0.05 % Trypsin-EDTA and incubated at 37oC for 5-7 mins to allow the cells to detach.
3. Once the cells were detached, 7mL of complete medium was added to neutralize the trypsin.
4. The cell solution was then collected in a 15mL Falcon tube and centrifuged at 3000rpm for 5 minutes to collect the cell pellet.
5. The growth medium was removed without disturbing the pellet and resuspended with fresh complete growth medium accordingly.
6. 10uL of cell solution was taken in an Eppendorf tube and mixed with 10uL of trypan blue. 10uL of this mixture was then added to one side of the disposable cell

counting chamber slide and inserted into the Invitrogen Countess II Automated Cell Counter machine to count the number of cells in the cell solution.

Cell Plating. The cell solution was diluted to 100,000 cells/well and plated on uncoated or collagen-coated wells in a 12-well plate and allowed to grow overnight at 37oC in a humidified atmosphere of 5% CO2 and were treated with ultrasound the following day.

Cell Splitting. The remaining cell solution was split in a ratio of 1:10 into a new culture flask and sub-cultured every 2 days for further experiments.

6.2.2. Protocol 2 - 3D Cell culture

Materials. Fisherbrand sterile 12 well plates (used for all cell cultures) and phosphate buffer saline (PBS) were purchased from Fisher Scientific. Deionized water produced by a Millipore System (MilliQ water) was utilized post sterilization by autoclaving. Fetal Bovine Serum (FBS) was purchased from Peak Serum. Dulbecco's Modified Eagle Medium 1x (DMEM) with 4.5 g/L D-Glucose, L-Glutamine and 110 mg/L Sodium Pyruvate was purchased from Fisher Scientific. HEPES solution was purchased from Millipore Sigma. Penicillin and Streptomycin (P/S) were purchased from Invitrogen. Bovine tendon type I collagen was purchased from Organogenesis. Minimum essential medium with Earle's salts (MEM 10x), L-glutamine and sodium bicarbonate was purchased from Cambrex. All reagents were utilized as obtained from the vendor without additional purification, unless otherwise specified. All procedures were performed under sterile conditions in a BSL 2 facility inside a biosafety cabinet.

Procedure. The protocol described in ref 27 was utilized for fabricating the 3D cell cultures.

Step 1: Preparation of components 24 hr prior

1. The conditioned media was prepared by using Gibco's DMEM 1x and mixing it with 10% FBS, 1% P/S and 1% HEPES under sterile conditions.
2. The following were placed in the refrigerator at 4 ºC 24 hr before fabrication of gels - FBS, glutamine, DMEM, sodium bicarbonate, pipette tips (p1000, p200), 15 mL Falcon tubes, and 12 well culture plates.
3. Sodium bicarbonate (1M) was sterilized using a PTFE syringe filter with pore size 0.22um. Forceps were sterilized by autoclaving prior to use.
4. Cells were thawed and cultured in a T-75 flask through the procedure described above and grown to 80-90% confluency before the next step.

Step 2: Preparation of the cell seeding solution.

1. Once the cells reached 80-90% confluency, the growth medium was carefully extracted from the flask and replaced with 5 mL of PBS that was warmed in a water bath at 37 ºC.
2. Cells were then washed by gentle swirling and the PBS was carefully removed and discarded from the flask.
3. Following this, 2 mL of 0.05% trypsin-EDTA was added to the flask and incubated at 37°C for 8-10 minutes to detach the cells.
4. Once the cells were detached, ~ 6 mL of conditioned DMEM medium was added to neutralize the trypsin and dilute the solution.

5. The cell solution was then placed in a 15 mL Falcon tube and centrifuged at 1,000 rpm for 10 min at 4 ^{o}C.
6. Excess medium was carefully extracted without disturbing the cell pellet and the cells were resuspended in 15 mL of fresh growth medium.
7. 10 µL of cell solution from above was added to a sterile 1.5 mL Eppendorf tube along with 40 µL of fresh growth DMEM medium and 50 µL of Trypan Blue. Cells were resuspended and 10 µL was extracted and placed on a hemocytometer for counting.
8. Finally, 3.22 mL of cell seeding solution was prepared at the concentration of 300,000 cells/ mL.

Step 3: Casting 3D collagen gels

1. The cell seeding solution, growth medium, two 50 mL Falcon tubes, collagen 1 solution, sterile $NaHCO_3$ solution, 12 well plates, and transfer pipets were all placed in an ice bath to maintain low temperature. Care was taken to keep all components cold during the experiment.
2. One of the two Falcon tubes were used to prepare the cell-collagen solution (Tube 1) while the other was used to prepare the cell-free control collagen solution (Tube 2). Each tube was prepared with the components described in **Table 6.1** and mixed well by pipetting back and forth several times. The final solution should be a straw color or darker. If lighter, more $NaHCO_3$ solution was added in 80 µL increments until the desired color was formed.

3. **To Tube 1**, 3.22 mL of the cell seeding solution was added after thorough mixing. The contents of Tube 1 were then mixed well by pipetting back and forth several times. Following this 2 mL of solution was placed in each well of a 12 well plate. This solution formed about 18 gels. Care was taken to minimize formation of bubbles during mixing.
4. **To Tube 2,** 804 µL of DMEM was added to prepare the cell-free control gels. The solution was mixed well as described above and 2 mL of the solution was placed in each well of a 12 well plate. This solution formed about 4 gels.
5. Gels were incubated at 37 ^{o}C and 7.5% CO_2 for 1 hr, to firm up. A pink coloration was observed when the gels were firm.
6. The cells were fed with 2 mL of warm growth medium every other day for a total of 7 days before proceeding with ultrasound treatment.

omponents	**Amount in Tube 1**	**Amount in Tube 2**
0 x MEM	3.5 mL	875 µL
- Glutamine	316 µL	79 µL
BS	3.92 mL	980 µL
NaHCO3 solution	1089 µL	273 µL
ollagen	29.17 mL	7.3 mL

Table 6.1. Table summarizes volume of each component added to Tube 1 and Tube 2 to prepare 18 and 4 gels respectively. Components must be adjusted to prepare more gels while keeping the ratio same.

6.2.3. Protocol 3 – Ultrasound treatment

Equipment. Ultrasound treatment was done using a 130-watt vibracell ultrasonic processor (VCX 130) with a 6 mm probe purchased from Sonics & Materials INC and was utilized at 35% amplitude for the time durations specified.

Procedure

1. Each well was topped off with enough media to ensure a final volume of 2 mL.
2. The ultrasound probe was dipped into the center of the well to ~ 1-2 mm depth. This is to ensure proper ultrasound exposure throughout the treatment duration.
3. Ultrasound treatments were done for 75, 150 and 300 seconds on cells cultured on both the 2D and 3D cultures. Each ultrasound treatment condition was repeated on at least 3 different wells. At least 3 wells in each culture were left untreated to serve as negative (growth) controls. See **Figure 6.2** for experimental set up.
4. Step 3 was repeated on uncoated 12 well plates were also treated with 75, 150 and 300 seconds of ultrasound treatment to serve as positive controls.

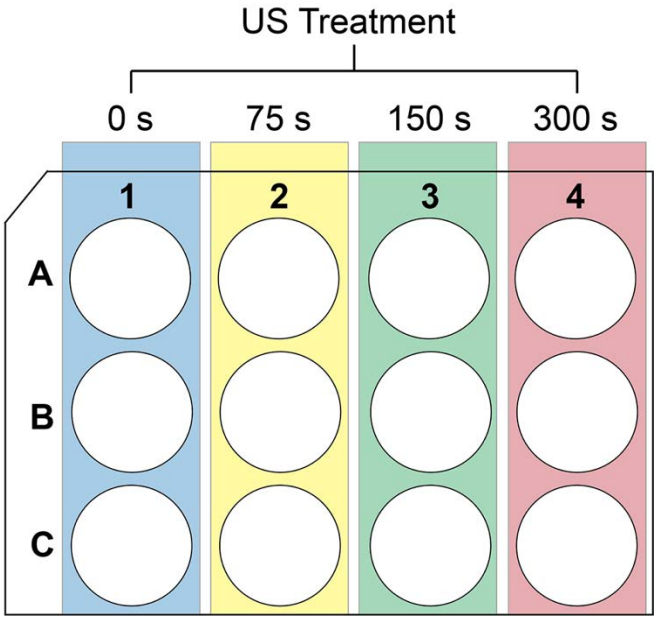

Figure 6.2. Schematic representation for conducting ultrasound treatment on a 12 well plate. Each treatment condition (yellow, green and red) were replicated three times. Blue column represents the untreated negative (growth) controls. A similar set up was utilized for uncoated or collagen-coated plates (2D cultures) or plates containing 3D collagen hydrogel cultures.

6.2.4. Protocol 4 – Determining cell viability post ultrasound treatment.

Materials and Equipment. The thermo scientific alamarBlue dye was purchased from Fisher Scientific. Fluorescence signal was measured on a SpectraMax 2 plate reader from Molecular Devices.

Procedure.

1. The protocol provided by the manufacturer for planktonic cells was utilized. This was done because ultrasound treatment may displace adherent cells but not necessarily result in cell death. Therefore, this strategy was able to measure all viable cells even if they are not adhered to the bottom of the well post treatment.

2. After the US treatment, each cell culture well of the 12 well plates was spiked with 200 μL of alamarBlue solution. The solution in each well was mixed by gently pipetting back and forth a few times and all the plates were incubated at 37 °C for 3 hours.

3. Simultaneously, 6 wells on a black 96 well plate were filled with 100 μL of the same DMEM media used for cell culture, spiked with 10 μL, mixed well, and incubated at 37 °C for 3 hours along with the cell culture plates. This will act as the reference value for the baseline signal from the media, when calculating the cell viability.

4. After 3 hours, 330 μL of supernatant was removed from each cell culture well (from step 2) and placed into three separate wells (110 μL each) of the black 96 well plate with the reference prepared in step 3. This ensures that each cell culture well is being measured at least 3 times.

5. As each treatment condition (described in the section - procedure for ultrasound treatment) was replicated 3 times and each cell culture well was sampled 3 times (described in step 4), the final measurements include 9 measurements per treatment condition. The final measurements must also include 9 measurements from both the positive and negative controls described previously.

6. Finally, the fluorescence signal from each well of the black 96 well plate was measured at excitation wavelength of 560 nm and emission of 590 nm.

7. % Cell viability was calculated for each treatment condition using the formula –

$$\%Cell\ viability = \frac{Fluor.signal\ from\ treated\ well - Fluor.signal\ from\ reference}{Fluor.signal\ from\ negative\ (growth) control - Fluor.\ signal\ from\ reference} \times 100$$

8. Average %Cell viability and standard deviation were obtained from the replicates described in step 5 and reported in Method Validation. This protocol was repeated two additional times to ensure reproducibility.

6.3. Protocol Validation

Figure 6.3 shows the %cell viability for different durations of ultrasound treatment for 2D cell cultures on uncoated and collagen coated substrates as well as a 3D cell culture in collagen hydrogels. As seen in Figure 3, cells grown on uncoated plates (green bars) show minimal resilience against ultrasound, with only ~10% of the cells surviving after 75 seconds of ultrasound treatment. By comparison, the 2D collagen scaffold (orange bars) increases the cell viability dramatically, with over 50% cells surviving 75 s of ultrasound treatment. However, prolonged treatment results in increased cell death. In the case of the 3D collagen hydrogels, > 80% of the cells survive even after 300 s of ultrasound treatment (as seen by the blue bars).

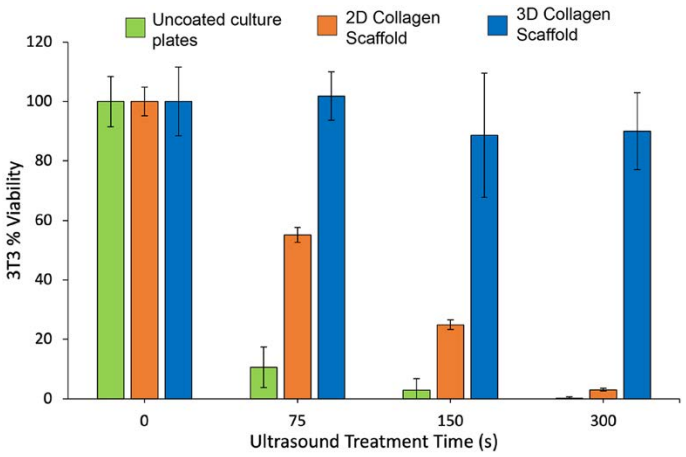

Figure 6.3. %Cell viability post ultrasound treatment for cells grown on uncoated plates (green), plates containing 2D collagen scaffold (orange), and plates containing 3D collagen scaffold (blue). 2D scaffold results in ~40% increase in cell viability while 3D scaffold results in ~90% increase.

6.4. Conclusions

We therefore concluded that collagen-based materials significantly increase the resilience of cells against ultrasound treatment by mimicking the extracellular matrix in tissue and absorbing some of the mechanical energy generated by the ultrasound. The 2D collagen scaffold offers a rapid and efficient way to test ultrasound-based treatments, as the experiment can be conducted within 24 hr and requires only a small amount of material. This strategy is therefore ideal for preliminary experiments or experiments with short duration of ultrasound exposure (~1 min). On the contrary, 3D cultures take ~1 week and significantly higher amounts of collagen to fabricate. However, the 3D cultures provide significantly more protection from prolonged exposure to ultrasound treatment and are therefore more representative of native tissue. Taken together, these collagen-based 2D and 3D cultures have the potential to serve as in vitro model for testing ultrasound-based treatment strategies for a variety of applications such as controlled drug delivery, anti-cancer, and antimicrobial strategies.

6.5. References

1. Deprez, J.; Lajoinie, G.; Engelen, Y.; De Smedt, S. C.; Lentacker, I. Opening Doors with Ultrasound and Microbubbles: Beating Biological Barriers to Promote Drug Delivery. *Adv. Drug Deliv. Rev.* **2021**, *172*, 9–36.

2. Low, S. S.; Lim, C. N.; Yew, M.; Chai, W. S.; Low, L. E.; Manickam, S.; Tey, B. T.; Show, P. L. Recent Ultrasound Advancements for the Manipulation of Nanobiomaterials and Nanoformulations for Drug Delivery. *Ultrason. Sonochem.* **2021**, *80*, 105805.

3. Miller, D. L.; Smith, N. B.; Bailey, M. R.; Czarnota, G. J.; Hynynen, K.; Makin, I. R. S. Overview of Therapeutic Ultrasound Applications and Safety Considerations. *J. Ultrasound Med.* **2012**, *31* (4), 623.

4. Xu, C.; Wang, Y.; Wang, E.; Yan, N.; Sheng, S.; Chen, J.; Lin, L.; Guo, Z.; Tian, H.; Chen, X.; et al. Effective Eradication of Tumors by Enhancing Photoacoustic-Imaging-Guided Combined Photothermal Therapy and Ultrasonic Therapy. *Adv. Funct. Mater.* **2021**, *31* (10), 2009314.

5. Kataoka, Y.; Kunimitsu, M.; Nakagami, G.; Koudounas, S.; Weller, C. D.; Sanada, H. Effectiveness of Ultrasonic Debridement on Reduction of Bacteria and Biofilm in Patients with Chronic Wounds: A Scoping Review. *Int. Wound J.* **2021**, *18* (2), 176–186.

6. El Tayeb, M. N.; Hassan, A. A.; Abuelnaga, Y. G.; Eid, P. M.; Tarkhan, Y. M.; Fathallah, M. M.; Awad, A. A.; Nabhan, A. F. Low Level Laser Therapy versus Ultrasonic Therapy for the Treatment of Shoulder Impingement Syndrome A Systematic Review of Randomized Controlled Trials. *QJM An Int. J. Med.* **2021**, *114* (Supplement_1).

7. Gorick, C. M.; Chappell, J. C.; Price, R. J. Applications of Ultrasound to Stimulate Therapeutic Revascularization. *Int. J. Mol. Sci. 2019, Vol. 20, Page 3081* **2019**, *20* (12), 3081.

8. Kamel, R. K.; Mahdy, E. W.; Elsayed, M. M. Updates on Role of Ultrasound in Intensive Care Unit. *Benha J. Appl. Sci.* **2021**, *6* (4), 133–140.

9. Kumar Sahu, A.; Rath, P.; Aggarwal, B. Ultrasound-Guided Injections in Musculo-Skeletal System - An Overview. *J. Clin. Orthop. Trauma* **2019**, *10* (4), 669–673.

10. Posarelli, C.; Covello, G.; Bendinelli, A.; Fogagnolo, P.; Nardi, M.; Figus, M. High-Intensity Focused Ultrasound Procedure: The Rise of a New Noninvasive Glaucoma

Procedure and Its Possible Future Applications. *Surv. Ophthalmol.* **2019**, *64* (6), 826–834.

11. Xu, Z.; Hall, T. L.; Vlaisavljevich, E.; Lee, F. T. Histotripsy: The First Noninvasive, Non-Ionizing, Non-Thermal Ablation Technique Based on Ultrasound. **2021**, *38* (1), 561–575.

12. Huebsch, N.; Kearney, C. J.; Zhao, X.; Kim, J.; Cezar, C. A.; Suo, Z.; Mooney, D. J. Ultrasound-Triggered Disruption and Self-Healing of Reversibly Cross-Linked Hydrogels for Drug Delivery and Enhanced Chemotherapy. *Proc. Natl. Acad. Sci. U. S. A.* **2014**, *111* (27), 9762–9767.

13. Ahmad, T.; McGrath, S.; Sirafim, C.; Do Amaral, R. J. F. C.; Soong, S. L.; Sitram, R.; Turkistani, S.; Santarella, F.; Kearney, C. J. Development of Wound Healing Scaffolds with Precisely Triggered Sequential Release of Therapeutic Nanoparticles. *Biomater. Sci.* **2021**, *9* (12), 4278–4288.

14. Kearney, C. J.; Skaat, H.; Kennedy, S. M.; Hu, J.; Darnell, M.; Raimondo, T. M.; Mooney, D. J. Switchable Release of Entrapped Nanoparticles from Alginate Hydrogels. *Adv. Healthc. Mater.* **2015**, *4* (11), 1634–1639.

15. Pourhajibagher, M.; Bahador, A. Synergistic Biocidal Effects of Metal Oxide Nanoparticles-Assisted Ultrasound Irradiation: Antimicrobial Sonodynamic Therapy against Streptococcus Mutans Biofilms. *Photodiagnosis Photodyn. Ther.* **2021**, *35*, 102432.

16. Chen, Y.; Yin, B.; Liu, Z.; Wang, H.; Fu, Z.; Ji, X.; Tang, W.; Ni, D.; Peng, W. Dual-Modality Magnetic Resonance/Optical Imaging-Guided Sonodynamic Therapy of Pancreatic Cancer with Metal—Organic Nanosonosensitizer. *Nano Res. 2022* **2022**, 1–8.

17. Wang, H.; Guo, J.; Lin, W.; Fu, Z.; Ji, X.; Yu, B.; Lu, M.; Cui, W.; Deng, L.; Engle, J. W.; et al. Open-Shell Nanosensitizers for Glutathione Responsive Cancer Sonodynamic Therapy. *Adv. Mater.* **2022**, *34* (15), 2110283.

18. Busch, J. J. The Role for MRI-Guided Transurethral Ultrasound Ablation in the Continuum of Prostate Cancer Care. *Br. J. Radiol.* **2022**, *95* (1131).

19. Zhou, Y.-F. High Intensity Focused Ultrasound in Clinical Tumor Ablation. *World J. Clin. Oncol.* **2011**, *2* (1), 8.

20. Hensel, K.; Mienkina, M. P.; Schmitz, G. Analysis of Ultrasound Fields in Cell Culture Wells for In Vitro Ultrasound Therapy Experiments. *Ultrasound Med. Biol.* **2011**, *37* (12), 2105–2115.

21. Kanta, J. Collagen Matrix as a Tool in Studying Fibroblastic Cell Behavior. *Cell Adh. Migr.* **2015**, *9* (4), 308.

22. Stamov, D. R.; Pompe, T. Structure and Function of ECM-Inspired Composite Collagen Type I Scaffolds. *Soft Matter* **2012**, *8* (40), 10200–10212.

23. Frantz, C.; Stewart, K. M.; Weaver, V. M. The Extracellular Matrix at a Glance. *J. Cell Sci.* **2010**, *123* (24), 4195.

24. Parenteau-Bareil, R.; Gauvin, R.; Berthod, F. Collagen-Based Biomaterials for Tissue Engineering Applications. *Mater. 2010, Vol. 3, Pages 1863-1887* **2010**, *3* (3), 1863–1887.

25. Rezvani Ghomi, E.; Nourbakhsh, N.; Akbari Kenari, M.; Zare, M.; Ramakrishna, S. Collagen-Based Biomaterials for Biomedical Applications. *J. Biomed. Mater. Res. Part B Appl. Biomater.* **2021**, *109* (12), 1986–1999.

26. Zhang, L.; Gopalakrishnan, S.; Li, K.; Wang, L.-S.; Han, Y.; Rotello, V. M. Fabrication of Collagen Films with Enhanced Mechanical and Enzymatic Stability through Thermal Treatment in Fluorous Media. *Cite This ACS Appl. Mater. Interfaces* **2020**, *12*, 6590–6597.

27. Carlson, M. W.; Alt-Holland, A.; Egles, C.; Garlick, J. A. Three-Dimensional Tissue Models of Normal and Diseased Skin. *Curr. Protoc. cell Biol.* **2008**, *Chapter 19* (SUPPL. 41).

28. Maione, A. G.; Brudno, Y.; Stojadinovic, O.; Park, L. K.; Smith, A.; Tellechea, A.; Leal, E. C.; Kearney, C. J.; Veves, A.; Tomic-Canic, M.; et al. Three-Dimensional Human Tissue Models That Incorporate Diabetic Foot Ulcer-Derived Fibroblasts Mimic *in vivo* Features of Chronic Wounds. *Tissue Eng. - Part C Methods* **2015**, *21* (5), 499–508.

CHAPTER 7

ULTRASOUND-ENHANCED ANTIBACTERIAL ACTIVITY OF POLYMERIC NANOPARTICLES FOR ERADICATING BACTERIAL BIOFILMS

7.1 Introduction

Bacterial infections are a major healthcare concern, presenting several acute threats such as chronic wounds[1] and implant-associated infections and failure.[2, 3] Approximately 1.7 million hospital-acquired infections occur in the United States alone annually, resulting in a financial burden of 11 billion USD.[4] This challenge is further exacerbated by formation of bacterial biofilms, which are bacterial communities surrounded by a self-secreted extracellular polymeric substance (EPS).[5, 6] Biofilms promote the spread of infection and development of drug resistance by protecting bacteria from the host immune response and antimicrobial agents.[7, 8] Conventional therapies like antibiotics are unable to effectively penetrate through the EPS,[9, 10] are deactivated in the matrix,[11] and are rapidly removed from the microenvironment through efflux pumps.[12] Aggressive treatment strategies are often employed to treat biofilm infections involving surgical debridement of infected tissue, high doses of antibiotics or the use of last-resort antibiotics.[13, 14] These strategies result in low patient compliance due to long and expensive treatments with the possibility of adverse side-effects. Therefore, recent efforts have focused on developing minimally invasive strategies that can disrupt the biofilm to enhance the penetration of therapeutics, while minimizing side-effects.

Nanomaterials are another recent approach that have gained interest as antimicrobials owing to their tunable morphological and physicochemical properties such

as size, shape, and surface chemistry.[15] Consequently, nanomaterials have been engineered to enhance biofilm penetration,[16] impart targeting or stimuli-responsive behavior,[17, 18] and facilitate localized delivery of antimicrobial agents.[19] For instance, cationic nanomaterials show enhanced penetration into biofilms and are also able to disrupt bacterial cell membranes due to the overall negative charge of the EPS.[20, 21] However, for the same reasons, cationic nanomaterials also show increased toxicity towards mammalian cells. Therefore, maximizing the therapeutic effect while minimizing host toxicity is a key challenge when designing antimicrobial nanomaterials.

Ultrasound (US)-based treatments have gained interest for eradicating biofilms due to its enhanced tissue penetration and the ability to localize treatment to infected area.[22] Ultrasonic waves (frequency > 20 kHz) are pressure waves transmitted through the expansion and contraction of a medium.[23, 24] The antimicrobial effect of US is mainly attributed to its thermal and cavitation effects. Heat generated from ultrasound has been utilized for ablation of infected tissue and for the localized release of drugs.[25, 26, 27, 28, 29] Cavitation is the process of formation of microbubbles in the media during US treatment resulting in shear forces inside bacterial cells. Cavitation leads to pore formation, disruption of bacterial biofilms, and eventually to bacterial cell membrane disruption.[30] However, prolonged exposure to ultrasound leads to tissue damage, either due to the hyperthermic effect on surrounding tissue or due to the cavitation-associated damage to healthy cells, thereby contributing to delayed wound-healing.[31]

Our strategy employs a combination of cationic antimicrobial polymeric nanoparticles (PNPs) and ultrasound for the rapid eradication of bacterial biofilms (as shown in **Figure 7.1**) with minimal toxicity to mammalian cells. We hypothesized that

ultrasound treatment would enhance the antimicrobial activity of nanomaterials by rapidly disrupting the biofilm matrix and increasing the susceptibility of bacterial cells to the treatment. Furthermore, the disruption of the bacterial membrane due to the combined activity of acoustic cavitation and cationic PNPs allows us to reduce both the concentration of PNPs utilized and exposure to US treatment. For this study, we utilized the polymer PONI-C11-TMA (synthesis described in **Figure D.1**). As shown in **Figure 7.1(a)**, PONI-C11-TMA is based on a poly(oxanorboroneneimide) (PONI) backbone, with a C_{11} alkyl sidechain and cationic trimethyl ammonium (TMA) headgroup. As demonstrated by **Figure D.2**, PNPs remained stable throughout ultrasound treatment, showing no significant change in size. We have previously shown that the PONI-C11-TMA polymer self-assembles into nanoparticles (size in **Figure 7.1(b)**) with antimicrobial activity against bacterial biofilms, while preventing the development of drug resistance. However, these studies employ longer incubation times (~ 3hr) to enable penetration into and disruption of biofilms. Furthermore, high concentrations and prolonged exposure to PNPs results in toxicity towards mammalian cells.[32, 33] In this study, we show rapid antibacterial activity through a combination treatment of ultrasound and PNPs, resulting in > 80% bacterial toxicity within 30 min of treatment. The combination treatment was tested against biofilms of both Gram-positive and Gram-negative strains and was demonstrated to be effective. Furthermore, we observed synergistic or additive behavior in most combinations, resulting in a 2- to 6- fold reduction in both the concentration of PNPs and the duration of ultrasound treatment. We also demonstrated through a co-culture model that this reduction in the concentration of PNPs and duration of ultrasound treatment resulted in minimized

cytotoxicity to fibroblast cells, while resulting in a 100- to 1000- fold reduction in bacterial cell concentration.

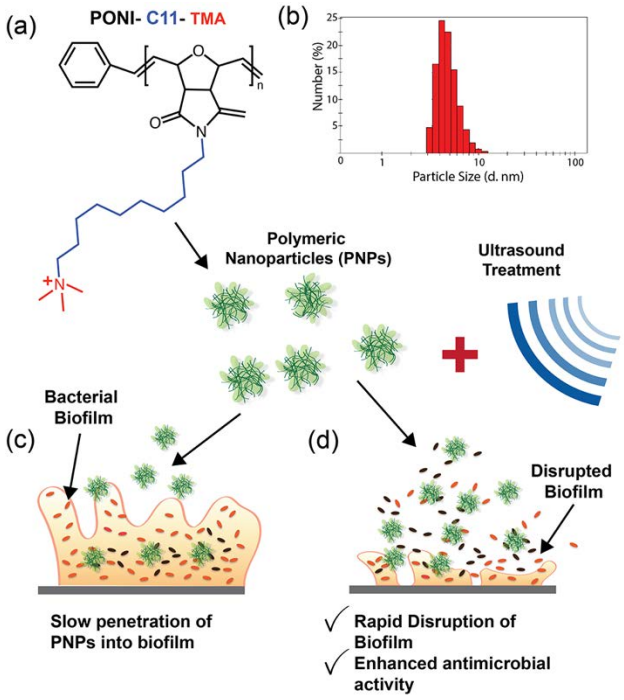

Figure 7.1. Schematic representation of effect of combination treatment on bacterial biofilms. (a) Chemical structure of cationic polymer PONI-C11-TMA with the poly(oxanorboroneneimide) backbone (in black), a C_{11} alkyl sidechain (in blue), and a cationic trimethyl ammonium headgroup (in red). (b) Hydrodynamic radius of PNPs, as measured by dynamic light scattering. (c) Scheme depicting slow penetration of PNPs into biofilms and (d) Scheme depicting rapid biofilm disruption and enhanced antibacterial activity due to ultrasound treatment.

7.2. Results and Discussion

7.2.1. Effect of Ultrasound Treatment on Biofilm Infections

Our initial studies focused on the effect of ultrasound treatment on bacterial biofilms by observing biofilms pre- and post-treatment using confocal microscopy. GFP-expressing MRSA were first grown to stationary phase in LB media. The culture tubes were then centrifuged to collect the bacteria and washed 3 times using a 0.85% NaCl

solution followed by resuspension in PBS. Following this, the concentration of bacteria was determined by measuring the optical density of the suspension at 600 nm (OD_{600}; 1 $O.D_{600} = 10^9$ cfu/mL). Seeding solutions were then prepared at 10^8 cfu/mL by diluting the bacteria in Tryptic Soy Broth (TSB) media. 2 mL of the seeding solution were then placed in a glass bottom confocal dish and incubated at 37 ^oC for 24 hr to generate MRSA biofilms. Mature biofilms were ~ 20 μm thick, as seen in **Figure 7.2**. Biofilms were then treated with ultrasound (conditions described in the Experimental Methods section) for varying durations. As shown in **Figure 7.2**, biofilm disruption begins ~40 s post exposure to ultrasound and is fully disrupted after about 300s of treatment. This demonstrated that short durations of exposure to ultrasound can cause significant disruption of the biofilm thereby enhancing penetration of antimicrobial agents.

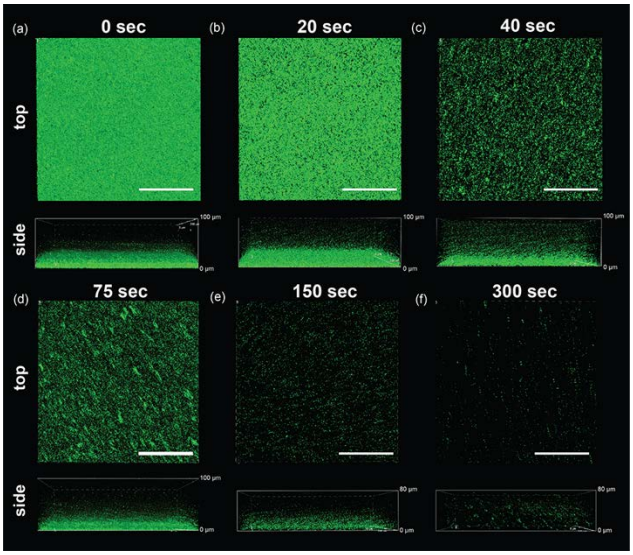

Figure 7.2. Top and side view confocal microscopy images demonstrating US-mediated biofilm disruption of MRSA-GFP biofilm. (a) Native untreated biofilm. Biofilms treated with ultrasound for (b) 20 s (c) 40 s (d) 75 s (e) 150 s and (f) 300 s. It can be seen that biofilm disruption begins at ~40s and is almost fully disrupted at ~300 s. Scale bar is 100 μm.

In addition to biofilm disruption, ultrasound treatment may also result in antimicrobial activity. We tested this on both Gram-positive and negative bacterial biofilms (results summarized in **Figure 7.3**). *E. coli* (CD2), *P. aeruginosa* (CD1006), MRSA (6169) and *S. epidermidis* (7073) biofilms were grown using the protocol described above. Mature biofilms were treated with ultrasound for varying durations. Following this, %bacterial viability was measured using alamarBlue assay and %toxicity was calculated and summarized in **Figure 7.3**. Ultrasound treatment resulted in ~80% toxicity across all strains, as seen in **Figure 7.3 (a, b, c and d)**. This is primarily attributed to cavitation and mechanical disruption of bacterial cell membranes. This is further evidenced by the disrupted cell membranes of MRSA (**Figure 7.3(e)**), *E. coli* (**Figure 7.3(f)**) and *P. aeruginosa* (**Figure 7.3(g)**) observed through propidium iodide staining. Furthermore, as seen in **Figure D.3**, the thermal effect from ultrasound treatment (increase in temperature from 25 ^{o}C to 40 ^{o}C) is not sufficient for antimicrobial activity. Additionally, ultrasound treatment over 600s did not result in sufficient changes Gram-positive strains were more resilient to the treatment. Both MRSA and *S. epidermidis* required ~600 s of ultrasound treatment to eliminate 60% of the bacteria, while *E. coli* and *P. aeruginosa* required ~200 s. This is explained by the presence of the peptidoglycan layer around Gram-positive bacteria which protects the cells from cavitation-associated membrane disruption.[34] **Figure 7.3(e), (f) and (g)** show fluorescence microscopy images of the dead bacteria stained by propidium iodide stain, which is further proof of the membrane disruption as a result of the ultrasound treatment.

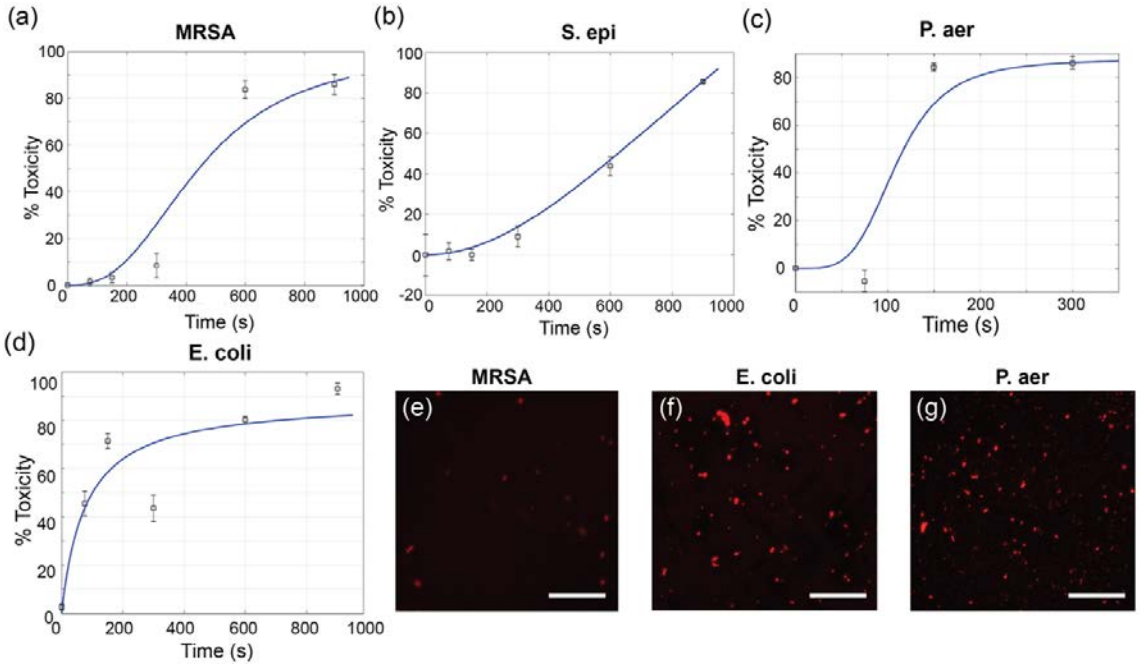

Figure 7.3. Broad-spectrum antibacterial activity of US treatment. Each graph represents %Biofilm toxicity at different durations of ultrasound treatment for Gram-positive (a) MRSA and (b) *S. epidermidis*, and negative (c) *P. aeruginosa* and (d) *E. coli* biofilms. Error bars represent standard deviation (n=4). Solid blue line in (a), (b) and (c) show trends consistent with Hill Equation while (d) is consistent with Michelis-Menten Equation. Fluorescence images post pI staining for (e) MRSA (f) *E. coli* and (g) *P. aeruginosa* show dead bacteria. Scale bar is 50 μm.

7.2.2. Synergistic or Additive Combination therapy of Ultrasound and PNPs

We next studied the potential for ultrasound treatment to enhance the antibacterial activity of polymeric nanomaterials. We have previously demonstrated the broad-spectrum antibacterial activity of the cationic PNPs.[32, 33] Furthermore, bacteria were unable to develop resistance against PNPs owing to its membrane disruption mechanism. However, higher concentrations and longer treatment time have to be utilized for effectively eliminating biofilms using PNPs, which contributes to increased cytotoxicity. Ultrasound treatment is expected to rapidly disrupt the bacterial biofilm and also enhance the bacterial membrane permeability. For this reason, we hypothesized that a combination of ultrasound

and PNPs will rapidly eliminate bacterial biofilms through a synergistic or additive behavior.

This combination therapy was tested on MRSA, *E. coli* and *P. aeruginosa* biofilms grown according to the protocol described previously. The mature biofilms were then treated with a combination of PNP solution, concentration ranging from 0 to 0.25 mg/mL, and ultrasound ranging from 0 to 600 s. The biofilms were then incubated at 37 ^{o}C for 30 min and tested with alamarBlue to calculate bacterial cell viability. **Figure 7.4** summarizes the results of %toxicity for each treatment condition in a heatmap where each cell represents a different treatment condition, and the color represents % toxicity. As seen in **Figure 7.4(a)**, MRSA has limited susceptibility to ultrasound treatment or PNPs individually, exhibiting 80% toxicity at 600s of ultrasound or 0.5 mg/mL of PNP solution. However, a 2- to 6- fold reduction of ultrasound treatment time and 2- to 4- fold reduction of PNP concentration may be obtained through combination treatment for the same level of toxicity. Similarly, a 4- fold reduction in both ultrasound treatment time and PNP concentration was observed in the case of *P. aeruginosa*, as observed in **Figure 7.4(b)** while a 2- to 6- fold reduction in both ultrasound treatment time and PNP concentration was observed for *E. coli*. These results demonstrate that a combination treatment of ultrasound and PNPs has broad-spectrum activity and can be utilized against both Gram-positive and negative infections. Furthermore, we tested the prolonged effect of ultrasound treatment on the susceptibility of bacteria to PNPs by increasing the duration of administration of PNPs after ultrasound treatment. As seen in **Figure D.4**, bacteria showed increased susceptibility towards PNPs up to 15 min post ultrasound treatment. **Figure 7.4(d), (e) and (f)** show fluorescence microscopy images of the dead bacteria stained by

propidium iodide stain, which is further proof of the membrane disruption as a result of the combination treatment.

The additive, synergistic or antagonistic behavior of the combination treatments was evaluated using the Bliss independence model.[35] Scores for each condition are shown in **Figure D.5** and synergistic conditions are marked with an asterisks in **Figure 7.4(a), (b) and (c)**. As expected, most combinations showed additive behavior. We observed that several synergistic conditions are observed for both MRSA and *E. coli*. In comparison, only one synergistic points are observed for *P. aeruginosa*. This is attributed to the significantly high susceptibility of *P. aeruginosa* to the ultrasound treatment alone (seen in **Figure 7.3**).

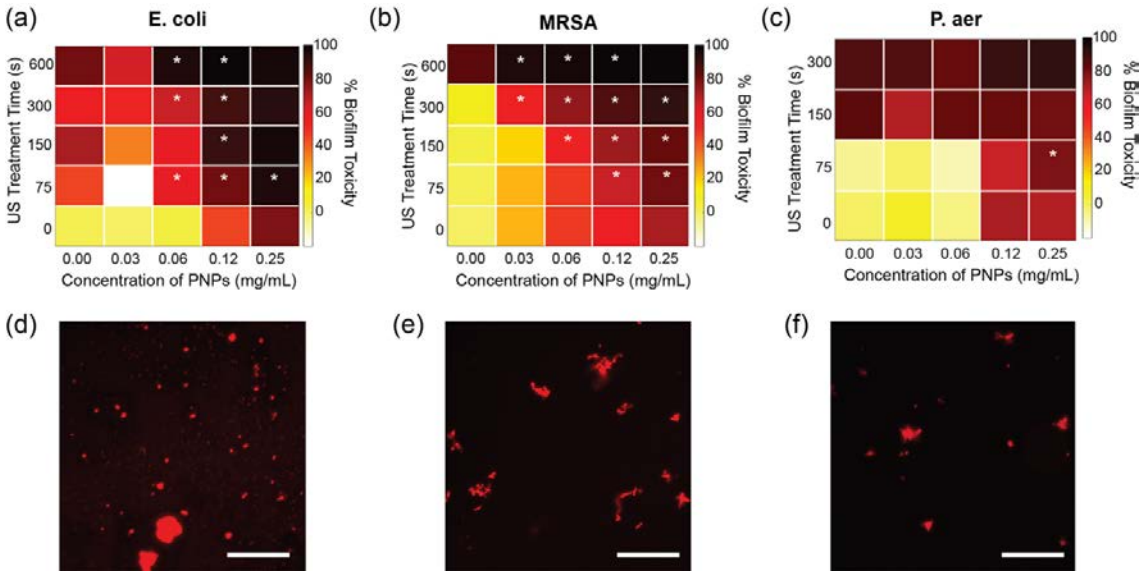

Figure 7.4. Antibacterial activity of combination therapy. % Biofilm toxicity due to combination therapy, as measured by alamarBlue assay for (a) *E. coli* (b) MRSA and (c) P. aeruginosa biofilms. Conditions where synergy was observed are marked by *. *E. coli* and MRSA show synergy at several combinations and additivity for most others. P. aeruginosa shows mostly additive behaviour, presumably due to the strong antibiofilm effect of ultrasound treatment alone on P. aer biofilms. (d), (e) and (f) show fluorescence microscopy images of dead bacteria visualized by propidium iodide staining. Scale bar is 50 μm.

5.2.4. *In vitro* Biofilm and Fibroblast Co-culture Model to Study the Effect of Combination Treatment

We have demonstrated that the combination treatment is successful at reducing both the duration of ultrasound treatment as well as the concentration of the PNPs utilized, while preserving the efficacy. This approach is not only beneficial for the rapid and efficient eradication of biofilms but can potentially limit side-target effects if it reduces the 'dosing' of each individual component. Ultrasound can be focused or directed to an area and therefore enables localized treatment of biofilm infections while minimizing significant damage to healthy tissue. However, prolonged exposure to ultrasound can result in cytotoxicity to healthy cells. On the other hand, PNPs also exhibit cytotoxicity at high concentrations that may be required to eradicate chronic biofilm infections. We therefore hypothesized that the combination treatment would allow us to preserve healthy cells, thereby promoting wound-healing by reducing both the intensity of ultrasound treatment and concentration of PNP utilized.

First, 3T3 fibroblast cells were cultured on collagen-coated wells of a 12 well plate. The collagen coating mimicked the extracellular matrix in native tissues and absorbed some energy from the ultrasound treatment, thereby protecting the cells.[36] As seen in **Figure D.6**, significant differences in fibroblast cell viability was observed on uncoated vs. collagen-coated plates. 100k cells were seeded onto collagen-coated plates and allowed to grow overnight. Non-pathogenic *E. coli* DH5α bacteria were grown to log phase in LB media and then washed and harvested. Bacteria seeding solution of 10^8 cfu/mL was prepared in DMEM media and placed on top of the 3T3 cell culture. Plates were then incubated at 37 ^{o}C for 6 hr to allow biofilms formation. Following this, co-cultured were treated with a combination of ultrasound and PNPs as shown in **Figure 7.5**. 3T3 %viability

was evaluated using the LDH cytotoxicity assay and colony-counting was performed to evaluate the bacterial viability. As seen in **Figure 7.5(a)**, the majority of the cells survived the combination treatment at lower concentrations of PNPs. Although some cytotoxicity was observed at 0.06 mg/mL, ~60% of the cells still survive the combination treatment. 3T3 viability did not significantly change due to ultrasound treatment for any of the treatment groups. However, for the same treatment conditions, a 100- to 1000- fold reduction in the concentration of bacteria was observed, as shown in **Figure 7.3(b)**. Ultrasound treatment results significant reduction as compared to PNP only for both lower concentrations of PNPs (0.007 mg/mL and 0.015 mg/mL). We therefore concluded that the combination treatment may be utilized to eradicate biofilm infections while minimizing significant tissue damage resulting from both ultrasound and PNP toxicity.

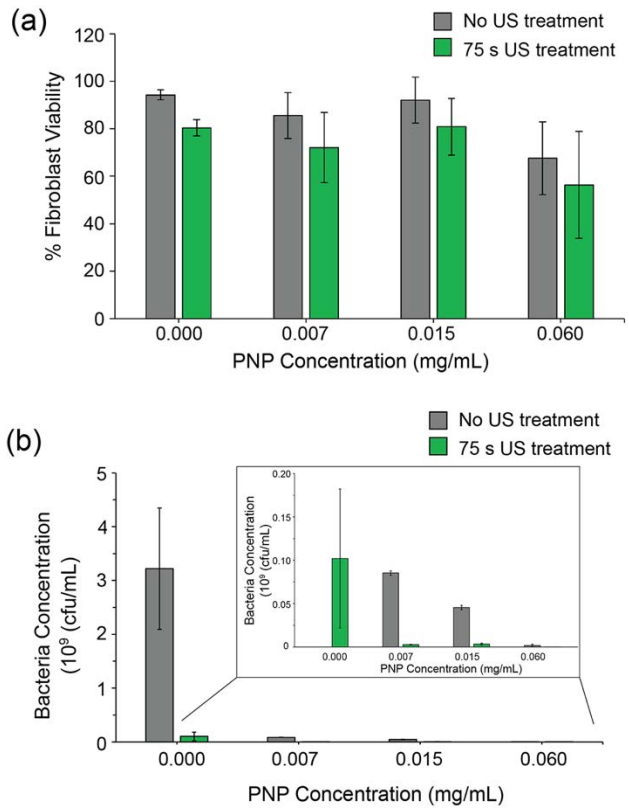

Figure 7.5. Effect of combination treatment on (a) fibroblast cells and (b) Non-pathogenic *E. coli* DH5α biofilms in an *in vitro* co-culture model. (a) % Fibroblast cell viability measured using LDH cytotoxicity assay shows that 60 to 80% of the cells survive the combination treatment. Error bars represent standard deviation (n=8). (b) 100- to 1000-fold reduction in bacteria concentration was observed during combination treatment. Bacteria concentration was measured by colony-counting. Error bars represent S.E.M. (n=4).

7.3. Conclusions

This study demonstrates the synergistic and additive therapeutic potential of combined ultrasound treatment and antimicrobial cationic PNPs. Ultrasound treatment rapidly disrupts bacterial biofilms and shows broad-spectrum antibacterial activity. Furthermore, when combined with our previously developed antimicrobial PNPs (PONI-C11-TMA) we observe enhanced antibacterial activity with a 2- to 6- fold reduction in the concentrations of PNPs and duration of ultrasound treatment. This combination treatment results in 100- to 1000- fold reduction in bacterial concentration with minimal toxicity to

fibroblast cells. Taken together, this approach provides a rapid and effective method to eradicate biofilm infections, while minimizing tissue damage. Additionally, PNPs minimize the risk of developing drug resistant infections. Therefore, this combined approach provides a robust and effective strategy for treating refractory conditions like chronic wound infections, implant-associated infections, and multi-drug resistant infections.

7.4 Experimental Methods

7.4.1. Materials.

All solvents, reagents, and chemicals for synthesis of PNPs were obtained from Fisher Scientific and Sigma Aldrich and used without further purification unless otherwise specified. Bacteria isolates with the code CD were obtained from the Cooley Dickinson Hospital Microbiology Laboratory, Northampton, MA. MRSA (IDRL-6169) and *S. epidermidis* (IDRL-7073) was from the Infectious Diseases Research Laboratory at Mayo Clinic, Rochester MN. NIH-3T3 fibroblast cells were purchased from ATCC (ATCC CRL-1658). Luria broth, tryptic soy broth, DMEM (Dulbecco's modified eagle medium) and agar were purchased from Fisher Scientific and used as received. AlamarBlue assay and CyQUANT LDH Cytotoxicity assay were purchased from Invitrogen on Fisher Scientific and used as suggested by the manufacturer. Rat-tail Collagen 1 solution (3-4 mg/mL) was purchased from ThermoFisher and used without further purification.

7.4.2. Bacterial and biofilm cultures

Growing bacteria for all experiments. All bacteria strains utilized throughout this study (MRSA eGFP, CD2, IDRL-6169, CD1006, IDRL-7073 and E. coli DH5α) were

first inoculated by transferring isolated colonies on agar plates into Luria broth (LB) media and grown to stationary phase overnight at 37 °C with aeration and agitation at 275 rpm. Bacteria were then collected and washed thrice through centrifugation at 3000 rpm for 5 min in 0.85% NaCl solution. Following this bacteria were resuspended in PBS media and their optical density ($O.D_{600}$) was measured at 600 nm (1 $O.D_{600}$ ~ 10^9 cfu/mL). Next, bacterial seeding solutions were prepared based on the experiment.

Confocal Imaging of Biofilm Disruption due to Ultrasound Treatment. MRSA eGFP bacteria were grown and washed according to the protocol described above. A seeding solution of 108 cfu/mL of bacteria was prepared in Tryptic soy broth (TSB) containing 1mM of IPTG. Next, 2 mL of seeding solution each was placed in confocal dishes and allowed to incubate at 37 °C overnight to form biofilms. Mature biofilms were then washed once with PBS and then replaced with 2 mL of M9 media before ultrasound treatment. Treated biofilms were then washed with PBS to remove free-floating planktonic bacteria and imaged on a Zeiss LSM 510 Meta microscope, from the Light Microscopy Facility and Nikon Center of Excellence at the Institute for Applied Life Sciences, UMass Amherst, by using a 40× objective. The settings of the confocal microscope were as follows: green channel, λ_{ex} = 488 nm and λ_{em} = LP 540 nm; red channel, λ_{ex} = 560 nm and λ_{em} = LP 640 nm; blue channel, λ_{ex} = 403 nm and λ_{em} = LP 495 nm. Emission filter: LP = high pass.

Propidium Iodide staining assay. MRSA (6169), E. coli (CD2), and P. aeruginosa (CD1006) solutions were prepared in M9 media to a concentration of 10^8 cfu/mL. 2 mL of this solution was added to each well of a 12 well plate and treated with either ultrasound for 600 s (**Figure 7.3**) or a combination of 150 s ultrasound and 0.125 mg/mL of PNPs

(**Figure 7.4**) and then then incubated for 30 min at 37 °C. Propidium iodide was then added to each treated bacteria solution such that the final PI concentration was 2 μM and then incubated in the dark at 37 °C for 30 min. 5 μL of each solution was then placed on a glass slide with a glass coverslip and observed with fluorescence microscopy, using an Olympus IX51 Inverted Phase Contrast Fluorescence Microscope with a 100W Mercury lamp and a QICAM fast 1394 digital camera from QICAM.

Biofilm growth for all eradication studies. MRSA (6169), E. coli (CD2), P. aeruginosa (CD1006) and S. epidermidis (7073) bacteria were grown and washed according to the protocol described above. A seeding solution of 10^8 cfu/mL of bacteria was prepared in Tryptic soy broth (TSB). Next, 1 mL of seeding solution was placed in each well of a 12-well plate and allowed to incubate at 37 °C overnight to form biofilms. Mature biofilms were washed once with PBS and then replaced with 2 mL of M9 media before ultrasound (**Figure 7.3**) or combination (**Figure 7.4**) treatment. Treated biofilms were resuspended through vigorous pipetting before transferring to multiple wells of a 96 well plate (90 μL per well, 3-4 replicates per treatment group).

%Toxicity Measurements. %Biofilm Toxicity (100 - %viability) was measured through the alamarBlue assay using the protocol for suspension cells, provided by the supplier. Each well was then spiked with 10 μL of alamarBlue solution and incubated at 37 °C for 30 min. Fluorescence was measured at 560 nm Ex and 590 nm Em. %Bacterial cell viability was calculated with respect to untreated growth control and then subtracted from 100 to calculate %Toxicity.

7.4.3. Co-culture model studies

Fibroblast cell culture. Briefly, NIH-3T3 fibroblast cells (ATCC CRL-1658) were cultured in DMEM in the presence of 10% fetal bovine serum and 1% antibiotic solution. 100,000 cells/well were plated on uncoated and collagen-coated wells and allowed to grow overnight at 37 °C in a humidified atmosphere of 5% CO2.

Biofilm culture and treatment. E. coli DH5α was to stationary phase overnight in LB media. Log-phase cultures were then prepared by spiking 160 µL of stationary phase in 3 mL of TSB media and allowed to grow for 3 hr in a shaker set at 37 °C, 300 rpm. Log-phase cultures were then washed and isolated per the protocol described above and diluted to 10^8 cfu/mL in antibiotic-free cell culture media (10% FBS + DMEM) to prepare seeding solutions. 1mL of the seeding solution was placed in each well of the fibroblast culture and allowed to incubate for 6 hr at 37 °C to prepare biofilms. Co-cultures were then treated with either a combination of ultrasound and PNPs, or individual treatments/ control groups and incubated at 37 °C for 30 min. Negative controls were co-culture groups that were left untreated. Positive controls (for LDH) were co-culture groups that were treated with Lysis buffer only.

Cell viability measurement. 3T3 viability was measured using the CyQUANT LDH cytotoxicity assay kit from Invitrogen. The protocol provided by the supplier was utilized for this assay. Briefly, the supernatant from treatment and control groups were harvested and placed in 96 well plates (50 µL x 4 per replicate (3) of each treatment/ control group). To these, 50 µL of the Reaction mixture (prepared by mixing the reactant and substrate mix) was added and mixed gently. Plates were then incubated for 30 min at 37 °C and finally 50 µL of the stop solution was added to each well. Absorbance of each

well was measured at 490 and 680 nm. To determine LDH activity, first the absorbance at 680 nm was subtract from the absorbance at 490 nm for each well. %Cytotoxicity was calculated as 100 x ((Treatment group Activity – Negative Control Activity)/(Positive Control Activity – Negative Control Activity)). %Cell viability was calculated as 100 - %cytotoxicity.

Colony counting. After collecting the supernatant for LDH assay, the remaining solution was homogenized through vigorous pipetting to resuspend the bacteria. Solutions were then collected and diluted up to 6 times (up to 10^{-6} of original solution). 10 μL from each dilution was then plated onto agar plates and allowed to grow overnight at 37 ^{o}C. Biofilm colonies in each plate were counted and multiplied with the appropriate dilution factor to calculate cfu/mL of bacteria that survived the treatment.

7.4.4. Ultrasound treatment

Ultrasound treatment was performed using a Vibracell 20 kHz 130-watt ultrasonic processor (VCX130) with a 6 mm probe at 35% amplitude for all studies. The duration for each treatment was varied from a range of 60 s to 900 s. It was ensured that at least 2 mL of media was present in the well prior to treatment.

7.5. References

1. Wolcott, R. D.; Ehrlich, G. D. Biofilms and Chronic Infections. *JAMA* **2008**, *299* (22), 2682–2684.

2. Van Epps, J. S.; Younger, J. G. Implantable Device Related Infection. *Shock* **2016**, *46* (6), 597.

3. Donlan, R. M. Biofilms and Device-Associated Infections. *Emerg. Infect. Dis.* **2001**, *7* (2), 277–281.

4. Römling, U.; Kjelleberg, S.; Normark, S.; Nyman, L.; Uhlin, B. E.; Åkerlund, B. Microbial Biofilm Formation: A Need to Act. *J. Intern. Med.* **2014**, *276* (2), 98–110.

5. Flemming, H. C.; Wingender, J. The Biofilm Matrix. *Nat. Rev. Microbiol.* **2010**, *8* (9), 623–633.

6. Arciola, C. R.; Campoccia, D.; Montanaro, L. Implant Infections: Adhesion, Biofilm Formation and Immune Evasion. *Nat. Rev. Microbiol.* **2018**, *16* (7), 397–409.

7. Sharma, D.; Misba, L.; Khan, A. U. Antibiotics versus Biofilm: An Emerging Battleground in Microbial Communities. *Antimicrob. Resist. Infect. Control 2019 81* **2019**, *8* (1), 1–10.

8. Ciofu, O.; Moser, C.; amp, P.; Jensen, strup; Hamp, N. Tolerance and Resistance of Microbial Biofilms. *Nat. Rev. Microbiol. 2022* **2022**, 1–15.

9. Cao, B.; Christophersen, L.; Thomsen, K.; Sønderholm, M.; Bjarnsholt, T.; Jensen, P. Ø.; Høiby, N.; Moser, C. Antibiotic Penetration and Bacterial Killing in a Pseudomonas Aeruginosa Biofilm Model. *J. Antimicrob. Chemother.* **2015**, *70* (7), 2057–2063.

10. Cao, B.; Christophersen, L.; Kolpen, M.; Jensen, P. Ø.; Sneppen, K.; Høiby, N.; Moser, C.; Sams, T. Diffusion Retardation by Binding of Tobramycin in an Alginate Biofilm Model. *PLoS One* **2016**, *11* (4), e0153616.

11. Kranjec, C.; Angeles, D. M.; Mårli, M. T.; Fernández, L.; García, P.; Kjos, M.; Diep, D. B. Staphylococcal Biofilms: Challenges and Novel Therapeutic Perspectives. *Antibiot. 2021, Vol. 10, Page 131* **2021**, *10* (2), 131.

12. Soto, S. M. Role of Efflux Pumps in the Antibiotic Resistance of Bacteria Embedded in a Biofilm. **2013**, *4* (3), 223–229.

13. Namgoong, S.; Jung, S. Y.; Han, S. K.; Kim, A. R.; Dhong, E. S. Clinical Experience with Surgical Debridement and Simultaneous Meshed Skin Grafts in Treating Biofilm-Associated Infection: An Exploratory Retrospective Pilot Study. *J. Plast. Surg. Hand Surg.* **2020**, *54* (1), 47–54.

14. Wu, H.; Moser, C.; Wang, H. Z.; Høiby, N.; Song, Z. J. Strategies for Combating Bacterial Biofilm Infections. *Int. J. Oral Sci.* **2015**, *7* (1), 1–7.

15. Makabenta, J. M. V.; Nabawy, A.; Li, C. H.; Schmidt-Malan, S.; Patel, R.; Rotello, V. M. Nanomaterial-Based Therapeutics for Antibiotic-Resistant Bacterial Infections. *Nat. Rev. Microbiol. 2020 191* **2020**, *19* (1), 23–36.

16. Mahmoudi, M.; Serpooshan, V. Silver-Coated Engineered Magnetic Nanoparticles Are Promising for the Success in the Fight against Antibacterial Resistance Threat. *ACS Nano* **2012**, *6* (3), 2656–2664.

17. Wu, J.; Li, F.; Hu, X.; Lu, J.; Sun, X.; Gao, J.; Ling, D. Responsive Assembly of Silver Nanoclusters with a Biofilm Locally Amplified Bactericidal Effect to Enhance Treatments against Multi-Drug-Resistant Bacterial Infections. *ACS Cent. Sci.* **2019**, *5* (8), 1366–1376.

18. Koo, H.; Allan, R. N.; Howlin, R. P.; Stoodley, P.; Hall-Stoodley, L. Targeting Microbial Biofilms: Current and Prospective Therapeutic Strategies. *Nat. Rev. Microbiol. 2017 1512* **2017**, *15* (12), 740–755.

19. Li, C. H.; Landis, R. F.; Makabenta, J. M.; Nabawy, A.; Tronchet, T.; Archambault, D.; Liu, Y.; Huang, R.; Golan, M.; Cui, W.; et al. Nanotherapeutics Using All-Natural Materials. Effective Treatment of Wound Biofilm Infections Using Crosslinked Nanoemulsions. *Mater. Horizons* **2021**, *8* (6), 1776–1782.

20. Carmona, A. M.; Id, R. Self-Assembled Antimicrobial Nanomaterials. *Int. J. Environ. Res. Public Heal. 2018, Vol. 15, Page 1408* **2018**, *15* (7), 1408.

21. Gupta, A.; Mumtaz, S.; Li, C. H.; Hussain, I.; Rotello, V. M. Combatting Antibiotic-Resistant Bacteria Using Nanomaterials. *Chem. Soc. Rev.* **2019**, *48* (2), 415–427.

22. Hayes, B. T.; Merrick, M. A.; Sandrey, M. A.; Cordova, M. L. Three-MHz Ultrasound Heats Deeper Into the Tissues Than Originally Theorized. *J. Athl. Train.* **2004**, *39* (3), 230.

23. LuTheryn, G.; Glynne-Jones, P.; Webb, J. S.; Carugo, D. Ultrasound-Mediated Therapies for the Treatment of Biofilms in Chronic Wounds: A Review of Present Knowledge. *Microb. Biotechnol.* **2020**, *13* (3), 613–628.

24. Nakonechny, F.; Nisnevitch, M.; Nakonechny, F.; Nisnevitch, M. Different Aspects of Using Ultrasound to Combat Microorganisms. *Adv. Funct. Mater.* **2021**, *31* (44), 2011042.

25. O'Brien, W. D. Ultrasound–Biophysics Mechanisms. *Prog. Biophys. Mol. Biol.* **2007**, *93* (1–3), 212–255.

26. Ouyang, J.; Tang, Z.; Farokhzad, N.; Kong, N.; Kim, N. Y.; Feng, C.; Blake, S.; Xiao, Y.; Liu, C.; Xie, T.; et al. Ultrasound Mediated Therapy: Recent Progress and Challenges in Nanoscience. *Nano Today* **2020**, *35*, 100949.

27. Huebsch, N.; Kearney, C. J.; Zhao, X.; Kim, J.; Cezar, C. A.; Suo, Z.; Mooney, D. J. Ultrasound-Triggered Disruption and Self-Healing of Reversibly Cross-Linked Hydrogels for Drug Delivery and Enhanced Chemotherapy. *Proc. Natl. Acad. Sci. U. S. A.* **2014**, *111* (27), 9762–9767.

28. Ahmad, T.; McGrath, S.; Sirafim, C.; Do Amaral, R. J. F. C.; Soong, S. L.; Sitram, R.; Turkistani, S.; Santarella, F.; Kearney, C. J. Development of Wound Healing Scaffolds with Precisely-Triggered Sequential Release of Therapeutic Nanoparticles. *Biomater. Sci.* **2021**, *9* (12), 4278–4288.

29. Kearney, C. J.; Skaat, H.; Kennedy, S. M.; Hu, J.; Darnell, M.; Raimondo, T. M.; Mooney, D. J.; Kearney, C. J.; Skaat, H.; Kennedy, S. M.; et al. Switchable Release of Entrapped Nanoparticles from Alginate Hydrogels. *Adv. Healthc. Mater.* **2015**, *4* (11), 1634–1639.

30. Kimmel, E. Cavitation Bioeffects. *Crit. Rev. Biomed. Eng.* **2006**, *34* (2), 105–161.

31. Ebbini, E. S.; Ter Haar, G. Ultrasound-Guided Therapeutic Focused Ultrasound: Current Status and Future Directions. *https://doi.org/10.3109/02656736.2014.995238* **2015**, *31* (2), 77–89.

32. Gupta, A.; Landis, R. F.; Li, C. H.; Schnurr, M.; Das, R.; Lee, Y. W.; Yazdani, M.; Liu, Y.; Kozlova, A.; Rotello, V. M. Engineered Polymer Nanoparticles with Unprecedented Antimicrobial Efficacy and Therapeutic Indices against Multidrug-Resistant Bacteria and Biofilms. *J. Am. Chem. Soc.* **2018**, *140* (38), 12137–12143.

33. Makabenta, J. M. V.; Park, J.; Li, C. H.; Chattopadhyay, A. N.; Nabawy, A.; Landis, R. F.; Gupta, A.; Schmidt-Malan, S.; Patel, R.; Rotello, V. M. Polymeric Nanoparticles Active against Dual-Species Bacterial Biofilms. *Molecules* **2021**, *26* (16).

34. Monsen, T.; Lövgren, E.; Widerström, M.; Wallinder, L. In Vitro Effect of Ultrasound on Bacteria and Suggested Protocol for Sonication and Diagnosis of Prosthetic Infections. *J. Clin. Microbiol.* **2009**, *47* (8), 2496.

35. Tang, J.; Wennerberg, K.; Aittokallio, T. What Is Synergy? The Saariselkï¿½ Agreement Revisited. *Front. Pharmacol.* **2015**, *6* (SEP), 181.

36. Baker, K. G.; Robertson, V. J.; Duck, F. A. A Review of Therapeutic Ultrasound: Biophysical Effects. *Phys. Ther.* **2001**, *81* (7), 1351–1358.

CHAPTER 8

SUMMARY AND OUTLOOK

This dissertation is primarily centered around the development of novel polymeric biomaterials for different biomedical applications. Biomaterials are defined as substances fabricated to interact with biological systems for a medical purpose - for diagnostic or therapeutic applications. Consequently, biomaterials must be non-toxic, biocompatible, and sterile/ easily sterilizable in addition to the specific functions they were designed to fulfill. Polymers are excellent candidates for fabricating functional biomaterials due to their wide availability and varied properties. Polymers may be natural or synthetic and are often fabricated into coatings, foams, scaffolds, gels, composites, and nanomaterials. This dissertation focused on the development of two types of polymeric biomaterials – protein-based materials and synthetic polymeric nanoparticles – for varied potential applications as diagnostic sensors, antimicrobial materials, wound-healing, tissue engineering, and drug delivery applications. Additionally, the application of exogenous stimuli, such as ultrasound, in enhancing the activity of these materials was highlighted.

Proteins are biopolymers that naturally occur with a large variety of structural, chemical, and biological properties that may be harnessed to fabricate functional materials. Furthermore, they are inherently biodegradable, sustainable, and often biocompatible making them ideal precursors for biomaterials. However, their high aqueous solubility often results in poor structural and mechanical stability, significantly limiting their biomedical applications. Chapter 2 highlights the different fabrication strategies that stabilize protein films, including our fluorous-curing based thermal treatment approach. We hypothesized that the fluorous effect will minimize the interaction of the proteins with

the environment including the fluorous solvent, thereby preventing protein rearrangement at the interface and forming stable protein films. Our results also indicated that these protein films retain surface properties of native protein such as charge and hydrophilicity. Chapter 3 and 4 highlighted two different applications of charged protein films. Chapter 3, described the fabrication of anti-fouling and antimicrobial implant coatings by translating the anionic charge of BSA into films. This anionic charge resulted in anti-fouling properties and also enabled loading cationic antibiotics into the BSA coating. Chapter 4 described the fabrication of charge-patterned surfaces using cationic Lysozyme and anionic BSA through inkjet printing. These patterned substrates were u in combination with an acoustic streaming device (GHz Hypersonic Resonator) to size sort microparticles. This device successfully sorted a small volume of particles with high efficiency and has potential applications in microfluidic devices and lab-on-a-chip sensors. Chapter 5 focused on the fabrication of mechanically robust collagen coatings for medical implants. We hypothesized that thermal treatment of collagen films will result in tighter packing of collagen fibers, while minimizing denaturation, thereby resulting in enhanced structural, mechanical, and enzymatic stability. These coatings have also been utilized bone regenerative coatings for medical implants in a follow-up study. Chapter 6 focused on developing 2D and 3D cell cultures for ultrasound treatment using collagen-based materials. Ultrasound has been widely employed in clinic for diagnostic applications and is now gaining interest for its therapeutic applicability, due to enhanced tissue penetration and minimal invasiveness. However, development of ultrasound-based therapies have been limited by the lack of effective *in vitro* models to study the effects of ultrasound treatment. We hypothesized that collagen-based materials (films and hydrogels) mimic the

extracellular matrix in the native tissue absorbing most of the energy from the ultrasound and preventing uncontrolled cell lysis. These collagen-based cell cultures were then employed in Chapter 7, where ultrasound treatment was used in combination with antimicrobial polymeric nanoparticles to elicit synergistic antibacterial therapy against bacterial biofilm infections. The combination showed significant decrease in bacterial concentration with minimal damage to healthy mammalian cells and provide an effective strategy for treating refractive infections while minimizing side-effects. This study also highlights the application of techniques like ultrasound to enhance the activity of functional biomaterials.

Future work on protein films should focus on the development of scalable and cost-effective strategies for a larger variety of protein-based coatings. Furthermore, the development of 2D and 3D patterning techniques, such as inkjet printing, roll-to-roll processing, and 3D printing using proteins, will enable the development of hierarchical protein-based materials and medical devices. Protein-patterned materials may be utilized for generating complex multi-cell culture by regulating cell adhesion, and have potential applications in tissue engineering scaffolds, *in vitro* models for high throughput screening, and diagnostic sensors. Additionally, the employment of techniques like ultrasound in combination with biomaterials must be further investigated. In addition to the example demonstrated in Chapter 7, ultrasound may also be utilized to target and enhance the penetration of therapeutics into tissues, including the penetration of nanomaterials, where targeted delivery has posed a significant challenge and has gained significant interest recently. Ultrasound may also be used as a trigger in combination with responsive materials, such calcium-crosslinked alginate hydrogels, to release therapeutics

controllably and locally. An ongoing area of interest is the use of ultrasound as an on-off switch for bioorthogonal nanocatalysts for on-demand production of drugs. By encapsulating these nanocatalysts into ultrasound-responsive alginate hydrogels, we can modulate their catalytic activity, such that the nanocatalysts are only able to catalyze the activation of drugs when ultrasound is turned on.

Overall, these studies have demonstrated the wide applicability of polymeric biomaterials and future research will pave the way for sophisticated material design, development of novel biomedical devices, and clinical translation of therapeutic strategies.

APPENDIX A

SUPPLEMENTARY INFORMATION: PROTEIN-BASED FILMS AS ANTI-FOULING AND DRUG ELUTING ANTIMICROBIAL COATINGS FOR MEDICAL IMPLANTS

A.1. Stability of Protein Films

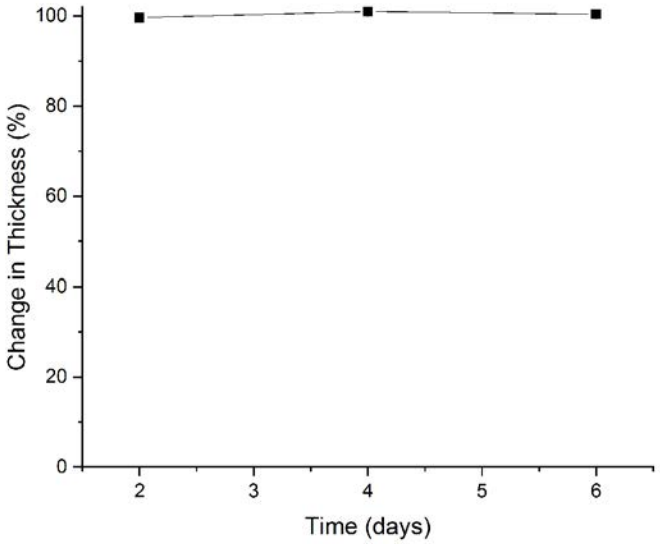

Figure A.1. Thickness change of FCP films after incubating in PBS for 6 days. No change in thickness indicates water-stable films.

A.2. Calibration Curves for Cationic and Anionic Dyes

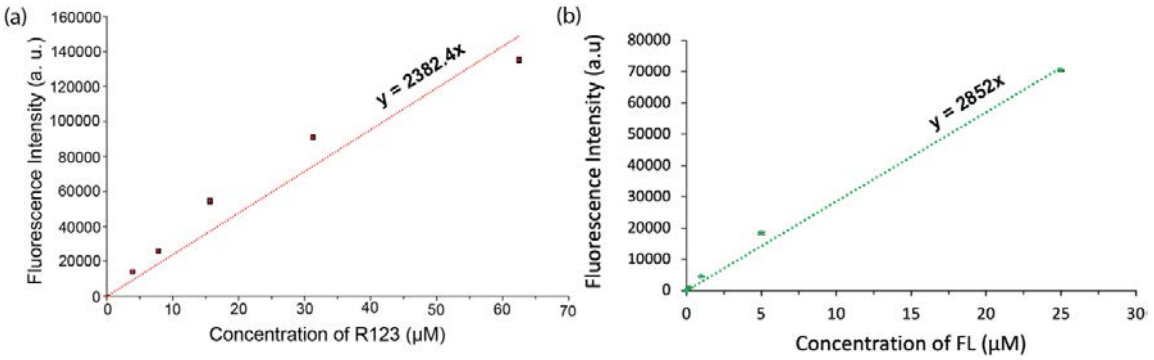

Figure A.2. Calibration curves for (a) R123 and (b) FL dyes measured in PSB buffer. Concetration of R123 and FL in Figure 1(c), Figure 2, Figure 3, and Figure S3 were measured by plugging the Fluorescence Intensity of each sample (y) into the appropriate equation to calculate the concentration (x).

A.3. Loading and Release of Dyes from BSA and Lyso Films

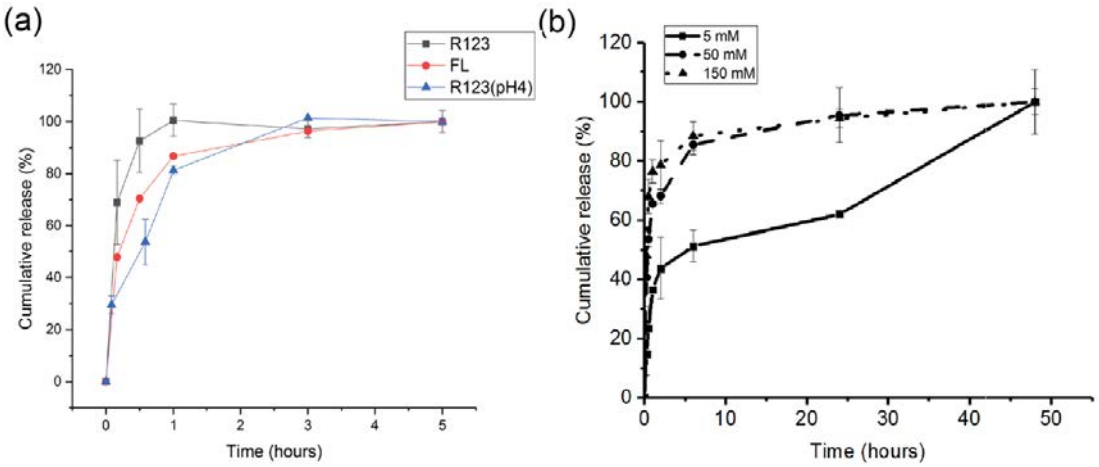

Figure A.3. (a) Cumulative release % of R123 (loaded at pH 7 and 4) and FL from BSA films. The trend shows that normalized release behavior is similar for different conditions. (b) Cumulative release (%) of R123 from BSA films at different salt concentrations over 50 hr. Release behavior demonstrates that most of the dye is released within the first 10 h at higher salt concentrations, however, is slow at low salt concentration. The sudden increase at 25 hr may be attributed to lack of data points between 25-50 hr and error resulting from evaporation of supernatant and photo-bleaching of dye.

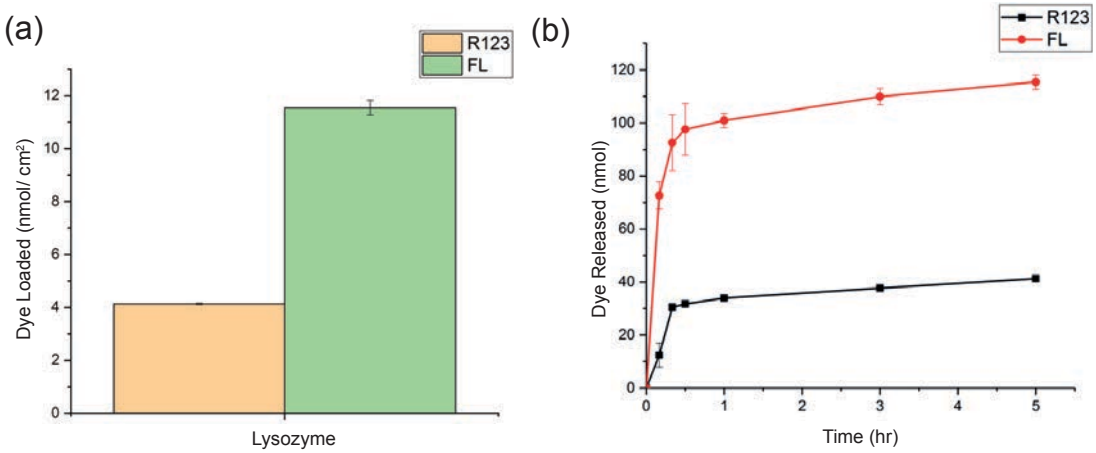

Figure A.4. (a) Loading and (b) release behavior of dyes in Lysozyme films. As expected, higher loading of anionic FL was observed in Lyso films as compared to cationic R123. The overall charge of Lysozyme is estimated as +8 [1] while that of BSA is estimated at -18 [2] at a pH of 7 which may be the primary cause of higher loading of R123 in lysozyme as compared to FL in BSA.

A.4. Colistin Loading in BSA Films

Sample Thickness (nm)	Intensity Ratio (Colistin/ Vancomycin)	Concentration of Colistin (µg/ mL)	St. Dev Intensity Ratio	St. Dev Concentration
85	1.01550713	507.7535652	0.264131724	132.065862
180	1.684150181	842.0750904	0.155603451	77.80172543
450	1.702795774	851.3978868	0.256676832	128.3384161

Table A.1. Calculations for colistin loading shown in Figure 4c. Intensity ratio and standard deviation were obtained through LDI-MS. BSA samples of different thickness were loaded with colistin and allowed to release for 15 h. Following this, the supernatant was collected and spiked with 500 µg/ mL of Vancomycin solution. Intensity ratio and standard deviation were obtained using three replicates and multiplied with the concentration of vancomycin to obtain the concentration of colistin

A.5. Calculation of Inhibition Zone of Colistin-Loaded BSA Films with Different Thicknesses

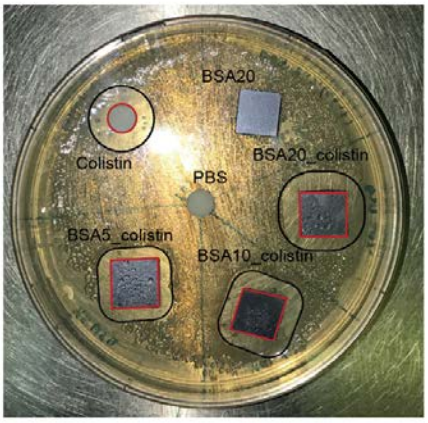

Inhibition Area - A (Black)	Sample Area - B (Red)	Normalized Inhibition Zone (A/B)
1039.03	200.50	5.18
1389.35	596.13	2.33
1786.37	710.95	2.51
1657.80	514.04	3.22

Figure A.5. Calculation of Normalized Inhibition zone for colistin-loaded BSA films of varying thicknesses. Inhibition area (marked in black) and area of the samples (Marked in red) were measured in pixels on Adobe Illustrator. Normalized inhibition zone (A/B) was then calculated as shown in the table. Experiment was repeated 3 times.

A.6. Supplementary References

1. Steudle, A.; Pleiss, J. Modelling of Lysozyme Binding to a Cation Exchange Surface at Atomic Detail: The Role of Flexibility. *Biophys. J.* **2011**, *100* (12), 3016.

2. Fologea, D.; Ledden, B.; McNabb, D. S.; Li, J. Electrical Characterization of Protein Molecules by a Solid-State Nanopore. *Appl. Phys. Lett.* **2007**, *91* (5), 053901–1.

APPENDIX B

SUPPLEMENTARY INFORMATION: HYPERSOUND-ASSISTED SIZE SORTING OF MICROPARTICLES ON INKJET-PATTERNED PROTEIN FILMS

B.1. Optical micrographs of printed protein pattern

10% w/w of protein solution (in 20% v/v ethanol in water) was loaded into magenta and yellow cartridges for printing. Optical micrograph shows protein droplets on Si surface post printing. Resolution of pattern is~ 5 μm.

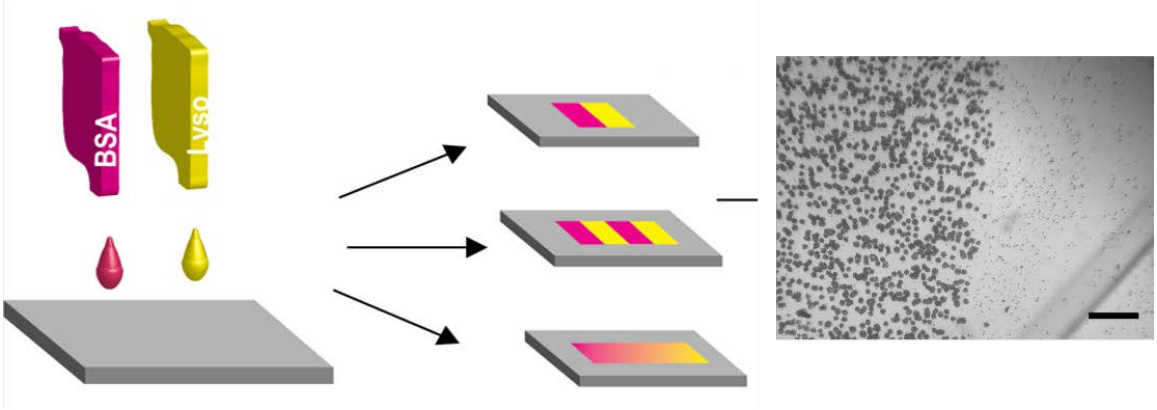

Figure B.1. Schematic representation of printing protocol and (right) optical micrograph of printed protein post PFHP treatment. Scale bar is 100 μm.

B.2. Silica Microparticle Functionalization Scheme

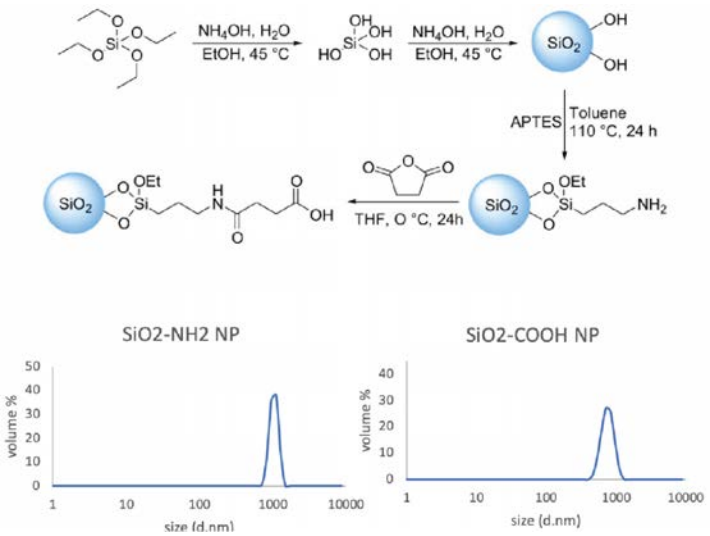

Figure B.2. Synthesis scheme for Si-COOH and DLS of 2 μm particles post -NH_2 functionalization as well as post -COOH functionalization. NO significant changes in size is observed due to treatment. Particles remain stable through treatment.

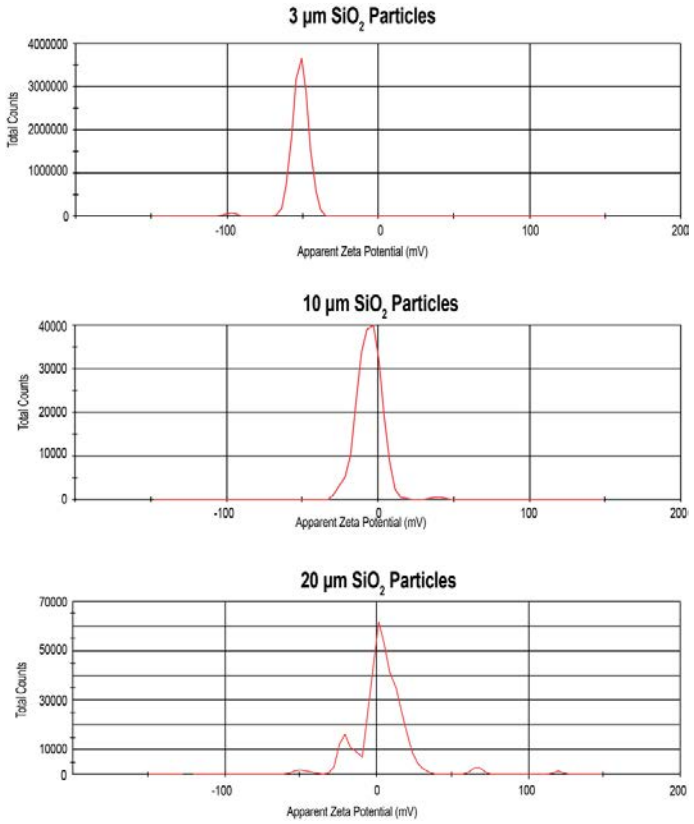

Figure B.3. Zeta potential of unfunctionalized SiO_2 microparticles of 3, 10 and 20 μm.

B.3. Surface functionalization of silica particles with -NH_2

500 mg of 3 um, 10 um and 20 um SiO_2 particles were charged separately in 2 neck round-bottom flasks. 5 mL toluene was added to the above and dispersed by sonication for 30 min. The dispersion was purged with Argon for 10 minutes, followed by the addition of 1.75 mL (3-Aminopropyl)triethoxysilane (APTES). The mixture was refluxed at 110 °C under inert condition for 12 h.

The mixture was then centrifuged at 4.4 rpm for 1 h, the precipitate collected, re-dispersed into 25 mL dry toluene, sonicated for 20 min and centrifuged again at 4.4 rpm for 20 min. The precipitate was washed with ethanol 2X and the final product lyophilized. Figure S2 shows zeta potential of particles after amine functionalization.

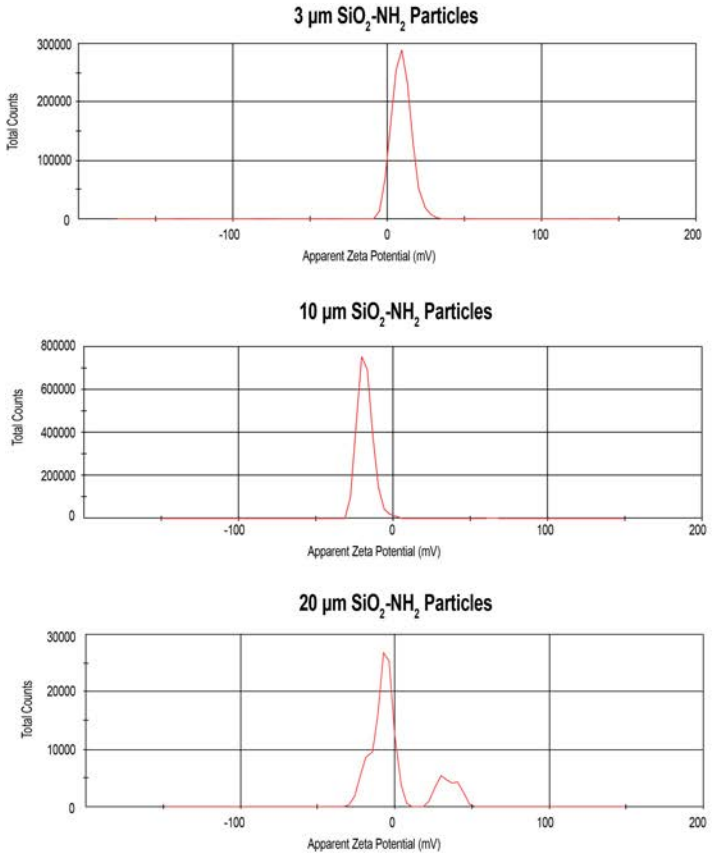

Figure B.4. Zeta potential of SiO_2-NH_2 microparticles of 3, 10 and 20 µm. Slight positive shift observed due to amine functionalization.

B.4. Surface functionalization of silica particles with -COOH

120 mg of SiO_2- NH_2 was dispersed in 6 mL THF and the suspension sonicated for 30 minutes. 420 mg succinic anhydride was added in 2 portions and stirred at 0 °C for 2 h, followed by stirring at room temperature overnight.

10 mL distilled water was then added to quench unreacted succinic anhydride, sonicated for 15 min and centrifuged at 4.4 rpm. for 1 h. The precipitate was re-dispersed in THF and centrifuged again for 15 min at the same rpm. The precipitate was collected, re-dispersed in water and centrifuged for 30 min, and lyophilized.

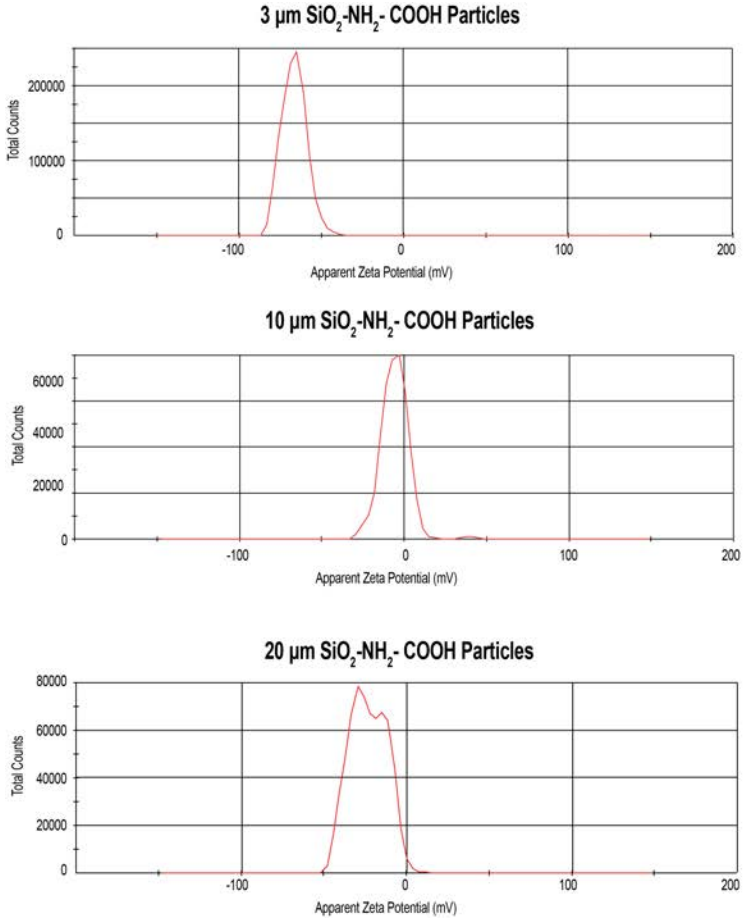

Figure B.5. Zeta potential of SiO_2-NH_2-COOH microparticles of 3, 10 and 20 µm. Negative shift observed due to carboxylate functionality.

B.5. Calculating efficiency of sorting

As shown in Figure 4 in the manuscript, several optical micrographs were obtained before and after hypersonic treatment in three regions of the surface – Lyso, BSA and drop area. Number of particles of 20 and 3 μm were manually counted in the areas of interest before and after treatment in ~3 images for each area. Table S1 summarizes the average number of particles rounded to the smallest integer observed in each region. Efficiency was calculated as follows –

$$\%\ Sorting\ efficiency\ of\ 3\ \mu m\ particles$$

$$= \frac{Number\ of\ 3\ \mu m\ particles\ in\ drop\ area}{Total\ number\ of\ particles} \times 100$$

$$\%\ Sorting\ efficiency\ of\ 20\ \mu m\ particles$$

$$= \frac{Number\ of\ 20\ \mu m\ particles\ in\ lyso}{Total\ number\ of\ particles} \times 100$$

Sorting efficiency was calculated to be **95.08%** for 3 μm particles and **91.95%** for 20 μm particles.

	Drop Area	**Lyso**	**BSA**
Total # of particles	122	87	0
20 μm	6	80	0
3 μm	116	7	0

Table B.1. Average number of particles rounded to the smallest integer for each region.

B.6. Translocation of silica particles of other sizes

Size-dependent translocation was also tested on particles of other sizes – 7 and 50 μm SiO_2-COOH particles. As seen in Figure S7 the drag force exerted by microvortices on both 7 and 50 μm particles can overcome the non-specific interactions with BSA but not the electrostatic interaction with Lyso. Magnification of 5X was used to analyze both images.

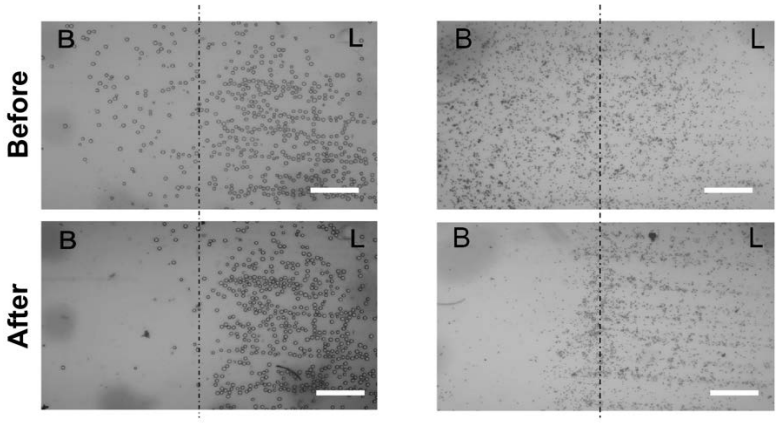

Figure B.6. Effect of hypersonic treatment on (a) 7 μm particles and (b) 50 μm particles. Drag force exerted due to hypersonic treatment is able to overcome non-specific interaction with BSA in the case of both particles. Scale bar is 160 μm.

APPENDIX C

SUPPLEMENTARY INFORMATION: HYPERSOUND-ASSISTED SIZE SORTING OF MICROPARTICLES ON INKJET-PATTERNED PROTEIN FILMS

C.1 Morphological characterization of collagen films post-treatment.

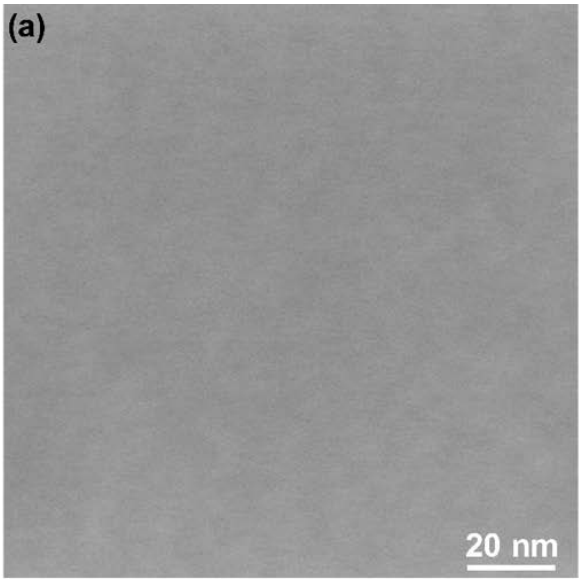

Figure C.1. Surface morphology image of Col-1 treated at 180 °C is in agreement with the results obtained using AFM. The surface and cross-section morphologies of FC were examined by a field emission scanning electron microscope (FESEM, SU6600, Hitachi, Japan) operating at 5 kV.

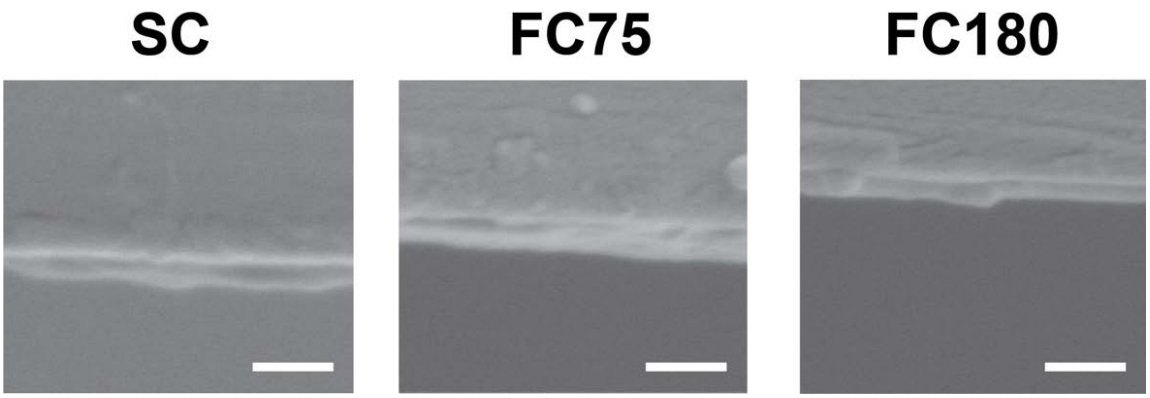

Figure C.2. Cross-sectional SEM images of SC, FC75 and FC180. It can be seen that the thickness of SC and FC75 are similar while that of FC180 is significantly lesser. Scale bars are 200 nm. Results are in agreement with ellipsometry results in Figure 3(a).

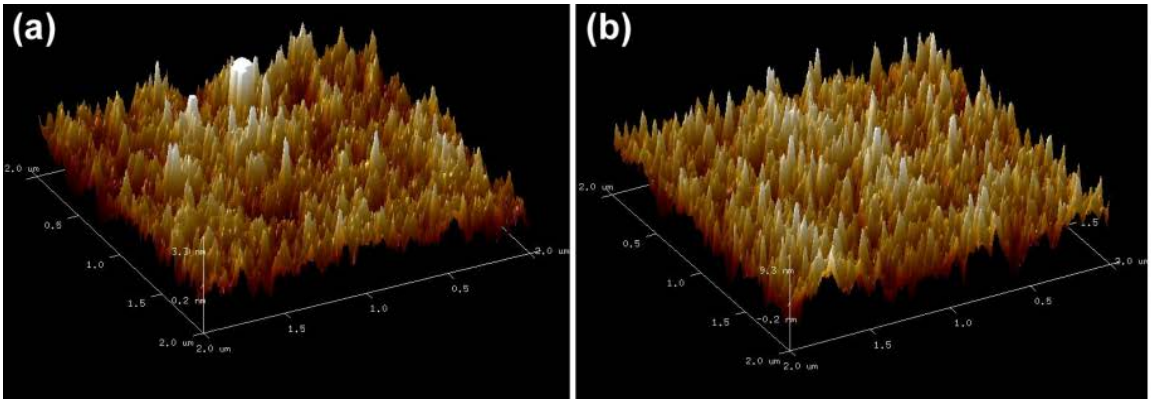

Figure C.3. 3D AFM topographical images of (a)FC180 and (b) AC180

C.2. Structural Integrity of collagen films treated at different temperatures

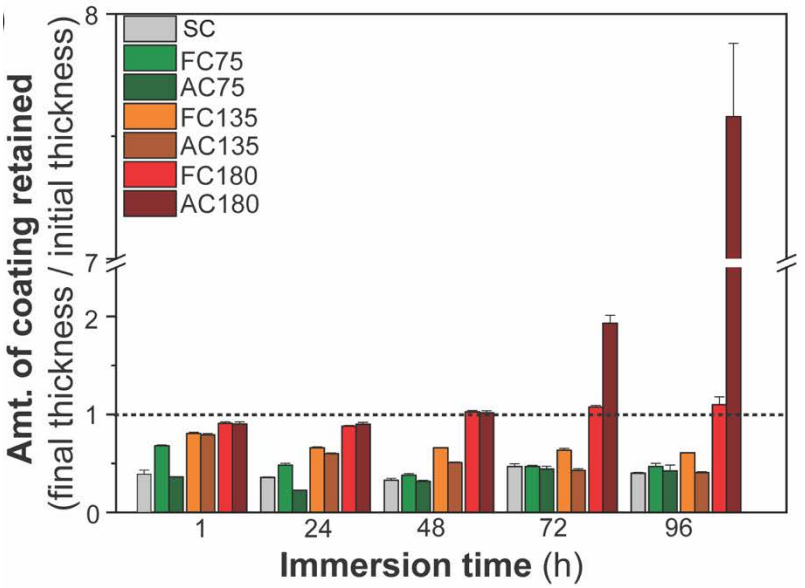

Figure C.4. Stability of heat-treated collagen films at different temperatures. At lower temperatures, thickness of collagen film rapidly reduces post-treatment. FC180 remains stable and shows no swelling behavior while AC180 shows significant swelling after 72 h.

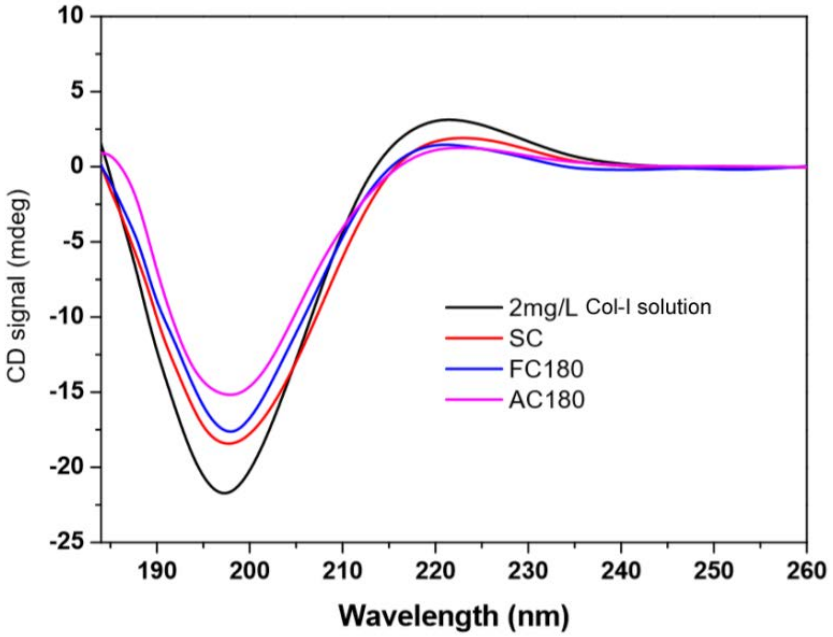

Figure C.5. CD spectra of SC, FC180 and AC180 after storing at 4 °C for 4 days. Results indicate no significant change or denaturation after incubation. This indicates that post-treatment there is no loss of structural features during swelling studies and is consistent with our explanation that loss of structure is prevented by PFHP treatment.

C.3. Cohesion strength of collagen films post treatment at different temperatures

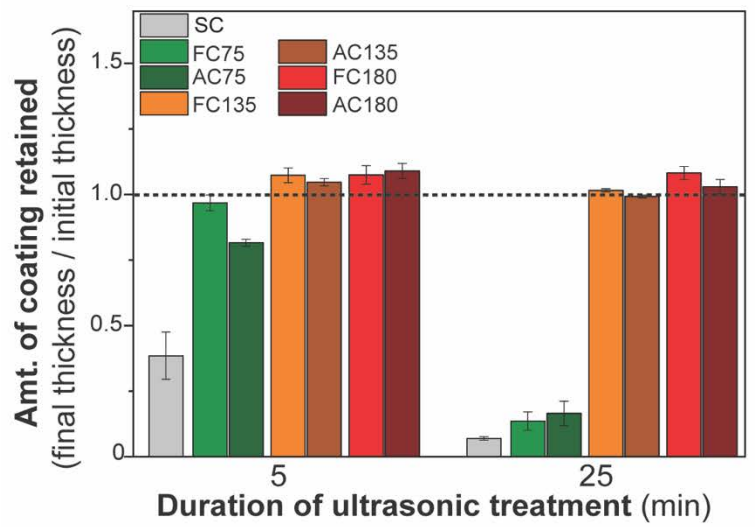

Figure C.6. Ultrasonic treatment of heat-treated films at different temperatures. Films treated at higher temperatures show greater cohesion strength.

C.4. XPS surface characterization for detecting traces of PFHP post treatment

The chemical species of the coatings were examined with a monochromatic X-ray photoelectron spectroscope (XPS; Axis Ultra, UK). In XPS tests, Mg-Ka radiation was used as an X-ray source and the photoelectron take-off angle was set at 45°. The obtained XPS spectra were corrected to the C 1s (hydrocarbon C/C, C/H) contribution at the binding energy of 284.6 eV.

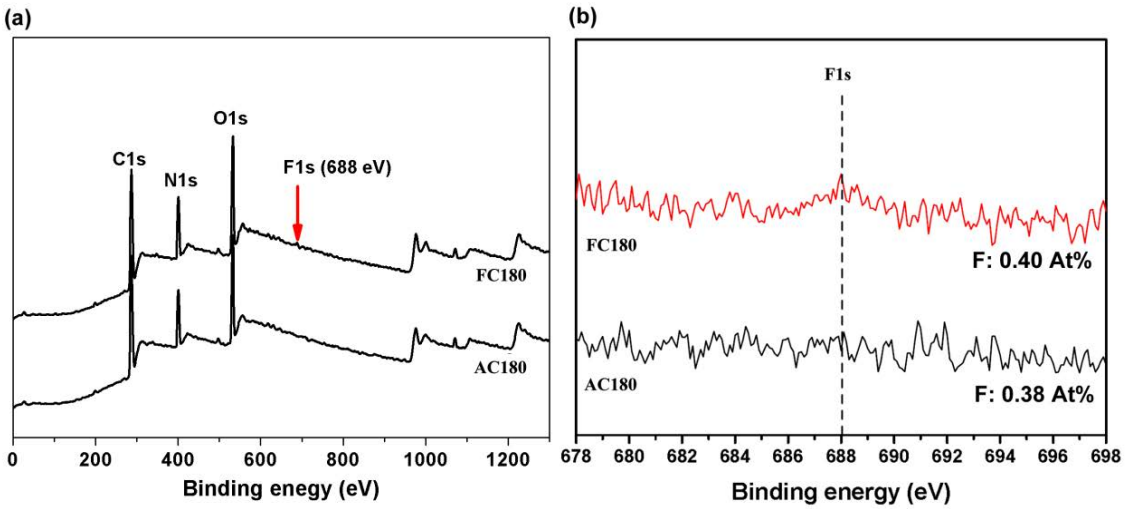

Figure C.7. XPS spectra of AC180 and FC180: (a) survey spectra, (b) high-resolution spectra of F1s. The F peak observed in XPS is beyond the limit of detection, indicating that there is no residual F on surface of PFHP treated samples

APPENDIX D

SUPPLEMENTARY INFORMATION: ULTRASOUND-ENHANCED ANTIBACTERIAL ACTIVITY OF POLYMERIC NANOPARTICLES FOR ERADICATING BACTERIAL BIOFILMS

D.1. Synthesis and characterization of PONI-C11-TMA

The protocol described in ref 1 was followed for the synthesis of PONI-C11-TMA, as depicted in Figure S1(a). Briefly, Monomer **1** (1 mg, 2.51 mmol, 1.0 eq) and 4 mL of DCM were added to a 10 mL pear-shaped air-free flask. In a separate flask, **Grubbs 3rd generation catalyst** (34.16 mg, 0.038 mmol, 0.02 eq) and 1 mL DCM were added. Both flasks were sealed with septa and attached to a Schlenk nitrogen/vacuum line. Both flasks were freeze pump-thawed three times. After thawing, Grubbs 3rd generation catalyst was syringed out and added to **1** and allowed to react for 10 min. Following this, ethyl vinyl ether (200 μL) was added and allowed to stir for 15 min. Afterwards, the reaction was diluted to twice the volume and precipitated into hexane (300 mL). The precipitated polymer **2** was filtered and directly used for the next reaction. Polymer **2** (50 mg) was added to 20 mL vials with an excess of trimethylamine (10 mL of 1 M in THF), purged with nitrogen, and stirred for 30 min at 80 °C. Half of the THF was evaporated by this time and replaced with methanol, to redissolve the polymers. The reaction was then allowed to proceed overnight at 50 °C. Next, the resultant product was washed with hexanes twice and dissolved into a minimal amount of water. The polymers were added to 10,000 MWCO dialysis membranes for purification and allowed to stir for 3 days, changing the water periodically. The polymers were filtered through PES syringe filters and freeze-dried to

yield polymer **3**. Polymer **3** was then dissolved in Milli-Q water to prepare PNP solutions for further experiments.

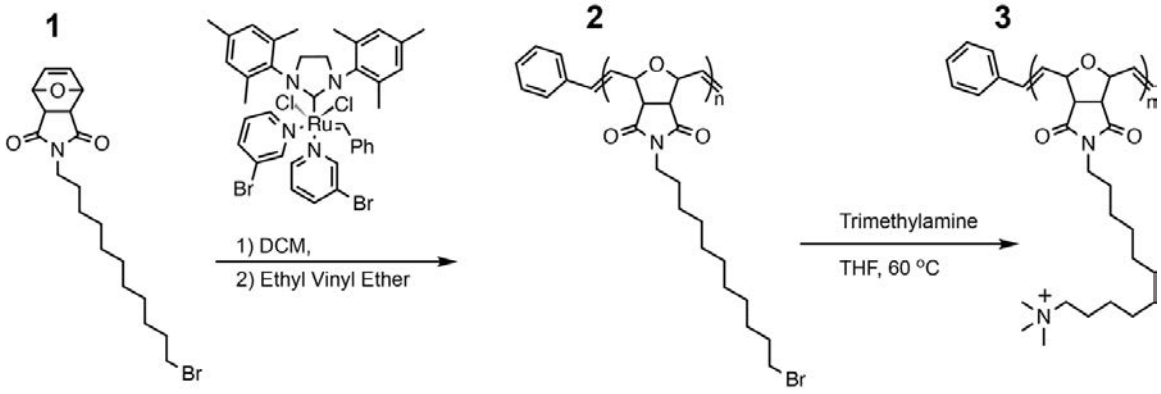

Figure D.1. Synthesis scheme for PONI-C11-TMA. Protocol and figure adapted with permission from ref 1.

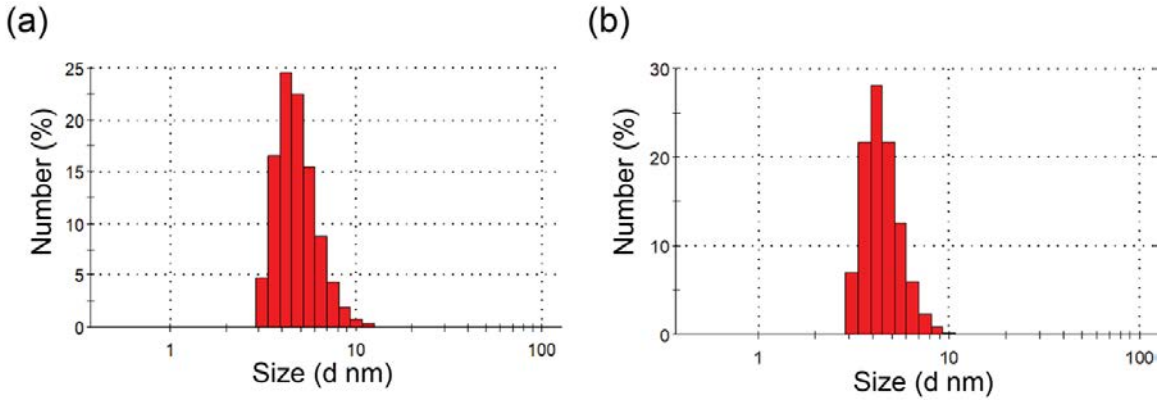

Figure D.2. (a) Particle size of the self-assembled PNPs formed by PONI-C11-TMA and (b) PNP particle size post ultrasound treatment, as measured by dynamic light scattering. The PNPs form particles of ~6 nm in size and the size does not change due to ultrasound treatment, indicating stability of the particles.

D.2 .Thermal Effect of Ultrasound Treatment

Thermal effect of ultrasound is evaluated by measuring the changes in temperature during ultrasound treatment. 2 mL of milliQ water was placed in a vial and treated with ultrasound (20 kHz; 130 W at 35% amplitude) for up to 600 s and the temperature was recorded at different intervals. Although ultrasound treatment results in some increase in

temperature from 25 ºC to 40 ºC, the thermal effect alone cannot be responsible for antimicrobial activity as significantly higher temperatures and longer durations of heat are required for eradicating bacteria.[2]

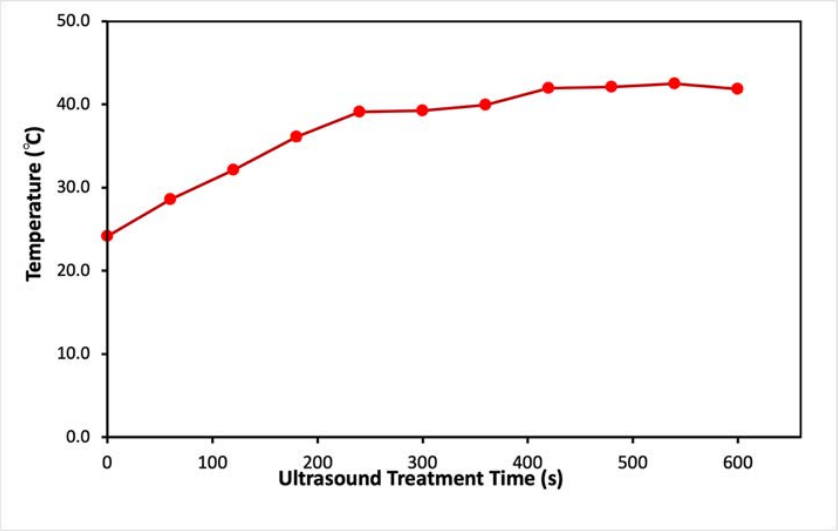

Figure D.3. Changes in temperature during ultrasound treatment in 2mL of water

Antibacterial Activity of Ultrasound and PNPs

D.3. Antibacterial Activity of Ultrasound and PNPs

Bacterial susceptibility towards antimicrobial PNP treatment was evaluated by increasing the duration between ultrasound and PNP treatment. Mature E. coli biofilms were first treated with 150 s of ultrasound and allowed to rest at room temperature for varying durations from 0 - 60 min. Following this, 0.125 mg/mL PNP solution was added to each well. Biofilms were then incubated at 37 ºC for 30 min before measuring %biofilm viability using alamarBlue assay. A significant reduction in biofilm viability was observed due to the combination treatment, as compared to US alone, even when there was a 30 min

delay between US and PNP treatments, indicating that biofilms remained susceptible up to 30 min after US treatment.

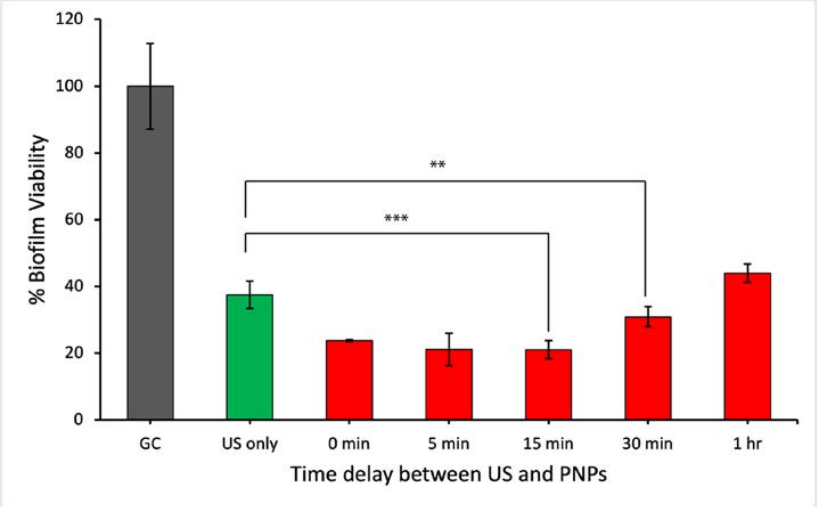

Figure D.4. Prolonged bacterial susceptibility post ultrasound treatment. Grey bar represents untreated growth control (GC), green bar represents ultrasound treatment only for 150 s, and red bars represent time delay between ultrasound and PNP treatment. Error bars represent standard deviation (n=3). *, **, *** = P values < 0.05, 0.01, 0.001, respectively calculated by a two-tailed test.

Antibacterial efficacy of combination treatment was evaluated by varying both - the concentration of PNPs from 0 - 0.25 mg/mL, and duration of US treatment from 0 – 600 s. Following this, %biofilm viability was measured by alamarBlue assay and %biofilm toxicity was reported as shown below. The degree of synergy was calculated for each combination through the Bliss independence model of synergy. [3] Briefly, the expected effect for each combination was defined as $\boldsymbol{E_{xy} = E_x + E_y - E_x E_y}$, wherein $\boldsymbol{E_x}$ (%biofilm Toxicity/100) is the probability of bacterial death from PNPs alone, and $\boldsymbol{E_y}$ is the probability of bacterial death from US alone. The experimentally observed effect $\boldsymbol{E_{exp}}$ for each combination is compared to $\boldsymbol{E_{xy}}$ and the ratio of $\boldsymbol{E_{exp}}$: $\boldsymbol{E_{xy}}$ is then calculated. The combination xy is considered synergistic if $\boldsymbol{E_{exp}}$: $\boldsymbol{E_{xy} > 1.1}$, antagonistic if $\boldsymbol{E_{exp}}$: $\boldsymbol{E_{xy}} <$

$\mathbf{0.9}$, and additive if $\mathbf{0.9} < \boldsymbol{E_{exp}}$: $\boldsymbol{E_{xy}} < \mathbf{1.1}$. Conditions marked NaN denote situations where there was an overgrowth of bacteria due to hormesis.

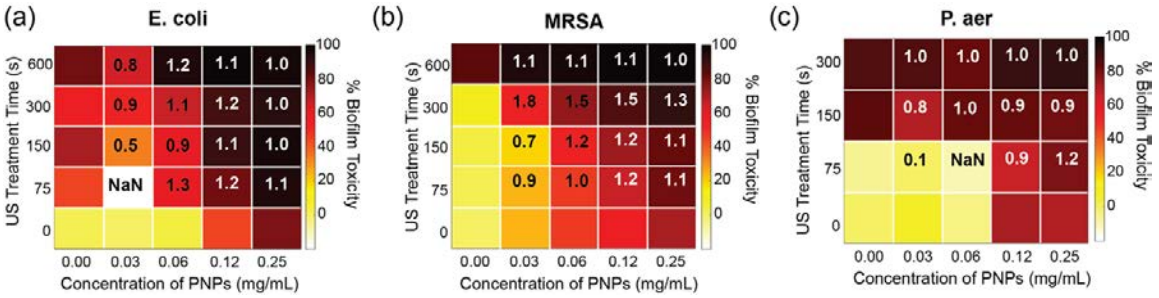

Figure D.5. Bliss synergy scores for combination treatment of PNPs and ultrasound. The combination is considered additive for scores between 0.9-1.1, synergistic for scores >1.1 and antagonistic for scores <0.9.

D.4. Effect of Ultrasound on Fibroblast cells

Ultrasound treatment is expected to produce excessive mechanical stress on cells in an *in vitro* culture due to the absence of the extracellular matrix. [4] Similar to bacteria, ultrasound is expected to lead to cell membrane disruption due to the mechanical perturbations and cavitation associated with ultrasound. However, in the native tissue environment most of this energy is absorbed by the extracellular matrix thereby protecting the cells. [5] Therefore, a collagen-based matrix was utilized to mimic this environment during the co-culture treatments shown in Figure 5. Rat-tail collagen 1 solution of concentration 1 mg/mL was utilized to coat the bottom of 12 well plates prior to cell culture. 1 mL of the collagen solution was placed into each well and incubated at 37 ºC for 1 hr to allow for the formation of stable coatings. Excess collagen solution was then removed, and the plates were washed with PBS and utilized immediately for culturing cells. 3T3 fibroblast cells were cultured in DMEM in the presence of 10% fetal bovine serum and 1% antibiotic solution. 100,000 cells/well were plated on uncoated and collagen-coated

wells and allowed to grow overnight at 37 °C in a humidified atmosphere of 5% CO2. The next day each well was washed once with PBS and replenished with 2 mL of cell culture media and treated with varying durations of ultrasound from 0 to 600 s. Treated wells were then incubated at 37 ºC for 30 min before treating with alamarBlue assay to measure the cell viability (summarized in Figure S6). As seen in Figure S6, coated collagen plates show significantly higher cell viability as compared to uncoated plates, post 75 and 150 s of ultrasound treatment. This is expected to increase further in the presence of a biofilm in a co-culture model (As seen in Figure 5) as the biofilm matrix provides an additional layer of protection to the cells.

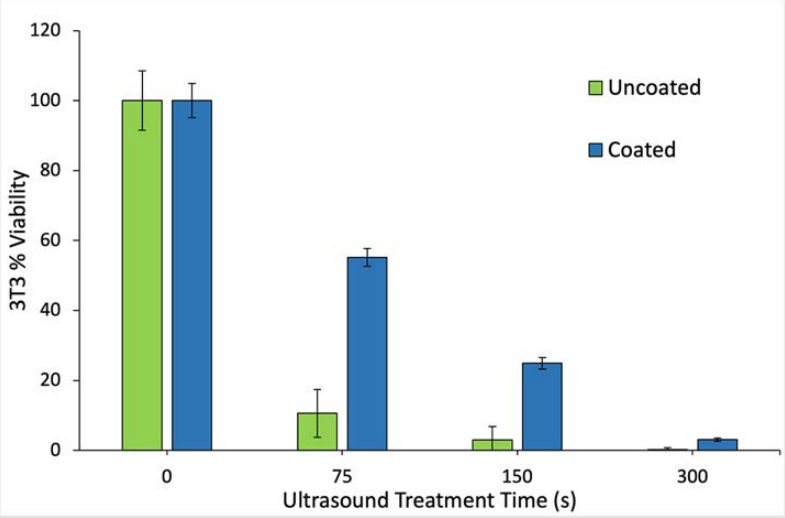

Figure D.6. Fibroblast viability due to collagen. Collagen coating (orange) shows 50% cell viability after 75 s and 30% viability after 150 s ultrasound treatment. By comparison, only 10% of the cells in the uncoated plates survive 75 s of ultrasound treatment.

D.5. Supplementary References

1. Makabenta, J. M. V.; Park, J.; Li, C. H.; Chattopadhyay, A. N.; Nabawy, A.; Landis, R. F.; Gupta, A.; Schmidt-Malan, S.; Patel, R.; Rotello, V. M. Polymeric Nanoparticles Active against Dual-Species Bacterial Biofilms. *Molecules* **2021**, *26* (16).

2. Espinosa, M. F.; Sancho, A. N.; Mendoza, L. M.; Mota, C. R.; Verbyla, M. E. Systematic Review and Meta-Analysis of Time-Temperature Pathogen Inactivation. *Int. J. Hyg. Environ. Health* **2020**, *230*, 113595.

3. Tang, J.; Wennerberg, K.; Aittokallio, T. What Is Synergy? The Saariselkï¿½ Agreement Revisited. *Front. Pharmacol.* **2015**, *6* (SEP), 181.

4. Baker, K. G.; Robertson, V. J.; Duck, F. A. A Review of Therapeutic Ultrasound: Biophysical Effects. *Phys. Ther.* **2001**, *81* (7), 1351–1358.

5. Kanta, J. Collagen Matrix as a Tool in Studying Fibroblastic Cell Behavior. *Cell Adh. Migr.* **2015**, *9* (4), 308.

BIBLIOGRAPHY

1. Menon, G. K.; Cleary, G. W.; Lane, M. E. The Structure and Function of the Stratum Corneum. *Int. J. Pharm.* **2012**, *435* (1), 3–9.

2. The cardiac muscle cell - Severs - 2000 - BioEssays - Wiley Online Library https://onlinelibrary.wiley.com/doi/10.1002/(SICI)1521-1878(200002)22:2%3C188::AID-BIES10%3E3.0.CO;2-T

3. Schuliga, M.; Read, J.; Knight, D. A. Ageing Mechanisms That Contribute to Tissue Remodeling in Lung Disease. Ageing Res. Rev. 2021, 70, 101405.

4. Frykberg, R. G.; Banks, J. Challenges in the Treatment of Chronic Wounds. Adv. Wound Care 2015, 4 (9), 560–582.

5. Tranquilli Leali, P.; Merolli, A. Fundamentals of Biomaterials. Biomater. Hand Surg. 2009, 1–11.

6. Gallo, J.; Holinka, M.; Moucha, C. S. Antibacterial Surface Treatment for Orthopaedic Implants. Int. J. Mol. Sci. 2014, Vol. 15, Pages 13849-13880 2014, 15 (8), 13849–13880.

7. Huebsch, N.; Mooney, D. J. Inspiration and Application in the Evolution of Biomaterials. Nat. 2009 4627272 2009, 462 (7272), 426–432.

8. Ralls, A.; Kumar, P.; Misra, M.; Menezes, P. L. Material Design and Surface Engineering for Bio-Implants. JOM 2020, 72 (2), 684–696.

9. Kokubo, T.; Kim, H. M.; Kawashita, M. Novel Bioactive Materials with Different Mechanical Properties. Biomaterials 2003, 24 (13), 2161–2175.

10. Islam, M. M.; Shahruzzaman, M.; Biswas, S.; Nurus Sakib, M.; Rashid, T. U. Chitosan Based Bioactive Materials in Tissue Engineering Applications-A Review. Bioact. Mater. 2020, 5 (1), 164–183.

11. Pan, H.; Zheng, M.; Ma, A.; Liu, L.; Cai, L. Cell/Bacteria-Based Bioactive Materials for Cancer Immune Modulation and Precision Therapy. Adv. Mater. 2021, 33 (50), 2100241.

12. Mart, R. J.; Osborne, R. D.; Stevens, M. M.; Ulijn, R. V. Peptide-Based Stimuli-Responsive Biomaterials. Soft Matter 2006, 2 (10), 822–835.

13. Godavitarne, C.; Robertson, A.; Peters, J.; Rogers, B. Biodegradable Materials. Orthop. Trauma 2017, 31 (5), 316–320.

14. Griffith, L. G. Polymeric Biomaterials. Acta Mater. 2000, 48 (1), 263–277.

15. Baranwal, J.; Barse, B.; Fais, A.; Delogu, G. L.; Kumar, A. Biopolymer: A Sustainable Material for Food and Medical Applications. Polymers (Basel). 2022, 14 (5).

16. Kaplan, D. L. Introduction to Biopolymers from Renewable Resources. Biopolym. from Renew. Resour. 1998, 1–29.

17. Cui, C.; Fu, Q.; Meng, L.; Hao, S.; Dai, R.; Yang, J. Recent Progress in Natural Biopolymers Conductive Hydrogels for Flexible Wearable Sensors and Energy Devices: Materials, Structures, and Performance. ACS Appl. Bio Mater. 2021, 4 (1), 85–121.

18. Shuborna, N. S.; Chaiyasamut, T.; Sakdajeyont, W.; Vorakulpipat, C.; Rojvanakarn, M.; Wongsirichat, N. Generation of Novel Hyaluronic Acid Biomaterials for Study of Pain in Third Molar Intervention: A Review. J. Dent. Anesth. Pain Med. 2019, 19 (1), 11.

19. Jin, M.; Shi, J.; Zhu, W.; Yao, H.; Wang, D. A. Polysaccharide-Based Biomaterials in Tissue Engineering: A Review. https://home.liebertpub.com/teb 2021, 27 (6), 604–626.

20. Gopalakrishnan, S.; Xu, J.; Zhong, F.; Rotello, V. M. Strategies for Fabricating Protein Films for Biomaterial Applications. Adv. Sustain. Syst. 2021, 5 (1), 2000167.

21. Wang, L. S.; Gopalakrishnan, S.; Lee, Y. W.; Zhu, J.; Nonnenmann, S. S.; Rotello, V. M. Translation of Protein Charge and Hydrophilicity to Materials Surface Properties Using Thermal Treatment in Fluorous Media. Mater. Horizons 2018, 5 (2), 268–274.

22. Xu, X.; Zhang, D.; Gao, S.; Shiba, T.; Yuan, Q.; Cheng, K.; Tan, H.; Li, J. Multifunctional Biomaterial Coating Based on Bio-Inspired Polyphosphate and Lysozyme Supramolecular Nanofilm. Biomacromolecules 2018, 19 (6), 1979–1989.

23. Yue, L.; Wang, S.; Zhou, Z.; Willner, I. Nucleic Acid Based Constitutional Dynamic Networks: From Basic Principles to Applications. J. Am. Chem. Soc. 2020, 142 (52), 21577–21594.

24. Yuan, Y.; Gu, Z.; Yao, C.; Luo, D.; Yang, D. Nucleic Acid–Based Functional Nanomaterials as Advanced Cancer Therapeutics. Small 2019, 15 (26), 1900172.

25. Becker, M. L.; Burdick, J. A. Introduction: Polymeric Biomaterials. Chem. Rev. 2021, 121 (18), 10789–10791.

26. Angelova, N.; Hunkeler, D. Rationalizing the Design of Polymeric Biomaterials. Trends Biotechnol. 1999, 17 (10), 409–421.

27. Teo, A. J. T.; Mishra, A.; Park, I.; Kim, Y. J.; Park, W. T.; Yoon, Y. J. Polymeric Biomaterials for Medical Implants and Devices. ACS Biomater. Sci. Eng. 2016, 2 (4), 454–472.

28. Pandolfino, J. Ambulatory Esophageal PH Monitoring Using a Wireless System. Am. J. Gastroenterol. 2003, 98 (4), 740–749..

29. Mir, M.; Ali, M. N.; Barakullah, A.; Gulzar, A.; Arshad, M.; Fatima, S.; Asad, M. Synthetic Polymeric Biomaterials for Wound Healing: A Review. *Prog. Biomater. 2018 71* **2018**, *7* (1), 1–21.

30. Jenks, M.; Craig, J.; Green, W.; Hewitt, N.; Arber, M.; Sims, A. Tegaderm CHG IV Securement Dressing for Central Venous and Arterial Catheter Insertion Sites: A NICE Medical Technology Guidance. Appl. Health Econ. Health Policy 2016, 14 (2), 135–149.

31. Khil, M. S.; Cha, D. Il; Kim, H. Y.; Kim, I. S.; Bhattarai, N. Electrospun Nanofibrous Polyurethane Membrane as Wound Dressing. J. Biomed. Mater. Res. Part B Appl. Biomater. 2003, 67B (2), 675–679.

32. Ramakrishna, S.; Mayer, J.; Wintermantel, E.; Leong, K. W. Biomedical Applications of Polymer-Composite Materials: A Review. Compos. Sci. Technol. 2001, 61 (9), 1189–1224.

33. Cools, P.; De Geyter, N.; Vanderleyden, E.; Barberis, F.; Dubruel, P.; Morent, R. Adhesion Improvement at the PMMA Bone Cement-Titanium Implant Interface Using Methyl Methacrylate Atmospheric Pressure Plasma Polymerization. Surf. Coatings Technol. 2016, 294, 201–209.

34. Moszner, N.; Salz, U. New Developments of Polymeric Dental Composites. Prog. Polym. Sci. 2001, 26 (4), 535–576.

35. Chen, L.; Yu, Q.; Wang, Y.; Li, H. BisGMA/TEGDMA Dental Composite Containing High Aspect-Ratio Hydroxyapatite Nanofibers. Dent. Mater. 2011, 27 (11), 1187.

36. Saito, N.; Aoki, K.; Usui, Y.; Shimizu, M.; Hara, K.; Narita, N.; Ogihara, N.; Nakamura, K.; Ishigaki, N.; Kato, H.; et al. Application of Carbon Fibers to Biomaterials: A New Era of Nano-Level Control of Carbon Fibers after 30-Years of Development. Chem. Soc. Rev. 2011, 40 (7), 3824–3834.

37. Iha, R. K.; Wooley, K. L.; Nyström, A. M.; Burked, D. J.; Kade, M. J.; Hawker, C. J. Applications of Orthogonal, "Click" Chemistries in the Synthesis of Functional Soft Materials. Chem. Rev. 2009, 109 (11), 5620.

38. O'reilly, R. K.; Hawker, C. J.; Wooley, K. L. Cross-Linked Block Copolymer Micelles: Functional Nanostructures of Great Potential and Versatility. Chem. Soc. Rev. 2006, 35 (11), 1068–1083.

39. Elsabahy, M.; Wooley, K. L. Design of Polymeric Nanoparticles for Biomedical Delivery Applications. Chem. Soc. Rev. 2012, 41 (7), 2545.

40. Makabenta, J. M. V.; Nabawy, A.; Li, C. H.; Schmidt-Malan, S.; Patel, R.; Rotello, V. M. Nanomaterial-Based Therapeutics for Antibiotic-Resistant Bacterial Infections. Nat. Rev. Microbiol. 2021, 19 (1), 23.

41. Kalhapure, R. S.; Jadhav, M.; Rambharose, S.; Mocktar, C.; Singh, S.; Renukuntla, J.; Govender, T. PH-Responsive Chitosan Nanoparticles from a Novel Twin-Chain Anionic Amphiphile for Controlled and Targeted Delivery of Vancomycin. Colloids Surf. B. Biointerfaces 2017, 158, 650–657.

42. Song, J.; Jang, J. Antimicrobial Polymer Nanostructures: Synthetic Route, Mechanism of Action, and Perspective. Adv. Colloid Interface Sci. 2014, 203, 37–50.

43. Mei, L.; Lu, Z.; Zhang, X.; Li, C.; Jia, Y. Polymer-Ag Nanocomposites with Enhanced Antimicrobial Activity against Bacterial Infection. ACS Appl. Mater. Interfaces 2014, 6 (18), 15813–15821.

44. Landis, R. F.; Gupta, A.; Lee, Y. W.; Wang, L. S.; Golba, B.; Couillaud, B.; Ridolfo, R.; Das, R.; Rotello, V. M. Crosslinked Polymer-Stabilized Nanocomposites for the Treatment of Bacterial Biofilms. ACS Nano 2017, 11 (1), 946.

45. González-Toro, D. C.; Ryu, J. H.; Chacko, R. T.; Zhuang, J.; Thayumanavan, S. Concurrent Binding and Delivery of Proteins and Lipophilic Small Molecules Using Polymeric Nanogels. *J. Am. Chem. Soc.* **2012**, *134* (16), 6964.

46. Sgolastra, F.; Backlund, C. M.; Ilker Ozay, E.; deRonde, B. M.; Minter, L. M.; Tew, G. N. Sequence Segregation Improves Non-Covalent Protein Delivery. J. Control. Release 2017, 254, 131.

47. Zhang, X.; Landis, R. F.; Keshri, P.; Cao-Milán, R.; Luther, D. C.; Gopalakrishnan, S.; Liu, Y.; Huang, R.; Li, G.; Malassiné, M.; et al. Intracellular Activation of Anticancer Therapeutics Using Polymeric Bioorthogonal Nanocatalysts. Adv. Healthc. Mater. 2021, 10 (5), 2001627.

48. Fedeli, S.; Im, J.; Gopalakrishnan, S.; Elia, J. L.; Gupta, A.; Kim, D.; Rotello, V. M. Nanomaterial-Based Bioorthogonal Nanozymes for Biological Applications. Chem. Soc. Rev. 2021, 50 (24), 13467–13480.

49. Huang, R.; Li, C. H.; Cao-Milán, R.; He, L. D.; Makabenta, J. M.; Zhang, X.; Yu, E.; Rotello, V. M. Polymer-Based Bioorthogonal Nanocatalysts for the Treatment of Bacterial Biofilms. J. Am. Chem. Soc. 2020, 142 (24), 10723–10729.

50. Raza, A.; Rasheed, T.; Nabeel, F.; Hayat, U.; Bilal, M.; Iqbal, H. M. N. Endogenous and Exogenous Stimuli-Responsive Drug Delivery Systems for Programmed Site-Specific Release. Molecules 2019, 24 (6).

51. Colson, Y. L.; Grinstaff, M. W. Biologically Responsive Polymeric Nanoparticles for Drug Delivery. Adv. Mater. 2012, 24 (28), 3878–3886.

52. Gupta, P.; Vermani, K.; Garg, S. Hydrogels: From Controlled Release to PH-Responsive Drug Delivery. Drug Discov. Today 2002, 7 (10), 569–579.

53. Alkekhia, D.; LaRose, C.; Shukla, A. β-Lactamase-Responsive Hydrogel Drug Delivery Platform for Bacteria-Triggered Cargo Release. ACS Appl. Mater. Interfaces 2022, 14 (24), 27538–27550.

54. Guo, B.; Ma, P. X. Conducting Polymers for Tissue Engineering. Biomacromolecules 2018, 19 (6), 1764.

55. Xie, Y. Q.; Wei, L.; Tang, L. Immunoengineering with Biomaterials for Enhanced Cancer Immunotherapy. Wiley Interdiscip. Rev. Nanomedicine Nanobiotechnology 2018, 10 (4), e1506.

56. Oberli, M. A.; Schoellhammer, C. M.; Langer, R.; Blankschtein, D. Ultrasound-Enhanced Transdermal Delivery: Recent Advances and Future Challenges. Ther. Deliv. 2014, 5 (7), 843.

57. Wu, T.; Zhang, D.; Qiao, Q.; Qin, X.; Yang, C.; Kong, M.; Deng, H.; Zhang, Z. Biomimetic Nanovesicles for Enhanced Antitumor Activity of Combinational Photothermal and Chemotherapy. Mol. Pharm. 2018, 15 (3), 1341–1352.

58. Chatterjee, S.; Hui, P. C. L.; Kan, C. wai. Thermoresponsive Hydrogels and Their Biomedical Applications: Special Insight into Their Applications in Textile Based Transdermal Therapy. Polymers (Basel). 2018, 10 (5).

59. Li, J.; Pu, K. Semiconducting Polymer Nanomaterials as Near-Infrared Photoactivatable Protherapeutics for Cancer. Acc. Chem. Res. 2020, 53 (4), 752–762.

60. Miller, D. L.; Smith, N. B.; Bailey, M. R.; Czarnota, G. J.; Hynynen, K.; Makin, I. R. S. Overview of Therapeutic Ultrasound Applications and Safety Considerations. J. Ultrasound Med. 2012, 31 (4), 623. https://doi.org/10.7863/JUM.2012.31.4.623.

61. Deprez, J.; Lajoinie, G.; Engelen, Y.; De Smedt, S. C.; Lentacker, I. Opening Doors with Ultrasound and Microbubbles: Beating Biological Barriers to Promote Drug Delivery. Adv. Drug Deliv. Rev. 2021, 172, 9–36.

62. Bos, J. D.; Meinardi, M. M. H. M. The 500 Dalton Rule for the Skin Penetration of Chemical Compounds and Drugs. Exp. Dermatol. 2000, 9 (3), 165–169.

63. Mitragotri, S. Sonophoresis: A 50-Year Journey. Drug Discov. Today 2004, 9 (17), 735–736.

64. Ryu, Y. C.; Kim, D. I.; Kim, S. H.; Wang, H. M. D.; Hwang, B. H. Synergistic Transdermal Delivery of Biomacromolecules Using Sonophoresis after Microneedle Treatment. Biotechnol. B*ioprocess Eng*. *2018 233* **2018**, *23* (3), 286–292.

65. Mitragotri, S. Sonophoresis: Ultrasound-Mediated Transdermal Drug Delivery. Percutaneous Penetration Enhanc. Phys. Methods Penetration Enhanc. 2017, 3–14.

66. Tharkar, P.; Varanasi, R.; Wong, W. S. F.; Jin, C. T.; Chrzanowski, W. Nano-Enhanced Drug Delivery and Therapeutic Ultrasound for Cancer Treatment and Beyond. Front. Bioeng. Biotechnol. 2019, 7, 324.

67. van den Bijgaart, R. J. E.; Eikelenboom, D. C.; Hoogenboom, M.; Fütterer, J. J.; den Brok, M. H.; Adema, G. J. Thermal and Mechanical High-Intensity Focused Ultrasound: Perspectives on Tumor Ablation, Immune Effects and Combination Strategies. Cancer Immunol. Immunother. 2017, 66 (2), 247–258.

68. Huebsch, N.; Kearney, C. J.; Zhao, X.; Kim, J.; Cezar, C. A.; Suo, Z.; Mooney, D. J. Ultrasound-Triggered Disruption and Self-Healing of Reversibly Cross-Linked Hydrogels for Drug Delivery and Enhanced Chemotherapy. Proc. Natl. Acad. Sci. U. S. A. 2014, 111 (27), 9762–9767.

69. Kearney, C. J.; Skaat, H.; Kennedy, S. M.; Hu, J.; Darnell, M.; Raimondo, T. M.; Mooney, D. J. Switchable Release of Entrapped Nanoparticles from Alginate Hydrogels. Adv. Healthc. Mater. 2015, 4 (11), 1634–1639.

70. Arrizabalaga, J. H.; Smallcomb, M.; Abu-Laban, M.; Liu, Y.; Yeingst, T. J.; Dhawan, A.; Simon, J. C.; Hayes, D. J. Ultrasound-Responsive Hydrogels for On-Demand Protein Release. ACS Appl. Bio Mater. 2022.

71. Pourhajibagher, M.; Bahador, A. Synergistic Biocidal Effects of Metal Oxide Nanoparticles-Assisted Ultrasound Irradiation: Antimicrobial Sonodynamic Therapy against Streptococcus Mutans Biofilms. Photodiagnosis Photodyn. Ther. 2021, 35.

72. Wang, H.; Guo, J.; Lin, W.; Fu, Z.; Ji, X.; Yu, B.; Lu, M.; Cui, W.; Deng, L.; Engle, J. W.; et al. Open-Shell Nanosensitizers for Glutathione Responsive Cancer Sonodynamic Therapy. Adv. Mater. 2022, 34 (15), 2110283.

73. DeFrates, K. G.; Moore, R.; Borgesi, J.; Lin, G.; Mulderig, T.; Beachley, V.; Hu, X. Protein-Based Fiber Materials in Medicine: A Review. Nanomater. (Basel, Switzerland) 2018, 8 (7).

74. Wang, L.-S.; Gopalakrishnan, S.; Rotello, V. M. Tailored Functional Surfaces Using Nanoparticle and Protein "Nanobrick" Coatings. 2019, 35, 23.

75. Andonegi, M.; Irastorza, A.; Izeta, A.; Cabezudo, S.; de la Caba, K.; Guerrero, P. A Green Approach towards Native Collagen Scaffolds: Environmental and Physicochemical Assessment. Polymers (Basel). 2020, 12 (7).

76. Lin, L.; Liao, X.; Cui, H. Cold Plasma Treated Thyme Essential Oil/Silk Fibroin Nanofibers against Salmonella Typhimurium in Poultry Meat. Food Packag. Shelf Life 2019, 21, 100337.

77. Pinheiro Bruni, G.; de Oliveira, J. P.; Gómez-Mascaraque, L. G.; Fabra, M. J.; Guimarães Martins, V.; Zavareze, E. da R.; López-Rubio, A. Electrospun β-Carotene–Loaded SPI:PVA Fiber Mats Produced by Emulsion-Electrospinning as Bioactive Coatings for Food Packaging. Food Packag. Shelf Life 2020, 23, 100426.

78. Holland, C.; Numata, K.; Rnjak-Kovacina, J.; Seib, F. P. The Biomedical Use of Silk: Past, Present, Future. Adv. Healthc. Mater. 2019, 8 (1), 1800465.

79. Goder, D.; Matsliah, L.; Giladi, S.; Reshef-Steinberger, L.; Zin, I.; Shaul, A.; Zilberman, M. Mechanical, Physical and Biological Characterization of Soy Protein Films Loaded with Bupivacaine for Wound Healing Applications. International Journal of Polymeric Materials and Polymeric Biomaterials 2020, 1.

80. Valentini, L.; Bittolo Bon, S.; Pugno, N. M. Combining Living Microorganisms with Regenerated Silk Provides Nanofibril-Based Thin Films with Heat-Responsive Wrinkled States for Smart Food Packaging. Nanomater. 2018, Vol. 8, Page 518 2018, 8 (7), 518.

81. Kuruwita, D. P.; Jiang, X.; Darby, D.; Sharp, J. L.; Fraser, A. M. Persistence of Escherichia Coli O157:H7 and Listeria Monocytogenes on the Exterior of Three Common Food Packaging Materials. Food Control 2020, 112, 107153.

82. Tao, H.; Kaplan, D. L.; Omenetto, F. G. Silk Materials – A Road to Sustainable High Technology. Adv. Mater. 2012, 24 (21), 2824–2837.

83. Arora, A.; Padua, G. W. Review: Nanocomposites in Food Packaging. J. Food Sci. 2010, 75 (1).

84. Zhao, S.; Wang, Z.; Kang, H.; Li, J.; Zhang, S.; Han, C.; Huang, A. Fully Bio-Based Soybean Adhesive in Situ Cross-Linked by Interactive Network Skeleton from Plant Oil-Anchored Fiber. Ind. Crops Prod. 2018, 122, 366–374.

85. Hassan, B.; Chatha, S. A. S.; Hussain, A. I.; Zia, K. M.; Akhtar, N. Recent Advances on Polysaccharides, Lipids and Protein Based Edible Films and Coatings: A Review. Int. J. Biol. Macromol. 2018, 109, 1095–1107.

86. Abaee, A.; Mohammadian, M.; Jafari, S. M. Whey and Soy Protein-Based Hydrogels and Nano-Hydrogels as Bioactive Delivery Systems. Trends Food Sci. Technol. 2017, 70, 69–81.

87. Perez-Puyana, V. M.; Jiménez-Rosado, M.; Romero, A.; Guerrero, A. Highly Porous Protein-Based 3D Scaffolds with Different Collagen Concentrates for Potential Application in Tissue Engineering. J. Appl. Polym. Sci. 2019, 136 (37), 47954.

88. Kord Forooshani, P.; Lee, B. P. Recent Approaches in Designing Bioadhesive Materials Inspired by Mussel Adhesive Protein. J. Polym. Sci. A. Polym. Chem. 2017, 55 (1), 9–33.

89. Zhu, L.; Yin, P.; Xie, T.; Liu, X.; Yang, L.; Wang, S.; Li, J.; Liu, H. Interaction between Soyasaponin and Soy β-Conglycinin or Glycinin: Air-Water Interfacial Behavior and Foaming Property of Their Mixtures. Colloids Surf. B. Biointerfaces 2020, 186.

90. Zhao, S.; Wang, Z.; Pang, H.; Li, Z.; Zhang, W.; Zhang, S.; Li, J.; Li, L. Designing Biomimetic Microphase-Separated Motifs to Construct Mechanically Robust Plant Protein Resin with Improved Water-Resistant Performance. Macromol. Mater. Eng. 2020, 305 (2), 1900462.

91. Borkner, C. B.; Elsner, M. B.; Scheibel, T. Coatings and Films Made of Silk Proteins. ACS Appl. Mater. Interfaces 2014, 6 (18), 15611–15625.

92. Hu, X.; Cebe, P.; Weiss, A. S.; Omenetto, F.; Kaplan, D. L. Protein-Based Composite Materials. Mater. Today 2012, 15 (5), 208–215.

93. Azeredo, H. M. C.; Waldron, K. W. Crosslinking in Polysaccharide and Protein Films and Coatings for Food Contact – A Review. Trends Food Sci. Technol. 2016, 52, 109–122.

94. Zhang, L.; Gopalakrishnan, S.; Li, K.; Wang, L. S.; Han, Y.; Rotello, V. M. Fabrication of Collagen Films with Enhanced Mechanical and Enzymatic Stability through Thermal Treatment in Fluorous Media. ACS Appl. Mater. Interfaces 2020, 12 (5), 6590–6597.

95. Pang, H.; Zhao, S.; Mo, L.; Wang, Z.; Zhang, W.; Huang, A.; Zhang, S.; Li, J. Mussel-Inspired Bio-Based Water-Resistant Soy Adhesives with Low-Cost Dopamine Analogue-Modified Silkworm Silk Fiber. J. Appl. Polym. Sci. 2020, 137 (23), 48785.

96. Zhang, S.; Xia, C.; Dong, Y.; Yan, Y.; Li, J.; Shi, S. Q.; Cai, L. Soy Protein Isolate-Based Films Reinforced by Surface Modified Cellulose Nanocrystal. Ind. Crops Prod. 2016, 80, 207–213.

97. Huang, W.; Ling, S.; Li, C.; Omenetto, F. G.; Kaplan, D. L. Silkworm Silk-Based Materials and Devices Generated Using Bio-Nanotechnology. *Chem. Soc. Rev.* **2018**, *47* (17), 6486–6504.

98. Feroz, S.; Muhammad, N.; Ranayake, J.; Dias, G. Keratin - Based Materials for Biomedical Applications. Bioact. Mater. 2020, 5 (3), 496–509.

99. Zubair, M.; Ullah, A. Recent Advances in Protein Derived Bionanocomposites for Food Packaging Applications. Crit. Rev. Food Sci. Nutr. 2020, 60 (3), 406–434.

100. Avramescu, S. M.; Butean, C.; Popa, C. V.; Ortan, A.; Moraru, I.; Temocico, G. Edible and Functionalized Films/Coatings—Performances and Perspectives. Coatings 2020, Vol. 10, Page 687 2020, 10 (7), 687.

101. Shavandi, A.; Silva, T. H.; Bekhit, A. A.; Bekhit, A. E. D. A. Keratin: Dissolution, Extraction and Biomedical Application. Biomater. Sci. 2017, 5 (9), 1699–1735.

102. Bax, D. V.; Smalley, H. E.; Farndale, R. W.; Best, S. M.; Cameron, R. E. Cellular Response to Collagen-Elastin Composite Materials. Acta Biomater. 2019, 86, 158–170.

103. Chen, X.; Knight, D. P.; Shao, Z.; Vollrath, F. Conformation Transition in Silk Protein Films Monitored by Time-Resolved Fourier Transform Infrared Spectroscopy: Effect of Potassium Ions on Nephila Spidroin Films. Biochemistry 2002, 41 (50), 14944–14950.

104. Jiang, C.; Wang, X.; Gunawidjaja, R.; Lin, Y. H.; Gupta, M. K.; Kaplan, D. L.; Naik, R. R.; Tsukruk, V. V. Mechanical Properties of Robust Ultrathin Silk Fibroin Films. Adv. Funct. Mater. 2007, 17 (13), 2229–2237.

105. You, R.; Zhang, J.; Gu, S.; Zhou, Y.; Li, X.; Ye, D.; Xu, W. Regenerated Egg White/Silk Fibroin Composite Films for Biomedical Applications. Mater. Sci. Eng. C. Mater. Biol. Appl. 2017, 79, 430–435.

106. Liu, H.; Fan, H.; Wang, Y.; Toh, S. L.; Goh, J. C. H. The Interaction between a Combined Knitted Silk Scaffold and Microporous Silk Sponge with Human Mesenchymal Stem Cells for Ligament Tissue Engineering. Biomaterials 2008, 29 (6), 662–674.

107. Jin, H. J.; Park, J.; Karageorgiou, V.; Kim, U. J.; Valluzzi, R.; Cebe, P.; Kaplan, D. L. Water-Stable Silk Films with Reduced β-Sheet Content. Adv. Funct. Mater. 2005, 15 (8), 1241–1247.

108. Lu, Q.; Hu, X.; Wang, X.; Kluge, J. A.; Lu, S.; Cebe, P.; Kaplan, D. L. Water-Insoluble Silk Films with Silk I Structure. Acta Biomater. 2010, 6 (4), 1380–1387.

109. Xu, J.; Liu, F.; Goff, H. D.; Zhong, F. Effect of Pre-Treatment Temperatures on the Film-Forming Properties of Collagen Fiber Dispersions. Food Hydrocoll. 2020, 107, 105326.

110. Diaz Quiroz, J. F.; Rodriguez, P. D.; Erndt-Marino, J. D.; Guiza, V.; Balouch, B.; Graf, T.; Reichert, W. M.; Russell, B.; Höök, M.; Hahn, M. S. Collagen-Mimetic Proteins with Tunable Integrin Binding Sites for Vascular Graft Coatings. ACS Biomater. Sci. Eng. 2018, 4 (8), 2934–2942.

111. Chattopadhyay, S.; Raines, R. T. Review Collagen-Based Biomaterials for Wound Healing. Biopolymers 2014, 101 (8), 821–833.

112. McManamon, C.; Cameron, A.; de Silva, J. P.; Daly, R.; O'Brien, F. J.; Cross, G. L. W. Effect of Cross-Linking and Hydration on Microscale Flat Punch Indentation Contact to Collagen-Hyaluronic Acid Films in the Viscoelastic Limit. Acta Biomater. 2020, 111, 279–289.

113. Xu, J.; Liu, F.; Wang, T.; Goff, H. D.; Zhong, F. Fabrication of Films with Tailored Properties by Regulating the Swelling of Collagen Fiber through PH Adjustment. Food Hydrocoll. 2020, 108, 106016.

114. Costa, M. J.; Marques, A. M.; Pastrana, L. M.; Teixeira, J. A.; Sillankorva, S. M.; Cerqueira, M. A. Physicochemical Properties of Alginate-Based Films: Effect of Ionic Crosslinking and Mannuronic and Guluronic Acid Ratio. Food Hydrocoll. 2018, 81, 442–448.

115. Ostrowska-Czubenko, J.; Gierszewska-Druzyńska, M. Effect of Ionic Crosslinking on the Water State in Hydrogel Chitosan Membranes. Carbohydr. Polym. 2009, 77 (3), 590–598.

116. Guan, Y.; You, H.; Cai, J.; Zhang, Q.; Yan, S.; You, R. Physically Crosslinked Silk Fibroin/Hyaluronic Acid Scaffolds. Carbohydr. Polym. 2020, 239.

117. Stern, R.; Maibach, H. I. Hyaluronan in Skin: Aspects of Aging and Its Pharmacologic Modulation. Clin. Dermatol. 2008, 26 (2), 106–122.

118. Cheung, D. T.; Nimni, M. E. Mechanism of Crosslinking of Proteins by Glutaraldehyde I: Reaction with Model Compounds. Connect. Tissue Res. 1982, 10 (2), 187–199.

119. Chen, X.; Zhou, L.; Xu, H.; Yamamoto, M.; Shinoda, M.; Tada, I.; Minami, S.; Urayama, K.; Yamane, H. The Structure and Properties of Natural Sheep Casing and Artificial Films Prepared from Natural Collagen with Various Crosslinking Treatments. Int. J. Biol. Macromol. 2019, 135, 959–968.

120. Iahnke, A. O. e. S.; Stoll, L.; Bellé, A. S.; Hertz, P. F.; Rios, A. de O.; Rahier, H.; Flôres, S. H. Gelatin Capsule Residue-Based Films Crosslinked with the Natural Agent Genipin. Packag. Technol. Sci. 2020, 33 (1), 15–26.

121. Mi, X.; Chang, Y.; Xu, H.; Yang, Y. Valorization of Keratin from Food Wastes via Crosslinking Using Non-Toxic Oligosaccharide Derivatives. Food Chem. 2019, 300.

122. Bajpai, S. K.; Shah, F. F.; Bajpai, M. Dynamic Release of Gentamicin Sulfate (GS) from Alginate Dialdehyde (AD)-Crosslinked Casein (CAS) Films for Antimicrobial Applications. Des. monomers Polym. 2016, 20 (1), 18–32.

123. Sarheed, O.; Abdul Rasool, B. K.; Abu-Gharbieh, E.; Aziz, U. S. An Investigation and Characterization on Alginate Hydogel Dressing Loaded with Metronidazole Prepared by Combined Inotropic Gelation and Freeze-Thawing Cycles for Controlled Release. AAPS PharmSciTech 2015, 16 (3), 601–609.

124. Zheng, T.; Yu, X.; Pilla, S. Mechanical and Moisture Sensitivity of Fully Bio-Based Dialdehyde Carboxymethyl Cellulose Cross-Linked Soy Protein Isolate Films. Carbohydr. Polym. 2017, 157, 1333–1340.

125. Buchert, J.; Cura, D. E.; Ma, H.; Gasparetti, C.; Monogioudi, E.; Faccio, G.; Mattinen, M.; Boer, H.; Partanen, R.; Selinheimo, E.; et al. Crosslinking Food Proteins for Improved Functionality. Annu. Rev. Food Sci. Technol. 2010, 1 (1), 113–138.

126. Cheng, S.; Wang, W.; Li, Y.; Gao, G.; Zhang, K.; Zhou, J.; Wu, Z. Cross-Linking and Film-Forming Properties of Transglutaminase-Modified Collagen Fibers Tailored by Denaturation Temperature. Food Chem. 2019, 271, 527–535.

127. Kchaou, H.; Benbettaieb, N.; Jridi, M.; Nasri, M.; Debeaufort, F. Influence of Maillard Reaction and Temperature on Functional, Structure and Bioactive Properties of Fish Gelatin Films. Food Hydrocoll. 2019, 97, 105196.

128. Li, S.; Donner, E.; Thompson, M.; Zhang, Y.; Rempel, C.; Liu, Q. Preparation and Characterization of Cross-Linked Canola Protein Isolate Films. Eur. Polym. J. 2017, 89, 419–430.

129. Rhim, J.-W.; Gennadios, A.; Lee, J.-J.; Weller, C. L.; Hanna, M. A. Biodegradation of Cast Soy Protein Films by Aspergillus Oryzae and Bacillus Subtilis. Food Sci. Biotechnol 2003, 12 (1), 96–99.

130. Olsson, E.; Hedenqvist, M. S.; Johansson, C.; Järnström, L. Influence of Citric Acid and Curing on Moisture Sorption, Diffusion and Permeability of Starch Films. Carbohydr. Polym. 2013, 94 (2), 765–772.

131. Amin, S.; Ustunol, Z. Solubility and Mechanical Properties of Heat-Cured Whey Protein-Based Edible Films Compared with That of Collagen and Natural Casings. Int. J. Dairy Technol. 2007, 60 (2), 149–153.

132. Rhim, J. W.; Gennadios, A.; Handa, A.; Weller, C. L.; Hanna, M. A. Solubility, Tensile, and Color Properties of Modified Soy Protein Isolate Films. J. Agric. Food Chem. 2000, 48 (10), 4937–4941.

133. Micard, V.; Belamri, R.; Morel, M. H.; Guilbert, S. Properties of Chemically and Physically Treated Wheat Gluten Films. J. Agric. Food Chem. 2000, 48 (7), 2948–2953.

134. Ali, Y.; Ghorpade, V. M.; Hanna, M. A. Properties of Thermally-Treated Wheat Gluten Films. Ind. Crops Prod. 1997, 6 (2), 177–184.

135. Neo, Y. P.; Perera, C. O.; Nieuwoudt, M. K.; Zujovic, Z.; Jin, J.; Ray, S.; Gizdavic-Nikolaidis, M. Influence of Heat Curing on Structure and Physicochemical Properties of Phenolic Acid Loaded Proteinaceous Electrospun Fibers. J. Agric. Food Chem. 2014, 62 (22), 5163–5172.

136. Shi, D.; Liu, F.; Yu, Z.; Chang, B.; Goff, H. D.; Zhong, F. Effect of Aging Treatment on the Physicochemical Properties of Collagen Films. Food Hydrocoll. 2019, 87, 436–447.

137. Jeoung, E.; Duncan, B.; Wang, L. S.; Saha, K.; Subramani, C.; Wang, P.; Yeh, Y. C.; Kushida, T.; Engel, Y.; Barnes, M. D.; et al. Fabrication of Robust Protein Films Using Nanoimprint Lithography. Adv. Mater. 2015, 27 (40), 6251–6255.

138. Cametti, M.; Crousse, B.; Metrangolo, P.; Milani, R.; Resnati, G. The Fluorous Effect in Biomolecular Applications. *Chem. Soc. Rev.* **2011**, *41* (1), 31–42.

139. Marsh, E. N. G. Fluorinated Proteins: From Design and Synthesis to Structure and Stability. *Acc. Chem. Res.* **2014**, *47* (10), 2878–2886.

140. Puerta, M.; Arango, M. C.; Jaramillo-Quiceno, N.; Álvarez-López, C.; Restrepo-Osorio, A. Influence of Ethanol Post-Treatments on the Properties of Silk Protein Materials. SN Appl. Sci. 2019, 1 (11), 1–7.

141. Xie, W. Y.; Wang, F.; Xu, C.; Song, F.; Wang, X. L.; Wang, Y. Z. A Superhydrophobic and Self-Cleaning Photoluminescent Protein Film with High Weatherability. Chem. Eng. J. 2017, 326, 436–442.

142. Liu, H.; Xie, W. Y.; Song, F.; Wang, X. L.; Wang, Y. Z. Constructing Hierarchically Hydrophilic/Superhydrophobic ZIF-8 Pattern on Soy Protein towards a Biomimetic Efficient Water Harvesting Material. Chem. Eng. J. 2019, 369, 1040–1048.

143. Gao, A.; Wu, Q.; Wang, D.; Ha, Y.; Chen, Z.; Yang, P. A Superhydrophobic Surface Templated by Protein Self-Assembly and Emerging Application toward Protein Crystallization. Adv. Mater. 2016, 28 (3), 579–587.

144. Wang, D.; Ha, Y.; Gu, J.; Li, Q.; Zhang, L.; Yang, P. 2D Protein Supramolecular Nanofilm with Exceptionally Large Area and Emergent Functions. Adv. Mater. 2016, 28 (34), 7414–7423.

145. Hu, X.; Tian, J.; Li, C.; Su, H.; Qin, R.; Wang, Y.; Cao, X.; Yang, P. Amyloid-Like Protein Aggregates: A New Class of Bioinspired Materials Merging an Interfacial Anchor with Antifouling. Adv. Mater. 2020, 32 (23), 2000128.

146. Wang, D.; Deng, J.; Deng, X.; Fang, C.; Zhang, X.; Yang, P. Controlling Enamel Remineralization by Amyloid-Like Amelogenin Mimics. Adv. Mater. 2020, 32 (31).

147. Liu, C.; Ye, X.; Wang, X.; Liao, X.; Huang, X.; Shi, B. Collagen Fiber Membrane as an Absorptive Substrate to Coat with Carbon Nanotubes-Encapsulated Metal Nanoparticles for Lightweight, Wearable, and Absorption-Dominated Shielding Membrane. Ind. Eng. Chem. Res. 2017, 56 (30), 8553–8562.

148. Meiyazhagan, A.; Thangavel, S.; Daniel P., H.; Pulickel M., A.; Palanisamy, T. Electrically Conducting Nanobiocomposites Using Carbon Nanotubes and Collagen Waste Fibers. Mater. Chem. Phys. 2015, 157, 8–15.

149. Wang, J.; He, C.; Cheng, N.; Yang, Q.; Chen, M.; You, L.; Zhang, Q. Bone Marrow Stem Cells Response to Collagen/Single-Wall Carbon Nanotubes-COOHs Nanocomposite Films with Transforming Growth Factor Beta 1. J. Nanosci. Nanotechnol. 2015, 15 (7), 4844–4850.

150. Li, J.; Mei, H.; Zheng, W.; Pan, P.; Sun, X. J.; Li, F.; Guo, F.; Zhou, H. M.; Ma, J. Y.; Xu, X. X.; et al. A Novel Hydrogen Peroxide Biosensor Based on Hemoglobin-Collagen-CNTs Composite Nanofibers. Colloids Surf. B. Biointerfaces 2014, 118, 77–82.

151. Xing, H.; Lee, H.; Luo, L.; Kyriakides, T. R. Extracellular Matrix-Derived Biomaterials in Engineering Cell Function. Biotechnol. Adv. 2020, 42.

152. Keirouz, A.; Zakharova, M.; Kwon, J.; Robert, C.; Koutsos, V.; Callanan, A.; Chen, X.; Fortunato, G.; Radacsi, N. High-Throughput Production of Silk Fibroin-Based Electrospun Fibers as Biomaterial for Skin Tissue Engineering Applications. Mater. Sci. Eng. C. Mater. Biol. Appl. 2020, 112.

153. Arthe, R.; Arivuoli, D.; Ravi, V. Preparation and Characterization of Bioactive Silk Fibroin/Paramylon Blend Films for Chronic Wound Healing. Int. J. Biol. Macromol. 2020, 154, 1324–1331.

154. Chen, G.; Matsuhisa, N.; Liu, Z.; Qi, D.; Cai, P.; Jiang, Y.; Wan, C.; Cui, Y.; Leow, W. R.; Liu, Z.; et al. Plasticizing Silk Protein for On-Skin Stretchable Electrodes. Adv. Mater. 2018, 30 (21).

155. Pereda, M.; Ponce, A. G.; Marcovich, N. E.; Ruseckaite, R. A.; Martucci, J. F. Chitosan-Gelatin Composites and Bi-Layer Films with Potential Antimicrobial Activity. Food Hydrocoll. 2011, 25 (5), 1372–1381.

156. Li, S.; Donner, E.; Xiao, H.; Thompson, M.; Zhang, Y.; Rempel, C.; Liu, Q. Preparation and Characterization of Soy Protein Films with a Durable Water Resistance-Adjustable and Antimicrobial Surface. Mater. Sci. Eng. C. Mater. Biol. Appl. 2016, 69, 947–955.

157. Wang, L. S.; Gupta, A.; Duncan, B.; Ramanathan, R.; Yazdani, M.; Rotello, V. M. Biocidal and Antifouling Chlorinated Protein Films. ACS Biomater. Sci. Eng. 2016, 2 (11), 1862–1866.

158. Egozi, D.; Baranes-Zeevi, M.; Ullmann, Y.; Gilhar, A.; Keren, A.; Matanes, E.; Berdicevsky, I.; Krivoy, N.; Zilberman, M. Biodegradable Soy Wound Dressings with Controlled Release of Antibiotics: Results from a Guinea Pig Burn Model. Burns 2015, 41 (7), 1459–1467.

159. Kodal Coşkun, B.; Çalikoğlu, E.; Karagöz Emiroğlu, Z.; Candoğan, K. Antioxidant Active Packaging with Soy Edible Films and Oregano or Thyme Essential Oils for Oxidative Stability of Ground Beef Patties. J. Food Qual. 2014, 37 (3), 203–212.

160. Musso, Y. S.; Salgado, P. R.; Mauri, A. N. Smart Edible Films Based on Gelatin and Curcumin. Food Hydrocoll. 2017, 66, 8–15.

161. Moraes, M. L.; Lima, L. R.; Vicentini-Oliveira, J. C.; de Souza, A. V. G.; Oliveira, O. N.; Deffune, E.; Ribeiro, S. J. L. Immunosensor for the Diagnostics of Autoimmune Hemolytic Anemia (AIHA) Based on Immobilization of a Monoclonal Antibody on a Layer of Silk Fibroin. J. Nanosci. Nanotechnol. 2019, 19 (7), 3772–3776.

162. Wang, X.; Gu, Y.; Xiong, Z.; Cui, Z.; Zhang, T.; Wang, X. W.; Gu, Y.; Xiong, Z. P.; Zhang, T.; Cui, Z. Silk-Molded Flexible, Ultrasensitive, and Highly Stable Electronic Skin for Monitoring Human Physiological Signals. Adv. Mater. 2014, 26 (9), 1336–1342.

163. Liu, J.; Chen, Q.; Liu, Q.; Zhao, B.; Ling, S.; Yao, J.; Shao, Z.; Chen, X.; Liu, J.; Chen, Q.; et al. Intelligent Silk Fibroin Ionotronic Skin for Temperature Sensing. Adv. Mater. Technol. 2020, 5 (7), 2000430.

164. Liu, X.; Fu, T.; Ward, J.; Gao, H.; Yin, B.; Woodard, T.; Lovley, D. R.; Yao, J. Multifunctional Protein Nanowire Humidity Sensors for Green Wearable Electronics. Adv. Electron. Mater. 2020, 6 (9), 2000721.

165. Li, C.; Adamcik, J.; Mezzenga, R. Biodegradable Nanocomposites of Amyloid Fibrils and Graphene with Shape-Memory and Enzyme-Sensing Properties. 2012.

166. X. Wang, D. Kong, Z. Ma, R. Zhao, Effect of carrot puree edible films on quality preservation of fresh-cut Irish Journal of Agricultural and Food Research 2015, 54, 64.

167. Badr, K. R.; Ahmed, Z. S.; El Gamal, M. S. Evaluation of the Antimicrobial Action of Whey Protein Edible Films Incorporated with Cinnamon, Cumin and Thyme against Spoilage Flora of Fresh Beef. *Int. J. Agric. Res.* **2014**, *9* (5), 242–250.

168. Thaker, M.; Hanjabam, M. D.; Gudipati, V.; Kannuchamy, N. Protective Effect of Fish Gelatin-Based Natural Antimicrobial Coatings on Quality of Indian Salmon Fillets during Refrigerated Storage. J. Food Process Eng. 2017, 40 (1), e12270.

169. Di Pierro, P.; Sorrentino, A.; Mariniello, L.; Giosafatto, C. V. L.; Porta, R. Chitosan/Whey Protein Film as Active Coating to Extend Ricotta Cheese Shelf-Life. LWT - Food Sci. Technol. 2011, 44 (10), 2324–2327.

170. Ünalan, I. U.; Arcan, I.; Korel, F.; Yemenicioğlu, A. Application of Active Zein-Based Films with Controlled Release Properties to Control Listeria Monocytogenes Growth and Lipid Oxidation in Fresh Kashar Cheese. Innov. Food Sci. Emerg. Technol. 2013, 20, 208–214.

171. Su, J. F.; Huang, Z.; Yuan, X. Y.; Wang, X. Y.; Li, M. Structure and Properties of Carboxymethyl Cellulose/Soy Protein Isolate Blend Edible Films Crosslinked by Maillard Reactions. Carbohydr. Polym. 2010, 79 (1), 145–153.

172. Clemmens, J.; Hess, H.; Lipscomb, R.; Hanein, Y.; Böhringer, K. F.; Matzke, C. M.; Bachand, G. D.; Bunker, B. C.; Vogel, V. Mechanisms of Microtubule Guiding on Microfabricated Kinesin-Coated Surfaces: Chemical and Topographic Surface Patterns. Langmuir 2003, 19 (26), 10967–10974.

173. Gilbert, V.; Rouabhia, M.; Wang, H.; Arnould, A. L.; Remondetto, G.; Subirade, M. Characterization and Evaluation of Whey Protein-Based Biofilms as Substrates for in Vitro Cell Cultures. Biomaterials 2005, 26 (35), 7471–7480.

174. Chen, Y.; Zhang, L.; Lu, Y.; Ye, C.; Du, L. Preparation and Properties of Water-Resistant Soy Dreg/Benzyl Konjac Glucomannan Composite Plastics. J. Appl. Polym. Sci. 2003, 90 (14), 3790–3796.

175. Lévesque, S. G.; Lim, R. M.; Shoichet, M. S. Macroporous Interconnected Dextran Scaffolds of Controlled Porosity for Tissue-Engineering Applications. Biomaterials 2005, 26 (35), 7436–7446.

176. Khalili, H.; Sheikhbabayi, M.; Samadi, N.; Jamalifar, H.; Dalili, D.; Samadi, N. Bacterial Contamination of Single- and Multiple-Dose Vials after Multiple Use and Intravenous Admixtures in Three Different Hospitals in Iran. Iran. J. Pharm. Res. IJPR 2013, 12 (1), 205–209.

177. Kramer, A.; Schwebke, I.; Kampf, G. How Long Do Nosocomial Pathogens Persist on Inanimate Surfaces? A Systematic Review. BMC Infect. Dis. 2006, 6 (1), 130.

178. Khan, H. A.; Ahmad, A.; Mehboob, R. Nosocomial Infections and Their Control Strategies. Asian Pac. J. Trop. Biomed. 2015, 5 (7), 509–514.

179. Klevens, R. M.; Edwards, J. R.; Chesley L. Richards, J.; Horan, T. C.; Gaynes, R. P.; Pollock, D. A.; Cardo, D. M. Estimating Health Care-Associated Infections and Deaths in U.S. Hospitals, 2002. Public Health Rep. 2007, 122 (2), 160–166.

180. Magill, S. S.; Edwards, J. R.; Bamberg, W.; Beldavs, Z. G.; Dumyati, G.; Kainer, M. A.; Lynfield, R.; Maloney, M.; McAllister-Hollod, L.; Nadle, J.; et al. Multistate Point-Prevalence Survey of Health Care–Associated Infections. N. Engl. J. Med. 2014, 370 (13), 1198–1208.

181. Crijns, F. R. L.; Keinänen-Toivola, M. M.; Dunne, C. P. Antimicrobial Coating Innovations to Prevent Healthcare-Associated Infection. J. Hosp. Infect. 2017, 95 (3), 243–244.

182. Cloutier, M.; Mantovani, D.; Rosei, F. Antibacterial Coatings: Challenges, Perspectives, and Opportunities. Trends Biotechnol. 2015, 33 (11), 637–652.

183. Mei, L.; Teng, Z.; Zhu, G.; Liu, Y.; Zhang, F.; Zhang, J.; Li, Y.; Guan, Y.; Luo, Y.; Chen, X.; Wang, Q. Silver Nanocluster-Embedded Zein Films as Antimicrobial Coating Materials for Food Packaging. ACS Appl. Mater. Interfaces 2017, 9 (40), 35297–35304.

184. Yuan, G.; Chen, X.; Li, D. Chitosan Films and Coatings Containing Essential Oils: The Antioxidant and Antimicrobial Activity, and Application in Food Systems. Food Res. Int. 2016, 89, 117–128.

185. Zhang, R.; Liu, Y.; He, M.; Su, Y.; Zhao, X.; Elimelech, M.; Jiang, Z. Antifouling Membranes for Sustainable Water Purification: Strategies and Mechanisms. Chem. Soc. Rev. 2016, 45 (21), 5888–5924.

186. Miller, D. J; Dreyer, D. R; Bielawski C. W; Paul. D. R; Freeman, B. D; Surface Modification of Water Purification Membranes. Angew. Chemie Int. Ed. 2017, 56 (17), 4662–4711.

187. Keum, H.; Kim, J. Y.; Yu, B.; Yu, S. J.; Kim, J.; Jeon, H.; Lee, D. Y.; Im, S. G.; Jon, S. Prevention of Bacterial Colonization on Catheters by a One-Step Coating Process Involving an Antibiofouling Polymer in Water. *ACS Appl. Mater. Interfaces* **2017**, *9* (23), 19736–19745.

188. Percival, S. L.; Suleman, L.; Donelli, G. Healthcare-Associated Infections, Medical Devices and Biofilms: Risk, Tolerance and Control. J. Med. Microbiol. 2015, 64 (4), 323–334.

189. Cheng, H.; Yue, K.; Kazemzadeh-Narbat, M.; Liu, Y.; Khalilpour, A.; Li, B.; Zhang, Y. S.; Annabi, N.; Khademhosseini, A. Mussel-Inspired Multifunctional Hydrogel Coating for Prevention of Infections and Enhanced Osteogenesis. ACS Appl. Mater. Interfaces 2017, 9 (13), 11428–11439.

190. Raphel, J.; Holodniy, M.; Goodman, S. B.; Heilshorn, S. C. Multifunctional Coatings to Simultaneously Promote Osseointegration and Prevent Infection of Orthopaedic Implants. Biomaterials 2016, 84, 301–314.

191. Yazici, H.; O'Neill, M. B.; Kacar, T.; Wilson, B. R.; Oren, E. E.; Sarikaya, M.; Tamerler, C. Engineered Chimeric Peptides as Antimicrobial Surface Coating Agents toward Infection-Free Implants. ACS Appl. Mater. Interfaces 2016, 8 (8), 5070–5081.

192. Lejars, M.; Margaillan, A.; Bressy, C. Fouling Release Coatings: A Nontoxic Alternative to Biocidal Antifouling Coatings. Chem. Rev. 2012, 112 (8), 4347–4390.

193. Tobin, E. J. Recent Coating Developments for Combination Devices in Orthopedic and Dental Applications: A Literature Review. Adv. Drug Deliv. Rev. 2017, 112, 88–100.

194. Masahiro, I.; L., de M. B. K.; J., M. B.; Sonny, B. B.; M., S. E.; Chao, X. Surface Topography of Silicon Nitride Affects Antimicrobial and Osseointegrative Properties of Tibial Implants in a Murine Model. J. Biomed. Mater. Res. Part A 2017, 105 (12), 3413–3421.

195. Knowles, B. R.; Wagner, P.; Maclaughlin, S.; Higgins, M. J.; Molino, P. J. Silica Nanoparticles Functionalized with Zwitterionic Sulfobetaine Siloxane for Application as a Versatile Antifouling Coating System. ACS Appl. Mater. Interfaces 2017, 9 (22), 18584–18594.

196. Bastarrachea, L. J.; Goddard, J. M. Antimicrobial Coatings with Dual Cationic and N-Halamine Character: Characterization and Biocidal Efficacy. J. Agric. Food Chem. 2015, 63 (16), 4243–4251.

197. Yu, M.; You, D.; Zhuang, J.; Lin, S.; Dong, L.; Weng, S.; Zhang, B.; Cheng, K.; Weng, W.; Wang, H. Controlled Release of Naringin in Metal-Organic Framework-Loaded Mineralized Collagen Coating to Simultaneously Enhance Osseointegration and Antibacterial Activity. ACS Appl. Mater. Interfaces 2017, 9 (23), 19698–19705.

198. Lischer, S.; Körner, E.; Balazs, D. J.; Shen, D.; Wick, P.; Grieder, K.; Haas, D.; Heuberger, M.; Hegemann, D. Antibacterial Burst-Release from Minimal Ag-Containing Plasma Polymer Coatings. J. R. Soc. Interface 2011, 8 (60), 1019–1030.

199. Huang, X.; Brazel, C. S. On the Importance and Mechanisms of Burst Release in Matrix-Controlled Drug Delivery Systems. J. Control. Release 2001, 73 (2–3), 121–136.

200. Joseph, M.; J., W. T.; Garima, B. Biocompatibility and Medical Device Coatings. Medical Coatings and Deposition Technologies. August 8, 2016.

201. Zheng, W.; Jia, Y.; Chen, W.; Wang, G.; Guo, X.; Jiang, X. Universal Coating from Electrostatic Self-Assembly to Prevent Multidrug-Resistant Bacterial Colonization on Medical Devices and Solid Surfaces. ACS Appl. Mater. Interfaces 2017, 9 (25), 21181–21189.

202. Wang, L. S.; Duncan, B.; Tang, R.; Lee, Y. W.; Creran, B.; Elci, S. G.; Zhu, J.; Tonga, G. Y.; Doble, J.; Fessenden, M.; Bayat, M.; Nonnenmann, S.; Vachet, R. W.; Rotello, V. M. Gradient and Patterned Protein Films Stabilized via Nanoimprint Lithography for Engineered Interactions with Cells. ACS Appl. Mater. Interfaces 2017, 9 (1), 42–46.

203. Aigner, T. B.; Desimone, E.; Scheibel, T. Biomedical Applications of Recombinant Silk-Based Materials. Adv. Mater. 2018, 1704636, 1–28.

204. Gu, J.; Su, Y.; Liu, P.; Li, P.; Yang, P. An Environmentally Benign Antimicrobial Coating Based on a Protein Supramolecular Assembly. ACS Appl. Mater. Interfaces 2017, 9 (1), 198–210.

205. Chen, L.; Zhou, M.-L.; Qian, Z.-G.; Kaplan, D. L.; Xia, X.-X. Fabrication of Protein Films from Genetically Engineered Silk-Elastin-Like Proteins by Controlled Cross-Linking. ACS Biomater. Sci. Eng. 2017, 3 (3), 335–341.

206. Murphy, A. R.; John, P. St.; Kaplan, D. L. Modification of Silk Fibroin Using Diazonium Coupling Chemistry and the Effects on hMSC Proliferation and Differentiation. Biomaterials 2008, 29 (19), 2829–2838.

207. Heichel, D. L.; Burke, K. A. Enhancing the Carboxylation Efficiency of Silk Fibroin through the Disruption of Noncovalent Interactions. Bioconjug. Chem. 2020, 31 (5), 1307–1312.

208. X, Hu.; J, Tian.; C, Li.; H, Su.; R, Qin.; Y, Wang.; X, Cao.; P, Yang. Amyloid-Like Protein Aggregates: A New Class of Bioinspired Materials Merging an Interfacial Anchor with Antifouling. Adv. Mater. 2020, 32 (23).

209. Xu, Y.; Liu, Y.; Hu, X.; Qin, R.; Su, H.; Li, J.; Yang, P. The Synthesis of a 2D Ultra-Large Protein Supramolecular Nanofilm by Chemoselective Thiol–Disulfide Exchange and Its Emergent Functions. Angew. Chemie Int. Ed. 2020, 59 (7), 2850–2859.

210. Wang, L.-S.; Gopalakrishnan, S.; Lee, Y.-W.; Zhu, J.; Nonnenmann, S. S.; Rotello, V. M. Translation of Protein Charge and Hydrophilicity to Materials Surface

Properties Using Thermal Treatment in Fluorous Media. Mater. Horizons 2018, 5, 268-274

211. Gopalakrishnan, S.; Pan, S.; Fernandez, A.; Lee, J.; Bai, Y.; Wang, L.-S.; Thayumanavan, S.; Duan, X.; Rotello, V. M. Hypersound-Assisted Size Sorting of Microparticles on Inkjet-Patterned Protein Films. Langmuir 2021, 37 (8), 2826–2832.

212. Jeoung, E.; Duncan, B.; Wang, L. S.; Saha, K.; Subramani, C.; Wang, P.; Yeh, Y. C.; Kushida, T.; Engel, Y.; Barnes, M. D.; Rotello, V. M. et al. Fabrication of Robust Protein Films Using Nanoimprint Lithography. Adv. Mater. 2015, 27 (40), 6251–6255.

213. Blinder, K. J.; Peyman, G. A.; Paris, C. L.; Dailey, J. P.; Alturki, W.; Lui, K. R.; Gremillion, C. M.; Clark, L. C. Vitreon, a New Perfluorocarbon. Br. J. Ophthalmol. 1991, 75 (4), 240–244.

214. Lin, Y.; Liu, K.; Wang, C.; Li, L.; Liu, Y. Electrochemical Immunosensor for Detection of Epidermal Growth Factor Reaching Lower Detection Limit: Toward Oxidized Glutathione as a More Efficient Blocking Reagent for the Antibody Functionalized Silver Nanoparticles and Antigen Interaction. Anal. Chem. 2015, 87, 8047–8051.

215. Cai, B.; Hu, K.; Li, C.; Jin, J.; Hu, Y. Bovine Serum Albumin Bioconjugated Graphene Oxide: Red Blood Cell Adhesion and Hemolysis Studied by QCM-D. Appl. Surf. Sci. 2015, 356, 844–851.

216. Wang, L.-S.; Gupta, A.; Duncan, B.; Ramanathan, R.; Yazdani, M.; Rotello, V. M. Biocidal and Antifouling Chlorinated Protein Films. ACS Biomater. Sci. Eng. 2016, 2 (11), 1862–1866.

217. ter Boo, G. J. A.; Richards, R. G.; Moriarty, T. F.; Grijpma, D. W.; Eglin, D. Hyaluronic Acid Derivatives and Its Polyelectrolyte Complexes with Gentamicin as a Delivery System for Antibiotics. Polym. Adv. Technol. 2017, 28 (10), 1325–1333.

218. Garnacho-Montero, J.; Ortiz-Leyba, C.; Jiménez-Jiménez, F. J.; Barrero-Almodóvar, A. E.; García-Garmendia, J. L.; Bernabeu-Wittell, M.; Gallego-Lara, S. L.; Madrazo-Osuna, J. Treatment of Multidrug-Resistant Acinetobacter Baumannii Ventilator-Associated Pneumonia (VAP) with Intravenous Colistin: A Comparison with Imipenem-Susceptible VAP. Clin. Infect. Dis. 2003, 36 (9), 1111–1118.

219. Bae, J.; Lee, J.; Zhou, Q.; Kim, T. Micro-/Nanofluidics for Liquid-Mediated Patterning of Hybrid-Scale Material Structures. Adv. Mater. 2019, 31 (20), 1804953.

220. Zhang, D.; Bi, H.; Liu, B.; Qiao, L. Detection of Pathogenic Microorganisms by Microfluidics Based Analytical Methods. Anal. Chem. 2018, 90 (9), 5512–5520.

221. Haidas, D.; Bachler, S.; Köhler, M.; Blank, L. M.; Zenobi, R.; Dittrich, P. S. Microfluidic Platform for Multimodal Analysis of Enzyme Secretion in Nanoliter Droplet Arrays. Anal. Chem. 2019, 91 (3), 2066–2073.

222. Bandodkar, A. J.; Gutruf, P.; Choi, J.; Lee, K. H.; Sekine, Y.; Reeder, J. T.; Jeang, W. J.; Aranyosi, A. J.; Lee, S. P.; Model, J. B.; et al. Battery-Free, Skin-Interfaced Microfluidic/Electronic Systems for Simultaneous Electrochemical, Colorimetric, and Volumetric Analysis of Sweat. Sci. Adv. 2019, 5 (1), 3294.

223. Devendran, C.; Choi, K.; Han, J.; Ai, Y.; Neild, A.; Collins, D. J. Diffraction-Based Acoustic Manipulation in Microchannels Enables Continuous Particle and Bacteria Focusing. Lab Chip 2020, 20 (15), 2674–2688.

224. Gençer, A.; Schütz, C.; Thielemans, W. Influence of the Particle Concentration and Marangoni Flow on the Formation of Cellulose Nanocrystal Films. Langmuir 2017, 33 (1), 228–234.

225. Kim, J. H.; Jeon, T. Y.; Choi, T. M.; Shim, T. S.; Kim, S. H.; Yang, S. M. Droplet Microfluidics for Producing Functional Microparticles. Langmuir 2014, 30 (6), 1473–1488.

226. Yin, C. Y.; Nikoloski, A. N.; Wang, M. Microfluidic Solvent Extraction of Platinum and Palladium from a Chloride Leach Solution Using Alamine 336. Miner. Eng. 2013, 45, 18–21.

227. Khoshmanesh, K.; Tang, S. Y.; Zhu, J. Y.; Schaefer, S.; Mitchell, A.; Kalantar-Zadeh, K.; Dickey, M. D. Liquid Metal Enabled Microfluidics. Lab on a Chip. Royal Society of Chemistry March 14, 2017, pp 974–993.

228. Chen, G.; Zheng, J.; Liu, L.; Xu, L. Application of Microfluidics in Wearable Devices. Small Methods 2019, 3 (12), 1900688.

229. Gao, B.; Li, X.; Yang, Y.; Chu, J.; He, B. Emerging Paper Microfluidic Devices. Analyst. Royal Society of Chemistry November 21, 2019, pp 6497–6511.

230. Tan, Y. C.; Fisher, J. S.; Lee, A. I.; Cristini, V.; Lee, A. P. Design of Microfluidic Channel Geometries for the Control of Droplet Volume, Chemical Concentration, and Sorting. Lab Chip 2004, 4 (4), 292–298.

231. Dalili, A.; Samiei, E.; Hoorfar, M. A Review of Sorting, Separation and Isolation of Cells and Microbeads for Biomedical Applications: Microfluidic Approaches. Analyst. Royal Society of Chemistry January 7, 2019, pp 87–113.

232. Yew, M.; Ren, Y.; Koh, K. S.; Sun, C.; Snape, C. A Review of State-of-the-Art Microfluidic Technologies for Environmental Applications: Detection and Remediation. Glob. Challenges 2019, 3 (1), 1800060.

233. Sun, J.; Wu, K.; Su, D.; Guo, G.; Shi, Z. Continuous Separation of Magnetic Beads Using a Y-Shaped Microfluidic System Integrated with Hard-Magnetic Elements. J. Phys. D. Appl. Phys. 2020, 53 (3), 035004.

234. Jeon, J.; Choi, N.; Chen, H.; Moon, J. Il; Chen, L.; Choo, J. SERS-Based Droplet Microfluidics for High-Throughput Gradient Analysis. Lab Chip 2019, 19 (4), 674–681.

235. Shang, L.; Cheng, Y.; Zhao, Y. Emerging Droplet Microfluidics. Chemical Reviews. American Chemical Society June 28, 2017, pp 7964–8040.

236. Waheed, S.; Cabot, J. M.; Macdonald, N. P.; Lewis, T.; Guijt, R. M.; Paull, B.; Breadmore, M. C. 3D Printed Microfluidic Devices: Enablers and Barriers. Lab on a Chip. Royal Society of Chemistry May 24, 2016, pp 1993–2013.

237. Sollier, E.; Go, D. E.; Che, J.; Gossett, D. R.; O'Byrne, S.; Weaver, W. M.; Kummer, N.; Rettig, M.; Goldman, J.; Nickols, N.; et al. Size-Selective Collection of Circulating Tumor Cells Using Vortex Technology. Lab Chip 2014, 14 (1), 63–77.

238. Zhou, Y.; Ma, Z.; Ai, Y. Dynamically Tunable Elasto-Inertial Particle Focusing and Sorting in Microfluidics. Lab Chip 2020, 20 (3), 568–581.

239. Gokaltun, A.; Yarmush, M. L.; Asatekin, A.; Usta, O. B. Recent Advances in Nonbiofouling PDMS Surface Modification Strategies Applicable to Microfluidic Technology. TECHNOLOGY 2017, 05 (01), 1–12.

240. Duffadar, R. D.; Davis, J. M. Dynamic Adhesion Behavior of Micrometer-Scale Particles Flowing over Patchy Surfaces with Nanoscale Electrostatic Heterogeneity. J. Colloid Interface Sci. 2008, 326 (1), 18–27.

241. Schachermeyer, S.; Ashby, J.; Kwon, M. J.; Zhong, W. Impact of Carrier Fluid Composition on Recovery of Nanoparticles and Proteins in Flow Field Flow Fractionation. J. Chromatogr. A 2012, 1264, 72–79. https://doi.org/10.1016/j.chroma.2012.09.050.

242. Liu, Y.; Cánovas, R.; Crespo, G. A.; Cuartero, M. Thin-Layer Potentiometry for Creatinine Detection in Undiluted Human Urine Using Ion-Exchange Membranes as Barriers for Charged Interferences. Anal. Chem. 2020, 92 (4), 3315–3323.

243. Gou, Y.; Jia, Y.; Wang, P.; Sun, C. Progress of Inertial Microfluidics in Principle and Application. Sensors (Switzerland). MDPI AG June 1, 2018.

244. Paiè, P.; Zandrini, T.; Vázquez, R.; Osellame, R.; Bragheri, F. Particle Manipulation by Optical Forces in Microfluidic Devices. Micromachines 2018, 9 (5), 200.

245. Haehnel, V.; Khan, F. Z.; Mutschke, G.; Cierpka, C.; Uhlemann, M.; Fritsch, I. Combining Magnetic Forces for Contactless Manipulation of Fluids in Microelectrode-Microfluidic Systems. Sci. Rep. 2019, 9 (1), 1–11.

246. Wu, M.; Ozcelik, A.; Rufo, J.; Wang, Z.; Fang, R.; Jun Huang, T. Acoustofluidic Separation of Cells and Particles. Microsystems and Nanoengineering. Nature Publishing Group December 1, 2019, pp 1–18.

247. Schultz, T.; Vogt, S.; Schlupp, P.; Von Wenckstern, H.; Koch, N.; Grundmann, M. Influence of Oxygen Deficiency on the Rectifying Behavior of Transparent-Semiconducting-Oxide-Metal Interfaces. Phys. Rev. Appl. 2018, 9 (6).

248. Mutafopulos, K.; Spink, P.; Lofstrom, C. D.; Lu, P. J.; Lu, H.; Sharpe, J. C.; Franke, T.; Weitz, D. A. Traveling Surface Acoustic Wave (TSAW) Microfluidic Fluorescence Activated Cell Sorter (MFACS). Lab Chip 2019, 19 (14), 2435–2443.

249. Hu, X. J.; Liu, H. L.; Jin, Y. X.; Liang, L.; Zhu, D. M.; Zhu, X. Q.; Guo, S. S.; Zhou, F. L.; Yang, Y. Precise Label-Free Leukocyte Subpopulation Separation Using Hybrid Acoustic-Optical Chip. Lab Chip 2018, 18 (22), 3405–3412.

250. Song, K.; Li, G.; Zu, X.; Du, Z.; Liu, L.; Hu, Z. The Fabrication and Application Mechanism of Microfluidic Systems for High Throughput Biomedical Screening: A Review. Micromachines 2020, 11 (3), 297.

251. Pan, S.; Zhang, H.; Liu, W.; Wang, Y.; Pang, W.; Duan, X. Biofouling Removal and Protein Detection Using a Hypersonic Resonator. ACS Sensors 2017, 2 (8), 1175–1183.

252. Pan, S.; Jeon, T.; Luther, D. C.; Duan, X.; Rotello, V. M. Cytosolic Delivery of Functional Proteins In Vitro through Tunable Gigahertz Acoustics. ACS Appl. Mater. Interfaces 2020, 12 (13), 15823–15829.

253. Feifel, S. C.; Lisdat, F. Silica Nanoparticles for the Layer-by-Layer Assembly of Fully Electro-Active Cytochrome c Multilayers. J. Nanobiotechnology 2011, 9 (1), 59.

254. Cui, W.; Zhang, H.; Zhang, H.; Yang, Y.; He, M.; Qu, H.; Pang, W.; Zhang, D.; Duan, X. Localized Ultrahigh Frequency Acoustic Fields Induced Micro-Vortices for Sub-milliseconds Microfluidic Mixing. Appl. Phys. Lett. 2016, 109 (25), 253503.

255. Sorushanova, A.; Delgado, L. M.; Wu, Z.; Shologu, N.; Kshirsagar, A.; Raghunath, R.; Mullen, A. M.; Bayon, Y.; Pandit, A.; Raghunath, M.; Zeugolis, D.I. The

Collagen Suprafamily: From Biosynthesis to Advanced Biomaterial Development. Advanced Materials. Wiley-VCH Verlag 2019.

256. Hosseinkhani, H.; Hiraoka, Y.; Li, C. H.; Chen, Y. R.; Yu, D. S.; Hong, P. Da; Ou, K. L. Engineering Three-Dimensional Collagen-IKVAV Matrix to Mimic Neural Microenvironment. *ACS Chem. Neurosci.* **2013**, *4* (8), 1229–1235.

257. karimizade, A.; takallu, sakine; Mirzaei, E. Evaluating the Effect of PH on Mechanical Strength and Cell Compatibility of Nanostructured Collagen Hydrogel by the Plastic Compression Method. Nanomedicine J. 2018, 5 (3), 180–185.

258. Sun, L.; Li, B.; Yao, D.; Song, W.; Hou, H. Effects of Cross-Linking on Mechanical, Biological Properties and Biodegradation Behavior of Nile Tilapia Skin Collagen Sponge as a Biomedical Material. J. Mech. Behav. Biomed. Mater. 2018, 80, 51–58.

259. Gautieri, A.; Vesentini, S.; Redaelli, A.; Buehler, M. J. Hierarchical Structure and Nanomechanics of Collagen Microfibrils from the Atomistic Scale Up. Nano Lett. 2011, 11 (2), 757–766.

260. Tapeinos, C.; Larrañaga, A.; Sarasua, J. R.; Pandit, A. Functionalised Collagen Spheres Reduce H2O2 Mediated Apoptosis by Scavenging Overexpressed ROS. Nanomedicine Nanotechnology, Biol. Med. 2018, 14 (7), 2397–2405.

261. Kaczmarek, B.; Sionkowska, A.; Gołyńska, M.; Polkowska, I.; Szponder, T.; Nehrbass, D.; Osyczka, A. M. In Vivo Study on Scaffolds Based on Chitosan, Collagen, and Hyaluronic Acid with Hydroxyapatite. Int. J. Biol. Macromol. 2018, 118 (Pt A), 938–944.

262. Pettian, M. S.; Plepis, A.M.G.; Martins, V.D.C.A; Dos Santos, G.R..; Pinto, C.A.L.; Galdeano, E. A.; Calegari, A.R.A; de Moraes, C.A.; Cunha, M.R.D. Use of an Anionic Collagen Matrix Made from Bovine Intestinal Serosa for in Vivo Repair of Cranial Defects. 2018.

263. Gaspar-Pintiliescu, A.; Seciu, A. M.; Miculescu, F.; Moldovan, L.; Ganea, E.; Craciunescu, O. Enhanced Extracellular Matrix Synthesis Using Collagen Dressings Loaded with Artemisia Absinthium Plant Extract. J. Bioact. Compat. Polym. 2018, 33 (5), 516–528.

264. Zhang, D.; Wu, X.; Chen, J.; Lin, K. The Development of Collagen Based Composite Scaffolds for Bone Regeneration. Bioactive Materials. KeAi Communications Co. March 1, 2018, pp 129–138.

265. Ferreira, A. M.; Gentile, P.; Chiono, V.; Ciardelli, G. Ferreira, A. M., Gentile, P., Chiono, V., & Ciardelli, G. (2012). Collagen for Bone Tissue Regeneration. Acta Biomater. 2012, 8 (9), 3191–3200.

266. Ryan, A. J.; Kearney, C. J.; Shen, N.; Khan, U.; Kelly, A. G.; Probst, C.; Brauchle, E.; Biccai, S.; Garciarena, C. D.; Vega-Mayoral, V.; Loskill, P.; Kerrigan, S.W.; Schenke-Leyland, K.; Coleman, J.N.; O'Brien, F.J. Electroconductive Biohybrid Collagen/Pristine Graphene Composite Biomaterials with Enhanced Biological Activity. Adv. Mater. 2018, 30 (15), e1706442.

267. Terzi, A.; Storelli, E.; Bettini, S.; Sibillano, T.; Altamura, D.; Salvatore, L.; Madaghiele, M.; Romano, A.; Siliqi, D.; Ladisa, M.; De Caro, L.; Quattrini, A.; Valli, L.; Sannino, A.; Giannini, C. Effects of Processing on Structural, Mechanical and Biological Properties of Collagen-Based Substrates for Regenerative Medicine. Sci. Rep. 2018, 8 (1).

268. Koide, M.; Osaki, K.; Konishi, J.; Oyamada, K.; Katakura, T.; Takahashi, A.; Yoshizato, K. A New Type of Biomaterial for Artificial Skin: Dehydrothermally Cross-Linked Composites of Fibrillar and Denatured Collagens. J. Biomed. Mater. Res. 1993, 27 (1), 79–87.

269. Sionkowska, A.; Skopinska-Wisniewska, J.; Gawron, M.; Kozlowska, J.; Planecka, A. Chemical and Thermal Cross-Linking of Collagen and Elastin Hydrolysates. Int. J. Biol. Macromol. 2010, 47 (4), 570–577.

270. Samouillan, V.; Delaunay, F.; Dandurand, J.; Merbahi, N.; Gardou, J.-P.; Yousfi, M.; Gandaglia, A.; Spina, M.; Lacabanne, C. The Use of Thermal Techniques for the Characterization and Selection of Natural Biomaterials. J. Funct. Biomater. 2011, 2 (3), 230–248.

271. Zhu, D.-W. Perfluorocarbon Fluids: Universal Suspension Polymerization Media. Macromolecules 1996, 29 (8), 2813–2817.

272. Marsh, E. N. G. Fluorinated Proteins: From Design and Synthesis to Structure and Stability. Acc. Chem. Res. 2014, 47 (10), 2878–2886.

273. Asakura, T.; Adachi, K.; Schwartz, E. Stabilizing Effect of Various Organic Solvents on Protein. J Bio. Chem. 1978 253, 6423-6423.

274. Uversky, V. N.; Narizhneva, N. V.; Kirschstein, S. O.; Winter, S.; Löber, G. Conformational Transitions Provoked by Organic Solvents in β-Lactoglobulin: Can a Molten Globule like Intermediate Be Induced by the Decrease in Dielectric Constant? Fold. Des. 1997, 2 (3), 163–172.

275. Madaghiele M.; Calo E.; Salvatore L.; Bonfrate V.; Pedone D.; Frigione M.; Sannino A.; Assessment of collagen crosslinking and denaturation for the design of regenerative scaffolds. J Biomed Mater Res Part A: 2016 104A: 186-194,

276. Millington, K. R.; Ishii, H.; Maurdev, G. Chemiluminescence from Thermal Oxidation of Amino Acids and Proteins. Amino Acids 2010, 38 (5), 1395–1405.

277. Bozec, L.; Odlyha, M. Thermal Denaturation Studies of Collagen by Microthermal Analysis and Atomic Force Microscopy. Biophys. J. 2011, 101 (1), 228–236.

278. Payne, K. J.; Veis, A. Fourier Transform Ir Spectroscopy of Collagen and Gelatin Solutions: Deconvolution of the Amide I Band for Conformational Studies. Biopolymers 1988, 27 (11), 1749–1760.

279. Silva, Z. S.; Botta, S. B.; Ana, P. A.; França, C. M.; Fernandes, K. P. S.; Mesquita-Ferrari, R. A.; Deana, A.; Bussadori, S. K. Effect of Papain-Based Gel on Type I Collagen - Spectroscopy Applied for Microstructural Analysis. Sci. Rep. 2015, 5.

280. De Campos Vidal, B.; Mello, M. L. S. Collagen Type I Amide I Band Infrared Spectroscopy. Micron 2011, 42 (3), 283–289.

281. Kandamchira, A.; Selvam, S.; Marimuthu, N.; Janardhanan, S. K.; Fathima, N. N. Influence of Functionalized Nanoparticles on Conformational Stability of Type I Collagen for Possible Biomedical Applications. Mater. Sci. Eng. C. Mater. Biol. Appl. 2013, 33 (8), 4985–4988.

282. Prasad, K.; Bazaka, O.; Chua, M.; Rochford, M.; Fedrick, L.; Spoor, J.; Symes, R.; Tieppo, M.; Collins, C.; Cao, A.; Markwell, D.; Ostrikov, K.K.; Bazaka, K. Metallic Biomaterials: Current Challenges and Opportunities. Materials. MDPI AG July 31, 2017.

283. Meyer, M. Processing of Collagen-Based Biomaterials, and the Resulting Materials Properties. Biomed. Eng. Online 2019, 18 (1).

284. Akhmanova, M.; Osidak, E.; Domogatsky, S.; Rodin, S.; Domogatskaya, A. Physical, Spatial, and Molecular Aspects of Extracellular Matrix of in Vivo Niches and Artificial Scaffolds Relevant to Stem Cells Research. Stem Cells Int. 2015, 2015.

285. Guarino, V.; Raucci, M. G.; Ronca, A.; Cirillo, V.; Ambrosio, L. Multifunctional Scaffolds for Bone Regeneration. In Bone Substitute Biomaterials; Elsevier Inc., 2014; pp 95–117.

286. Zhang, L.; Liu, X.; Li, G.; Wang, P.; Yang, Y. Tailoring Degradation Rates of Silk Fibroin Scaffolds for Tissue Engineering. J. Biomed. Mater. Res. Part A 2019, 107 (1), 104–113.

287. Richbourg, N. R.; Peppas, N. A.; Sikavitsas, V. I. Tuning the Biomimetic Behavior of Scaffolds for Regenerative Medicine through Surface Modifications. Journal of Tissue Engineering and Regenerative Medicine. John Wiley and Sons Ltd 2019.

288. Low, S. S.; Lim, C. N.; Yew, M.; Chai, W. S.; Low, L. E.; Manickam, S.; Tey, B. T.; Show, P. L. Recent Ultrasound Advancements for the Manipulation of Nanobiomaterials and Nanoformulations for Drug Delivery. Ultrason. Sonochem. 2021, 80, 105805.

289. Miller, D. L.; Smith, N. B.; Bailey, M. R.; Czarnota, G. J.; Hynynen, K.; Makin, I. R. S. Overview of Therapeutic Ultrasound Applications and Safety Considerations. J. Ultrasound Med. 2012, 31 (4), 623.

290. Xu, C.; Wang, Y.; Wang, E.; Yan, N.; Sheng, S.; Chen, J.; Lin, L.; Guo, Z.; Tian, H.; Chen, X.; et al. Effective Eradication of Tumors by Enhancing Photoacoustic-Imaging-Guided Combined Photothermal Therapy and Ultrasonic Therapy. Adv. Funct. Mater. 2021, 31 (10), 2009314.

291. Kataoka, Y.; Kunimitsu, M.; Nakagami, G.; Koudounas, S.; Weller, C. D.; Sanada, H. Effectiveness of Ultrasonic Debridement on Reduction of Bacteria and Biofilm in Patients with Chronic Wounds: A Scoping Review. Int. Wound J. 2021, 18 (2), 176–186.

292. El Tayeb, M. N.; Hassan, A. A.; Abuelnaga, Y. G.; Eid, P. M.; Tarkhan, Y. M.; Fathallah, M. M.; Awad, A. A.; Nabhan, A. F. Low Level Laser Therapy versus Ultrasonic Therapy for the Treatment of Shoulder Impingement Syndrome A Systematic Review of Randomized Controlled Trials. QJM An Int. J. Med. 2021, 114 (Supplement_1).

293. Gorick, C. M.; Chappell, J. C.; Price, R. J. Applications of Ultrasound to Stimulate Therapeutic Revascularization. Int. J. Mol. Sci. 2019, Vol. 20, Page 3081 2019, 20 (12), 3081.

294. Kamel, R. K.; Mahdy, E. W.; Elsayed, M. M. Updates on Role of Ultrasound in Intensive Care Unit. Benha J. Appl. Sci. 2021, 6 (4), 133–140.

295. Kumar Sahu, A.; Rath, P.; Aggarwal, B. Ultrasound-Guided Injections in Musculo-Skeletal System - An Overview. J. Clin. Orthop. Trauma 2019, 10 (4), 669–673.

296. Posarelli, C.; Covello, G.; Bendinelli, A.; Fogagnolo, P.; Nardi, M.; Figus, M. High-Intensity Focused Ultrasound Procedure: The Rise of a New Noninvasive Glaucoma Procedure and Its Possible Future Applications. Surv. Ophthalmol. 2019, 64 (6), 826–834.

297. Xu, Z.; Hall, T. L.; Vlaisavljevich, E.; Lee, F. T. Histotripsy: The First Noninvasive, Non-Ionizing, Non-Thermal Ablation Technique Based on Ultrasound. 2021, 38 (1), 561–575.

298. Ahmad, T.; McGrath, S.; Sirafim, C.; Do Amaral, R. J. F. C.; Soong, S. L.; Sitram, R.; Turkistani, S.; Santarella, F.; Kearney, C. J. Development of Wound Healing Scaffolds with Precisely Triggered Sequential Release of Therapeutic Nanoparticles. Biomater. Sci. 2021, 9 (12), 4278–4288.

299. Pourhajibagher, M.; Bahador, A. Synergistic Biocidal Effects of Metal Oxide Nanoparticles-Assisted Ultrasound Irradiation: Antimicrobial Sonodynamic Therapy against Streptococcus Mutans Biofilms. Photodiagnosis Photodyn. Ther. 2021, 35, 102432.

300. Chen, Y.; Yin, B.; Liu, Z.; Wang, H.; Fu, Z.; Ji, X.; Tang, W.; Ni, D.; Peng, W. Dual-Modality Magnetic Resonance/Optical Imaging-Guided Sonodynamic Therapy of Pancreatic Cancer with Metal—Organic Nanosonosensitizer. Nano Res. 2022 2022, 1–8.

301. Busch, J. J. The Role for MRI-Guided Transurethral Ultrasound Ablation in the Continuum of Prostate Cancer Care. Br. J. Radiol. 2022, 95 (1131).

302. Zhou, Y.-F. High Intensity Focused Ultrasound in Clinical Tumor Ablation. World J. Clin. Oncol. 2011, 2 (1), 8.

303. Hensel, K.; Mienkina, M. P.; Schmitz, G. Analysis of Ultrasound Fields in Cell Culture Wells for In Vitro Ultrasound Therapy Experiments. Ultrasound Med. Biol. 2011, 37 (12), 2105–2115.

304. Kanta, J. Collagen Matrix as a Tool in Studying Fibroblastic Cell Behavior. Cell Adh. Migr. 2015, 9 (4), 308.

305. Stamov, D. R.; Pompe, T. Structure and Function of ECM-Inspired Composite Collagen Type I Scaffolds. Soft Matter 2012, 8 (40), 10200–10212.

306. Frantz, C.; Stewart, K. M.; Weaver, V. M. The Extracellular Matrix at a Glance. J. Cell Sci. 2010, 123 (24), 4195.

307. Parenteau-Bareil, R.; Gauvin, R.; Berthod, F. Collagen-Based Biomaterials for Tissue Engineering Applications. Mater. 2010, Vol. 3, Pages 1863-1887 2010, 3 (3), 1863–1887.

308. Rezvani Ghomi, E.; Nourbakhsh, N.; Akbari Kenari, M.; Zare, M.; Ramakrishna, S. Collagen-Based Biomaterials for Biomedical Applications. J. Biomed. Mater. Res. Part B Appl. Biomater. 2021, 109 (12), 1986–1999.

309. Zhang, L.; Gopalakrishnan, S.; Li, K.; Wang, L.-S.; Han, Y.; Rotello, V. M. Fabrication of Collagen Films with Enhanced Mechanical and Enzymatic Stability through Thermal Treatment in Fluorous Media. Cite This ACS Appl. Mater. Interfaces 2020, 12, 6590–6597.

310. Carlson, M. W.; Alt-Holland, A.; Egles, C.; Garlick, J. A. Three-Dimensional Tissue Models of Normal and Diseased Skin. Curr. Protoc. cell Biol. 2008, Chapter 19 (SUPPL. 41).

311. Maione, A. G.; Brudno, Y.; Stojadinovic, O.; Park, L. K.; Smith, A.; Tellechea, A.; Leal, E. C.; Kearney, C. J.; Veves, A.; Tomic-Canic, M.; et al. Three-Dimensional Human Tissue Models That Incorporate Diabetic Foot Ulcer-Derived Fibroblasts Mimic in vivo Features of Chronic Wounds. Tissue Eng. - Part C Methods 2015, 21 (5), 499–508.

312. Wolcott, R. D.; Ehrlich, G. D. Biofilms and Chronic Infections. JAMA 2008, 299 (22), 2682–2684.

313. Van Epps, J. S.; Younger, J. G. Implantable Device Related Infection. Shock 2016, 46 (6), 597.

314. Donlan, R. M. Biofilms and Device-Associated Infections. Emerg. Infect. Dis. 2001, 7 (2), 277–281.

315. Römling, U.; Kjelleberg, S.; Normark, S.; Nyman, L.; Uhlin, B. E.; Åkerlund, B. Microbial Biofilm Formation: A Need to Act. J. Intern. Med. 2014, 276 (2), 98–110.

316. Flemming, H. C.; Wingender, J. The Biofilm Matrix. Nat. Rev. Microbiol. 2010, 8 (9), 623–633.

317. Arciola, C. R.; Campoccia, D.; Montanaro, L. Implant Infections: Adhesion, Biofilm Formation and Immune Evasion. Nat. Rev. Microbiol. 2018, 16 (7), 397–409.

318. Sharma, D.; Misba, L.; Khan, A. U. Antibiotics versus Biofilm: An Emerging Battleground in Microbial Communities. Antimicrob. Resist. Infect. Control 2019 81 2019, 8 (1), 1–10.

319. Ciofu, O.; Moser, C.; amp, P.; Jensen, strup; Hamp, N. Tolerance and Resistance of Microbial Biofilms. Nat. Rev. Microbiol. 2022 2022, 1–15.

320. Cao, B.; Christophersen, L.; Thomsen, K.; Sønderholm, M.; Bjarnsholt, T.; Jensen, P. Ø.; Høiby, N.; Moser, C. Antibiotic Penetration and Bacterial Killing in a Pseudomonas Aeruginosa Biofilm Model. J. Antimicrob. Chemother. 2015, 70 (7), 2057–2063.

321. Cao, B.; Christophersen, L.; Kolpen, M.; Jensen, P. Ø.; Sneppen, K.; Høiby, N.; Moser, C.; Sams, T. Diffusion Retardation by Binding of Tobramycin in an Alginate Biofilm Model. PLoS One 2016, 11 (4), e0153616.

322. Kranjec, C.; Angeles, D. M.; Mårli, M. T.; Fernández, L.; García, P.; Kjos, M.; Diep, D. B. Staphylococcal Biofilms: Challenges and Novel Therapeutic Perspectives. Antibiot. 2021, Vol. 10, Page 131 2021, 10 (2), 131.

323. Soto, S. M. Role of Efflux Pumps in the Antibiotic Resistance of Bacteria Embedded in a Biofilm. 2013, 4 (3), 223–229.

324. Namgoong, S.; Jung, S. Y.; Han, S. K.; Kim, A. R.; Dhong, E. S. Clinical Experience with Surgical Debridement and Simultaneous Meshed Skin Grafts in Treating Biofilm-Associated Infection: An Exploratory Retrospective Pilot Study. J. Plast. Surg. Hand Surg. 2020, 54 (1), 47–54.

325. Wu, H.; Moser, C.; Wang, H. Z.; Høiby, N.; Song, Z. J. Strategies for Combating Bacterial Biofilm Infections. Int. J. Oral Sci. 2015, 7 (1), 1–7.

326. Makabenta, J. M. V.; Nabawy, A.; Li, C. H.; Schmidt-Malan, S.; Patel, R.; Rotello, V. M. Nanomaterial-Based Therapeutics for Antibiotic-Resistant Bacterial Infections. Nat. Rev. Microbiol. 2020 191 2020, 19 (1), 23–36.

327. Mahmoudi, M.; Serpooshan, V. Silver-Coated Engineered Magnetic Nanoparticles Are Promising for the Success in the Fight against Antibacterial Resistance Threat. ACS Nano 2012, 6 (3), 2656–2664.

328. Wu, J.; Li, F.; Hu, X.; Lu, J.; Sun, X.; Gao, J.; Ling, D. Responsive Assembly of Silver Nanoclusters with a Biofilm Locally Amplified Bactericidal Effect to Enhance Treatments against Multi-Drug-Resistant Bacterial Infections. ACS Cent. Sci. 2019, 5 (8), 1366–1376.

329. Koo, H.; Allan, R. N.; Howlin, R. P.; Stoodley, P.; Hall-Stoodley, L. Targeting Microbial Biofilms: Current and Prospective Therapeutic Strategies. Nat. Rev. Microbiol. 2017 1512 2017, 15 (12), 740–755.

330. Li, C. H.; Landis, R. F.; Makabenta, J. M.; Nabawy, A.; Tronchet, T.; Archambault, D.; Liu, Y.; Huang, R.; Golan, M.; Cui, W.; et al. Nanotherapeutics Using All-Natural Materials. Effective Treatment of Wound Biofilm Infections Using Crosslinked Nanoemulsions. Mater. Horizons 2021, 8 (6), 1776–1782.

331. Carmona, A. M.; Id, R. Self-Assembled Antimicrobial Nanomaterials. Int. J. Environ. Res. Public Heal. 2018, Vol. 15, Page 1408 2018, 15 (7), 1408.

332. Gupta, A.; Mumtaz, S.; Li, C. H.; Hussain, I.; Rotello, V. M. Combatting Antibiotic-Resistant Bacteria Using Nanomaterials. Chem. Soc. Rev. 2019, 48 (2), 415–427.

333. Hayes, B. T.; Merrick, M. A.; Sandrey, M. A.; Cordova, M. L. Three-MHz Ultrasound Heats Deeper Into the Tissues Than Originally Theorized. J. Athl. Train. 2004, 39 (3), 230.

334. LuTheryn, G.; Glynne-Jones, P.; Webb, J. S.; Carugo, D. Ultrasound-Mediated Therapies for the Treatment of Biofilms in Chronic Wounds: A Review of Present Knowledge. Microb. Biotechnol. 2020, 13 (3), 613–628.

335. Nakonechny, F.; Nisnevitch, M.; Nakonechny, F.; Nisnevitch, M. Different Aspects of Using Ultrasound to Combat Microorganisms. Adv. Funct. Mater. 2021, 31 (44), 2011042.

336. O'Brien, W. D. Ultrasound–Biophysics Mechanisms. Prog. Biophys. Mol. Biol. 2007, 93 (1–3), 212–255.

337. Ouyang, J.; Tang, Z.; Farokhzad, N.; Kong, N.; Kim, N. Y.; Feng, C.; Blake, S.; Xiao, Y.; Liu, C.; Xie, T.; et al. Ultrasound Mediated Therapy: Recent Progress and Challenges in Nanoscience. Nano Today 2020, 35, 100949.

338. Ahmad, T.; McGrath, S.; Sirafim, C.; Do Amaral, R. J. F. C.; Soong, S. L.; Sitram, R.; Turkistani, S.; Santarella, F.; Kearney, C. J. Development of Wound Healing Scaffolds with Precisely-Triggered Sequential Release of Therapeutic Nanoparticles. Biomater. Sci. 2021, 9 (12), 4278–4288.

339. Kearney, C. J.; Skaat, H.; Kennedy, S. M.; Hu, J.; Darnell, M.; Raimondo, T. M.; Mooney, D. J.; Kearney, C. J.; Skaat, H.; Kennedy, S. M.; et al. Switchable Release of Entrapped Nanoparticles from Alginate Hydrogels. Adv. Healthc. Mater. 2015, 4 (11), 1634–1639.

340. Kimmel, E. Cavitation Bioeffects. Crit. Rev. Biomed. Eng. 2006, 34 (2), 105–161.

341. Ebbini, E. S.; Ter Haar, G. Ultrasound-Guided Therapeutic Focused Ultrasound: Current Status and Future Directions. https://doi.org/10.3109/02656736.2014.995238 2015, 31 (2), 77–89.

342. Gupta, A.; Landis, R. F.; Li, C. H.; Schnurr, M.; Das, R.; Lee, Y. W.; Yazdani, M.; Liu, Y.; Kozlova, A.; Rotello, V. M. Engineered Polymer Nanoparticles with Unprecedented Antimicrobial Efficacy and Therapeutic Indices against Multidrug-Resistant Bacteria and Biofilms. J. Am. Chem. Soc. 2018, 140 (38), 12137–12143.

343. Makabenta, J. M. V.; Park, J.; Li, C. H.; Chattopadhyay, A. N.; Nabawy, A.; Landis, R. F.; Gupta, A.; Schmidt-Malan, S.; Patel, R.; Rotello, V. M. Polymeric Nanoparticles Active against Dual-Species Bacterial Biofilms. Molecules 2021, 26 (16).

344. Monsen, T.; Lövgren, E.; Widerström, M.; Wallinder, L. In Vitro Effect of Ultrasound on Bacteria and Suggested Protocol for Sonication and Diagnosis of Prosthetic Infections. J. Clin. Microbiol. 2009, 47 (8), 2496.

345. Tang, J.; Wennerberg, K.; Aittokallio, T. What Is Synergy? The Saariselkï¿½ Agreement Revisited. Front. Pharmacol. 2015, 6 (SEP), 181.

346. Baker, K. G.; Robertson, V. J.; Duck, F. A. A Review of Therapeutic Ultrasound: Biophysical Effects. Phys. Ther. 2001, 81 (7), 1351–1358.

347. Steudle, A.; Pleiss, J. Modelling of Lysozyme Binding to a Cation Exchange Surface at Atomic Detail: The Role of Flexibility. Biophys. J. 2011, 100 (12), 3016.

348. Fologea, D.; Ledden, B.; McNabb, D. S.; Li, J. Electrical Characterization of Protein Molecules by a Solid-State Nanopore. Appl. Phys. Lett. 2007, 91 (5), 053901–1.

349. Espinosa, M. F.; Sancho, A. N.; Mendoza, L. M.; Mota, C. R.; Verbyla, M. E. Systematic Review and Meta-Analysis of Time-Temperature Pathogen Inactivation. Int. J. Hyg. Environ. Health 2020, 230, 113595.